University of Technology, Sydney

Improvement in Seismic Performance of Stone Masonry Using Galvanized Steel Wire

Rudra Pun

A Thesis submitted in fulfilment of the requirement for the degree of

Doctor of Philosophy

School of Civil and Environmental Engineering

Faculty of Engineering and Information Technology

University of Technology, Sydney

April 2015

Certificate of original authorship

I certify that the work in this thesis has not previously been submitted for a degree nor has it been submitted as part of requirements for a degree except as fully acknowledged within the text.

I also certify that the thesis has been written by me. Any help that I have received in my research work and the preparation of the thesis itself has been acknowledged. In addition, I certify that all information sources and literature used are indicated in the thesis.

Rudra Pun

April 2015

In the Memory of Precious Lives Lost in Earthquakes

Abstract

This research is about using either freely available natural stone or rubble left behind earthquake disasters to build a seismic resistant house. The bottom line of this research is to develop a simple and effective technique for building a stone masonry house that will not collapse during the seismic event.

Traditionally constructed stone masonry houses are highly vulnerable to seismic loadings. In the past, most of the un-reinforced stone masonry buildings had collapsed causing many casualties during the earthquake events. In order to address this problem, various options have been recommended by the researchers for reinforcing new stone masonry buildings as well as strengthening existing buildings. However, developing an economically viable and socially acceptable option for improving seismic performance of the residential stone masonry houses is still remaining a great challenge.

In this context, a system of reinforcing rubble masonry using galvanized steel wire (GSW) mesh has been proposed in this research. A gabion like technique is adopted for wrapping the wall with a mesh. It is a simple technique, which can be easily learnt by the users and applied to build their houses. This method is suitable even in remote and isolated areas, where access to the technical inputs is not available. In addition, this technique seems to be useful during reconstruction phase after the earthquake disaster, for clearing up sites and building safer houses side by side.

The performance of the proposed reinforcement system was investigated both experimentally and analytically under static and dynamic loadings. Suitable materials for this research were identified and the required materials were collected. All specimens were prepared and cured in the laboratory environment. Wall specimens were constructed with due considerations to the owner builder construction mode, where owners themselves construct their houses. Both unreinforced and reinforced wall specimens were prepared for static test as well as shake table testing simulating strong earthquakes.

Two types of reinforcement schemes have been proposed in this research. In the first method, reinforcement mesh is woven around the wall using steel wire, whereas in the second method, pre-fabricated meshes are used.

Developing connecting techniques between adjacent meshes are some of the significant contributions of this investigation. This method makes this reinforcement system practicable using pre-fabricated meshes. Moreover, a simple method for tightening the mesh has been developed in this research. This tightening technique makes the proposed reinforcement system more effective in seismic performance than other types of external mesh by allowing limited deformation of the building during ground motions.

Most of the testing procedures required for this research were not covered in the existing standard methods. Therefore, several additional techniques required for preparing the specimens and testing have been developed during this research, which are given in the relevant sections. Two terminologies have been proposed for describing the strength of rubble wall in flexure.

Materials were tested for some basic properties as well as few reference parameters, which can be used for comparing the results of this research to the relevant cases. Static tests on unreinforced wall specimens have provided the basic strength properties of the wall, whereas testing on reinforced specimens have indicated potential effectiveness of the proposed scheme under dynamic loading. This has been verified by shake table testing.

A theory has been proposed for explanation of the behaviour of an externally reinforced beam and some relations have been derived. Deformation characteristics of a hexagonal mesh have been derived so that the theory developed for externally reinforced beam could be applied to the GSW reinforced wall. A set of analytical procedures have been developed and applied for the assessment of a single storey and two storey buildings.

[Blank Page]

Acknowledgements

I would like to extend my sincere gratitude to the University of Technology Sydney and all individuals whose direct or indirect contributions have made it possible to accomplish this research.

In particular, I am very grateful to my supervisor Prof. Bijan Samali for providing comprehensive support, guidance, and encouragement throughout the whole period. My deep appreciation goes to my co-supervisor Dr. Hamid Valipour for his kind guidance during this research.

I would also like to thank Mr. Rami Haddad for managing experimental activities in the laboratory, Mr. David Hooper for arranging the materials, Mr. David Dicker for assisting in preparing accessories, setting up and testing, Mr. Peter Brown and Mr. Mulugheta Hailu for technical advice and supports during testing, Mr. Antonio Reyno for assisting in soils laboratory. I also appreciate the efforts of all other laboratory staff for assisting during the experimental phase of my works.

My sincere thanks go to A/Prof. Robert J Wheen, Ms Penny Rosier, and Mr. Ian Brumby for sharing their expertise and concept in the field of gabion system. I am also thankful to A/Prof. Jianchun Li, and Dr. Kirk Vessalas for their helpful comments and suggestions.

I am truly indebted to my friend Dr. Binod Shrestha for helping in various occasions of the research activities. I also appreciate the help from my friends and colleagues for assisting in one or another form during this research.

I am grateful to National Society for Earthquake Technology-Nepal (NSET), Dr. Ulrike Dackermann and Mr. Shambhu Raj Kandel for few photographs used in this thesis. I am thankful to all authors and institutions whose contributions towards the knowledge have been referred in this research.

I wish to express my sincere gratitude to my mum and other family members for their loving support. Finally, I would like to express appreciation to my wife Tika for her love, encouragement, patience and support throughout the journey.

Table of Contents

[Blank Page]

List of Figures

[Blank Page]

List of Tables

Abbreviations and Acronyms

A	Cross-sectional Area
AEM	Applied Element Method
A_h	Design Horizontal Seismic Coefficient
AS	Australian Standard
ASTM	American Society for Testing and Materials
B	Breadth
BS	British Standard
CFRP	Carbon Fibre Reinforced Polymer
cm	Centimetre
D	Depth of beam / thickness of wall
DEM	Discrete Element Method
E	Modulus of Elasticity
ε	Strain
F	Failure Load
f_a	Axial Stress
f_b	Bending Stress
f_c	Compressive Stress
FEM	Finite Element Method
f_s	Shear Strength
G	Modulus of Rigidity
g	Acceleration due to Gravity
GFRP	Glass Fibre Reinforced Polymer
GPa	Gigapascal
GSW	Galvanized Steel Wire
h, H	Height
HB	Hand Book
Hz	Hertz
I	Second Moment of Area, Importance Factor
IAEE	International Association for Earthquake Engineering
IS	Indian Standard
kg	Kilogram
kPa	Kilopascal
L	Length
l	Span
LL	Liquid Limit
LS	Lateral Span
LVDT	Linear Variable Differential Transformer
m	Metre
M	Moment
min	Minute

mm	Millimetre
MMI	Modified Mercalli Intensity
MPa	Megapascal
N	Newton
NBC	Nepal National Building Code
NSET	National Society of Earthquake Technology-Nepal
NSW	New South Wales
P	Point Load
PI	Plasticity Index
PL	Plastic Limit
PP	Polypropylene
R	Response Reduction Factor
RC	Reinforced Concrete
s	Second
s_m	Strain mobilising length
STP	Scrap Tyre Pads
T_a	Approximate Time Period
USGS	Unites States Geological Survey
UTS	University of Technology, Sydney
V_B	Design Base Shear
VS	Vertical Span
Z	Zone Factor
ν	Poisson's Ratio

Publications

Pun, R., Samali, B. & Shreshta, B. 2010, 'Major factors in reinforcing stone masonry for sustainable construction practice', *21st Australasian Conference on the Mechanics of Structurers and Materials*, Melbourne, Australia, pp. 547-552.

Pun, R., Samali, B. & Valipour, H. 2012a, 'Flexural strength of stone wall in mud mortar', *Australasian Structural Engineering Conference 2012*, Perth, Australia.

Pun, R., Samali, B. & Valipour, H. 2012b, 'Seismic performance improvement of stone masonry buildings in mud mortar', *22nd Australasian Conference on the Mechanics of Structures and Materials*, Sydney, New South Wales, Australia, pp. 479-484.

[Blank Page]

1. Introduction

1.1 General

Stone masonry has been used in practice since ancient times and is still being widely used these days. As stone is naturally available in handy shapes and sizes, and also hard enough to sustain loads, one can easily deduce that this material could have been in use for building houses since early human civilization. For example, Natufian used stone to build round stone huts as early as 10,000 BC in western Asia (Brooks, Adams & Fowler 2001). Gradual improvement in building skills in stone masonry went on over centuries. The Egyptians introduced complexity in the building architecture, which was elaborated by Greeks and much more refined by Romans with the invention of pozzolanic cement (Hendry & Khalaf 2001). As a consequence, stone masonry reached to an advanced level of development thorough the Middle Ages. After the invention of cement and steel, the use of stone masonry gradually declined in economically active regions. With advancements in building technology and construction materials, a land mark shift in construction practice has occurred. However, there are several regions around the world lagging behind the main stream of development, where stone houses with mud mortar are the only prevailing construction practice.

Stone masonry buildings still exist in old historic towns, often in buildings of art, cultural and historical significance (Lutman n.d.). These type of buildings range from monumental buildings with cultural and historical significance, often built by highly skilled stonemasons, to simple dwellings built by their owners (Bothara & Brzev 2011). For instance, in Sydney, there are few historical buildings made from stone

masonry around the city (Figure 1.1). The residential stone buildings are popular in developing countries (Figure 1.2), where these types of buildings represent affordable and cost-effective alternatives for housing construction. Most often, such buildings are made with rubble laid in mud mortar.

Figure 1.1 Stone masonry building in Sydney

The stone masonry possesses several advantages, such as durability, fire resistance, thermal and sound insulation, and is environmentally friendly. Unlike clay bricks, natural stone need not be processed further to increase its strength and durability. Stone masonry is normally thicker than other types of masonry. Therefore, it is effective in thermal and sound insulation. Use of locally available materials helps for reducing energy consumption during transportation. In this regard, a significant amount of energy can be saved by using local stone for the construction of houses

(Morel et al. 2001). Therefore, stone masonry has been proven to be one of the most sustainable construction materials and deserves due attention for its promotion.

Figure 1.2 A stone masonry house in developing region. *(Photo: S. Kandel)*

On the other hand, traditional stone masonry buildings have shown poor performance in seismic events (Bothara & Hiçyılmaz 2008; Karantoni & Bouckovalas 1997; Spence & Coburn 1992). Most of the casualties in devastating earthquakes in the past were caused by the collapse of poorly constructed masonry buildings (Bayraktar, CoSkun & Yalçin 2007). In spite of being most pleasingly built, stone buildings suffered heavy damage in the Christchurch Earthquake (22 February 2011) as shown in Figure 1.3. There are still large stocks of stone masonry buildings in earthquake prone regions of the world, such as South Asia, Middle East, North Africa, and Mediterranean Europe (World Housing Encyclopedia).

Figure 1.3 Damaged Cathedral in Christchurch Earthquake (Stuff 2011)

It is almost impossible to replace all these buildings at once by modern materials, either because of socioeconomic reasons or due to conservation of cultural and historical values. Therefore, improving the seismic performance of such buildings is the only viable option for safer construction practice. In order to address this problem, research has been undertaken around the world, and various reinforcing and strengthening options of stone masonry are developed. However, large variations in structural typology and construction practices make it really difficult to generalise these options. In addition, the applicability of each method is influenced by various factors: socioeconomics, traditions, availability of materials, accessibility to technical skills, transportation facilities, cultural and historical significance, topographical landscape, geographical location, political decisions, and awareness of

risks (Coburn & Spence 2002; Pun, Samali & Shreshta 2010). Overall, sustainability has become one of the major aspects to be considered while developing and selecting the most appropriate option for implementation.

In these scenarios, a reinforcing option for stone masonry with Galvanized Steel Wire (GSW) has been proposed in this study. The background on selecting this type of reinforcement system is given in detail in section 3.1. In this scheme, walls are enclosed within a mesh of GSW. The effectiveness of the stone masonry wall with new intervention for resisting seismic loads has been thoroughly investigated and presented in this thesis.

In order to accomplish any mission, setting certain realistic objectives are essential at the beginning. The following objectives have been set for this research.

1.2 Objectives of the research

The major objective of this research is to develop a simple and effective technique to build enhanced stone masonry houses that will, at least, not collapse during major seismic events. The specific objectives are:

1. To determine the strength related parameters of un-reinforced rubble masonry in mud mortar and its constituents.
2. To investigate the effectiveness of GSW reinforcement system under static loading.
3. To observe the overall performance of an un-reinforced model house subjected to seismic loading.
4. To study the improvements in seismic performance of reinforced houses.

These research objectives have been set within the following scope of investigation.

1.3 Scope of the study

This research presents a concept of stone masonry reinforcement using galvanized steel wire mesh. The performances of this system have been investigated both experimentally and numerically. Experimental works were broadly divided into two parts: static and dynamic tests. Static tests were carried out to find the strength of materials and wall specimens. Dynamic tests included shake table testings on reduced scale (1:2) physical models. The static test results of the materials were used in order to explain the behaviour of the wall under static load. Based upon these parameters, the response of the wall under dynamic loading were analysed.

1.4 Research methodology

The following methodologies were adopted for setting the scope of investigation of this research.

A. Literature Review

The relevant information required to conduct this research was collected through reviewing numerous literature, which is presented in Chapter 2. Initially, existing information regarding stone masonry and its constituents were gathered. Then, the performance of the stone masonry buildings in the past earthquakes along with available techniques for improving the seismic resistance of those buildings were explored. On the basis of this information, the necessity for further investigation on the improvement methods of the stone masonry was identified and research on

proposed reinforcement system was validated. The details of the reinforcement system were further refined, which are presented in Chapter 3.

Due to limited data available on the properties of stone masonry in mud mortar, the experimental work was commenced with finding the properties of materials. For this purpose, various standard testing methods, as well as research activities in similar fields carried out around the world, were studied. Mostly, Australian Standards have been referred to whenever relevant. Other standards have also been adopted for those materials not covered in the Australian Standards. These standards have been quoted in the corresponding sections. In most cases, certain modifications in the existing methods were implemented because these were not covered in the standard procedures. These adaptations are explained in the relevant sections.

Static test results were inadequate to confirm the performance of the proposed system under seismic loading. Therefore, various research works on dynamic tests on masonry were also studied. Furthermore, attempts on numerical analysis of the stone masonry by numerous researchers were observed. Based on this information, a detailed experimental investigation plan has been worked out.

B. Experimental Investigation

According to the detailed plan prepared after extensive literature search, several experimental investigations were conducted. Following the standard procedures and by developing new techniques not covered in the standards, specimens were prepared and tested in the laboratory. These are explained in detail in Chapter 4 and

Chapter 5. Material testing is given in Chapter 4, whereas Chapter 5 covers testing on wall specimens.

C. Analytical and Numerical Studies

In addition to experimental investigations, analytical and numerical studies were also carried out. Analytical studies were performed for explaining the performance of loosely wrapped external reinforcement (straight). Deformation characteristics of the GSW mesh were investigated using analytical as well as numerical approach. Some useful relations of the hexagonal GSW mesh have been derived so that the theory of external reinforcement could be applied to the mesh system. Using these parameters, adequacy of the mesh have been assessed for a single storey and a double storey buildings. These are covered in detail in Chapter 6.

D. Discussions on the results

The results of both experimental and numerical results were investigated thoroughly. Various influencing factors on the results were discussed. These were compared with the results in the literature. These are given in Chapter 7.

E. Conclusions and Recommendations

On the logics of discussions, the outcomes of the research were summarised through various conclusions and recommendations. These are presented in Chapter 8.

2. Literature Review

This chapter begins with the review of existing literature relevant to the building materials used in this research. This is followed by the types of stone walling, which are commonly used around the world. Then, the common deficiencies in traditional stone masonry buildings for resisting seismic loadings are addressed. Afterwards, current reinforcing options available for new construction and strengthening methods for existing stone masonry buildings are presented. Based on these facts, the requirement for the new reinforcement system is critically analysed.

Subsequently, brief descriptions on relevant testing methods are described. After that, static and dynamic testings carried out by various researchers on the stone masonry are presented. Finally, existing information on the numerical studies of the stone masonry are included.

2.1 Building Materials

Four types of building materials were used in this research: natural building stone, mud mortar, galvanised steel wire and timber. Properties of timber were not the major concern of this research. Therefore, the other three building materials have been briefly explained in this section.

2.1.1 Natural building stone

In rural part of hilly regions, natural building stones are still abundantly available in handy sizes scattered either along the terrains or along the river banks (Figure 2.1).

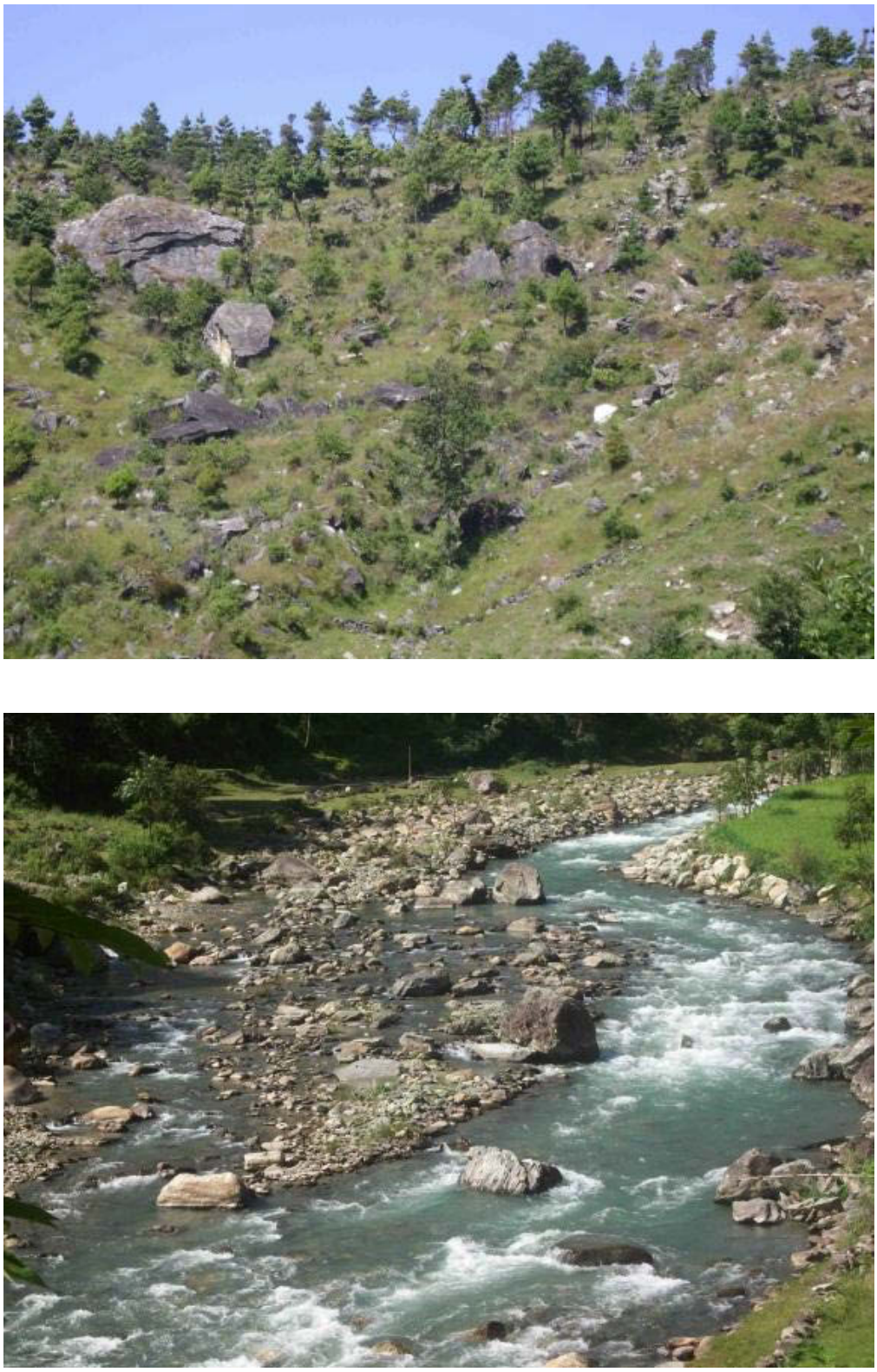

Figure 2.1 Natural sources of building stones

As the stone can be easily picked up with little effort, it has become one of the most economical options for building construction over centuries.

Naturally available building stone can be categorised in to three major groups: igneous; sedimentary and metamorphic (BS 5628-3 : 2001). According to this standard, the most popular igneous building stones are granite, basalt diorite and serpentine. Igneous rocks are the most difficult to build because they are hard to split and shape. The major sedimentary building stones are limestone and sandstone. Sedimentary rocks are relatively soft and easy to work with, but wear out faster than other types of rocks. Slate and marble are the most commonly used metamorphic building stones. Shale and schist are the best building stones as they can be split nicely (Chiras 2000).

The size of the stone used in the stone masonry should be handy so that one can easily lift and place by hand. According to Indian Standard (IS 1597.1 : 1992), the maximum length of any stone piece should not be larger than three times the thickness of stone, whereas the width of the stone should be greater than 150 mm and less than three-fourth of the thickness of wall.

2.1.2 Mud mortar

Usage of mud mortar in stone masonry is a very ancient technique (Maxlow & Maxlow 1984). Usually, soil available at a building site can be used for preparing mud mortar.

Mud mortar soil is composed of sand, silt and clay particles. The recommended proportions of sand, silt and clay in mud mortar soil are 30% to 75 %, 10% to 30%

and 10% to 40%, respectively (HB 195 - 2002). According to this reference, soil for mud mortar is pulverised well and screened to remove material sizes larger than 5 mm and unwanted organic matters. A sufficient quantity of potable water is added to the soil and mixed until the mortar achieves uniform consistency so that it is easy to spread during construction. However, the mortar must be firm enough to support the weight of the wall without squeezing out. The exact quantity of water to be added depends on the nature of the soil, which is to be determined by trial and error.

2.1.3 Galvanized steel wire

Galvanized steel wire for gabion basket have been used since late 19th century, although similar structures made from rock filled wicker basket was initially developed by Chinese and improved by British and French in the 16th century (Global Synthetics n.d.). Further improvements to steel wire coating and manufacturing techniques have been achieved and implemented in the earth retaining structures around the world.

Australian/New Zealand standard (AS/NZS 4534: 2006) has recommended six standard classes of zinc and zinc/aluminium-alloy coatings and a range of special coating on steel wire of circular or non-circular cross-section. The standard classes are intended for using in normal atmospheric corrosion conditions, whereas the special classes are for using under severe to extreme service conditions, such as marine environments. The recommended tensile strength of galvanized wire for weaving ranges from 380 MPa to 550 MPa (AS 2423-2002).

According to ASTM standard, galvanized steel (GS) wire comes under six different classes of zinc coating and tensile strength (ASTM A 641/A 641M: 2009). Double twisted hexagonal gabion basket is prepared using soft tempered steel wire with zinc coating of class 3 (ASTM A 975 : 2003). The exact value of tensile strength and zinc coating is specified based on diameter of wire used. The gabion baskets are also available in other standard coatings for protection of wire from corrosion in different environments such as zinc-aluminium alloy coating, polyvinyl chloride (PVC) coating over zinc coating, and aluminium coating.

2.2 Walling types

Throughout the history of human civilization, stone masonry has undergone various stages of refinement; from a simple dwelling to the extreme level of architecture (Brooks, Adams & Fowler 2001). Depending upon the type of locally available building stones, climatic conditions, culture, workmanship and research, wide ranges of walling types have been developed in various regions around the world. In spite of many variations, stone masonry walls can broadly be divided in to two major categories: ashlar walling and rubble walling.

2.2.1 Ashlar walling

Ashlar walling consists of blocks of stone, finely square dressed to given dimensions and laid in courses with thin joints, which is generally used for buildings in urban settings or formal type of construction (BS 5390 : 1976). In each course, stone blocks of equal height are used. If every stone is fine tooled on all sides, such masonry is called plain ashlar (Figure 2.2). Based on exposed faces, the ashlar

masonry can be rock or quarry faced ashlar, chamfered ashlar, and sunk or moulded ashlar, rough tooled or punched (Figure 2.3). If hammer-faced large stone blocks

Figure 2.2 Plain ashlar masonry

(a) Chamfered

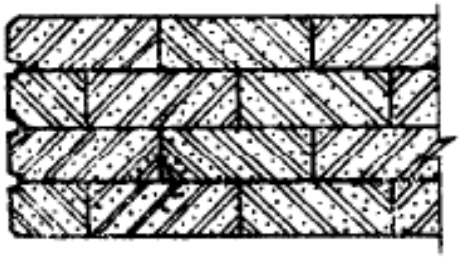

(b) Sunk or Moulded

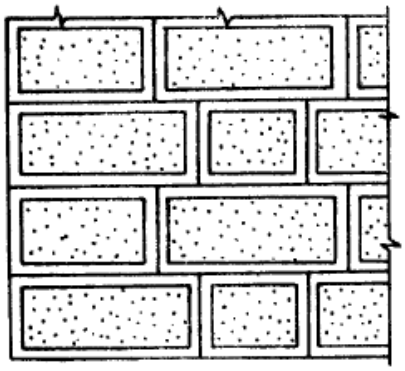

(c) Rough tooled or Punched

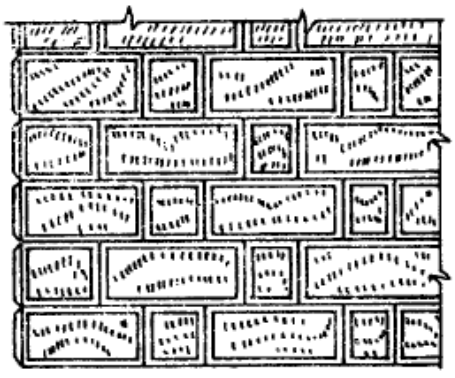

(d) Rock faced

Figure 2.3 Ashlar masonry based on exposed face (IS 1597.2 : 1992)

are used to build a regular coursed masonry, these are known as block-in-course ashlar (IS 1597.2 : 1992). As fine dressing of stone blocks involves a major investment of time and efforts, the ashlar masonry is relatively expensive as compared to rubble walling.

2.2.2 Rubble walling

Rubble walling is built of stone blocks essentially of irregular shapes, sizes and having comparatively thick mortar joints (IS 1597.1 : 1992). This type of walling is used, where a less formal character is required, or in village and rural setting (BS 5628-3 : 2001). It covers a wide range of masonry types available in various regions, which can be broadly categorised in three categories: random rubble, squared rubble and miscellaneous rubble walling as given below.

2.2.2.1 Random rubble

This type of wall is constructed by selecting the stones of all shapes and sizes randomly and placing them in position to obtain a good bond (BS 5390 : 1976). A bond stone is normally inserted along certain horizontal and vertical intervals in order to hold the wall together transversally (IS 1597.1 : 1992). The walling can be either un-coursed for the whole height or roughly levelled up to courses at intervals of 600 mm to 900 mm (Figure 2.4).

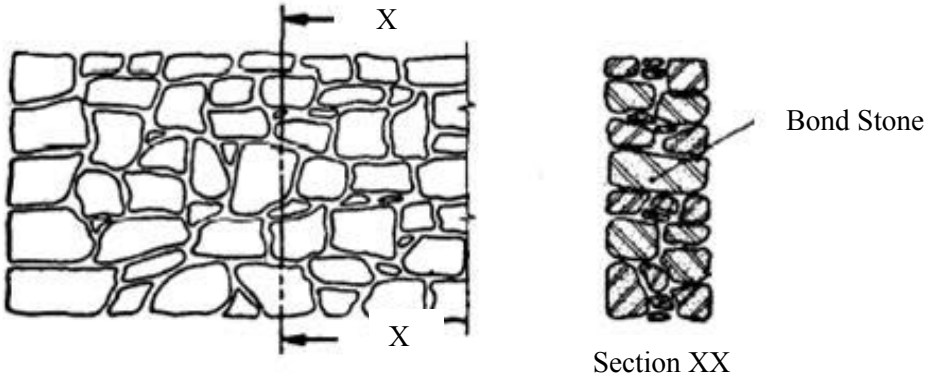

(a) Un-coursed

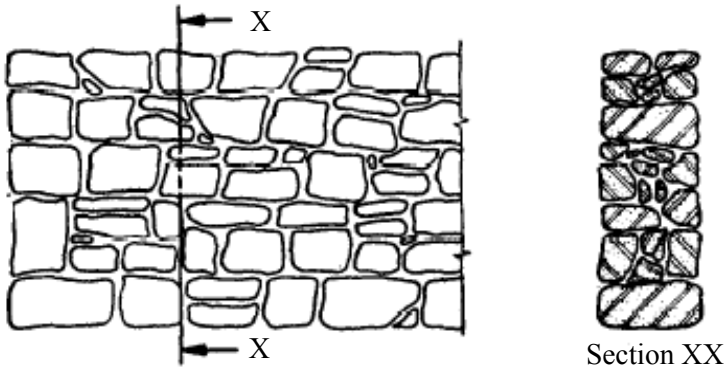

(b) Brought to coursed

Figure 2.4 Random rubble masonry (IS 1597.1 : 1992)

2.2.2.2 Squared rubble

In squared rubble masonry, the stone units are roughly squared as risers and stretchers of varying height (BS 5390 : 1976). This type of walling can also be laid in different ways, such as, leaving the entire wall un-coursed throughout the height or levelling up in the interval of varying height from 300 mm to 900 mm or fully coursed in an interval of 100 mm to 300 mm (Figure 2.5). In all cases, the stones at any course are maintained roughly of same height (IS 1597.1 : 1992).

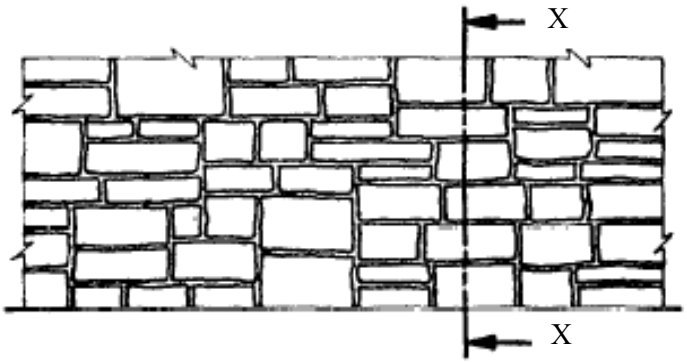

Section XX

(a) Un-coursed

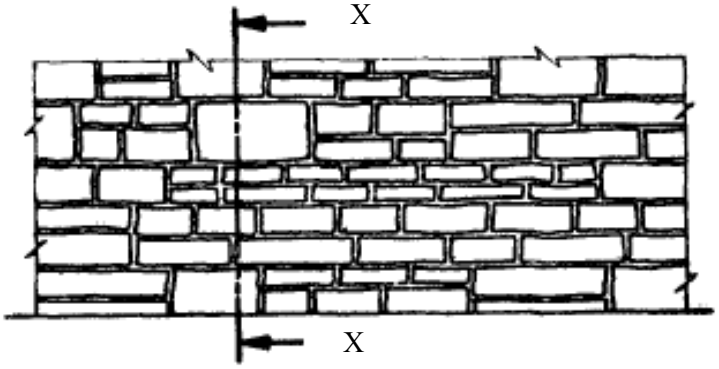

Section XX

(b) Brought to course

Figure 2.5 Squared rubble masonry (IS 1597.1 : 1992)

2.2.2.3 Miscellaneous rubble walling

Besides above mentioned types, there are many varieties of rubble masonry. The variations are mainly governed by specific characteristics of local materials and traditional forms of construction (BS 5390 : 1976). One such form is cobble or flint walling. In this type, a wall is built up with a facing of selected flints or cobbles of varying sizes and shapes and a core of the same material or other type of rubble. Usually, joints are deeply raked back to emphasise the roundness of the stones (Maxlow & Maxlow 1984). Polygonal rubble walling is another variation of rubble

walling, in which stone pieces without clear lamination is hammered into irregular polygonal shapes, and bedded to show the face joints running irregularly (Figure 2.6).

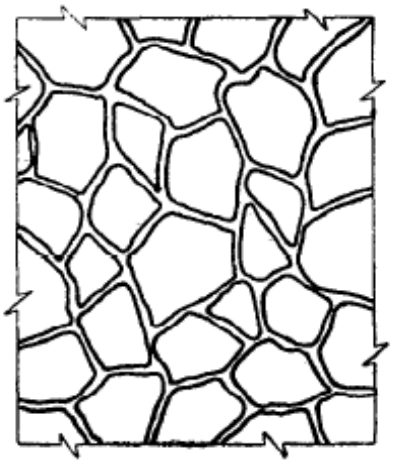

Figure 2.6 Polygonal rubble walling (IS 1597.1 : 1992)

(a) Flat bedded walling

(b) Dry stone walling

Figure 2.7 Miscellaneous rubble walling *(Photo S. Kandel)*

Moreover, using irregular flat bedded stones of various sizes brings another variation in rubble walling (Figure 2.7 a). In this type of wall, flat stones are placed layer upon layer, usually horizontally, and are often roughly coursed. Dry stone walling is a

special type of rubble masonry in which a wall is constructed using relatively flat stones without using mortar (Figure 2.7 b).

2.3 Common seismic deficiencies and modes of failure in traditional stone masonry houses

In general, a traditional stone house consists of detached, single to double storey rubble masonry with a flexible timber floor covered with mud and pitched or flat roof (Figure 1.2). The wall system ranges from partly dressed to fully dressed stones masonry laid in mud mortar. Partially dressed rubble masonry is most commonly used due to ease of construction and economic reasons. Undressed or partly dressed walls are usually covered with mud plaster.

Some historical earthquakes have offered abundance of evidence of the weakness and extreme vulnerability of the traditional stone masonry dwellings in many earthquake prone regions. Random rubble and semi dressed stone masonry buildings have suffered extensive damage to complete collapse in the seismic events exceeding intensity of ground shaking over MMI VI (Arya 2001).

The most common deficiencies of traditional stone buildings are given in this section. Supporting photographs presented in this section were taken by the author (except quoted) during his visit to the earthquake affected areas, which created much motivation for this research.

2.3.1 De-lamination

De-lamination is a unique and most common failure mechanism observed in stone masonry (Bothara & Hiçyılmaz 2008). During vigorous shaking, outer and inner

layers of the stone masonry get separated through the middle of the wall thickness (Figure 2.8).

Figure 2.8 De-lamination of stone masonry *(Photo: NSET)*

This type of weakness is related to the constructional features of rubble masonry. In this type of masonry, the stone units are not in full contact to each other. Due to irregular shapes, stone blocks are only in partial contact near the outer face. The voids between rubble are filled with mortar and gravels. Because of this feature, stone pieces are in an unstable equilibrium in rubble masonry. During earthquake, equilibrium is easily disturbed and the stone pieces simply crumble away (Arya 2001). The absence of through stone or any other interlocking elements between the outer and inner layer of stones increases the chance of de-lamination of the wall

during seismic event. This phenomenon is more severe in rubble walls with weak mortar, such as mud mortar.

2.3.2 Out of plane bending failure

Usually, traditional stone masonry construction is composed of a flexible floor and roof structure. Out of plane bending failure of wall is common in such buildings (Figure 2.9).

Figure 2.9 Out of plane bending failure

This type of failure is mainly because of the lack of connection between orthogonal walls and between walls and floors or roofs (Bayraktar, Nart & Ali 2007). Initially, orthogonal external walls separate at roof level, which allows outward movement of the major walls leading to out of plane failure (Spence & D'Ayala 1999). Even in a

building with a rigid floor, once the wall cracks, either due to in-plane shear failure or bulged due to de-lamination, it cannot sustain the out of plane component of seismic load. Long unsupported slender walls are highly susceptible to out of plane loading (Bothara & Brzev 2011). If the connection between cross walls and outer walls are not adequate, the outer walls will be subjected to significant out of plane bending, leading to the collapse of wall.

2.3.3 In-plane shear or bending failure

In-plane shear or bending failure is another type of failure mechanism, particularly in buildings with rigid floors. Damage to stone building with flexible roof due to in-plane shear is relatively less common than out of plane bending (Bothara & Brzev 2011; Spence & D'Ayala 1999). If the connection between a rigid roof and the wall can transfer seismic loads induced in the roof in to the walls, the load is distributed among the walls, based on their relative stiffness. The higher stiffness of in-plane walls attract more of the seismic load than flexible out of plane walls. Depending upon the aspect ratio of wall or pier, quality of materials and boundary conditions, the wall fails either in shear or bending (Tomazevic 1999).

Such damage can also be observed in buildings with flexible floor with inadequate spacing between openings or having insufficient distance between an opening and the corner of the building. Besides these, presence of opening makes the walls more critical for in-plane shear strength than a solid wall. In such cases, crack is usually initiated from the corner of the opening and extends diagonally (Figure 2.10). Distance between door and window also has a significant effect on in-plane behaviour of stone masonry.

Figure 2.10 In-plane shear failure and corner separation

2.3.4 Corner or junction separation

A junction or a corner is usually the most vulnerable part of un-reinforced stone masonry buildings. The corner failure is one of the predominant failure modes of masonry in earthquakes (Spence & D'Ayala 1999). It is due to the interaction between adjoining walls and poor connection between orthogonal walls. Reversible bending stress at the end of wall induces vertical cracks at the corner, leading to subsequent collapse (Figure 2.11).

Figure 2.11 Damage along the corner (*Photo NSET*)

The formation of vertical crack at the junction is a common phenomenon in masonry buildings, when subjected to earthquake loadings (Bayraktar, CoSkun & Yalçin 2007; Bayraktar, Nart & Ali 2007; Decanini et al. 2004). Due to poor connection, separation of walls at T-junction (junction between main wall and cross wall) in stone masonry is more likely than brick masonry (IAEE 1986). If the external walls are constructed before the partition walls, there will be no proper connections at the junctions. Also, in the case of a opening being very close to the corner or junction, the integrity of the wall gets reduced. As a result, separation of the walls commences easily at the junction.

2.4 Seismic performance improving methods for new stone masonry

In order to address the most common deficiencies explained in the last section along with other weaknesses in traditional masonry buildings, some recommendations are available in the literature for reinforcing new constructions as well as strengthening existing buildings. These are briefly presented in the following sections.

2.4.1 A system of reinforcements at critical locations and limits on openings

A set of guidelines for reinforcing non engineered buildings was published by the International Association for Earthquake Engineering (1986) including stone masonry buildings. However, it has been advised to avoid mud mortar as far as possible. In these guidelines, a system of horizontal and vertical reinforcement is specified at the critical locations. For horizontal reinforcement, a reinforced concrete (RC) band is provided at lintel and roof level along with an optional band at plinth level (Figure 2.12).

Vertical steel reinforcement, encased in a cement concrete core is specified at corners, junction and jambs of openings. Alternatively, a timber band is suggested instead of RC band, wherever it is economically available. It consists of wooden planks of rectangular section, effectively spliced longitudinally and held in position by lateral members in lattice form as shown in Figure 2.13.

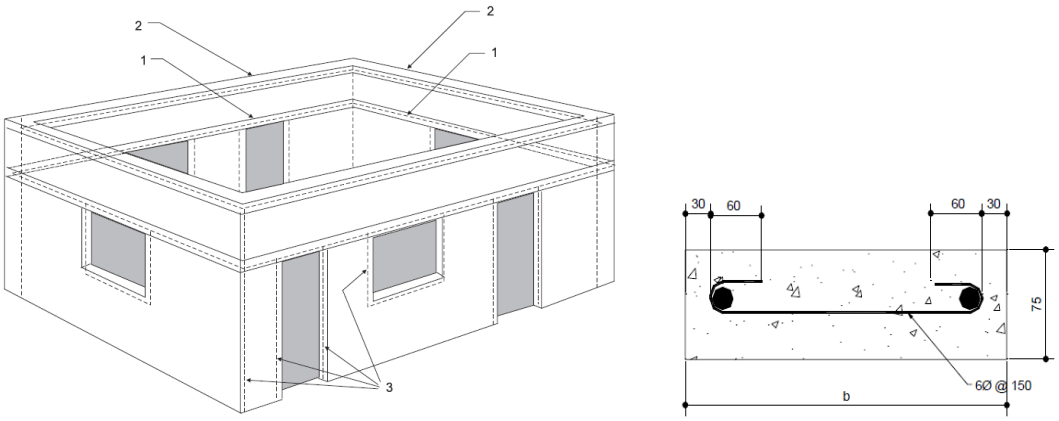

(Notes: 1-lintel band, 2-roof band, and 3-vertical steel)

(a) Location of reinforcement (b) Cross-section of band

Figure 2.12 Reinforced concrete bands and vertical reinforcement (IAEE 1986)

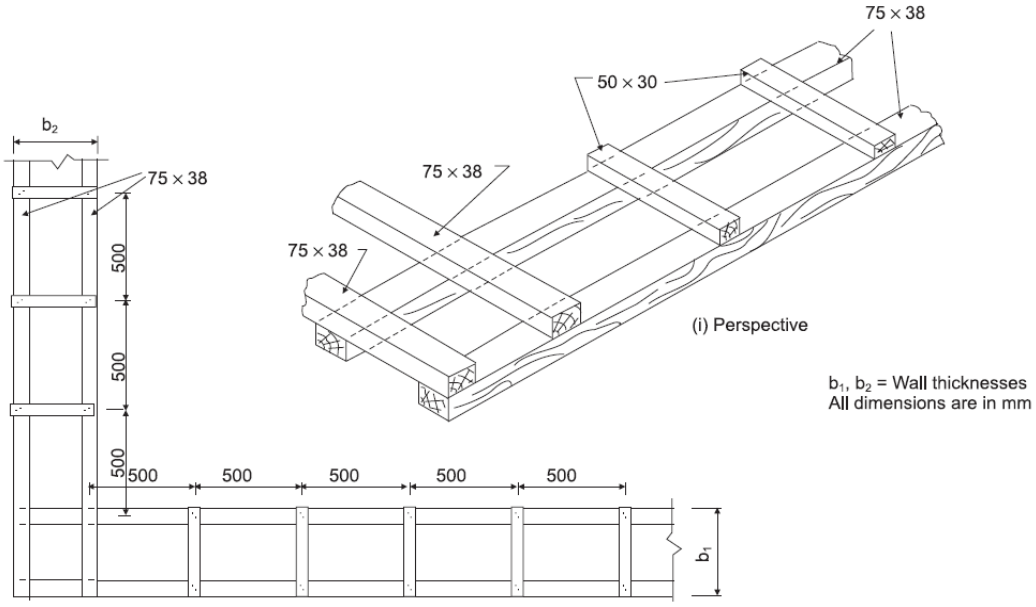

Figure 2.13 Wooden band (IAEE 1986)

Moreover, it has been suggested to use through stones in every 600 mm lift and 1.2 m apart as well as to bring the courses level at 600 mm lift. Besides, centrally located small openings with certain limits on size and spacing of the openings are also specified (Figure 2.14).

Spence and Coburn (1992) investigated the effectiveness of timber band and RC band and found that load at failure of random masonry wall in mud mortar with timber reinforcement was much higher than un-reinforced wall, whereas it was substantially higher in case of reinforced with concrete ring beam. Vintzileou (2008) observed similar improvement with wooden band. The timber reinforced rubble masonry withstood substantially higher shear load than plain masonry and also sustained large shear cracks without disintegration.

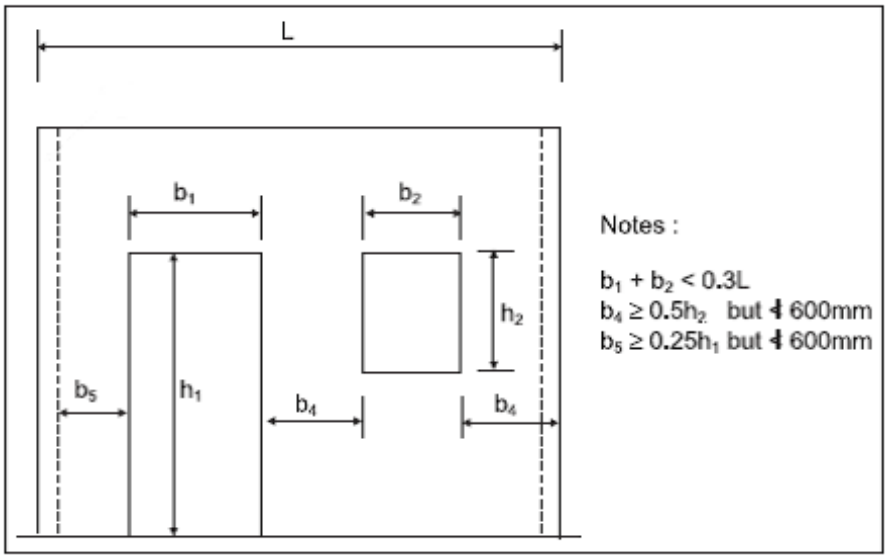

Figure 2.14 Recommended openings in rubble masonry (IAEE 1986)

2.4.2 Internal galvanized wire-mesh reinforcement

Nienhuys (1999) proposed a galvanized wire-mesh wall reinforcement as a simple and cost effective solution for making earthquake resistant houses. It does not require masonry with strong cement mortar and can be used in dry stone construction as well. In this method, a long ladder-like strip is knitted from the galvanized wire in such a way that the knots provide optimum grip with the surrounding stone. In

foundation, wire mesh is applied in every layer, covering the whole width and the ends of the wire mesh folded up to provide anchorage to the vertical reinforcement (Figure 2.15). A single wire mesh is placed at window sill level and double layers are provided at lintel level. Additional layer of wire mesh is recommended to be added in the case of small pier section between wall openings. At lintel level, a tie beam is constructed and a double 3 mm galvanized wire is anchored to provide anchorage for floor or roof beam.

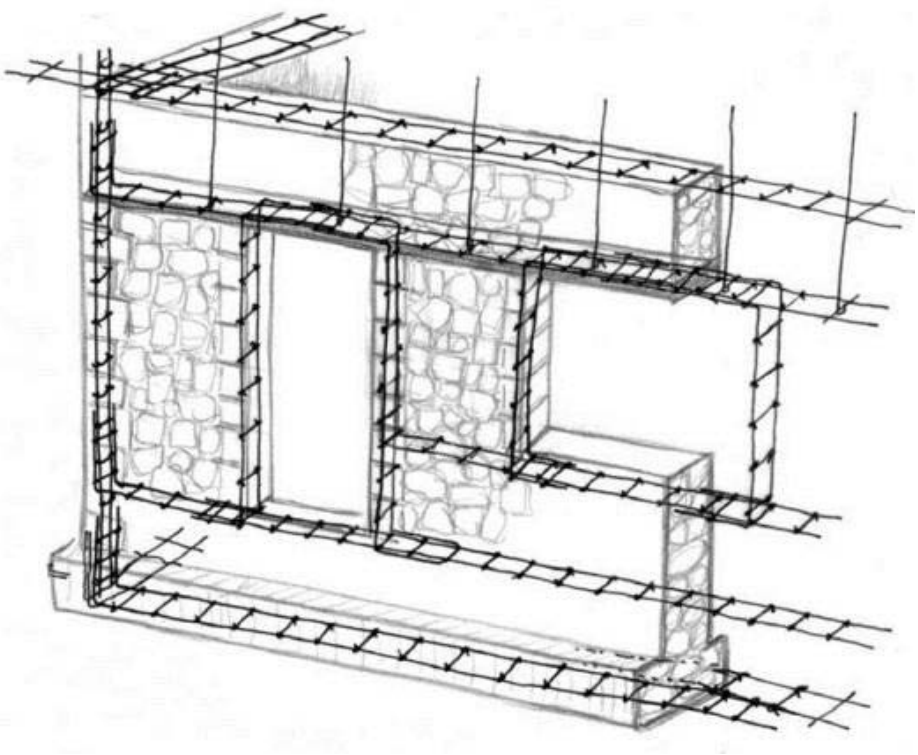

Figure 2.15 Internally applied galvanized steel wire (Nienhuys 1999)

2.4.3 Polymeric grids

Use of polymeric grids with fibre reinforced plaster for reinforcing the stone masonry buildings has shown great potential in improving their seismic performance

(Bairrão & Falcão Silva 2009). The synthetic grid placed in horizontal layers and embedded in lime-cement mortar, in the intervals of 240 to 400 mm along the height of the wall increases the ductility and strength capacity of the building (Figure 2.16).

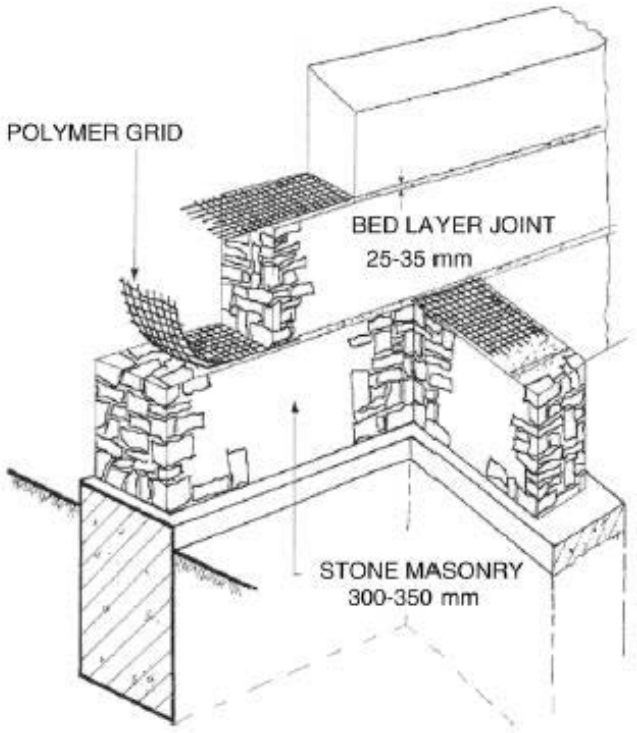

Figure 2.16 Polymeric grids in horizontal layer (Bairrão & Falcão Silva 2009)

When horizontal reinforcement placed in bed layer, is combined with vertical reinforcement of polymeric grid attached to the wall with special connecting elements and covered with fibre added cement-lime plaster, the compressive and shear strength of the wall increases significantly. If only the vertical reinforcement of polymeric grid is used, this technique is also applicable for strengthening existing buildings.

Another variation of wall reinforcement using polymeric mesh can be made by wrapping the mesh around the wall (Blondet, Vargas & Rubiños 2009). In this system, geo-mesh is anchored to the concrete foundation and the wall is built over it. A set of plastic strings are placed across the wall in regular intervals along the horizontal and vertical direction. When the wall is complete, a wooden crown beam is placed on the top of each wall and a polymeric mesh is wrapped around the wall including the top beam (Figure 2.17).

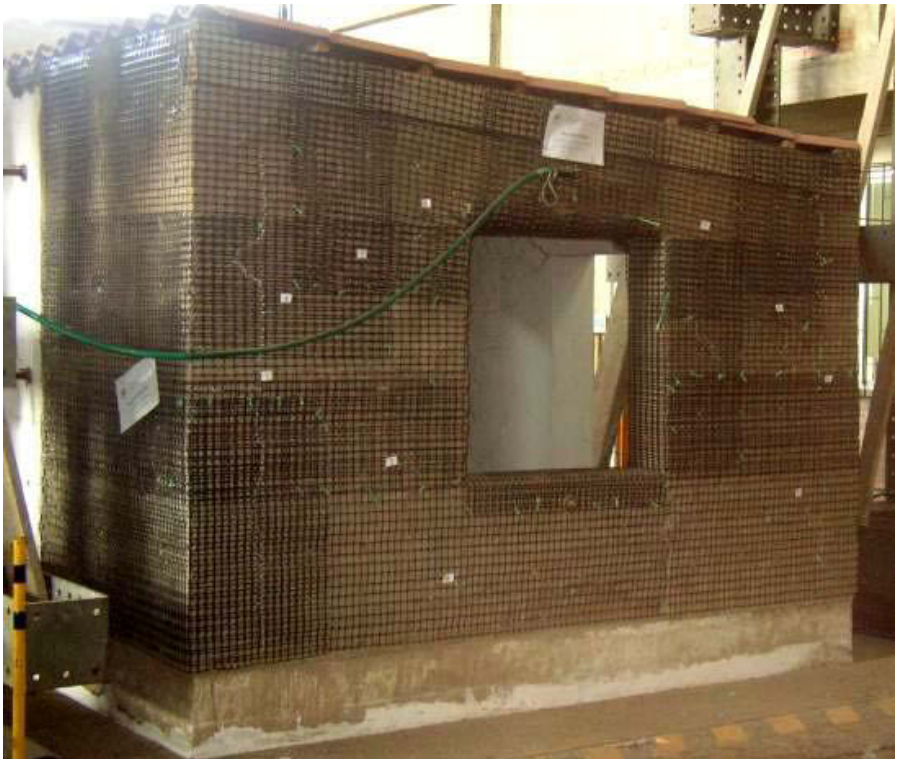

Figure 2.17 Geo-mesh reinforcement (Blondet, Vargas & Rubiños 2009)

A minimum overlap of 150 mm is recommended between two pieces of geo-mesh. The mesh is tied firmly to both sides of walls using the plastic strings placed in the

wall. This scheme increases the stiffness and strength of the wall, and maintains the integrity of the house. Though this system of reinforcement was originally developed for adobe houses, it also seems applicable to stone masonry.

2.4.4 External bamboo reinforcement with internal chicken wire mesh

External bamboo reinforcement, which was developed and verified in adobe houses, (Dowling, Samali & Li 2005) may be applicable to stone masonry as well. This reinforcement system consists of external bamboo reinforcement, internal chicken wire mesh and a wooden ring beam at the top. In this technique, strips of chicken wire mesh are prepared and polypropylene strings are weaved through the strips. The mesh is laid in the mortar joints every three courses during construction of walls. A two mm wire loop is laid in the mortar joint, four coursed below the top of the wall at 150 mm spacing to tie down the wooden beam. After the completion of walls, bamboo poles are placed vertically on both sides of the walls and tied using polypropylene strings (Figure 2.18).

A wooden ring beam is connected to the top of wall using wire loops and also securely attached with external bamboo. Such a scheme has shown a significant improvement in the seismic performance of adobe houses.

Figure 2.18 External bamboo reinforcement (Dowling, Samali & Li 2005)

2.4.5 Low cost techniques for seismic base isolation

Seismic base isolation is an effective way to reduce the level of earthquake excitation on the structure. Using a layer of round-grain sand of size around 1 mm between two terrazzo plates at the top of wall footing can be an effective and low cost solution in isolating horizontal strong ground motion (Li 1984).

Likewise, scrap tyre pad (STP) may be used as a cost effective base isolation system for masonry houses (Turer & Özden 2008). In this method, side walls of a used tyre are cut, and the remaining strap ring are further divided into smaller pieces and placed on top of each other to form a base isolator (Figure 2.19). The friction

between tyre layers is enough to keep layers intact. Up to 22% equivalent damping ratio was obtained using STP as a base isolator.

Figure 2.19 Scraped tyre pads used as a base isolator (Turer & Özden 2008)

Similarly, effectiveness of sliding type stone isolators for the prospective use in low cost masonry houses were studied by Yamaguchi et al (2008). Mirror finished granite and marble pads (Figure 2.20) were prepared and tested using a shake table. Such pads performed well in reducing the base excitation up to 90%.

(a) Granite (b) Marble

Figure 2.20 Sliding type stone isolators (Yamaguchi et al. 2008)

2.5 Strengthening options for existing stone masonry

The overall performance of existing stone masonry buildings can be improved by increasing the strength and stiffness of individual walls. The most common methods are discussed in the following sections.

2.5.1 Grout injection

Grout injection is a very common technique for strengthening and repairing stone masonry walls (Valluzzi, Binda & Modena 2002). It helps restoring the original integrity of the walls by filling the voids and cracks present inside the walls. It does not alter the aesthetic and architectural features of the existing buildings.

In this process, about 2 to 4 holes per square metre are drilled in the wall and water is injected to remove dust and loose materials (IS 13935: 1993). This helps improving the bond between the grout and the wall. Then, the grout is injected through the holes starting from holes at the bottom and moving upwards.

Compatible grouting with original materials is effective in improving the mechanical characteristics of the stone walls by homogenizing the layers, improving the bond among the layers and increasing the ultimate load capacity significantly (Valluzzi, da Porto & Modena 2004). In addition to grouting, application of transverse ties through the thickness of the walls can improve the connection between the layers and reduce the transverse deformation. Similarly, hydraulic lime-based grout can efficiently delay the separation of leaves in stone masonry (Vintzileou & Miltiadou-Fezans 2008). However, grouting in undamaged structures requires a careful analysis

of the texture and characteristics in order to understand whether the grout can be properly distributed within the masonry (Corradi, Borri & Vignoli 2002).

2.5.2 Jacketing

Strengthening by jacketing consists of applying a thin reinforced concrete coating on one or both sides of the walls. A reinforcement mesh is attached to the walls by a series of transverse ties or shear connectors and micro concrete is applied over the reinforcement (Valluzzi, Binda & Modena 2002). Such an intervention improves the strength and stiffness of the walls, depending upon the amount of reinforcement, thickness of the concrete coatings and distribution of ties. For an economical option, the covering may be limited to the width of at least 400 mm in the form of vertical splints located around the corners as well as both sides of an opening, and horizontal bandage at lintel level (IS 13935: 1993) as shown in Figure 2.21.

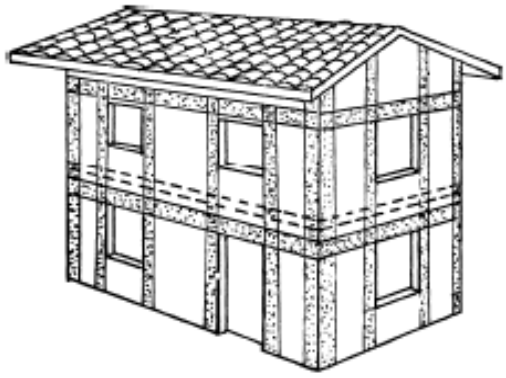

Figure 2.21 Splint and bandage technique (IS 13935: 1993)

2.5.3 Externally bonded fibre reinforced polymer

Externally bonded glass fibre reinforced polymer (GFRP) or Carbon Fibre Reinforced Polymer (CFRP) can be used for strengthening stone masonry houses. In

this method, GFRP strips are attached to one or both wall faces by using epoxy resin and mechanical anchorage (Gago et al. 2009). It enhances the out of plane bending behaviour by improving bending strength, shear strength, ductility and energy dissipation capacity. The anchorage system also increases compressive strength by preventing slip and de-bonding of strips, and providing lateral confinement. Use of concrete based mortar, instead of epoxy resin is not effective in such case (Corradi, Borri & Vignoli 2002). These systems slightly add to mass and wall thickness. Also, the reinforcement materials are non-corrosive.

2.5.4 Post tensioning

Low tensile strength of stone masonry can be improved by applying post tensioning. This technique is also helpful for increasing the shear strength of wall and for improving the connection of orthogonal walls (IS 13935: 1993). Post tensioning tendons are usually in the form of alloy steel bars threaded on two ends and anchored with thick or specially stiffened plates. Karantoni and Fardis (1992) observed that combined horizontal post tensioning along the spandrel and vertical post tensioning along the piers were more effective than when applied individually.

Turer, Korkmaz & Korkmaz (2007) introduced an alternative method for post tensioning using scrap rubber tyre as a cost effective solution. In this method, two sides of a scrap tyre are cut to obtain a strap ring and two steel pipes of 5 cm diameter, with a hole on both ends are passed through the ring. Then, the strap ring is stretched with a steel pipe at each end to achieve a double layered strap (Figure 2.22). Such a strap is connected with other straps by means of nuts and bolts passed through the holes on either side of the pipes and a chain of straps is formed.

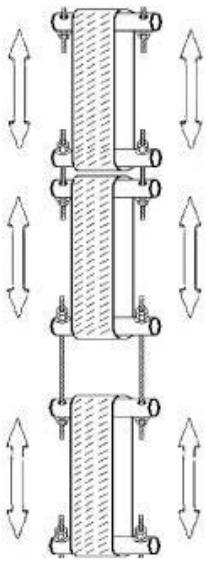

Figure 2.22 Scrap rubber tyre chain (Turer, Korkmaz & Korkmaz 2007)

These chains are applied vertically and horizontally in selected locations and post tensioning is applied by tightening the nuts. Such a scheme significantly increases the seismic performance of the building.

An improved method of strengthening adobe houses using scrap type was proposed by Charleson (2011). In this method, a circumferentially cut strap of width 40 mm from the treads of used car tyres is used as tension reinforcement (Figure 2.23). This is more economical and less bulky than tyre chain with nut-bolt system. However, a ratchet device is required to stretch the straps lightly during installation. The ends of the straps are overlapped for 150 mm and joined with 4 nails. This technique is applicable for strengthening existing houses as well as reinforcing new construction. Though, this technique was investigated for adobe houses, it might also be applicable to stone masonry houses.

(a) tyre strap (b) scrap tyre applied to a masonry house

Figure 2.23 Scrap tyre strips reinforcement system (Charleson 2011)

2.5.5 Polypropylene band mesh

Polypropylene band (PP-band) mesh technique was proposed as a low cost option for retrofitting masonry houses by Mayorca and Meguro (2004). PP-bands are commonly used for packing, which are resilient, inexpensive, durable and commonly available worldwide. Initially, its effectiveness was tested on brick and adobe masonry. After obtaining promising results from these investigations, this technique was also applied to shapeless stone masonry (Meguro et al. 2012) in order to check its effectiveness in rubble masonry.

In this method, the PP-bands are arranged in mesh fashion with a steel rod at the connection edge (Figure 2.24) for providing anchorage at bottom and top of the wall. Then, 6 mm- diameter holes are drilled through the wall at an interval of 250 to 300 mm. The prepared meshes are installed on both sides of the wall and wrapped around the corners overlapping about 300mm. A piece of wire is passed through each hole and the meshes are connected on both sides of the wall. The bottom and top edges of

the meshes containing steel bars are connected with the wall using epoxy. Finally, the meshes are covered with cement sand mortar (1:4.5).

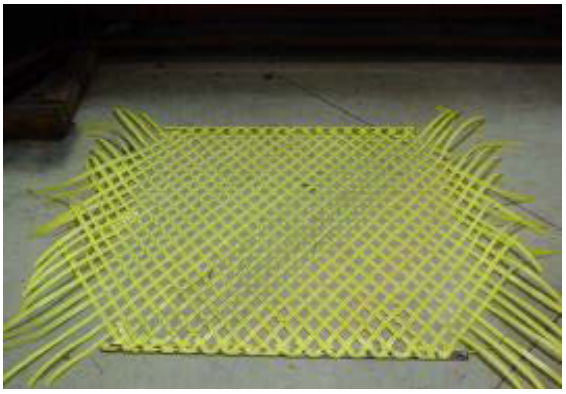

Figure 2.24 PP-band mesh (Mayorca and Meguro 2004)

Such intervention has shown considerable improvement in the performance of the building after crack occurrence though there is no improvement before cracking. The retrofitted walls have sustained post cracking strength for lateral drifts of more than 2%.

2.6 Critical analysis of the existing reinforcing and strengthening options

From sections 2.4 and 2.5 above, it is obvious that several reinforcing and strengthening options are available for earthquake resistant construction of stone masonry. However, all of these schemes are not directly applicable in all circumstances. Affordability and accessibility of the construction materials primarily govern the choice of appropriate construction techniques. As the rubble masonry in mud mortar is being practiced in rural and mountainous areas around the world, obviously both of the above aspects should be taken into considerations.

The use of local materials, such as timber or bamboo reinforcement seems a worthy option, but good quality timber has become scarce and expensive. Even with wooden reinforcement band, it is still likely to experience disintegration of the rubble from the wall during vigorous shaking in earthquakes (Figure 2.25), which may be the potential source of fatal injuries (Pun, Samali & Valipour 2012b).

The internal vertical bamboo reinforcement is not so effective due to a reduction in cross-section of wall and the different dynamic response of masonry and bamboo reinforcement (Dowling, Samali & Li 2005). As the diameter of a bamboo is comparable with the thickness of the wall, a weak section is created at the location of the bamboo reinforcement. In the absence of strong bond between the bamboo and the wall, the bamboo and wall vibrate in their own frequency. As a result, the wall cracks easily during the seismic event.

A reinforced concrete band at lintel and roof level, along with vertical reinforcements at critical locations, is a more efficient system than timber reinforcement. However, it may not be applicable in remote areas owing to lack of transportation facilities, poor quality control and being relatively expensive (Pun, Samali & Shreshta 2010). Cracking in the piers below the lintel band is still likely even after the introduction of such a system (Thakkar & Agarwal 2000).

Figure 2.25 Partial damage of rubble wall with wooden bands in an earthquake

Internally applied galvanized steel wire mesh seems a cost effective solution. Nonetheless, it is not useful in case of random rubble masonry because the grip between rubble and steel wire mesh may not be sufficient to retain the stability of wall during earthquake shaking (Nienhuys 2006).

Use of polymer mesh with fibre reinforced plaster seems an effective solution, but because of similar reasons mentioned in case of reinforced concrete band, it may not be applicable everywhere.

Seismic base isolation using scrap rubber tyre and stone isolators have shown probable alternatives for seismic risk mitigation. However, their applicability in the real situation is still under study.

Grout injection technique was specially developed for masonry with lime mortar or cement mortar. It is not so effective for stone masonry with mud mortar. Injection of clay slurry into the wall can be a potential area of study. Nonetheless, improvement in the strength of the wall may not be comparable with the efforts invested.

Jacketing can improve the strength of the wall considerably. The presence of large stones in the rubble masonry can make it difficult for inserting the ties (Valluzzi, Binda & Modena 2002).

Application of fibre reinforced polymer with epoxy resin seems incompatible to the wall with mud mortar because of fragility of mortar and dust particles. On the other hand, post tensioning with steel rods can be a potential solution for strengthening, provided such capability is available in the field. Instead of this technique, use of scrap tyre pads looks more applicable. Nevertheless, due to the requirement of steel pipes, nuts and bolts make it bulky. The second alternative of scrap tyre strip may be a pleasing option. Both these options are susceptible to damage by fire.

The external vertical bamboo reinforcement looks a good option for reinforcing stone walls as well. However, something needs to be done for covering the bamboo for improving the aesthetic value. It also reduces the usable space of the building because of the protruding parts of the bamboo reinforcement. Moreover, the bamboo is not available everywhere as compared to timber.

Use of geo-mesh wrapping around the walls seems a probable solution for stone masonry as well. Nevertheless, special considerations need to be given to protect the mesh from ultraviolet ray in order to lengthen the life of the reinforcement. In

addition, polymer is not a heat resistant material. Similar will be the case for the PP band. Both of these meshes cannot be wrapped tightly to the wall. This is the major drawback of these methods. A considerable overlap is necessary between two meshes for effective interconnection. As a result, this system of reinforcement will allow large deformations of the wall during a seismic event, which is undesirable.

From the above discussion, it is clear that there is still a need to develop a reinforcing technique for rubble masonry, which is effective, durable, requiring less maintenance, easily adoptable and relatively cheap. The realistic aims of fulfilling such a need for upgrading low cost traditional housings could be to limit the damage in the case of normal earthquakes and to provide enough time to the occupants to escape in the event of large earthquakes (Coburn & Spence 2002).

In this scenario, a reinforcing technique of stone masonry using galvanized steel wire, similar to a gabion basket is proposed in this research. The details of this reinforcement system are given in Chapter 3.

The major challenge for investigating the effectiveness of the proposed reinforcement system begins with the lack of enough data related to the properties of stone masonry with mud mortar. In such a case, the very first step to proceed is to carry out experimental investigation to generate some basic data. In this process, existing standard testing methods were reviewed, which are presented briefly in next section.

2.7 Brief description of relevant testing methods

Testing procedures for natural building stone, soil, mud mortar, galvanized steel wire and rubble masonry wall with mud mortar are relevant for this research. Some of the testing methods are covered in Australian standards. For other tests, British standards and ASTM standards have also been referred. Testing procedures for mud mortar and rubble masonry with mud mortar have not been included in any standards. In such cases, similar types of testing procedures have been taken as references, which were modified according to the need as given in Chapter 4. In order to provide a basis for adaptations followed in this research, brief descriptions of related testing methods have been included in this section.

2.7.1 Testing methods on natural building stone

The primary interests on testing of natural building stone in this research were for finding the compressive strength and the flexural strength. Testing methods for uniaxial compressive strength of natural stone are specified in British Standard (BS EN 1926:2006). According to this code, test specimens shall be either cubes with sizes (70 ± 5) mm or (50 ± 5) mm or right circular cylinders with diameter and height equal to (70 ± 5) mm or (50 ± 5) mm. Minimum of 10 specimens are to be tested to get reliable results. The loading rate shall be at a constant stress rate of 1±0.5 MPa/s. The uniaxial compressive strength, f_c, is given as:

$$f_c = \frac{F}{A} \tag{2.1}$$

where, F is the failure load and A is the cross-sectional area of the specimen before testing.

Similarly, testing methods for flexural strength of natural stone under a concentrated load are available in British Standard (BS EN 12372:2006). The preferred dimensions of the specimens are specified as 50 mm x 50 mm x 300 mm for the stone with the largest grain size below 25 mm. However, other possible dimensions are also specified based on certain requirements, such as, thickness shall be between 25 mm and 100 mm and shall be greater than twice the size of the largest grain in the stone; the total length shall be equal to 6 times the thickness; the width shall be between 50 mm and three times the thickness and in no case it shall be less than the thickness. The thickness between the supporting rollers shall be five times the thickness. Again, at least 10 specimens shall be tested. The loading rate shall be 0.25± 0.05 MPa/s until the specimen breaks. The flexural strength, f_b, is given by:

$$f_b = \frac{3Fl}{2bh^2} \tag{2.2}$$

where, F is the load at failure, l is the span, b is width of the specimen at the plane of fracture and h is the thickness of the specimen adjacent to the plane of fracture.

2.7.2 Testing methods on mud mortar soil

Some simplified field tests, along with more rigorous laboratory testing methods for soil, are covered in Australian Standard. Some of the most relevant testing methods have been selected for this research.

The type of soil can be determined using plastic limit (PL) test and liquid limit (LL) test following standard procedures. Australian standards (AS1289.3.2.1-2009) and (AS 1289.3.1.1-2009) have covered this procedures in detail, which have been used in this research as mentioned in section 4.3.1.

Sedimentation test has been adopted as a field test to find the approximate soil composition (HB 195 - 2002). These procedures were followed to determine the soil composition as given in section 4.3.2.

The composition of particles sized from 32 μm to 125 mm can be determined by sieving procedures (AS 3638-1993). Though there is no adequate information regarding the effect of particle size distribution in the properties of mud mortar soil, sieving procedures were adopted to determine the composition of particle sizes greater than 75 μm as explained in section 4.3.3.

2.7.3 Testing methods on wet mud mortar

Testing methods on workability of mud mortar could not be found in any standard. The amount of water to be added to the soil to get the proper workability depends on the type of soil, which is determined by trial and error (HB 195 - 2002).

2.7.4 Testing methods on dried mud mortar

As in case of wet mud mortar, testing method for dried mud mortar was not found in any of the standards. In such case, testing procedures specified in British Standard (BS EN 1015-11:1999) for hardened mortar has been adopted in this research to determine the flexural and compressive strength of mud mortar. According to this standard, the flexural strength of hardened mortar is determined by three point loading of mortar prism specimen to failure. The two halves of the broken prisms obtained from the flexural strength test are used for compression test.

The specimen for bending test is a prism of size 160 mm x 40 mm x 40 mm. At least three specimens are required to be tested. The loading is applied at a uniform rate of 10 N/s to 50 N/s so that failure occurs within 30 s to 90 s. The flexural strength is calculated using similar relation as Equation (2.2).

For compression testing, the specimen is placed between two square shaped steel bearing plates of width equal to the width of mortar prism and 10 mm thick. The broken prism is arranged in such a way that the cast end is 160 ± 0.1 mm from the nearer edge of the bearing plates. The suggested loading rate for a mortar specimen with compressive strength of about 1 MPa is 50 N/s.

The detailed procedures of few modifications adopted for mud mortar prisms have been covered in section 4.2.1.

2.7.5 Testing methods on galvanized steel wire

In this research, testing on the coating of zinc or zinc/aluminium alloy in steel wire was not included. Only the tensile strength of steel wire was tested following the procedures mentioned in Australian Standard (AS 1391 - 2007). According to this standard, the original gauge length is to be taken as 200 mm ± 2 mm for wire with a diameter less than 4 mm. The strain rate of loading for determining the tensile strength is recommended not to exceed 0.008/s throughout the test.

2.7.6 Testing methods on rubble masonry with mud mortar

In spite of numerous testing methods for masonry covered by various standards, testing procedures of rubble masonry with mud mortar could not be traced in any of

those standards. The detailed process for finding the flexural strength of masonry perpendicular to the bed joints are given in Australian Standard (AS 3700 - 2011) either by means of bond wrench test method or beam test method. These methods are intended for masonry specimens built using bricks, blocks and square dressed natural stones. British Standard (BS EN 1052-5: 2005) provides bond wrench method for determining the bond strength of horizontal bed joints in masonry. Likewise, ASTM International Standard (ASTM C 1072 - 2006) specifies the test method for determining the flexural bond strength of non-reinforced masonry using bond wrench testing apparatus. Bond wrench method is appropriate only for squared or rectangular shaped masonry units.

British Standard (BS EN 1052-2:1999) specifies methods for determining the flexural strength of masonry along two principal axes of loading: one for a plane of failure parallel to the bed joints and the other for plane of failure perpendicular to the bed joints. For each type, at least five specimens are required to be prepared and tested. The principle of four point bending test has been adopted for these tests.

The specimen for the flexural strength test for a plane of failure parallel to the bed joints consists of a wall panel with thickness equal to the width of a single masonry unit. The length of such a wall panel shall be at least equal to 400 mm and 2 times the length of the masonry unit. The height of the specimen shall be such that there are at least two bed joints between two loadings in a four point bending test scheme. Also, the distance between the top and bottom of the specimen from the supports at the respective ends shall be at least 50 mm.

The thickness of the specimen for a plane of failure perpendicular to the bed joints is similar to the other type. The height of such specimen consists of at least four masonry units and 240 mm, whichever is more. The length of the specimen shall be such that there is at least one head joint between two loadings in a four point bending test scheme. Similarly, the distance between the left and right ends of the specimen from the end supports shall be least 50 mm.

In both cases, the distance between the two loadings shall be 0.4 to 0.6 times the spacing between end supports. Also, the spacing between end supports and the loadings on the corresponding sides shall not be less than the thickness of the masonry specimen. In order to ensure the base of the specimen is free from frictional restraints, the specimens can be placed on two layers of polytetrafluoroethylene with grease between them or on ball, needle or roller bearings.

The loading rate is maintained between 0.03 N/mm^2/min and 0.3 N/mm^2/min until the specimen breaks. The flexural strength, $f_{b,}$ is calculated using the following formula:

$$f_b = \frac{3F(l_2 - l_1)}{2bt^2} \quad (2.3)$$

where,

F = maximum load applied to an individual specimen

l_1 = spacing between end supports

l_2 = spacing between loading strips

b = height or width of the specimen perpendicular to the direction of span

t = width of specimen

These methods are applicable for the masonry made with regular units such as bricks, blocks and properly shaped stones.

In order to determine the compressive strength of masonry, Australian Standard (AS 3700 - 2011) has set out the method for constructing and testing of specimen. Minimum of three specimens are to be tested for compression. Stack-bonded piers having at least three courses and height to width ratio of two to five have been recommended as specimens. For testing, the specimen is placed between strips of plywood of 4 to 6 mm thick. A steady loading at a rate of 350 kN/min to 700 kN/min is applied until the specimen fails. The compressive strength of the specimen, f_c, is calculated as:

$$f_c = k_a \frac{F}{A_d} \tag{2.4}$$

where,

k_a = aspect ratio factor for the specimen (Table 2.1),

F = total load at which specimen fails,

A_d = combined bedded and grouted area

Table 2.1 Aspect ratio factor, k_a (AS 3700 - 2011)

Height/thickness ratio	0.00	0.40	1.00	≥ 5
k_a	0.00	0.50	0.70	1.00

British standard (BS EN1052-1:1999) also specifies the dimension of the masonry specimen for compressive strength testing based on the size of the masonry unit

(Table 2.2). At least three specimens are required for testing in compression. In order to achieve uniform load distribution, use of steel plates at the top and bottom of the specimen is recommended with a thin layer of gypsum plaster or an appropriate mortar if necessary. If the modulus of elasticity is to be determined, axial deformation of central one third of the height of the specimen is recorded. For testing, a steady loading rate (0.15 MPa/min to 1.25 MPa/min) is applied so that failure is reached after 15 to 30 minutes from the start of loading.

Table 2.2 Specimen sizes for compressive strength test (BS EN1052-1:1999)

Face Size of unit (mm)		Masonry specimen size				
Length, l_u	*Height,*h_u	Length, l_s	Height, h_s			Thickness, t_s
≤ 300	≤ 150	$\geq 2\ l_u$	$\geq 5\ h_u$	$3\ t_s \leq h_s \leq 15\ t_s$	$\geq\ l_s$	$\geq t_u$
≤ 300	> 150	$\geq 2\ l_u$	$\geq 3\ h_u$	$3\ t_s \leq h_s \leq 15\ t_s$	$\geq\ l_s$	$\geq t_u$
> 300	≤ 150	$\geq 1.5\ l_u$	$\geq 5\ h_u$	$3\ t_s \leq h_s \leq 15\ t_s$	$\geq\ l_s$	$\geq t_u$
> 300	> 150	$\geq 1.5\ l_u$	$\geq 3\ h_u$	$3\ t_s \leq h_s \leq 15\ t_s$	$\geq\ l_s$	$\geq t_u$

Note: t_u = *width of masonry unit*

The compressive strength is calculated using similar relation as Equation (2.1).

The modulus of elasticity, E, is calculated as a secant modulus at a stress equal to one third of the maximum stress reached.

$$E = \frac{F}{3\,\varepsilon A} \tag{2.5}$$

where,

$\mathcal{E}$ = strain in an individual specimen at one third of the maximum strength achieved.

These test methods are suitable for bricks or blocks or squared shaped stone masonry units laid in lime or cement mortar.

For the shear strength testing of masonry block, British Standard (BS EN1052-3: 2002) specifies a set of procedures for squared or rectangular shaped masonry units. Similarly, British Standard (BS EN 1052-4: 2000) provides a method for determining the in plane shear strength of horizontal bed joints in masonry including a damp proof course sheet. These methods are not applicable to random rubble masonry.

ASTM International Standard (ASTM E519/E519M-2010) has included a testing method for determining the diagonal tensile or shear strength of masonry assemblages by loading the specimen in compression along one diagonal as a means of more accurate methods than other available method. The nominal size of specimen recommended in this method is 1.2 m x 1.2 m x thickness of wall. At least three similar specimens are to be constructed and tested. The loading rate should be such that the maximum load is reached between one to two minutes. The shear stress, f_s, is to be calculated using the relation:

$$f_s = \frac{0.707F}{A_n} \tag{2.6}$$

where,

F = applied load,

A_n = net area of the specimen, calculated as follows

$$A_n = \left(\frac{w+h}{2}\right)\text{t n} \quad (2.7)$$

where,

w = width of specimen,

h = height of specimen,

t = total thickness of specimen,

n = percentage of the gross area of the unit that is solid, expressed as decimal.

The shear strain is calculated as follows:

$$\gamma = \frac{\Delta V + \Delta H}{g} \quad (2.8)$$

where,

γ = shearing strain,

ΔV = vertical shortening

ΔH = horizontal extension

g = vertical gauge length

Though this method was intended for masonry with lime or cement mortar, it may be applicable to the masonry with mud mortar. However, due to fragile nature of mud mortar, handling such a bulky and weak wall specimen seems challenging.

Based on aforementioned testing methods, an outline of the experimental program was set up, which was refined and a detailed testing plan was prepared with due consideration to the observations of the research activities carried out by other researchers as given below.

2.8 Existing trend of testing on soil and mud mortar

Investigating the liquid limit and the plastic limit of soil sample used in adobe, rammed earth and other similar construction is useful for comparing the results based on type of the soil. A relatively recent trend of such an observation can be traced in the literature. For instance, Zhong et al. (2008) used soil samples from two sites with liquid limit of 36.6% and 42.0% respectively for constructing specimens for rammed earth walls. The corresponding plastic limit of the soil samples were observed as 22.7% and 24.9%. Similarly, Wu et al. (2011) studied the shear behaviour of adobe made from soil having 36.3% liquid limit and 19.2% plastic limit.

In the research activities related to mud brick (adobe), the properties of mud mortar are not investigated separately. The properties of mud mortar are considered similar to the properties of mud brick. For example, Silveira et al. (2012) conducted extensive studies on the available data on the adobe constructions to compare with the properties of specimens extracted from ancient adobe buildings. Cylindrical specimens were extracted (diameters of 80 to 90 mm with a height to diameter ratio of approximately 2) and tested in compression and splitting. It was reported that the

mean compressive strength, modulus of elasticity and tensile strength of adobe were 1.32 MPa, 225 MPa and 0.17 MPa respectively.

Dowling (2006) investigated the properties of adobe for finding the strengthening measures of adobe houses. Ten specimens (stack bonded prisms of three layers of mud bricks joined with mud mortar) were prepared and tested in compression according to ASTM standard (ASTM C 1314-02). The compressive strength of the prisms was 1.5 MPa. Modulus of elasticity of the adobe prism (calculated within 5% to 30% of ultimate stress) was observed as 151 MPa. Shear test on nine triplet specimens was conducted according to European standard (EN1052-3-2002). The average shear strength of the triplet was 49 kPa. Flexural strength of the adobe unit was not determined. However, flexural bond strength of 7 specimens (stack bonded prisms) was 0.085 MPa, which was measured according to Australian Standard (AS 3700-2001)

2.9 Research on static testing of stone masonry

Despite being the oldest building material, few data are available on stone masonry. Only recently, researchers have shown interest in the field of stone masonry focusing mainly in historical buildings. Such monumental buildings were mostly built with lime mortar. Therefore, results on rubble masonry with mud mortar are very scarce.

2.9.1 Behaviour of rubble masonry with mud mortar

Few research works on rubble masonry with mud mortar could be traced in literature. Spence and Coburn (1992) investigated the deflection of a wall specimen for out-of-plane loading by devising a simple testing scheme (Figure 2.26).

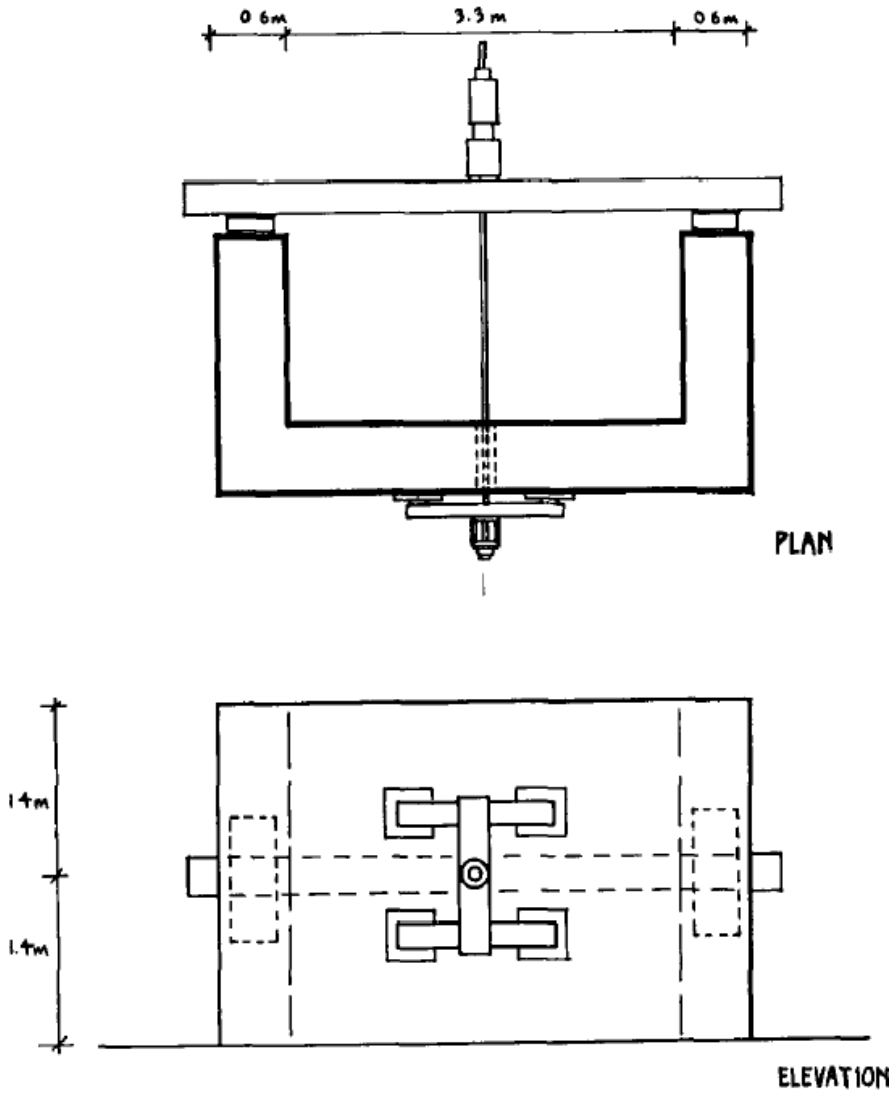

Figure 2.26 Static testing set up (Spence & Coburn 1992)

An H-shaped loading yoke was designed to distribute a single concentrated load into four equal loads on square shaped spreader plates of size 40 cm and 1.5 cm thick. In order to ensure proper contact, a pad of gypsum plaster was created between the wall and the spreader plates. Load was applied to the yoke via a 30 mm diameter bar passing through the wall and coupled with a hydraulic ram. The ram was attached to

a steel beam, which was supported on the ends of the side walls through a timber spreading beam.

Four similar wall specimens were built using four different types of construction practice. Wall 1 was prepared as an un-strengthened random-rubble wall with mud mortar, wall 2 was similar to wall 1 but reinforced with wooden band, wall 3 was a random-rubble wall with cement mortar and reinforced with RC beams, and wall 4 was built as cut and dressed stone work with cement mortar. Load was applied at a uniform rate and the displacement was measured at loading face.

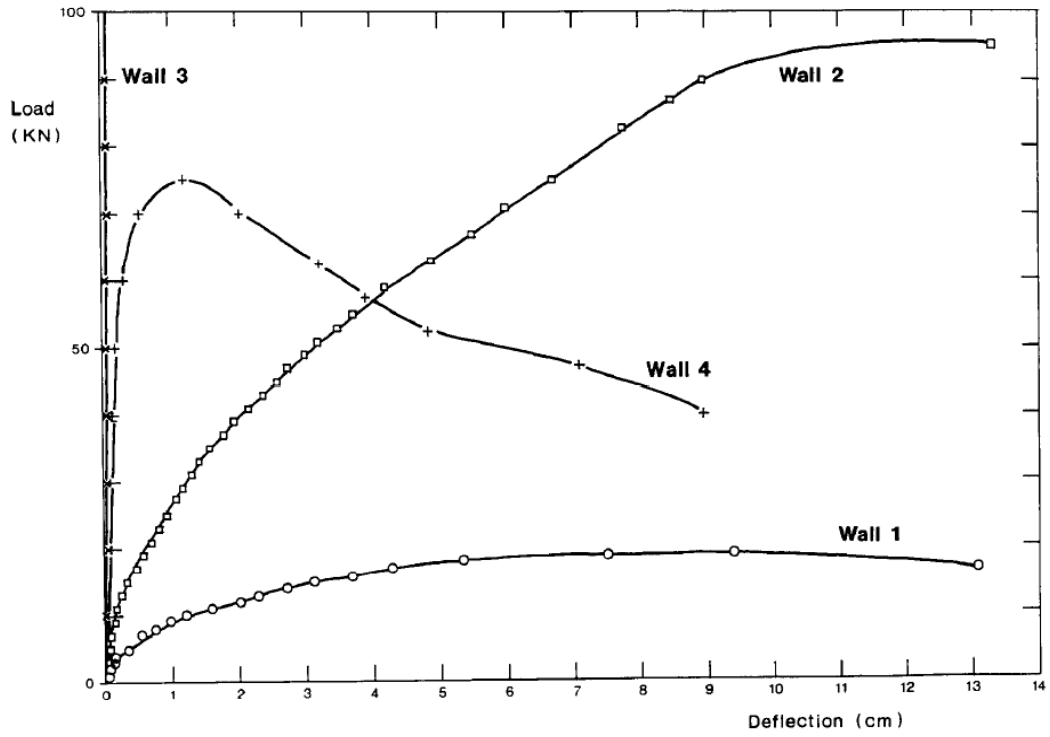

(Notes: Wall 1: un-strengthened random- rubble wall with mud mortar, Wall 2: random-rubble wall with mud mortar and horizontal timber reinforcement, Wall 3: random-rubble wall with cement mortar and reinforced concrete beam, Wall 4: Cut and dressed stone wall with cement mortar)

Figure 2.27 Load deflection curves for midpoint of a wall (Spence & Coburn 1992)

The results showed that the load at failure of a random-rubble wall in mud mortar with timber reinforcement was four times more than the unreinforced wall (Figure 2.27). The stiffness of mud mortar wall was observed to be very low with considerable displacement before the maximum load was reached.

No significant cracking was observed in random rubble wall specimen with cement mortar and RC band, when the load reached up to the capacity of loading machine (100 kN). The cut stone block specimens in cement mortar showed much higher stiffness than the wall specimens in mud mortar. The peak strength reached at small displacements. However, the strength reduced considerably as the displacement increased further.

2.9.2 Experiments on rubble masonry with lime mortar

Experimental studies on traditional stone masonry under compressive load were investigated by Gracía et al. (2012) using rubble masonry. Sand stone was selected as masonry unit and lime-cement-sand mortar was used as representative of historical masonry with total water/binder ratio of 1. The compressive strength of sandstone was 40 MPa, which was determined using cylindrical specimen of diameter 50 mm and height of 115 mm. Cylindrical mortar specimens of diameter 100 mm and height of 200 mm were prepared and tested in compression. The compressive strength of lime mortar at 120 days was 0.26 MPa.

Stone masonry prisms of dimensions 400 mm high, 500 mm long and 300 mm wide were prepared. The specimens were constructed over steel plates and covered with mortar at the top to provide a smooth surface. After allowing 120 days of curing at

normal temperature and humidity conditions, the specimens were tested at a loading rate of 10 N/s. The axial deformation was measured by the movement of cross head travel. Therefore, a deformability value was calculated instead of Young's modulus following similar procedures as modulus of elasticity between the stress levels of 30% to 60% of ultimate stress. The average compressive strength of rubble masonry was 1.84 MPa. The deformability value was 62 MPa.

Milosevic et al. (2013) performed diagonal compression tests on four rubble panels of size 120 cm x 120 cm x 70 cm following ASTM E 519-02. Roughly cut lime stone pieces having the compressive strength of 48 MPa were used for constructing wall panels. Two specimens were built using hydraulic lime-sand (1:3) mortar and the other two specimens were built using air lime-sand (1:3) mortar. The compressive strengths of hydraulic lime mortar and air lime mortar were 1.47 MPa and 0.56 MPa, respectively, whereas the flexural strengths were 0.35 MPa and 0.25 MPa, respectively. The panels were built in the test position on a lower loading shoe and also supported on the two lower faces during construction (Figure 2.28). The specimens were cured for 8 months before relocating to the testing facility. Another loading shoe was placed on the top edge and tested in diagonal compression. The compression and extension of both diagonals were also measured using LVDTs.

Figure 2.28 Panels for diagonal compression test (Milosevic et al. 2013)

A major crack was developed at the centre of the panel and propagated along the vertical diagonal dividing the whole panel into almost two halves. The crack appeared through the mortar without any damage to the stones. The shear strength of the panels with air lime mortar was 24 kPa, whereas for hydraulic lime mortar, it was considerably higher exhibiting 258 kPa. Similarly, shear modulus of air lime mortar panel was 75 MPa. This value for of hydraulic lime mortar was 252 MPa.

Vintzileou (2008) investigated the effect of timber band on the compression and shear behaviour of three leaf rubble masonry built with lime mortar. A portion of wall reinforced with one horizontal timber tie and enclosed between two consecutive transverse timber elements was chosen for preparing a specimen. Eight wall specimens of size 0.7 m long, 0.9 m high and 0.5 m wide were prepared. Two

specimens were unreinforced and six specimens were reinforced with timber elements. The size of longitudinal element was 60 mm x 60 mm and the size of transverse element was 50 mm x 50 mm. Longitudinal and transverse elements were connected by 80 mm long steel nails of 3.5 mm diameter.

The lime stone with compressive strength of 50 MPa was chosen. The compressive strength of lime mortar at the age of one month was 0.8 MPa. Four of the wall specimens were tested in compression and the remaining four in diagonal tension. In each group, one of the specimens was unreinforced. Testing was conducted under load control conditions.

It was observed that timber band helped to increase compressive strength by 10% to 20%. Significant reductions in the width of vertical cracks were noticed in timber reinforced masonry. Both these results were attributed to the confinement provided by the timber element.

The effect of timber band on diagonal compression was considerably high. An improvement of shear capacity of up to 5 times was measured. Also, a significant enhancement in large shear cracks without disintegration of the masonry was observed.

2.9.3 Ashlar masonry in static testing

Research activities on ashlar masonry with lime or cement mortar are comparatively higher than rubble masonry with mud mortar. Characteristics of ashlar masonry more closely resemble the bricks masonry. However, in the absence of extensive research activities available on rubble masonry with mud mortar, investigations carried out on

the ashlar masonry with lime or cement mortar have also been considered as an indirect indication for the behaviour of rubble masonry.

An experimental study on the strength of stone masonry laid in cement mortar was investigated by Rao, Reddy and Jagadish (1997). A metamorphic rock, gneiss was chosen as a building stone. The compressive strength of the stone was determined using 5 specimens of 80 mm cube following Indian standards IS:1121-1976. While loading perpendicular to the mineral bands, the compressive strength of the stone was found to be 86.1 MPa.

In addition, six stack bonded prisms of three layers of stone cubes (size 80 mm) joined with 10 mm cement mortar were used for the compressive strength testing of stone masonry following ASTM - E447. Two proportions of cement-sand mortar (1:4 and 1:8) were used for preparing stone prisms. The 28 day compressive strengths of cement-sand mortars of proportions 1:4 and 1:8 were 9.4 MPa and 2.8 MPa, respectively. The compressive strength of stone prisms with 1:4 cement-sand mortar was 38.6 MPa. With the proportion of 1:8 cement-sand mortar, the compressive strength was reduced to 30.4 MPa. In most cases, vertical cracks were observed in the middle stone cube.

Besides, flexural bond strength of stone masonry was determined by bond wrench method according to ASTM C1072. Three-block high stack bonded prisms were prepared using 305 mm x125 mm x 100 mm manually dressed stones. In addition to two cement sand mortar combinations used in compression testing, 1:1:6 soil-cement-sand mortar was also used. The bond strengths for cement-sand mortars of 1:4 and 1:8 proportions were 0.16 and 0.12 MPa. The soil-cement-sand mortar

exhibited better performance than 1:8 cement-sand mortar with the bond strength of 0.14 MPa.

A more extensive experimental research program was carried out at the University of Catalunya, Barcelona, for finding the mechanical properties of historical masonry structures including stone masonry (Oliveira 2000). In this test, modulus of elasticity of the stone, as well as Poisson's ratio, was determined. This test was mainly focused on the strength of dry jointed masonry specimen.

Four cylindrical natural sand stone specimens of diameter 50 mm and height 120 mm were tested for uniaxial compression. Axial and lateral deformations were measured using strain gauges as well as LVDTs. The specimens were loaded at a rate of constant axial displacement of 5 μm/s. The average ultimate strength of the specimens was 91.6 MPa. The Young's modulus remained almost constant up to approximately 60% of ultimate load. Interestingly, the values of elastic modulus calculated from strain gauge data was just about 12 % higher than that calculated from LVDT data. The average value of elastic modulus was 18.8 GPa. The Poisson's ratio recorded at stress level of 25% of ultimate was 0.27, whereas this value crossed 0.5 around 50% of ultimate stress indicating the formation of micro cracks.

Compressive strength tests were also performed on dry jointed stone prisms. Each prism was constructed by placing a stone piece on the top of another stone without any mortar between them. Two prisms were constructed by stacking three pieces of 10 cm x 20 cm x 10 cm and the other two prisms were constructed by stacking four pieces of size 20 cm x 20 cm x 10 cm. All prisms were tested at natural moisture

content. The displacement control loading was applied at a rate of 3µm/s. Axial displacement was measured using three LVDTs placed between two platens.

The average compressive strength of prisms with three layers was 62.3 MPa, and average elastic modulus in the range of 30% - 60 % of ultimate stress was 15.2 GPa, whereas these values for the prisms of four layers were 52.0 MPa and 14.3 GPa, respectively. Comparing these results with the values for stone cylinder, there is no significant difference in the value of elastic modulus, but a considerable difference in values of the compressive strength. The large reduction in the compressive strength might be due to slenderness ratio as well as the presence of few weaker pieces of stone.

Vasconcelos and Lourenço (2009) conducted experimental investigations on the behaviour of stone masonry in shear and compression. The influence of surface roughness and bed joint material on the compressive strength was the major concern of this research.

Direct shear tests with three different levels of pre-compression were conducted on dry and low strength lime mortar masonry joints and uniaxial compression test on a set of stone masonry prisms (Figure 2.29). Tests were conducted both in dry and saturated conditions.

A coefficient of friction of 0.65 was observed in dry joint masonry, whereas it was 0.6 in the case of saturated joint. For the mortar joint, cohesion of 0.36 N/mm^2 and coefficient of friction of 0.63 were attained.

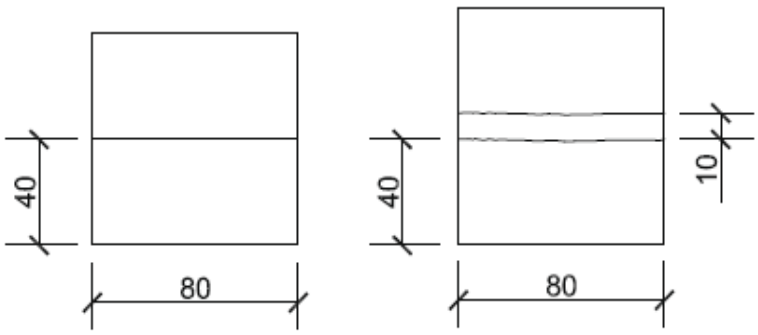

(a) Dry joint (b) Mortar joint

Figure 2.29 Specimen for direct shear test (Vasconcelos & Lourenço 2009)

Masonry prisms were constructed with three cubic stone blocks of 150 mm stacked one over the other (Figure 2.30). Both dry joint and mortar joint prisms were prepared. Two types of dry joint prisms were constructed: with smooth surface and rough surfaces. Similarly, two types of mortar were used: low strength lime mortar and granitic soil mortar. The thickness of the mortar joint adopted was 10 mm.

The failure modes of dry joint and mortar joint prisms were not similar. The crack pattern of dry joint prisms showed the continuous shear band. The failure of lime mortar joint prism was followed by vertical splitting cracks initiating in the central block and extended to other blocks, which was attributed to composite action. The granitic soil mortar joint prisms showed almost similar patterns as dry joint prisms.

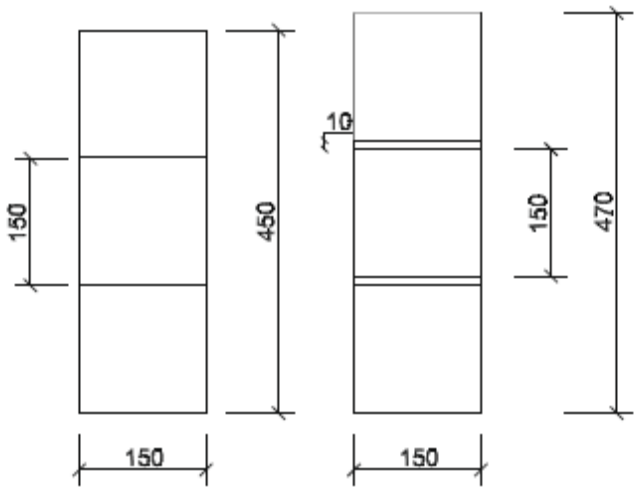

Figure 2.30 Masonry prisms for compression test (Vasconcelos & Lourenço 2009)

The stress-strain diagram obtained from the test showed that even the smooth surface dry joint prisms did have some upward concavity, which was attributed to the initial adjustment of bed joints (Figure 2.31). The large initial deformation of the prism with granitic clay mortar was relevant to the compaction of mortar at the bed joint. The modulus of elasticity was determined as the secant modulus in the range of 30% and 60% of the ultimate compressive strength.

The dry joint masonry prism with smooth surface exhibited the highest compressive strength (73 MPa) similar to compressive strength of stone units and the highest modulus of elasticity (14.7 GPa). The compressive strength of dry joint prisms with rough surface was about 29% lower than the smooth surface prism, whereas the modulus of elasticity was down by 46%.

The compressive strength and modulus of elasticity of the prisms in soil mortar were 64.2 MPa and 8.92 GPa, respectively, which are about 88% and 61% of the values

for smooth dry joint prism. These values for prism with lime mortar were further reduced to 50% and 31%, indicating the effect of tri-axial stress state for the stone blocks induced by dilation of the mortar.

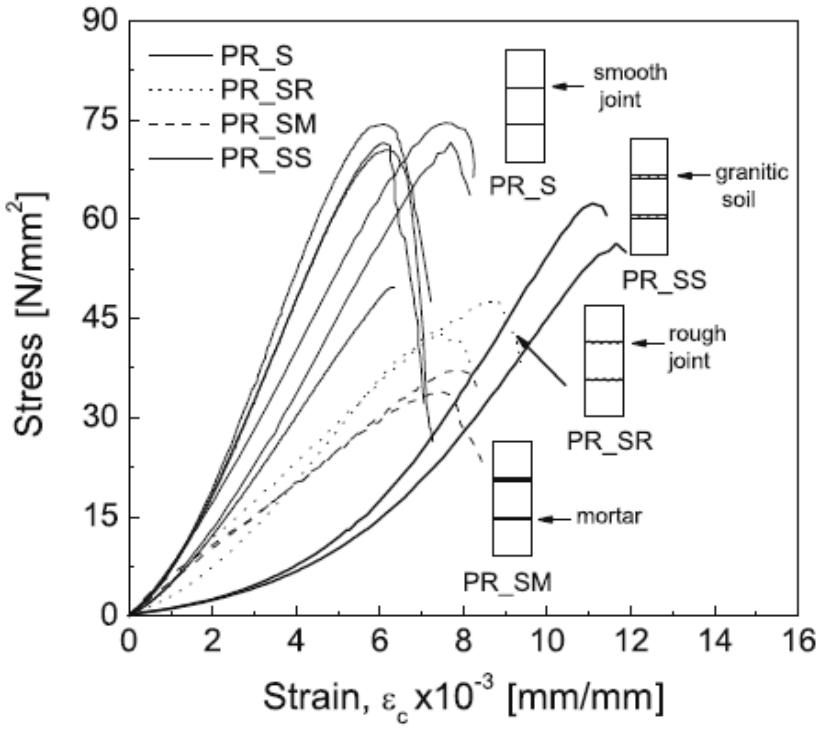

Figure 2.31 Stress-strain diagram of stone prisms (Vasconcelos & Lourenço 2009)

Compression testing on granite wall specimens with cement mortar was carried out by Zeng (2010) to examine the effect of granite units and mortar on the strength and elastic constant of the masonry. The unique feature of this experiment was the use of masonry prism with a single head joint.

The compressive strength of granite stone was determined using two types of prisms constructed by superimposing three equal pieces of granite with dimensions 50.8

mm x 50.8 mm x 50.8 mm (originally in inches) and 50.8 mm x 50.8 mm x 152.4 mm. This scheme was adopted to reduce the confinement effect for the middle cubic stone piece. The average compressive strength and modulus of elasticity of three granite stone specimens were 55.2 MPa and 36.9 GPa, respectively. A continuous vertical crack was observed from the top to the bottom of the specimen.

Using cylindrical specimens of diameter 50.8 mm and height 101.6 mm and also prismatic specimens of size 50.8 mm x 50.8 mm x 152.4 mm, the compressive strength of cement mortar at 28 days was observed. The average compressive strength of the three mortar specimens was 15.9 MPa, whereas the modulus of elasticity was 15.4 GPa. Mortar specimens showed more ductile behaviour than granite specimens.

The masonry specimen for compression test was a wall panel of size 203.2 mm long, 177.8 mm high and 127 mm thick as shown in Figure 2.32. The thickness of cement mortar joint was 12.7 mm.

Displacement controlled loading was applied at a rate of 0.125 mm/s. Strain was measured using Digital Image Correlation (DIC) technique proposed by Sutton et al. (1983). The failure of masonry specimen was mainly due to vertical splitting of granite units and no evidence of crushing of mortar was observed. The average compressive strength of 3 masonry specimens was 40.7 MPa. The masonry specimen exhibited much more ductility than granite stone and mortar specimens. The average modulus of elasticity of the masonry specimen was 30 GPa.

Figure 2.32 Wall specimen for compression test (Zeng 2010)

The properties of three-leaf stone masonry was investigated by Binda et al. (2006) using twelve specimens of size 310 mm x 510 mm x 790 mm. Two outer leaves were composed of ashlar masonry with 10 mm thick hydraulic lime mortar and the inner core was filled with rubble masonry. Two types of interconnection between outer leaves and inner core were provided: straight and with shear keys (Figure 2.33).

Locally available limestone and sandstone were used for building the specimen. The compressive strength of the stone was determined using three cylindrical specimens of 80 mm diameter and 145 mm height. Modulus of elasticity and Poisson's ratio were calculated within the range of 30% to 60% of ultimate strength. The compressive strength, modulus of elasticity and Poison's ratio of limestone were observed as 20.6 MPa, 9.47 GPa and 0.10, while loading perpendicular to the bedding. The respective values for sandstone were obtained as 104.2 MPa, 18.2 GPa, and 0.19. The tensile strength of the stone was determined using splitting test on six cylinders of diameter and height of 80 mm sawn along the direction of bedding. The splitting tensile strength of limestone and sandstone were 2.05 MPa and 6.00 MPa respectively.

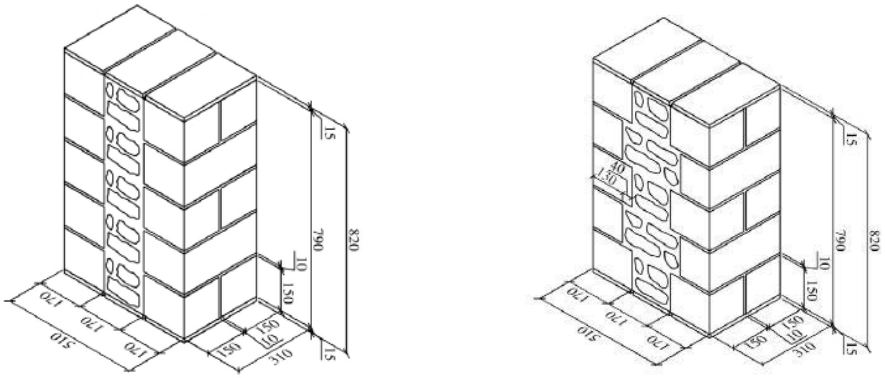

(a) Straight joint (b) Keyed joint

Figure 2.33 Three leaf stone masonry specimen (Binda et al. 2006)

The flexural strength of lime mortar was determined using 40 mm x 40 mm x 160 mm prisms. The compressive strength tests were conducted on two halves of the prisms obtained after flexural test. The average value of flexural strength and compressive strength at 28 days were 1.5 MPa and 7.4 MPa. These values at 75 days were 1.9 MPa and 9.2 MPa, respectively. The testing on the wall specimen begun on 75th day.

The shear strength of three leaf masonry was determined by testing two wall specimens similar to the compression test specimens. The wall specimen was treated as a triplet, supported on the bottom of two outer layers and a vertical load was applied on the top of the inner core. The shear strength for straight joint was calculated based on the shear area of 2 x 310 mm x790 mm. For keyed joint, a similar approach was taken to calculate equivalent shear strength assuming straight joints. The shear strength of lime stone with straight joint was 0.17 MPa. Sand stone with straight joint showed only 90 kPa. The equivalent shear strength of keyed joint

specimens of limestone and sand stone were 0.58 MPa and 0.81 MPa, reflecting the contribution of shear strength of the stone.

After the shear test on straight joint specimens, two outer leaves were tested in compression. Both outer leaves were tested simultaneously for limestone. Due to limited capacity of the testing facility, outer leaves of sandstone were tested separately. The test results showed that the outer leaves of limestone specimens could bear around 45% of the stone strength and the inner core only about 20%. These ratios for sandstone specimens were 40% and 4%. Besides, inner core of sandstone specimen exhibited less brittle behaviour as compared to limestone specimen. This was attributed to the higher strength of stones in the inner core, where cracks are developed around the unbroken stone.

Finally, compression tests were carried out on a single specimen of three-leaf wall of each type. The sandstone specimen was tested up to 2,380 kN, as the capacity of the machine (Maximum of 2,500 kN) was not enough to load up to the ultimate load. The compressive strength and modulus of elasticity of limestone specimen with straight joint was 5.8 MPa and 1.77 GPa. These values for keyed joint specimens were 6.4 MPa and 2.08 GPa. Thus, the key joint specimens were about 10% stronger than straight joint specimens. The keyed joint specimens showed less brittle behaviour than specimens with straight joint.

In rubble masonry, voids between outer layers are filled with mortar and gravel. However, a continuous vertical layer of mortar and gravel is not created due to certain overlapping between outer and inner layers. Therefore, it is not exactly similar to the three-leaf stone masonry. If the inner core of three-leaf masonry is

squeezed, then the keyed joint three-leaf masonry may be similar to rubble masonry provided the outer layers are made from rubble.

2.10 **Research on shake table testing of stone masonry**

Usefulness of shake table testing in the study of response of structures to dynamic loading has been realised after every disastrous earthquake in the past. Though the earliest history of shake table goes back to 1890 in Japan, with many improvements through various stages in USA, Japan, and Europe, sophisticated versions of the shake tables were developed only after 1970s (Severn, Stoten & Tagawa 2012). The technological advancements have been instrumental in the evolution of the shake table facilities for improving its capability and accuracy for reproducing the original records of ground motions. Due to economic reasons, reduced scale shake table testing is more common in order to study the overall response of the buildings as compared to full scale models.

While preparing reduced scale models, the relationship between the prototype and the model are determined using dynamic similitude requirements, which are based on the theory of models (Harris 1999). If every physical quantity in the model satisfies proper scaling with the prototype according to dimensional analysis, such models are true models or complete models. In order to achieve these requirements, new model materials are manufactured having properties scaled down proportionately. On the other hand, if the models are prepared using prototype materials, such models are called adequate or simple models. If L_M is the length measured on the model, the corresponding length on the prototype L_P is determined

by multiplying it by a scale factor S_L. Thus, $L_P = S_L L_M$. The scale factors for some of the most common physical quantities are summarised in Table 2.3.

Table 2.3 Similitude requirements for dynamic conditions

Quantity	Complete Model	Simple Model
Length (L)	S_L	S_L
Strain (Ɛ)	1	1
Stress (σ)	S_L	*1*
Young's modulus (E)	S_L	1
Specific weight (γ)	1	*1*
Force (F)	S_L^3	S_L^2
Time (t)	$S_L^{1/2}$	S_L
Frequency (*f*)	$S_L^{-1/2}$	S_L^{-1}
Displacement (δ)	S_L	S_L
Velocity (*v*)	$S_L^{1/2}$	1
Acceleration (a)	1	S_L^{-1}

Tomazevic & Velechovsky (1992) investigated the global seismic behaviour of reduced scale (1:4) two storey stone masonry model built with lime mortar using a simple earthquake simulator capable of simulating the uni-directional ground motions. The reduced scale model was constructed according to the laws of the complete model similarity. Though no special material was developed, the strength of the model was reduced proportionally using low strength lime mortar. The prime objective was to study the influence of rigidity of floors on the seismic behaviour of historic stone-masonry buildings. The seismic loading was the N-S component of the Petrovac ground acceleration record of the Montenegro Yugoslavia earthquake of 15 April 1979. Similar damage patterns in the walls of the upper part of the model, which were not connected to the flexible wood floors were observed during the test as in the real buildings after the earthquake.

Shaking table tests on 1:2 scale two-storey stone masonry building of size 5.5 m x 4.4 m x 6 m was undertaken by Benedetti, Cardis and Pezzoli (1998). Seven models were built of roughly squared stones with wall thickness of 225 mm using poor quality mortar (0.8 MPa compressive strength). Two types of configurations were prepared based on the position of windows either on north face or south face. One such configuration also had arches on the top of the windows as shown in Figure 2.34. Wooden slabs, supported on timber beams, were adopted as flooring structure. About 70% additional masses were placed on the slab and 30% additional masses were distributed among walls.

Three-component base excitations were used for each shock derived from records at Calitri during Irpinia earthquake (23 November 1980). Only response accelerations were recorded along the base, first floor and second floor. After testing up to severe damage stage, the models were repaired, strengthened and tested again. Major cracks were sealed using cement or gypsum. Connection between slabs and walls were improved using steel plates. Other various strengthening techniques were also used among different models, such as, using reinforced concrete band at each floor level, and applying horizontal tendons at each storey level. Four models with arches over windows and doors were strengthened using two light curved steel blades at both faces of the intrados.

In all unreinforced models, severe cracks appeared in spandrel beams. Diagonal cracks were observed in piers, mainly at first storey. Piers were heavily damaged at the top and bottom by wide horizontal cracks. Wall separation was also observed leading to collapse.

Figure 2.34 A stone masonry building model (Benedetti, Carydis & Pezzoli 1998)

Amplification factor of the unreinforced specimen at the first storey was detected as 1.46, whereas at the second storey, it was 2.23. The base shear coefficient for stone masonry was estimated in the range of 0.11 to 0.19 whereas the structural reduction factor was estimated as 2. Initial damping factor was obtained as 10%. The original frequency was reduced by up to 30% of the original at the ultimate stage. After repair, original frequency and damping was almost recovered.

A full scale shake table testing was conducted by Bairrao & Silva (2009) on a single storey asymmetric (plan) limestone masonry (squared rubble) building under two different reinforcement techniques. With the first technique, the specimen was horizontally reinforced with polymer grids (RichterGard 20 gridTM) inserted in the layers of fibre added lime-cement mortar, whereas in the second technique, it was also vertically confined with polymeric grids and covered with fibre added lime-cement mortar (Figure 2.35). The second technique was applied as a repair or

strengthening measure on the specimen after the first test. The lime-cement mortar was composed of 75% sand, 19% lime and 6% cement. Input signals for the shake table were semi-artificial loadings adapted from the Herceg Novi earthquake records considering two horizontal directions. In first phase of testing, input loading was varied with PGA levels from 0.02g to 0.25g at a rate of 0.05g. The variation was maintained at a rate of 0.1g from 0.1g to 0.9g in the second phase.

(a) after placing vertical reinforcement (b) covered with mortar

Figure 2.35 Polymeric grids reinforcement (Bairrão & Falcão Silva 2009)

The first ten vibration periods obtained were below 0.02 s, indicating high global stiffness of the structure. In the first phase, initial damage was detected at bottom of the specimen near the connection with the foundation slab. Considerable damage was observed near all the openings in the final stage. In the second phase, cracks also appeared in the interface zone between the specimen and foundation slab. The width of cracks in the second case were thin and densely populated which means the normal stresses were more uniformly distributed in the bed layers. All cracks were in the mortar and never passed through the limestone blocks. Fewer cracks were

observed in the lower part as compared to upper part of the model, which was supposed to be due to the effect of out of plane vibration along with general torsion. Surprisingly, few cracks were observed at the lower part of the openings. Cracks did not appear at the upper corners of the window. This means vertical reinforcement embedded in fibre added lime-cement mortar was acting as a lintel beam over the windows and door. On the other hand, the maximum lateral acceleration on the top of the specimen in the second phase was considerably reduced. As a consequence, the specimen in the second phase could sustain about three to four times the values of PGA in the first phase.

Magenes, Penna and Galasco (2010) conducted a full-scale shaking table test on a single room two storey stone masonry building with pitched roof in order to study the seismic performance of existing stone masonry buildings. The specimen was made of double-leaf stone masonry having thickness of 320 mm. The wooden floor was made of pine joists (160 mm x 120 mm) @ 500 mm with 30 mm planks nailed on the top. A pitch roof was constructed using a ridge beam (320 mm x 200 mm), a spreader beam (320 mm x 120 mm) on the top of each longitudinal wall, purlins (120mmx 80mm) @ 500 mm, wooden planks of 30 mm thick and clay tiles nailed to the timber structure (Figure 2.36).

Figure 2.36 Specimen before fixing clay tiles (Magenes, Penna & Galasco 2010)

As a retrofitting measure, a tie rod (18 mm diameter steel rebar) was inserted parallel to each wall adjacent to the inner face of the wall at floor and roof level. Also a steel x bracing (8 mm diameter) was provided on each side of pitch roof between the ridge beam and the spreader beam. The retrofitting scheme was to be activated after significant damage had been sustained by the specimen during incremental dynamic testing. Also additional masses were laid on the floor as a distributed load equalling to 3.2 tonnes.

As a seismic input, the strong motion recorded during Montenegro earthquake at Herceg-Novi station in 1979 was selected. The loading was applied with increasing values of PGA @ 0.05g, starting from 0.05g up to 0.4g. When the loading rate reached 0.3g, local failure was initiated. As a consequence, the gable walls tended to overturn out of plane, along with cracks around corners of the openings observed at the loading rate of 0.4g. After that, retrofitting measures were activated and the test

was repeated with 0.4g loading. This intervention prevented out-of-plane mechanisms of the walls and the response was mainly governed by in-plane wall response.

Meguro et al (2012) performed shaking table tests on 1:4 scaled shapeless stone masonry houses, with or without retrofitting with polypropylene band meshes. The specimens were a single room, one storey house with a pitched wooden roof but without gable walls. The dimensions of both models were 950 mm x 950 mm x 720 mm with 100 mm thick walls. The size of door and window were 290 mm x 480 mm and 370 mm x 240 mm respectively (Figure 2.37).

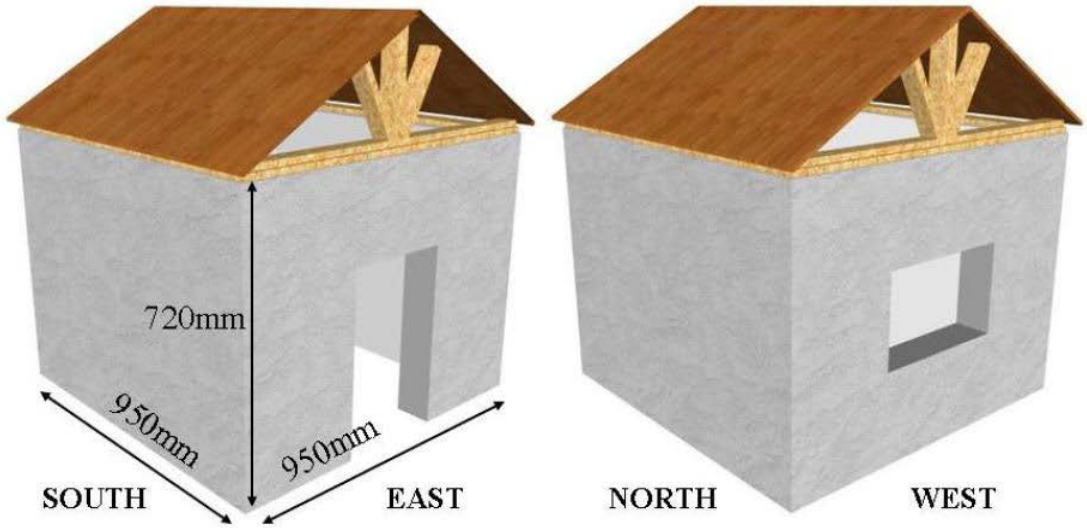

Figure 2.37 Schematic diagram of tested model (Meguro et al. 2012)

A sinusoidal input motion with frequencies ranging from 2 Hz to 35 Hz and amplitudes ranging from 0.05 g to 1.4 g were applied as input signals (Figure 2.38). At a time one frequency was chosen for the input motion. The simple input loading was chosen for simplicity in the numerical modelling. The loading was applied

starting from high fluency to low frequency and from lower amplitude to higher amplitude. The wall was constructed using pieces of stone of size 40 mm to 60 mm placed side by side in rows and gaps filled with gravels of size up to 10 mm and cement-lime-sand mortar (1:7:19). The water cement ratio of the mortar was chosen as 0.15. One of the specimens was retrofitted with PP-band mesh after construction.

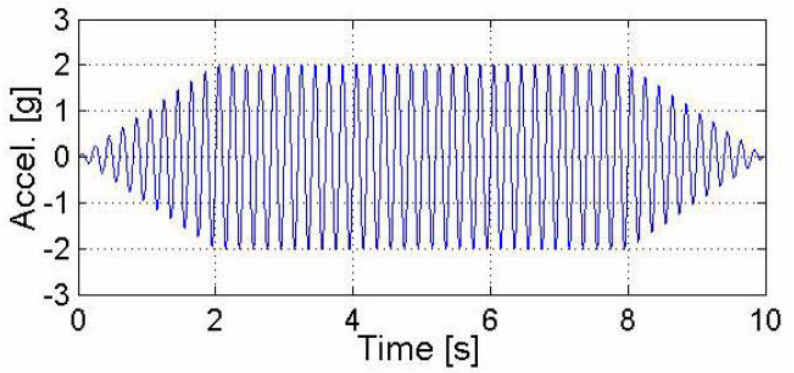

Figure 2.38 Typical shape of input loading (Meguro et al. 2012)

In the case of non-retrofitted specimen, cracks were initiated at the top of openings and propagated towards bottom of the wall. With increased loading rate, cracks widened further. As a consequence, the connection between walls gets separated leading to complete collapse.

The nature of crack initiation and propagation in the case of retrofitted specimen was almost similar as in non-retrofitted case. However, PP-band mesh maintained the overall integrity as well as stability and prevented the collapse of the structure even after the base displacement was more than 4 times greater than a non-retrofitted case.

2.11 **Research on numerical modelling of random stone masonry**

The numerical simulation of masonry is extremely complex due to various influencing factors, such as anisotropy of units, dimension of units, joint width, material properties of the units and mortar, arrangement of bed as well as head joints and quality of workmanship (Lourenço & Rots 1997). The complexities of numerical modelling increase further in the case of random stone masonry due to variation of shape and size of stone blocks. Besides, such type of wall consists of at least two vertical layers of stones overlapping each other and the remaining gaps filled with smaller pieces of stone and mortar.

Finite element method (FEM) is the most commonly used numerical tool for the analysis of masonry structures. However, discrete element method (DEM) is also gaining popularity. Both these methods have their own advantages and limitations. Therefore, a combined finite-discrete element method is also in use in the analysis of stone masonry, which possesses the advantages of both methods. Applied element method (AEM) is considered one of the most suitable numerical models to simulate masonry in large deformation range (Worakanchana et al. 2008).

Senthivel and Lourenço (2009) carried out two dimensional nonlinear finite element analysis to model deformation characteristics of historical stone masonry shear walls subjected to combined axial compression and lateral shear loading. Three types of stone masonry were considered: sawn dry joint stone masonry, irregular stone masonry with mortar and rubble masonry. A micro modelling technique based on plasticity theory was used for analysis. Stone units were treated as eight nodded iso-parametric continuum plane stress elements with quadratic interpolation and full

Gauss integration. The joints were modelled as six nodded zero thickness line interface elements with Lobatto integration. The finite element mesh for dry joint regular stone masonry was generated by using a special computer program developed for messing regular units. The nodal points for irregular masonry and rubble masonry were generated using a special image scanning software and Microsoft Excel and meshing was carried out as for regular masonry.

The vertical pre-compression load was applied in small steps at the top surface and horizontal load was applied in terms of incremental displacement. In all types of masonry models, axial pre-compression played a significant role in the behaviour of shear walls. Slight increase in the vertical load improved the shear strength of wall considerably due to improved bond resistance mechanism at joints. However, a substantial axial stress (1.25 MPa) changed the failure modes. At lower pre-compression load (100 kN, axial stress 0.5 MPa), wall failed either in flexure or rocking, whereas at higher axial stress, wall failed by toe crushing and diagonal shear failures. A good agreement between numerical and experimental load displacement curve was observed for regular masonry, however this trend for rubble masonry was not so good.

Smoljanović, Živaljić, & Nikolić (2013) applied the combined finite-discrete element method for a 2D analysis of dry stone masonry structures. Each stone block was modelled as a discrete element discretised by triangular finite elements. Material non linearity was treated using contact elements implemented within the finite element mesh (Figure 2.39). The model was validated by comparing it with three

experimental test results: rocking motion as a single block, shear tests on dry stone masonry joints and monotonic cyclic behaviour of in-plane dry stone masonry walls.

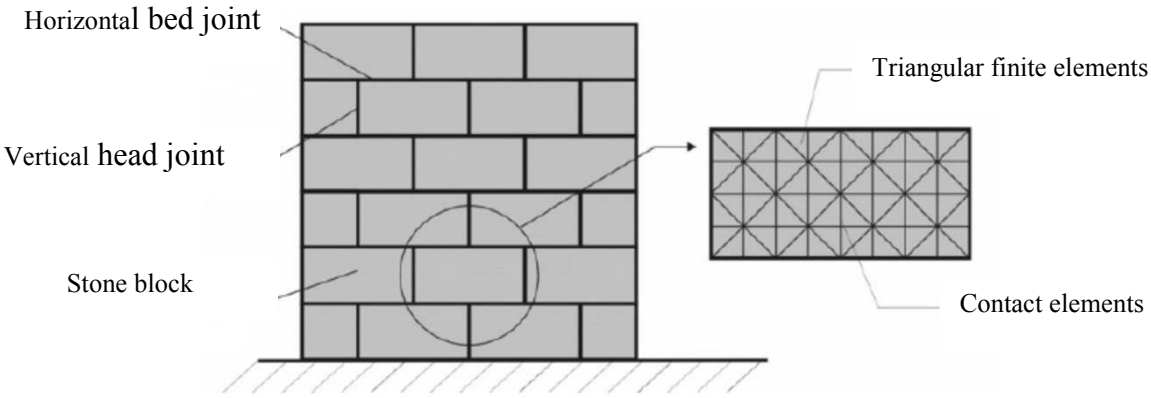

Figure 2.39 Dry stone masonry model (Smoljanović, Živaljić & Nikolić 2013)

The numerical results of the model simulated the main features of dry stone masonry, such as, shear behaviour in dry joints between stone blocks and rocking motion. Also, it provided a realistic prediction of the collapse load.

A nonlinear FEM model was developed by Ramalho et al. (2008) to simulate the nonlinear response of three-leaf stone masonry specimens subjected to compression testing. The specimens were composed of two external leaves of stone and mortar joints filled with an internal leaf of mortar and stone pieces. Eight nodded iso-parametric brick elements were used to model the one quarter of the wall specimen considering the symmetry of boundary conditions at the vertical mid planes of the specimens. Each leaf was assumed homogeneous having average mechanical properties derived from the tests on the individual leaf. The lower base was assumed completely or partially restrained and an increasing displacement was applied at the upper base. Initially, materials were assumed to be elastic. A non-rotating smeared

crack model was employed in order to represent the behaviour at the damage stage. In this model, crack closure effect was neglected, so that it was valid only for monotonically increasing loads or displacements. Analyses were carried out using ABAQUS and FEAP software. The peak load and the corresponding displacement were predicted with a very good degree of accuracy by using both tools, whereas the post peak softening behaviour was more closely represented by FEAP implemented with strain averaging procedure to avoid strain localization.

Milani (2010) proposed a 3D finite element model for analysing multi-layer masonry structures reinforced with FRP strips (Figure 2.40). In this model, stones and filler were modelled as infinitely rigid four nodded tetrahedron elements and joints are treated as interfaces with frictional properties as well as limited tensile and compressive strength. The main purpose of using tetrahedron elements was capturing probable diagonal failures along the thickness due to cracks inside bricks, mortar and filler.

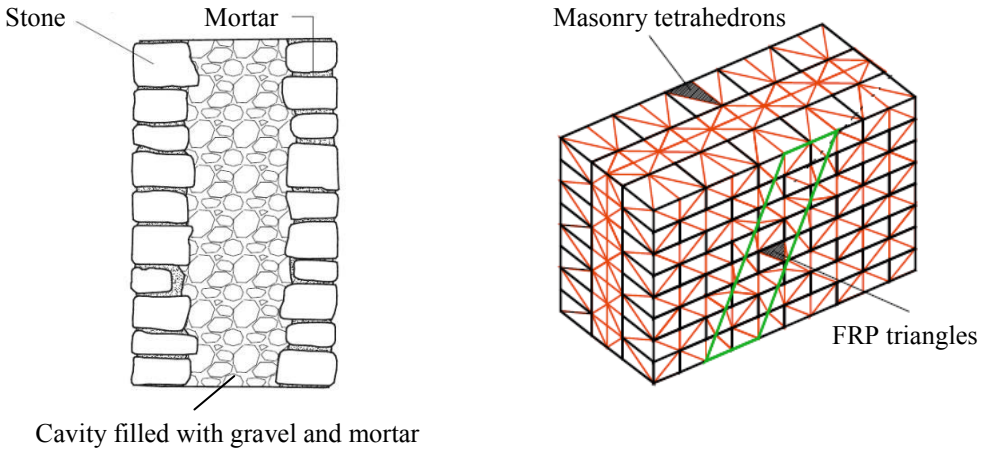

(a) Typical cross section (b) FEM model

Figure 2.40 Multi-layer masonry model (Milani 2010)

FRP strips were modelled as triangular rigid elements. The interaction between masonry and FRP layers were represented by interfacial tangential actions. Besides, a limited tensile strength of the FRP reinforcement was introduced at the interfaces between adjacent triangular elements to take account of tensile failure of the FRP.

In addition to mortar joint interface, stone-stone, filler-filler, and stone-filler interfaces were adopted in order to represent the stone layer, cavity filled with gravel and mortar, and interaction between them, respectively. For stone-stone interfaces, a piecewise linear approximation of a Mohr-Coulomb failure criterion with tension cut off was adopted. A linear Lourenço and Rots failure criterion (1997) was used for mortar joint interfaces. The failure criteria for filler-filler interfaces and filler-stone interfaces were similar to stone-stone interfaces, but having different cohesion, friction angles and tensile strength. For FRP masonry interaction, plastic dissipation was supposed to occur at the interface due to stress action parallel to the direction of fibres. The numerical results of such models have satisfactorily represented the behaviours of walls under both in-plane and out-of-plane loadings. The role played by the filler in the failure mechanism was crucial for the overall resistance of the wall.

2.12 **Summary**

Sand stone is one of the popular building stones used for rubble masonry houses built in mud mortar. In most cases, soil available at a building site can be used for preparing mud mortar. Relatively flat bedded stone pieces of various sizes are suitable for the construction of rubble walls with mud mortar.

The most common failure mechanisms of traditional stone houses in an earthquake event are de-lamination, out of plane bending failure, in-plane shear failure and corner or junction separation. In order to improve the seismic performance of new as well as existing stone masonry buildings, various options have been developed by the researchers. However, very few methods are applicable to the rubble houses built with mud mortar. Therefore, there is still a need to develop an effective, economically viable, and socially acceptable reinforcing technique suitable for rubble masonry houses.

In the literature, only a few research activities relevant to the rubble masonry are available. Therefore, extensive experimental investigation is necessary in order to determine various parameters required for understanding the behaviour of rubble masonry. On the other hand, the testing methods for rubble masonry are not explicitly covered in existing standards. As a consequence, a set of procedures for preparing specimens as well as testing needs to be established.

Seismic performance of rubble masonry cannot be fully understood through static testing alone. Investigation of such types of construction through analytical and numerical studies is extremely complex. Therefore, shake table testing is indispensable in the study of seismic behaviour of rubble masonry houses.

Based on these facts, a reinforcement scheme has been proposed for improving the seismic performance of rubble masonry built with mud mortar. The details of the reinforcement system has been given in the next chapter. The performance of such system in static and dynamic loading has been presented in the subsequent chapters.

3. Proposed Reinforcing System

In this chapter, the motivations behind the origin of the concept of proposed reinforcement system are explained. This is followed by the description on how the original concepts were further extended by exploring various alternatives. Then, details of the adopted options are described along with advantages and probable major mechanisms of the system. Finally, proposition on the effectiveness of this reinforcement system in reducing the common seismic deficiencies of the traditional buildings is explained.

3.1 Background

Generally, a large quantity of rubble is left behind the scene from damaged buildings after an earthquake disaster. The major motivation of this research is to utilise such rubble in the most effective way for building earthquake resistant houses after such events. However, it is always more useful if it could be implemented before an earthquake disaster.

If the proper reconstruction policies cannot be strictly implemented in the earthquake affected regions, tendency may be to rebuild as before using the same rubble. Without any improvements, these reconstructed buildings are likely to suffer heavy damage in the next earthquake and disaster cycle repeats again and again. This research is an attempt to break this disaster cycle either before an earthquake or immediately after an earthquake, if not possible to do so before the seismic event (Figure 3.1).

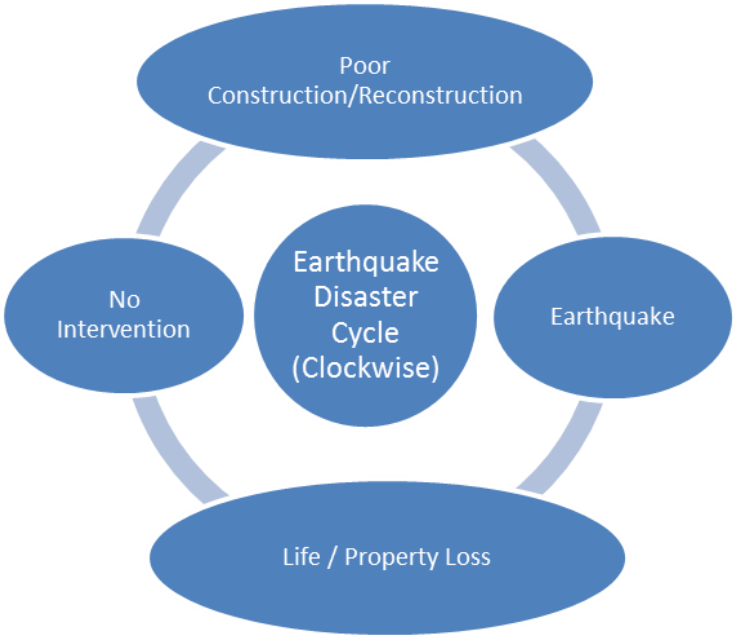

Figure 3.1 Schematic diagram of earthquake disaster cycle without intervention

Though, a number of disastrous earthquakes have struck within the last few years (Table 3.1), the origin of the concept of this research goes back to the Kashmir Earthquake in 2005. In the aftermath of the Kashmir Earthquake (8 Oct 2005), two renowned architects from Sydney (Penny Rosier and Ian Brumby), started thinking about new construction schemes using such rubble suitable for the reconstruction phase in devastated areas (Wheen 2009). This idea was influenced from the evidence of gabion performance in the Atico (Peru) earthquake (23 June 2001, Magnitude 8.4, depth 33 km). In that earthquake, gabion performed well undergoing a large deformation (about 40%) without rupture, as shown in Figure 3.2 (Koseki et al. 2002).

Penny and Ian invited a number of professionals including Prof. Bijan Samali from the University of Technology Sydney; A/Prof. Robert Wheen from the University of

Sydney; Davina Rooney and John Hewitt from Arup Consulting Engineers; Andrea Nield from Emergency Architects; and Vince Scolaro from Maunsell Consulting Engineers. This group of professionals was focused on devising simple yet earthquake resistant forms of dwelling construction. The rubble-filled gabion concept was at the centre of discussion from the very beginning.

Table 3.1 Disastrous earthquakes from 2005 to 2013 (USGS)

Date	Local Time	Location	Magnitude	Casualties	Depth, km
8 Oct 2005	08:52:37	Kashmir, Pakistan	7.6	73,338+	26.0
27 May 2006	05:53:58	Java, Indonesia	6.3	5749+	10.0
17 Jul 2006	15:19:28	Java Indonesia	7.7	686+	48.6
15 Aug 2007	18:40:57	Chincha Alta, Peru	8.0	514+	39.0
12 May 2008	14:28:01	Sichuan, China	7.9	87587+	19.0
6 Apr 2009	03:32:39	L'Aquila, Italy	6.3	287+	8.80
30 Sep 2009	17:16:09	Sumatra, Indonesia	7.6	1117+	81.0
12 Jan 2010	16:53:10	Port-au-Prince, Haiti	7.0	100,000+	13.0
27 Feb 2010	03:34:14	Maule, Chile	8.8	523+	35.0
14 Apr 2010	07:49:38	Yushu, China	6.9	2698+	17.0
25 Oct 2010	21:42:22	Sumatra, Indonesia	7.7	340+	20.6
22 Feb 2011	12:51:42	Christchurch, New Zealand	6.3	181	5.9
11 Mar 2011	14:46:24	Tohoku, Japan	9.0	20,896+	30.0
23 Oct 2011	13:41:21	Van, Turkey	7.1	534+	16.0
11 Aug 2012	15:53:17	North-western Iran	6.4	306+	9.9
24 Sept 2013	16:29:47	Awaran, Pakistan	7.7	825+	15.0

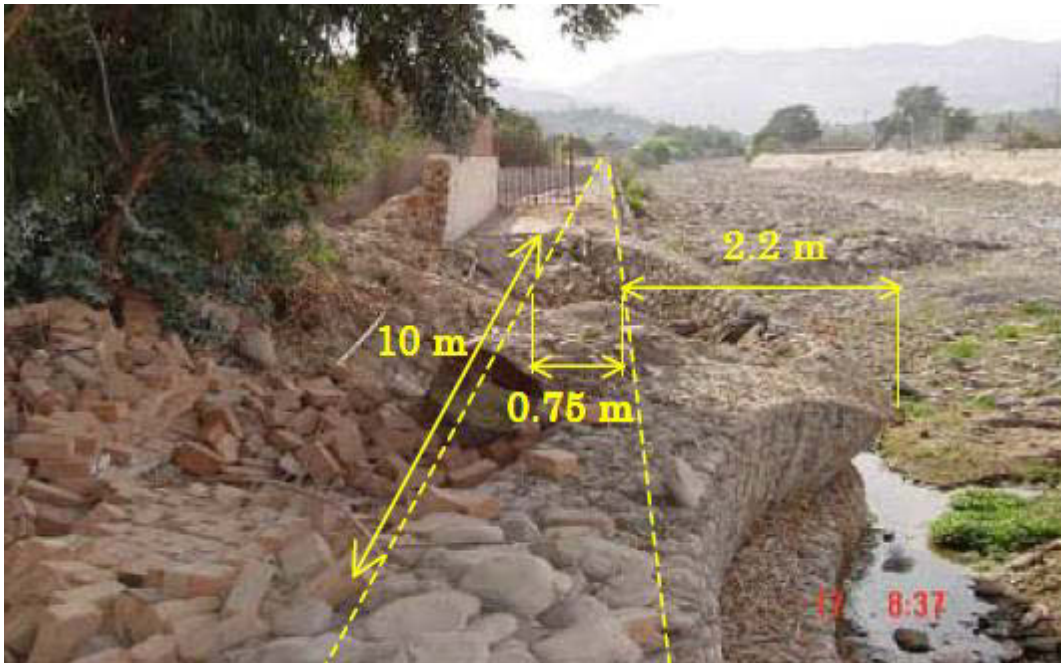

Figure 3.2 Performance of gabion wall in Atico earthquake (Koseki et al. 2002)

3.2 Concept development

When the author was introduced to this concept by his principal supervisor Prof. Bijan Samali, he was interested in extending this idea of using gabion in earthquake resistant houses. A couple of meetings were also organised by Prof. Samali to gain an insight from other experts including A/Prof. Robert Wheen during the first meeting and also Penny Rosier and Ian Brumby during the second meeting. In these meetings, ideas regarding the performance of gabions were exchanged among participants.

A/Prof. Wheen had conducted three types of tests in order to investigate the merits of gabion box for post-earthquake reconstruction (Wheen 2009). The first test was on a chain-wire panel (900 mm x 900 mm) fabricated by anchoring a wire-mesh (square opening with nominal size of 50mm, and wire diameter of 2 mm) along the sides of a

square steel frame having hinges at four corners. This frame was displaced along one diagonal; both in tension and compression, and corresponding loads were measured. A similar test was also conducted on an identical panel with chain wire encased in a layer of 10 mm thick low strength concrete. The chain-wire without concrete layer had taken loads only after a large deformation whereas the panel with a concrete layer displayed significant load carrying capacity and energy absorption within relatively small deformation.

The second test was a compression test on a stone filled 300 mm cubical gabion box fabricated with a plastic coated square mesh (nominal opening of 25mm, wire diameter of 1 mm). Three similar boxes were fabricated; two of them with an additional cylindrical mesh inside the box and the third box with a tie wire at mid height. The external mesh of the gabion box with an internal cylinder was effective only after the deformation of 60 mm (1/5 of the height of gabion). Those gabions had higher load carrying capacity as compared to gabion box without an internal cylinder.

The third test was a compression test on a river-gravel filled chain-wire (square opening with nominal size of 50 mm, wire diameter of 2 mm) cylinder. Though the deformation was very large, the ductility of the specimen was maintained.

These observations have clearly verified the ductile behaviour of the gabion box as observed in Atico earthquake. However, very large deformation was the main constraint, which could have undesirable effects on the building construction. Cylindrical box were more effective than square box. A tie wire at the mid height of the cubical box had a positive role for maintaining the load with limited deformation.

After getting these ideas on the behaviours of gabion box, a number of different options were tried for developing a system of reinforcement similar to the gabion. The other related information regarding existing practice of gabion basket, standard sizes, fabrication and relevant details were also studied.

Initially, a system of building a house using standard gabion baskets of width 500 mm, height 500 mm and length varying from 500 to 2000 mm was proposed. The minimum width of gabion basket available in the market was 500 mm with 2.7 mm nominal diameter of wire (MACCAFERRI). In this scheme, a wall could be built by stacking one basket on top of another which was based on following almost similar procedures to existing practice of gabion application in slope protection. The main advantage of such a system was the availability of standard gabion baskets in the market.

As a refining process, this reinforcement system was critically analysed to simplify and economise it. Few drawbacks of such a system were identified. Firstly, in this system, there was a continuous horizontal and vertical separation along the common sides of two gabion baskets, which could be a potential source of weakness. The system was supported just by the friction between two blocks of gabion and binding wire at the edge. Unlike a gravity structure, a building wall constitutes a relatively slender structure. Therefore, during earthquake shaking, there is a high chance of sliding and rotation of the wall about the common interface. Secondly, each common side had two layers of wire mesh, one from adjacent gabion, making it uneconomical (Figure 3.3).

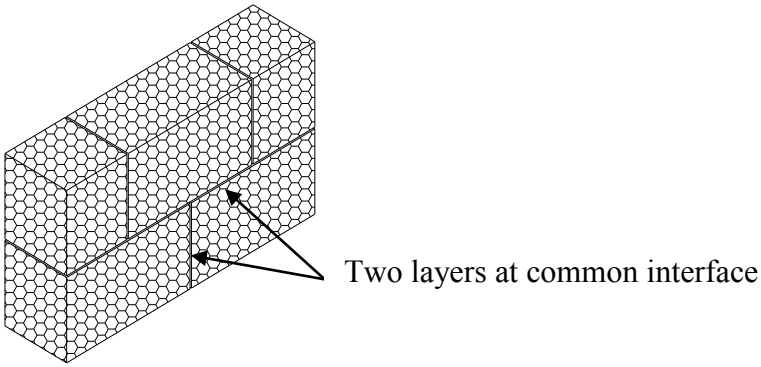

Figure 3.3 Initially proposed model

In order to economise the system, a gabion basket with a separate top lid and a side face was proposed so that only one lid or side could be used at the common interface (Figure 3.4). However, such a system still poses some difficulty in transportation. Therefore, further alternatives were tried to improve the system.

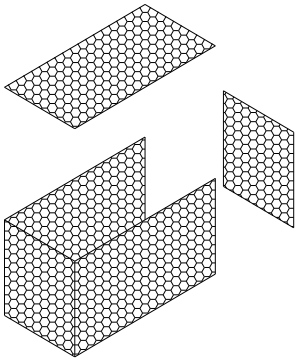

Figure 3.4 Gabion basket with separate side and top cover

During the search for different options of gabion system, it was realised that application of gabion like system in walling was actually very complex. It is due to the wire mesh carrying both vertical and lateral loads all the time. To simplify further, the whole scheme was divided into two major schemes:

a) A system in which walls remain stable in vertical load and reinforcement comes to action only when subjected to lateral loads
b) A system in which the reinforcement remains in action due to both vertical as well as lateral loads.

Then, it was decided to begin with option “a” and if time permits continue to option “b”. Nonetheless, due to the nature of the work and constraints in the laboratory, the first option was chosen, leaving the second option as a topic for further study.

For scheme “a”, dry stone masonry seems to be the best option. However, for making a relatively thin wall section stable, properly shaped stones are required. Fully dressed stones are labour intensive. Hence, such a system appears to be uneconomical. On the other hand, partly dressed rubble masonry built with mud mortar, could be an economical option. This is because mud mortar is naturally available, which can be collected with little efforts. Also with mud mortar, rubble of any shapes can be used, shaping only one side of the rubble facing to the wall surface. Once the performance of such system is fully understood, it will provide a basis for further analysis of true gabion like system if the mud mortar is removed.

In order to finalise the most economic and effective system, various options were considered. Use of gabion basket even after few modifications as mentioned above was still expensive. For self-stable system against vertical load like rubble masonry with mud mortar, the size of the steel wire could be reduced considerably. Eventually, a new system was conceptualised. The details of such system are given in the next section.

3.3 Details of the reinforcement scheme

The reinforcement system consists of wrapping around a wall with a galvanized steel wire (GSW) mesh. It can be prepared in two different ways. In the first method, the wire mesh is directly woven around the wall using GSW, whereas in the second method, a prefabricated mesh is wrapped around the wall.

The basic process of direct weaving method consists of fabricating a strip of mesh and laying it at the foundation level. Wall is built over the mesh. A pair of wires are inserted at a certain interval (preferably less than or equal to thickness of wall) along the horizontal as well as vertical direction during the construction of wall. When the wall is complete, meshes are woven around the wall. Finally, meshes are attached to the wall with twin wires inserted during the construction of the wall. Due to more corrosive environment below the plinth level, it is recommended to use either cement plaster up to the plinth level or wire coated with higher class of corrosion protection.

Almost similar procedures are followed for reinforcement with prefabricated mesh. Instead of twin wires, it is always better to insert a strip of wire mesh of width slightly larger than wall thickness during the construction of the wall. Once the wall is complete, required pieces of prefabricated mesh are cut and connected to foundation mesh as well as to each other forming a cage. The twin wires from the inserted strip are used to tie the mesh with the wall.

The first method has few inherent advantages over the second. This method can be applied to accommodate any shape of the wall precisely and it produces a continuous and seamless caging. However, this method has a drawback. It is time consuming

and hence labour intensive. In those regions, where labour is cheap, this method may still be economical. In the second method, the mesh can be either prefabricated in the factory or prepared on the building site. Prefabricated mesh is helpful for time saving during installation in the building site. Nevertheless, it might be slightly more expensive and little bit more difficult to transport as compared to rolls of wire. Therefore, the better option may be chosen based on field situations.

The detailed procedures of both direct weaving method and using prefabricated mesh method have been given in section 5.1.2. Connection details around openings as well as mesh tightening techniques are presented in section 5.2.

3.4 **Advantages of GSW**

The GSW reinforcing method is a simple technique. Generally, most targeted users are familiar with gabion technology in the form of either slope protection (Figure 3.5) or river bank protection from erosion. Even if they are not familiar with gabion system, this technique can be easily learnt and applied to reinforce their houses on their own with or without some technical support from skilled masons.

It is relatively easy to transport a roll of galvanized wire (or mesh) to the building sites. Also, it can be produced as a strip of prefabricated net which can be stored and transported in the form of a roll of mesh. It is relatively high heat resistant and lasts for a longer duration in a rural environment. This system of reinforcement creates a continuous caging around the wall. Any shapes and forms of the walls can easily be accommodated within the system.

Figure 3.5 Gabion wall during construction *(Photo: U. Dackermann)*

This type of mesh can be wrapped more tightly to the wall as compared to other types of mesh mentioned in section 2.4.3 and section 2.5.5. It is also useful in the reconstruction phase after a disaster, for clearing up the sites and building safer houses side by side. Thus, it has a widespread scope of applications.

3.5 **Governing principles of GSW reinforcement system**

The basic philosophy behind the GSW reinforcement system is to allow controlled damage to the wall but maintaining the overall stability of the building during the seismic events. Limited damage is permitted because of the nature of the material used in the building. It is not a wise idea to strive for constructing a building which remains intact in an earthquake in spite of using fragile materials such as stone with mud mortar. Therefore, allowing some degree of damage to the building seems

reasonable. With this little sacrifice of the wall, the collapse of the building might be prevented. This is the least performance level of the traditional buildings anticipated in extreme seismic events. Preventing the collapse of the buildings will reduce the chance of fatal injuries. As a result, probability of survival will increase significantly.

Figure 3.6 Localised damage of a wall during a seismic event (*Photo: NSET*)

Providing a certain level of confinement to the wall is the next important aspect of this reinforcement system. The combined effects of allowing limited damage and confinement result in a flexible but stable system. This is the most desired property in dealing with seismic loads. As the stiffness of the building reduces in a seismic event due to cracking, the vibration period will increase considerably. This will enable the building to have less amplification of seismic excitation. Due to flexible but confined system, it is expected that the energy dissipation capacity of the building will be improved extensively. In addition, the confinement will prevent

stones falling from the localised damaged (Figure 3.6) portion of the wall which reduces the risk of getting injured during a seismic event.

Another important aspect of this reinforcement scheme is associated with the nature of the stone masonry and the characteristic of seismic load. The low strength of the stone masonry with mud mortar has an inherent advantage over the overall seismic behaviour of the building. In most cases, the peak of seismic input does not occur at the onset of the earthquake (Figure 5.45). Therefore, during lower level of shaking, the masonry building will get cracked. However, with the help of the reinforcement caging, it will remain stable and acts as a flexible system. As a consequence, when the shaking level reaches its peak value, a drastically low value of the seismic load will be imparted to the building.

3.6 Performance of GSW in reducing the seismic deficiencies

The proposed reinforcement system is likely to reduce the most common seismic deficiencies of traditional stone masonry houses mentioned in section 2.3. The proposition of seismic performance of rubble masonry with GSW mesh has been explained below.

3.6.1 Reducing the effect of de-lamination

The GSW reinforcement system is expected to be very effective for reducing de-lamination of the stone wall. The de-lamination of the wall starts with the outward movement of stone layer in the rubble masonry. The reason for outward movement of the rubble is related to the shape of the stone, which can be explained through the failure mechanism of rubble masonry (Figure 3.7).

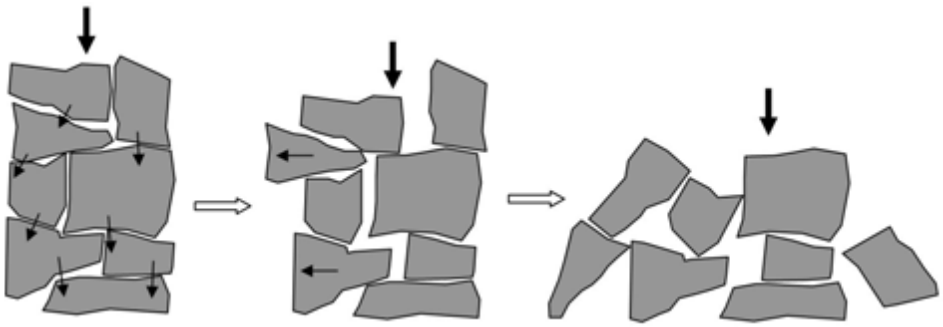

Figure 3.7 Failure mechanism of rubble masonry (Bothara & Hiçyılmaz 2008)

Thus, the rubble masonry is considered to be in unstable equilibrium in its initial state (Arya 2001). However, the rubble wall with mud mortar is stable up to a certain (large) displacement. This is evident from experimental observations (Spence & Coburn 1992) of rubble masonry with mud mortar.

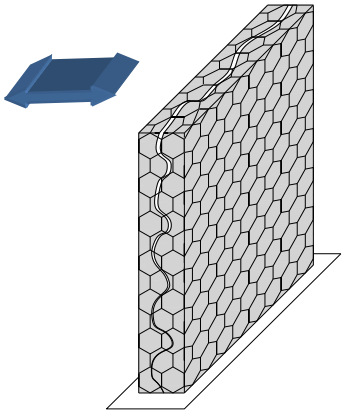

Figure 3.8 GSW reducing the effect of de-lamination

The proposed GSW mesh allows limited deformation to the separation of two layers of the wall. However, uniformly distributed tie wires/mesh throughout the wall limit the outward movement of the outer mesh. As a consequence, a confinement effect is

imparted to the wall. Thus, the bulging of the wall will be reduced significantly and the stability of the wall will be maintained (Figure 3.8).

3.6.2 Improvement on out of plane behaviour of the wall

Usually, out of plane load causes bending of the walls. Depending upon the aspect ratio of the wall, the bending of the wall may be either in lateral span or in the vertical span. The GSW reinforcement system will improve the out of plane bending behaviour of the wall in both ways (Figure 3.9).

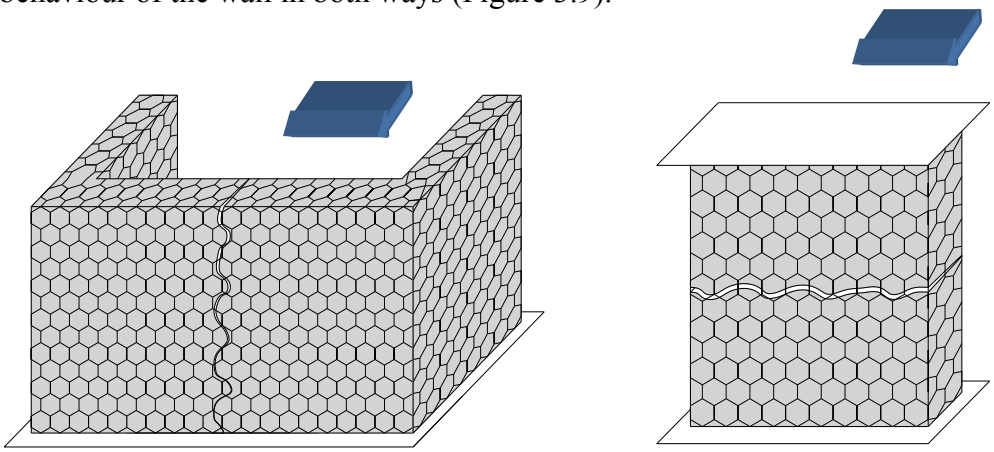

(a) lateral span (b) vertical span

Figure 3.9 Out of plane bending failure of wall

Once the flexural stress exceeds the tensile strength of the wall, cracks appear in the walls. The GSW mesh is anticipated to limit the width of cracking from further development as a result of the tensile stress developed in the mesh. Since the wall can sustain considerably larger compressive stress as compared to tensile stress, the wall will remain in equilibrium, mobilizing the high tensile strength of wire mesh as the crack width grows further. Due to large thickness of the wall, the wall will remain stable up to a significantly large rotation. This allows the wall to rock along

the crack. As a consequence, a considerable amount of energy is lost. Thus, further damage to other parts reduces significantly.

The inserted horizontal strips of wire mesh along the height make the wall more resilient and stronger in bending along the lateral span than in the vertical span. The self-weight of the wall above the horizontal crack is helpful for stabilizing the overturning moment in the vertical span.

3.6.3 Performance of in-plane behaviour of wall

As described in section 2.3.3, the wall subjected to in-plane loading may fail in sliding or shear or bending. The mechanisms of GSW reinforcement scheme at shear failure and bending failure of the wall are shown in Figure (3.10).

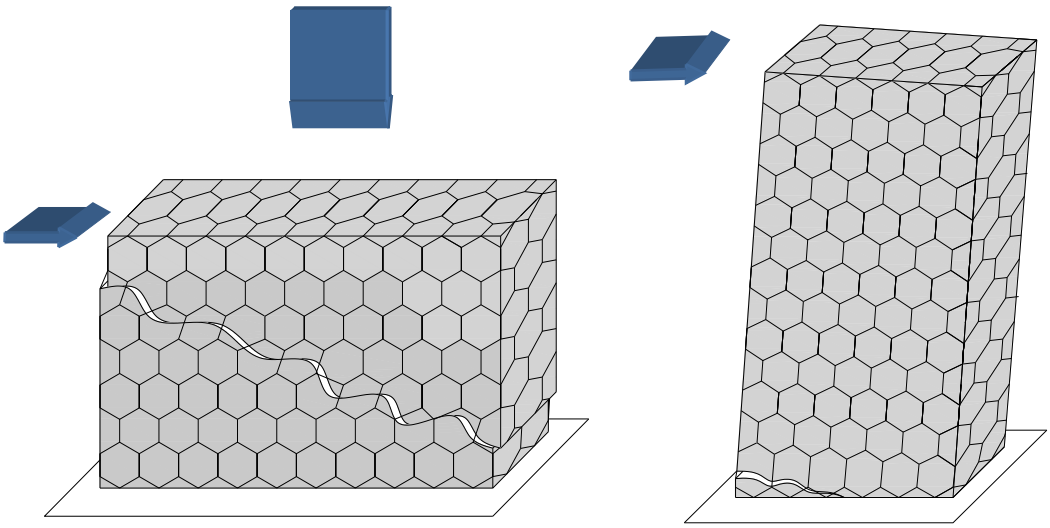

(a) Shear failure (b) Bending failure

Figure 3.10 In-plane behaviour of wall

The shear crack will be limited due to combined action of inserted horizontal strips as well as outer meshes. The in-plane bending action is resisted in similar way as in case of out of plane bending.

3.6.4 Improvement of integrity of corner or junction

The mesh of reinforcement improves the integrity of corners of the masonry building. During strong earthquake shaking, the wall may crack at the corner, but the GSW reinforcement will prevent widening the crack width. Thus, the wall remains stable even after separating from the orthogonal wall (Figure 3.11). The support to the separated wall will be provided by the rest of the walls through the tensile stress in the wire mesh. This will be helpful for preventing the collapse of the separated wall as well as the building as a whole. Also, the limited deformation to the wall will be favourable for supporting the floor or roof.

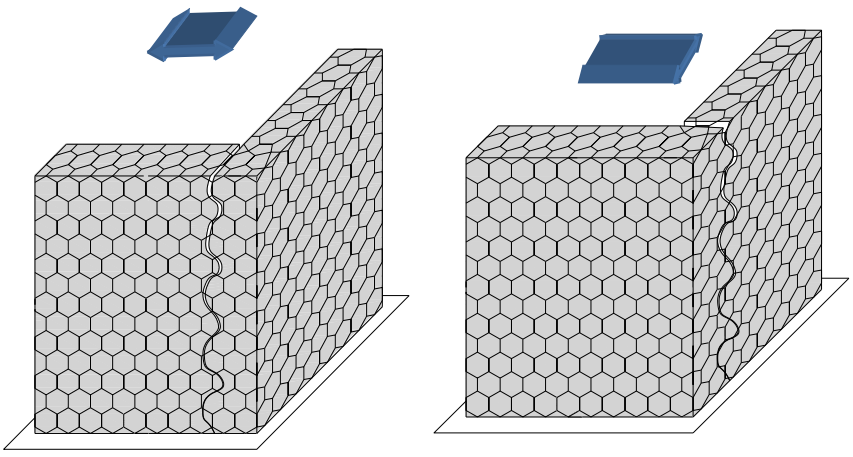

Figure 3.11 Reinforcement improves corner separation

3.7 **Summary**

The origin of the concept of this research goes back to the Kashmir Earthquake, which occurred in 2005. In the aftermath of the Kashmir Earthquake (8 Oct 2005), a team of professionals from Sydney, started thinking whether the rubble filled gabion can be useful for clearing the rubble left behind the earthquake disaster as well as building a new earthquake resistant house. This main idea was further refined and various alternatives were explored in this research. Eventually, a system of reinforcement scheme using GSW has been proposed.

Two methods were developed for fabricating the reinforcement system: direct weaving method and using pre-fabricated mesh method. Mesh connection technique was a significant step achieved during developing pre-fabricated mesh method.

The reinforcement scheme consists of establishing a continuous cage of reinforcement mesh around each and every wall. This reinforcing system has several inherent advantages. It is based on simple techniques, easy to transport, durable, highly thermal resistant, can be accommodated in any shape of wall and tightly fitted to the wall.

The basic working principle of GSW reinforcement system is to allow controlled damage to the wall but maintaining the overall stability of the building during the seismic events. In this way, it is very likely to reduce the most common seismic deficiencies of traditional stone masonry houses, which will be observed through experimental investigation in next chapter.

4. Experimental Investigation: Part I

This chapter includes the details about materials collection, preparation of the specimens for finding the material properties and testing on the specimens. The materials were selected to represent situations in rural and hilly areas around the world, where strict implementation of safer building policy is not enforced. The reasons behind such selection criteria are associated with the potential target group of this research as mentioned in Chapter 3. Specimens were prepared and tested based on specifications available in the standard codes as given in section 2.7 with due considerations to other research activities mentioned in sections 2.8. Specifications for some of the specimens were not covered in the standard codes. In such cases, few modifications were incorporated in preparing the specimens.

4.1 Collection of materials

Stone, mud, galvanized steel wire and timber were used to prepare specimens in this research. Though the stone and soil are both natural materials, it was very hard to find a supplier for these materials in Sydney. Five different sites were visited in order to find a suitable type of stone and soil for this research. Most of the stone suppliers were supplying either fully dressed stones or stone for paving purposes. Eventually, a sand stone quarry was approached located at Glenorie, NSW. Stone pieces of various sizes and shapes were randomly chosen (Figure 4.1 a). Random rubble was selected because this type of stone walling is the most common construction practice. As preparation of rubble for building a wall requires less effort as compared to fully dressed stone, it is an economically viable option.

(a) Rubble

(b) mud mortar soil

Figure 4.1 Major construction materials used in this research

In every site visited for the stone samples, soil for mud mortar was also investigated, but suitable soil was not available. In addition, a construction site was also

approached for the soil dug during excavation. However, due to some legal reasons, the site manager was hesitant to provide the excavated soil. Finally, mud mortar soil was brought form Nowra, NSW (Figure 4.1 b). Galvanized steel wire mesh and timber were purchased from the local market. After all required materials were secured, preparation of specimens commenced.

4.2 Preparation of specimens

All specimens were prepared in the laboratory. A considerable amount of time and effort have been invested by the author for the preparation of the specimens. Initially, specimens for testing the properties of mud mortar and stone were prepared. Then, specimens for testing the properties of wall in static test were constructed, followed by the specimens for shake table testing.

4.2.1 Mortar specimens

From the literature, it has been observed that mud mortar specimens are not separately prepared and tested. In the case of adobe, similar materials are used for both mud bricks as well as mud mortar. Therefore in such cases, there is no reason for a separate study on mud mortar.

In the current research, it was not logical to prepare mud bricks for the study of mud mortar. Therefore, it was decided to adapt the specifications for the hardened mortar with some modifications for preparing mud mortar specimens.

In order to determine the flexural strength of mud mortar, nine mortar prisms were prepared using steel moulds of size 285 mm x 75 mm x 75 mm (Figure 4.2). Because

of the fragile nature of mud mortar, a larger depth and width were chosen compared to the size of specimens specified in the code (BS EN 1015-11:1999).

The mould with a base was chosen for achieving a smooth bottom surface. Potable water was thoroughly mixed with the mortar soil to prepare mud mortar. Based on visual observations and with few trials, about 23 % moisture content was found to be appropriate for the type of soil used in this experiment.

Figure 4.2 Mud mortar specimens for flexure test

Using both palms some prepared mud mortar was rolled into a roughly cylindrical shape and dropped from about 30 cm to the mould for self-compaction. The wet mortar was compacted by hand tamping to ensure all corners are properly filled. Excess mortar was scraped off using a straightedge to provide a level surface. After a week, sides of the moulds were removed, allowing the mortar prism dry laying on

the base over four weeks in the laboratory environment. Usually, the top surface of the mortar prism gets uneven due to shrinkage (Figure 4.3).

Figure 4.3 Undulation on the top surface of mortar prism

Though the sides of the prism, which are in contact with the mould are smooth, these surface get slanted due to shrinkage. Therefore, there will not be full contact with the loading arm if such prisms are tested by placing casted sides over the support. Therefore, the uneven top surface of the mortar prism needs to be prepared before testing. A method was developed for that purpose in this experiment. After letting the mortar prism dry for three weeks, the top surface was prepared removing its undulation. For that purpose, the mortar prism was removed from the mould and a packing of steel plates (70 mm x 285 mm) of about 4 mm thickness was placed on the base of the mould and mortar prism were placed back on the plate. The steel

plates at the bottom of the specimen help to counterbalance the reduced height of mortar prism due to shrinkage. Both longer sides of the moulds were brought closer to the mortar prism and gently tightened with clamps on both ends (Figure 4.4). Care should be taken to ensure the clamp is just tight enough for holding both plates. Otherwise, the specimen may be broken.

Figure 4.4 Preparation for removing uneven part on top surface of mortar prism

In this stage, the top edges of the side plates of the mould should not be higher than the lowest height of the mortar prism. The undulating part of the mortar prism above the sides of the moulds was removed gently using a fine file. With few trials, it was found that the least disturbing strike of file could be achieved by adopting the following procedures.

At first, the file should be held at an inclined angle of approximately 45^0 with the top surface of the mortar prism. Starting from one side of the mortar prism at the middle length, the strike of the file should be sideways. As some parts of the mortar prism starts crumbling away, the inclination of the file should be lowered gradually until the rubbed part reaches the middle width of the prism. After that, the filing should be flipped to another side of the mortar prism just opposite to the initial strike. By following the same procedures, whole undulating part can be removed. Finally, the top surface is smoothened by holding the file horizontally on the top of the specimen and gently moving the file forward and backward along the length of the prism. The horizontal strike should always be from end to the middle of the prism in order to avoid breakage at the end of the specimen.

After removing the uneven top part, the dust should be removed with soft brush. Gentle blowing can also be helpful. Filing removes most of the undulations, but it will not ensure a smooth surface because of sand particles present in the mortar soil. Therefore, a thin layer of soil mortar paste was applied on the top.

For preparing mortar paste, some mortar soil was sieved through a 600 μm sieve. Half of the sieved soil was mixed with some water to get a paste. Some quantity of mortar paste was taken on a palm and a ball was formed rolling between both palms. This ball was placed on the top of the mortar prism and rolled back and forth. It created a thin layer of mortar on the top of the mortar prism. This process was carried out along the entire top surface. Excess mortar was removed with a straightedge. On top of it, some dry sieved soil was sprinkled and gently pressed with the straightedge (Figure 4.5). This process was done to reduce moisture content of the top layer so that it will not crack while drying. Then, clamps were released and

sides of the mould removed. The prepared specimens were left to dry for another week.

Figure 4.5 Mud mortar prism with a smooth top surface

4.2.2 Stone specimens for compression test

The test specimens for determining the compressive strength of stone were prepared as standard cubes of size 50 ± 5 mm edges (BS EN 1926:2006) using a diamond saw. Similar type of specimens with a larger size were used by Rao, Reddy and Jagadish (1997).

Twelve sandstone samples were prepared with axis of specimens normal to the bedding planes (Figure 4.6). These specimens were tested without using strain gauges. Another set of three specimens was prepared on which strain gauges were attached in order to measure the strain.

(a) Stone cubes without strain guage

(b) Stone cube with strain gauge

Figure 4.6 Stone samples for compression test

4.2.3 Stone specimens for flexure test

Ten specimens were prepared for determination of flexural strength of natural stone under a concentrated load (Figure 4.7). As per provisions in the code (BS EN 12372:2006), dimensions of the specimens were chosen. The dimensions of the specimens were maintained within the limit prescribed in the code (25 mm ≤ thickness ≤ 100 mm; 50 mm ≤ width ≤ 3 x thickness; length ≥ 6 x thickness).

Figure 4.7 Stone specimens for flexure test

4.2.4 Specimens for galvanized steel wire

Specimens were prepared from a straight portion of steel wire. The original cross sectional area was calculated by measuring diameter of the wire at two orthogonal directions (AS 1391 - 2007) without removing the galvanized layer.

4.3 Material testing

4.3.1 Plastic limit and liquid limit test of mortar soil

The type of soil used as mortar for preparing wall specimens was determined using plastic limit test and liquid limit test according to Australian Standards (AS1289.3.2.1-2009) and (AS 1289.3.1.1-2009) respectively.

For plastic limit test, a sample of about 40 g of soil obtained passing through 425 μm sieve was taken in a bowl and mixed thoroughly with potable water. The soil mass was kneaded until it becomes homogeneous and soft enough to be shaped into a ball. Then the sample was covered and allowed to cure for 24 hours at room temperature.

A ball of soil of about 8 g was taken and moulded between fingers to form a ball. Then, it was rolled between palms until slight cracks appeared on its surface. The ball was further rolled between palm and glass plate to form a soil thread of about 3 mm diameter. When the soil thread rolled down to 3 mm diameter without crumbling, thread was gathered, kneaded down and re-rolled again. This process was repeated until the thread crumbled when it reached 3 mm in diameter (Figure 4.8). Then, the crumbled portion was gathered into a container and covered with a lid. Repeating the same process, two sets of crumbled threads of about 5 to 10 g were gathered. The moisture content of the soil was determined using oven drying method (AS 1289.2.1.1-2005). The plastic limit of the mortar soil was obtained as 18%.

Figure 4.8 Figure Soil specimen during plastic limit test

Soil sample of about 250 g of soil was prepared and cured for 24 hours for liquid limit test following the similar process as in plastic limit test. A portion of the prepared soil sample was placed in the cup of liquid limit apparatus and levelled it parallel to the base using enough downward pressure from the palette knife. A depth of soil of about 10 mm was prepared. Holding the grooving tool normal to the surface of the cup and drawing along the centre line of the bowl, a groove was formed dividing the soil into two parts. Then, the crank was turned at the rate of 2 revolutions per second until the two parts of the soil came into contact along the bottom of the groove for a distance of 10 mm (Figure 4.9).

Figure 4.9 Soil specimen during liquid limit test

For the first trial, the number of blows was above 40. Therefore, soil was replaced back into the bowl, some water was added and the soil was remixed for about 3 minutes. Cup of the apparatus and grooving tools were cleaned and dried. This process was repeated until the required number of blows for closure was within 30 to 40. After getting the number of blows in this range for the first time, the process was repeated once more without adding water to ensure the compatibility of the test. The number of blows was recorded, when the difference in the number of blows in two consecutive tests was not more than one. Then, about 10 g of soil was removed with a spatula from the portions of the sample where two sides just came together and moisture content was determined using oven drying method (AS 1289.2.1.1-2005).

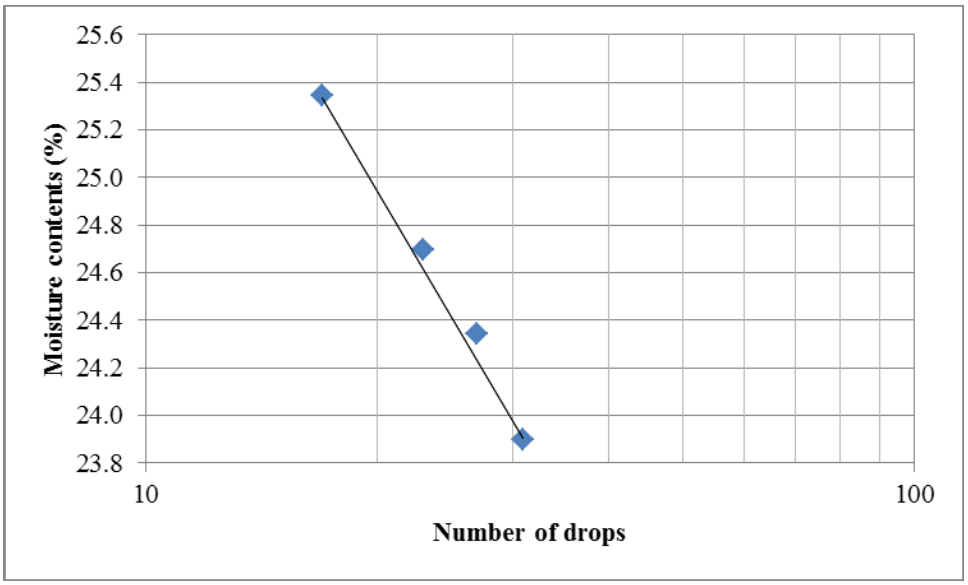

Figure 4.10 Liquid limit test result

The process was further repeated adding some water and thoroughly mixing it for about three minute so that the number of blows lies in the range of 40 to 15. A graph was plotted on a semi logarithmic chart with the percentage of moisture as ordinates on the linear scale and the number of blows as abscissa on the logarithmic scale. A line of best fit was plotted through the points and liquid limit was determined as the moisture content corresponding to 25 blows on the abscissa (Figure 4.10). This graph shows that the liquid limit of the soil used in this research was 25%.

4.3.2 Sedimentation test of mortar soil

The composition of the soil was determined following the procedures mentioned in the sedimentation test (HB 195 - 2002). This test was included in this study because it can be done in the field.

Figure 4.11 Sedimentation test

Some loose sample of the soil was kept in a glass jar of 500 ml capacity and filled with potable water. The jar was sealed and allowed the water to completely soak into the soil. Then, it was vigorously shaken for about two minutes and left undisturbed for one hour. After that, it was re-shaken for about a minute and placed on a firm flat surface out of direct sun light for about 24 hours for sedimentation. The height of each layer of sand, silt and clay was measured as shown in Figure 4.11.

Table 4.1 Sedimentation test results

Composition	Height, mm	Percentage
Clay	5	14
Silt	7	20
Sand	23	66
Total	35	100

The result showed that the mud mortar soil sample was composed of 14% clay, 20% silt and 66% sand (Table 4.1).

4.3.3 Sieve Analysis of mortar soil

The composition of the soil was also studied using sieve analysis (Australian Standard AS 3638-1993). The main purpose of this test was to provide a reference which may be useful for comparison in future studies.

Figure 4.12 Sieves under mechanical shaker

Some mortar soil was dried in the oven for 24 hours at 105^0 C. A set of sieves with aperture sizes varying from 4.75 mm to 75 μ m was chosen and cleaned. Weight of each sieve was noted. Then, all the sieves were stacked in descending order of their apertures with a pan at the bottom. An oven dried soil sample of 500 g was placed on

the top of a set of sieves. The whole set was transferred to a mechanical shaker (Figure 4.12). After shaking for 15 minutes, the weight of each sieve was noted again and the material retained on each sieve was determined.

When compared with results from sedimentation test, it was found that the material passing through 75 μ m sieve was much less. The reason behind such large discrepancy might be due to fine clay particles sticking around the sand particles. Therefore, material retained on each sieve was washed with water successively through a nest of sieves with the finest at the bottom. The suspension passing through the coarser sieve was transferred to the immediate next sieve. This process was repeated until the water passing through the sieve was clear. Then, all sieves were left for air drying followed by oven drying process at 105^0 C for 24 hours. The weight of each sieve was measured and the material retained on each sieve was determined (Table 4.2). The particle size distribution curve of the above result was plotted as shown in Figure 4.13.

Table 4.2 Wet sieve analysis results

Sieve size Particle Diam.(mm)	Mass of empty sieve (g)	Mass of sieve + soil (g)	Mass Retained (g)	Percent Retained (%)	Cumulative Percent Retained	Percent Passing (%)
4.750	405.60	410.70	5.10	1.02	1	99
2.360	390.80	409.50	18.70	3.74	5	95
1.180	350.80	378.80	28.00	5.60	10	90
0.600	316.90	372.50	55.60	11.12	21	79
0.425	297.80	371.90	74.10	14.82	36	64
0.300	289.60	338.80	49.20	9.84	46	54
0.150	268.30	332.30	64.00	12.80	59	41
0.075	259.80	306.70	46.90	9.38	68	32
Pan	449.60	607.90	158.30	31.67	100	0
Total			499.90			

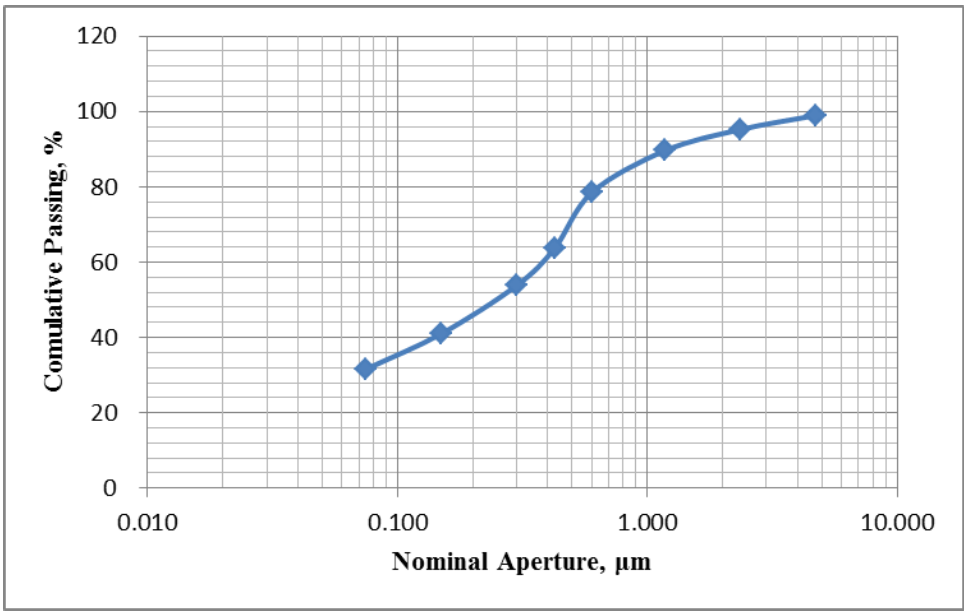

Figure 4.13 Particle Size Distribution Curve

4.3.4 Flexural strength of mud mortar

The procedure for bending test was adapted from British Standards (BS EN 1015-11:1999). The flexural strength of mud mortar was determined using three point bending test (Figure 4.14).

The span was set as 200 mm between roller supports. The displacement controlled load was applied at a uniform rate of 0.2 mm/min. The maximum load applied, F was noted (Table 4.3). The flexural strength was calculated using Equation (2.2). The contribution of self-weight of the beam to the flexural stress was 8 kPa, which was neglected.

Figure 4.14 Mud mortar beam under flexure test

Table 4.3 Flexural strength of mud mortar

Sample	Span	Breadth	Depth	Load	Stress
	mm	mm	mm	N	MPa
1	200	74.4	70.3	568	0.46
2	200	73.8	70.7	590	0.48
3	200	74.2	70.6	638	0.52
4	200	74.0	70.6	560	0.46
5	200	72.7	70.6	543	0.45
6	200	72.6	70.5	535	0.45
7	200	72.9	70.5	556	0.46
8	200	73.7	70.8	587	0.48
9	200	74.3	70.5	577	0.47
Average					0.47
Coefficient of Variation					4.25%

In addition, the mid-span deflection was measured using a LVDT during the test. The modulus of elasticity, E, of the mortar prism was calculated considering the

mid-span deflection, Δ, composed of bending as well as shear deflection (Newlin & Trayer 1956).

$$\Delta = \frac{Pl^3}{48EI} + \frac{0.375Pl}{AG} \quad (4.1)$$

where,

P = Point load

l = span

I = second moment of area

A = area of cross-section

G = modulus of rigidity = E/(2(1+ν))

ν = Poisson's ratio

Mid span deflection data from all specimens were plotted and a curve of the best fit was drawn (Figure 4.15). The slope of the curve (P/Δ) was used in the above equation to calculate the modulus of elasticity. With variation of the value of ν from 0 to 0.5, the corresponding value of E changes from 847 MPa to 962 MPa. On average, the modulus of elasticity can be taken as 900 MPa with the corresponding Poisson's ratio of 0.23.

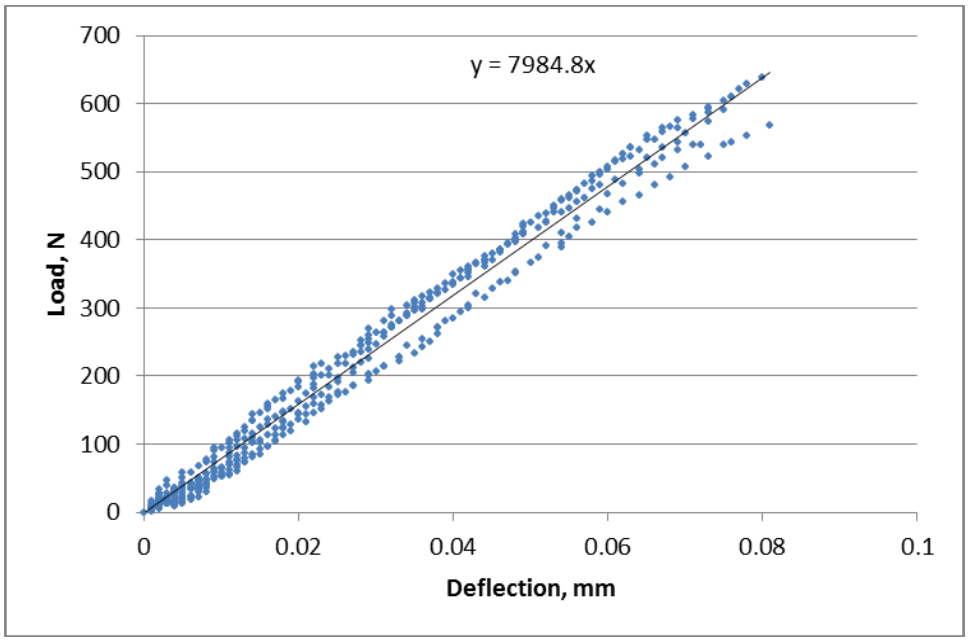

Figure 4.15 Load deflection curve of mortar prisms

4.3.5 Compressive strength of mud mortar

After the flexural strength test, each half of the broken mortar prism were used for compressive strength measurement (BS EN 1015-11:1999). Any loose grit or other materials were removed from the sides. Two bearing plates of size 75 mm x 75 mm x 10 mm were used one at the bottom and the other at the top of the specimen (Figure 4.16). The specimen was arranged in such a way that the cast end was 16mm±0.1 mm from the nearer edge of the platens or bearing plates. The Load was applied at a constant rate of 1 mm/min until failure occurred (HB 195 - 2002) and maximum load was noted (Table 4.4). Two specimens were discarded during testing because of some technical problems.

(a) During testing

(b) After testing

Figure 4.16 Mortar specimen under compression test

Table 4.4 Compressive strength of mud mortar

Sample	Length mm	Breadth mm	Height mm	Load kN	Stress MPa
1	75.0	73.5	70.3	8.978	1.63
2	75.0	74.2	70.2	8.522	1.53
3	75.0	73.9	70.7	8.129	1.47
4	75.0	73.3	70.5	9.427	1.71
5	75.0	74.0	70.6	8.540	1.54
6	75.0	73.9	70.6	8.564	1.55
7	75.0	72.2	70.5	8.695	1.61
8	75.0	73.5	70.6	8.703	1.58
9	75.0	72.7	70.5	8.523	1.56
10	75.0	72.8	70.6	8.938	1.64
11	75.0	72.3	70.5	8.316	1.53
12	75.0	73.0	70.4	7.864	1.44
13	75.0	73.7	70.9	8.095	1.46
14	75.0	73.4	70.8	7.922	1.44
15	75.0	73.6	70.6	9.032	1.64
16	75.0	73.6	70.5	8.692	1.57
Average					1.56
Coefficient of Variation					5.1%

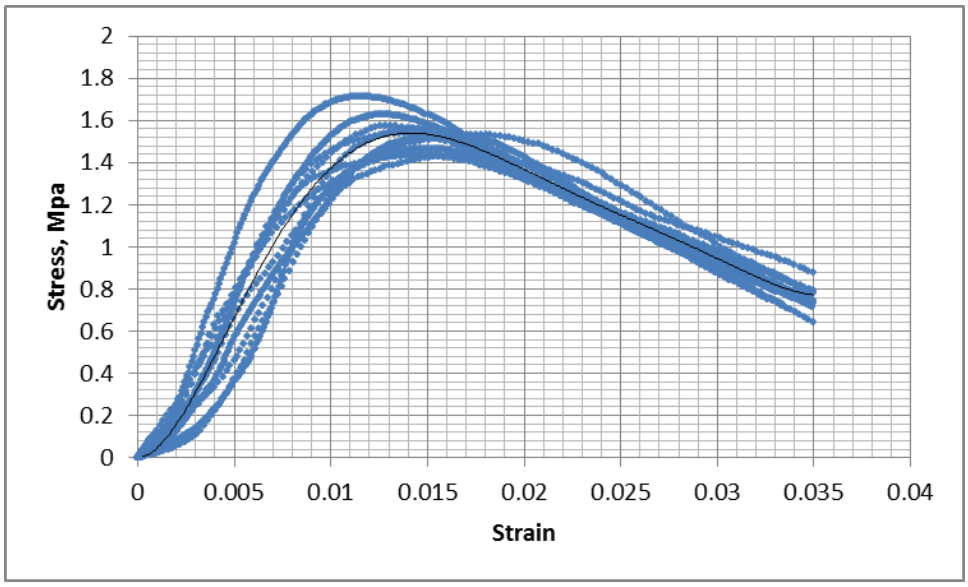

Figure 4.17 Stress strain diagram of mud mortar prisms in compression testing

Axial deformation was also measured using two LVDTs on each side of the mortar prisms and average deformation was calculated. The stress strain diagram was obtained as shown in Figure 4.17. From this curve, the elastic modulus between 30% to 60% ultimate stress seems to be 207 MPa.

A piece was taken from each mortar beam after the test. The moisture content of each of the samples was determined using oven drying method (Table 4.5). The moisture content was taken as a reference parameter as the strength of hardened mud mortar is highly susceptible to the moisture content.

Table 4.5 Moisture content of mortar samples

Sample	Wet g	Dry g	Water g	Moisture Content (%)
1	118.84	117.29	1.55	1.32
2	218.32	215.52	2.80	1.30
3	252.68	249.41	3.27	1.31
4	201.78	199.19	2.59	1.30
5	212.31	209.57	2.74	1.31
6	197.46	194.87	2.59	1.33
7	194.00	191.54	2.46	1.28
8	204.20	201.55	2.65	1.31
9	244.64	241.57	3.07	1.27
Average				1.30

4.3.6 Compressive strength of stone samples

The specimens prepared for the compressive strength of stone were allowed to dry in laboratory conditions for several days and tested under ambient condition. The moisture contents of the specimens were measured after the test. The logic behind testing in normal conditions was to create similar conditions of testing as in masonry testing so that results could be compared. The cross-sectional dimensions of the test

specimen were measured to the nearest 0.1 mm by averaging two measurements taken at right angles to each other at about upper height and lower height. The height of the specimen was also determined to the nearest 0.1 mm (BS EN 1926:2006).

The bearing surfaces of the testing machine were wiped and bed faces of the specimens were cleaned. The specimen was carefully aligned with the centre of the platen (Figure 4.18).

Figure 4.18 Stone cube under compression test

Load on the specimen was applied continuously at a constant rate of 0.25 mm/min and the maximum load was recorded (Table 4.6). The failure pattern was brittle leaving the central core as shown in Figure 4.19. The uniaxial compressive strength of the specimen was calculated using Equation (2.1).

Figure 4.19 Specimen after failure

Table 4.6 Compressive strength of stone

Sample	Length mm	Breadth mm	Height mm	Load kN	Stress MPa
1	49.6	49.5	49.6	83.7	34.13
2	49.3	49.3	49.7	89.5	36.86
3	49.6	49.6	49.8	100.3	40.85
4	49.4	49.5	49.5	100.8	41.26
5	49.2	49.2	49.4	88.9	36.76
6	49.2	49.3	49.0	97.2	40.11
7	49.7	48.3	49.2	65.9	27.48
8	49.4	48.2	49.2	85.8	36.03
9	49.4	49.4	49.5	85.4	34.99
10	49.6	49.4	50.0	100.0	40.85
11	49.2	49.1	49.5	95.6	39.61
12	49.5	49.7	49.7	87.4	35.56
Average					37.91
Coefficient of Variation					7.01%

In Table 4.6, the strength of sample 7 deviates more as compared to other samples. Hence, it was discarded while calculating the average and coefficient of variation. The moisture content of each sample at the time of testing was determined by oven drying method. The weight of a broken piece from each of the samples was measured after the test. It was kept in the oven for 24 hours at (100±5) ^{0}C and the dried weight was again measured. The moisture content was found to be insignificant (Table 4.7).

Table 4.7 Moisture content of stone sample

Sample	Air dried wt g	Oven dried wt g	Wt of water g	Moisture content (%)
1	43.61	43.52	0.09	0.23
2	38.72	38.61	0.11	0.26
3	44.00	43.90	0.10	0.23
4	63.10	63.02	0.08	0.13
5	70.03	69.90	0.13	0.19
6	91.60	91.20	0.40	0.44
7	65.50	65.30	0.20	0.31
8	36.21	36.09	0.12	0.33
9	71.14	71.00	0.14	0.20
10	48.54	48.42	0.12	0.25
11	65.32	65.10	0.22	0.34
12	82.10	81.80	0.30	0.37
Average				0.27

Axial strain was measured on another set of three specimens using polyester foil strain gauge of length 30 mm. However, one of the specimens was discarded because of unusual results caused by some technical problem. The remaining results are shown in Figure 4.20. From this graph, the elastic moduli in the range of 30% to 60% of ultimate stress of samples 1 and 2 are 16.5 GPa and 14 GPa respectively.

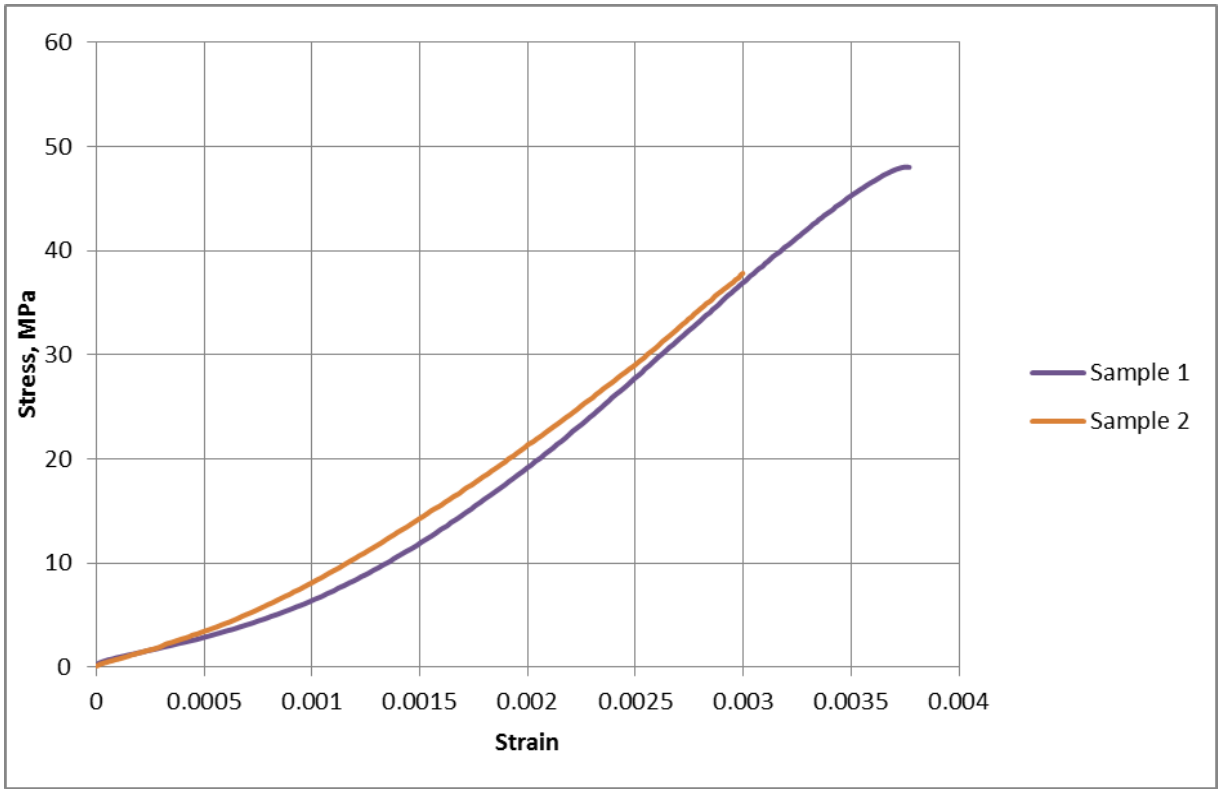

Figure 4.20 Stress strain curve for two stone samples

4.3.7 Flexure strength of stone samples

After preparing specimens for bending test of stone, the specimens were dried at ambient temperature for several days in laboratory conditions. The specimens were tested under three point loading (BS EN 12372:2006). Before testing, the surface of the rollers and the specimens were cleaned and specimens were placed centrally on the supporting rollers (Figure 4.21). The load was applied uniformly at 0.22 mm/min until the failure of the specimen. The flexural strength was calculated using Equation (2.2).

Figure 4.21 Bending test of a stone specimen

These results are shown in Table 4.8. The fracture was observed directly beneath the point load in all specimens.

Table 4.8 Flexural strength of stone samples

Specimen	Span (*l*) mm	Depth (d) mm	Width (b) mm	Load (F) N	Stress MPa
1	225	45.7	77.3	1671	3.5
2	225	42.6	77.9	1710	4.1
3	225	36.8	74.5	1265	4.2
4	225	43.4	72.6	3765	9.3
5	225	40.2	59.7	2453	8.6
6	225	45.7	77.2	1817	3.8
7	225	43.7	77.2	1284	2.9
8	225	34.9	77.6	740	2.6
9	225	44.9	77.0	947	2.1
10	225	42.6	74.5	1418	3.5

The flexural strengths of specimens 4 and 5 are comparatively higher than other specimens. Excluding these values, the average bending strength of the stone specimen was obtained as 3.3 MPa.

The moisture content of the specimen at the time of testing was measured using oven drying method (Table 4.9).

Table 4.9 Moisture content of stone specimens for bending test

Specimen	Wet weight (g)	Dry weight (g)	Moisture content (%)
1	2037.52	2021.96	0.77
2	2034.24	2017.42	0.83
3	1669.89	1659.85	0.60
4	2140.49	2123.14	0.82
5	1626.98	1614.12	0.80
6	2047.57	2041.67	0.29
7	1858.47	1854.50	0.21
8	1693.62	1686.04	0.45
9	2245.80	2231.35	0.65
10	2006.18	2001.42	0.24
Average			0.57

4.3.8 Tensile strength of galvanized steel wire

Galvanized wire specimens were fixed to the tensile testing machine using proper gripping device in such a way that the axis of the specimens were coincident with the centre line of the head of the testing machine. The original gauge length was taken as 200 mm (AS 1391 - 2007). The specimens were loaded at a constant rate of 90 mm/min (0.0075/s) until fracture (Figure 4.22).

Figure 4.22 Tensile strength testing of steel wire

The maximum force was noted and the corresponding stress was calculated as the tensile strength of the specimen (Table 4.10).

Table 4.10 Tensile strength of galvanized wire specimens

Specimen	Diameter, mm	Load, N	Tensile strength, MPa
1	0.60	113.4	401
2	0.60	115.7	409
3	0.60	108.2	383
Average			398
1	1.0	299.0	381
2	1.0	309.1	394
3	1.0	303.0	386
Average			387

4.4 **Summary**

Randomly selected sand stone pieces, mud mortar soil, timber and galvanized steel wire were collected for the experimental investigation. As the properties of timber were not the major concern of this research, testing on other three building materials were included in this research.

The plastic limit and the liquid limit of the soil sample for mud mortar was observed as 18% and 25% respectively. The soil was composed of 14% clay, 20% silt and 23% sand as determined through sedimentation test.

In order to determine the flexural strength of mud mortar, nine mortar prisms were prepared using steel mould of size 285 mm x 75 mm x 75 mm and tested in three point bending. The average flexural strength was observed as 0.47 MPa. A method was developed for removing the undulation on the top surface of the mud mortar prism caused by shrinkage. As a result, consistent results were obtained.

The compressive strength of mud mortar was determined by conducting compressive strength test on each half of the prism after bending test. The average compressive strength of mud mortar was 1.56 MPa. The modulus of elasticity of the mortar prism in compression was observed as 207 MPa.

Twelve sand stone specimens (standard cubes of size 50 ± 5 mm) were prepared for determining the compressive strength of stone. The average compressive strength of the stone specimens was obtained as 38 MPa. The modulus of elasticity of the stone specimens was 15 GPa. Ten stone prisms (25 mm $\leq$ thickness $\leq$ 100 mm; 50 mm $\leq$ width $\leq$ 3 x thickness; length $\geq$ 6 x thickness) were prepared and tested in three point

bending. The results of two specimens were relatively higher than other results. Therefore, these two values were discarded to get the average bending strength of 8 prisms as 3.3 MPa.

The average tensile strength of three specimens of galvanized steel wire was observed around 400 MPa.

[Blank Page]

5. Experimental Investigation: Part II

In this chapter, preparation of wall specimens for static and dynamic testing are covered. This is followed by the procedures followed in testing. The wall specimens were prepared and tested with due considerations to available standard methods presented in section 2.7 and other research activities as given in section 2.9 and section 2.10. As the testing procedures on rubble masonry built with mud mortar are barely covered in the research activities and the existing Standards, several modifications were incorporated in preparing the specimens and testing.

5.1 Wall specimens for static test

Since testing methods of rubble masonry in mud mortar were not covered in any standards, testing procedures and dimensions of the specimens were adapted based on the British Standards (BS EN 1052-1:1999 and BS EN 1052-2: 1999). Some additional information is also included in this code, which is not provided by other standards. For instance, specifications for the size of specimens are given based on the dimension of masonry units (Table 2.2). This was the main reason for choosing this code.

On the other hand, preparing each and every piece of stone was necessary for using it to build a wall specimen. The randomly collected lump of stones was composed of rubble of various sizes and shapes. Large pieces of stones were broken down in to handy sizes using hand tools such as hammer and brick bolster.

In addition, a smooth surface of the wall was necessary for ensuring a constant cross-section throughout the height of wall specimen. Also, a full contact along the support as well as along the loading strip was necessary. Therefore, every piece of stone was cut along one side using a diamond saw whereas the corner stone was cut along two adjacent orthogonal sides (Figure 5.1). The other sides of the stone were left undisturbed so that it could have represented the behaviour of a rubble wall.

Moreover, due considerations were taken for reflecting an owner-builder construction mode during the preparation of wall specimens. This approach was considered to address the intended user groups of this type of wall. Targeting to the construction practice, where owners themselves build their houses with little or no support from local builders is in accordance with the prime goal of this research.

(a) Stone for general use (b) Corner stone

Figure 5.1 Prepared stone blocks

5.1.1 Wall specimens for compression test

Three specimens were prepared for the compression test of the wall as specified in British standard (BS EN1052-1:1999) for regular masonry unit. The dimensions of the wall were finalised considering various parameters as given below.

Using random rubble, it is not practicable to build a wall with a single vertical layer of stones. All types of specimens used by other researchers for testing in compression included in section 2.9.3 are not suitable for rubble masonry.

Therefore, a wall specimen with two vertical layers was chosen with a thickness of 350 mm. This was selected on the basis of the minimum thickness of rubble wall being used in practice (NBC 203: 1994). The length of the specimen was selected as 500 mm (2 x length of a masonry unit). It was assumed that the maximum length of the stone piece was 240 mm. The specimen height was taken as 1050 mm (three times the wall thickness). Comparing to the specimen (length 500 mm, thickness 300 mm and height 400mm) used by Gracía et al. (2012), only the length was similar.

The wall specimen was built on a steel plate of dimension 700 mm x 450 mm x 25 mm. Mud mortar was prepared using potable water with about 23% moisture content. In order to maintain it within this limit, the moisture content of the soil was determined and the required amount of water was calculated to get the target value of moisture content. The soil was weighed and a measured quantity of water was added. Finally, moisture content of the fresh mortar was tested for confirmation using oven dry method (AS 1289.2.1.1-2005). It was found to be within the target range.

A working platform with a steel plate on the top was levelled and a sheet of builder's plastic was laid. A wall specimen was built over the sheet using stones laid in mud mortar with thicknesses of 20 – 30 mm similar to adobe wall construction (HB 195 - 2002). The stone laying process was followed as one stone over two stones or two stones over one stone to avoid the continuous joint along the height and sometimes two stones over a single stone (Maxlow & Maxlow 1984; McAfee 2001) were also used to match with adjacent rubble. While laying the stones, the smooth surface was maintained along the face of the wall. The irregular gap between two adjacent vertical layers of stone blocks was filled with mud mortar and small pieces of stones ensuring the most stable position of each and every stone. During the construction of the wall, a metal plate (120mm x 20 mm x 5mm) was inserted (about two third of its length) horizontally at a height of two layers of stones, lying exactly at the centre of wall thickness at both ends for measuring axial deformation. Similar provisions were made at the height of the wall just below two layers of stones from the top of the wall.

Creating a smooth surface at the top end of the wall was a great challenge for rubble masonry due to irregular shape of stones. In order to solve this problem, a layer of mud mortar was laid at the top of the wall and a piece of 17 mm thick form plywood of a size similar to the cross-section of the wall was placed over it. This plywood was firmly pressed against mortar. Then, it was levelled properly using a spirit level and gently striking with a rubber mallet from the top. The wall specimens were left for curing in air over four weeks in the laboratory environment (Figure 5.2).

Figure 5.2 Wall specimens for compression test

5.1.2 Wall specimens for bending test in vertical span

The terminology “flexural strength of wall with reference (parallel or perpendicular) to bed joint” as in case of brick masonry is not suitable in rubble masonry because it does not necessarily contain a perfect horizontal bedding layer. Therefore, two new terminologies are proposed in this research to address the bending strength of walls: flexural strength of wall spanning in vertical direction and flexural strength of wall spanning in lateral direction.

The thickness and length of the specimen were selected as 350 mm and 500 mm respectively, as in the case of compression testing of walls. The height of the specimen was taken as 1400 mm. This dimension was finalised based on the

conditions specified in British Standard (BS EN 1052-2:1999). Considering the provisions of the codes as mentioned in section 2.7.6 of this thesis, the total height of the specimen was calculated.

Suppose, h is the spacing between support bearings, and the distance between the support and loading be 375 mm > 350 mm to be on the safe side;

h = 375+ 0.4 x h +375;

h = 1250 mm.

In addition, the code suggests that the distance between outer support bearing and the end of the specimen should be at least 50 mm. Thus, the total height of the specimen needs to be 1350 mm. Moreover, the wall section at uppermost support is likely to fail in shear due to inadequate compressive stress provided by just 50 mm wall height above it. Therefore, to avoid shear failure at the upper support, a layer of stone was added on the top of the wall. Thus, the total height of the wall specimen was around 1400 mm.

A platform was prepared using a plank of structural plywood of size 700 mm x 450 mm x 17 mm stiffened with a machine graded pine (MGP10) of size 95x45 at the base. The platform was levelled and a sheet of builder plastic was laid on the platform. The wall specimen was built over it following similar procedures mentioned in the last section (Figure 5.3). Five similar wall specimens were prepared. The wall specimens were left for curing in air over four weeks in the laboratory environment (Figure 5.4).

Figure 5.3 Wall specimen during construction

Figure 5.4 Specimen for flexure test in vertical span

In order to test the effectiveness of GSW reinforcement system, three similar specimens of each type, as mentioned above, were prepared and reinforcement was applied. One of the walls was reinforced by directly weaving the wire mesh around the wall and the other two walls were reinforced using prefabricated mesh as given below.

Various techniques can be developed while weaving the mesh directly to the wall. One such option was developed to prepare sample reinforcement in the laboratory. In this method, wooden handles were prepared for holding the wire. U-shape slots were made at each end of the handles with smooth edge to avoid kinks in the wire. A piece of wire (GSW of diameter 1.25 mm) of required length was cut. The wire was wrapped around two handles starting with one handle from each end and finished at half-length of the wire so that both handles were holding equal length of wire (Figure 5.5).

A strip of wire net was prepared, using twin wires at a spacing of 100 mm centre to centre, and laid on the top of the platform (foundation in the case of building site) as shown in Figure 5.6.

Over the net, a wall was built. A pair of connecting wires was inserted across the wall thickness in regular spacing (at least equal to wall thickness) along the horizontal and vertical directions during the construction of wall.

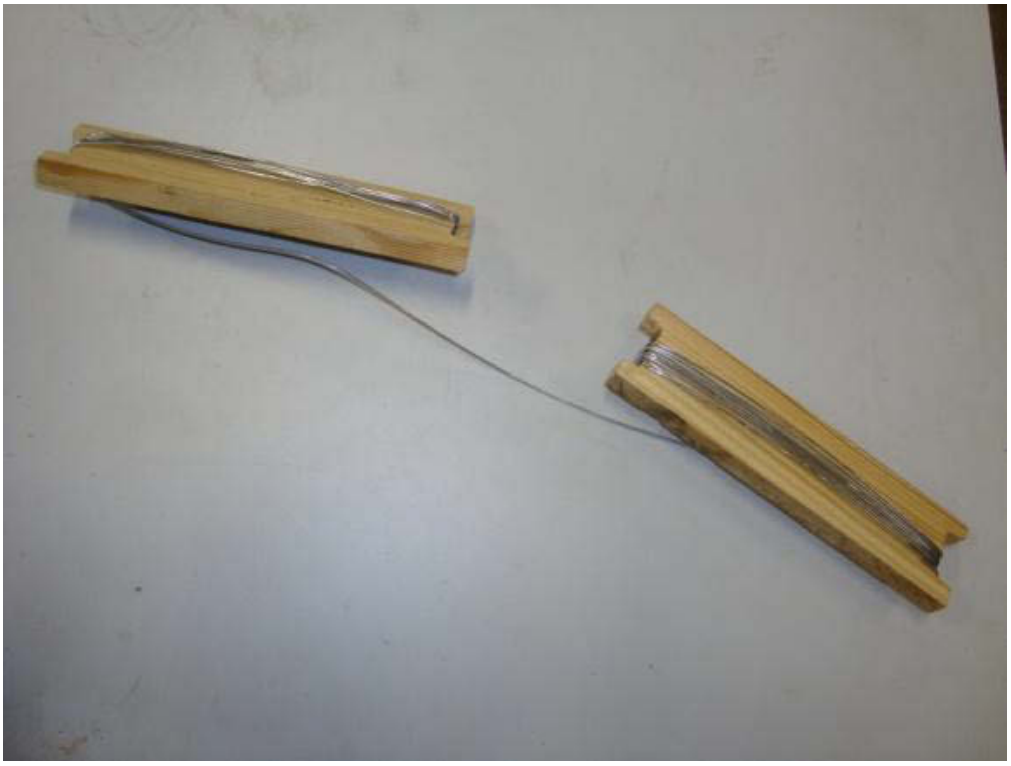

Figure 5.5 Wire wrapped around two handles

Figure 5.6 Wire net at the bottom of wall

Preparation for weaving of mesh started after the wall was complete. Before mesh fabrication, a dot was marked at the probable position of each node of the mesh along all sides of the wall. The positions of the nodes on the first row were marked at the middle of the spacing of twin wires and at a height equal to half of the spacing. The marks for the second row were located just above the position of the twin wires at the foundation at a height equal to the spacing of the twin wires. These positions were calculated for creating a square shape mesh.

In order to start mesh weaving, one wire from the twin wires was stretched to the right and double twisted with another wire stretched to left from the adjacent twin wires. The position of twist was maintained over location of the node marked on the

(a) First layer of nodes formation

(b) Second layer of nodes formation

(c) Weaving in progress

Figure 5.7 Reinforcement fabrication by direct weaving method

wall. This process was continued along the whole periphery of wall and repeated along the full height (Figure 5.7).

At the top of the wall, the twin wires were again brought together to form a thread and a net similar to the mesh at the bottom of the wall was created using wires from opposite sides. The mesh was attached to the wall using a pair of connecting wires inserted during the construction of the wall. A few pieces of smooth stones were inserted at the top of the wall to increase the tightness of the mesh. The completed reinforced specimen was as shown in Figure 5.8.

Figure 5.8 Reinforced wall specimen prepared by direct weaving method

The construction of reinforced wall specimen using prefabricated mesh was almost similar to the direct weaving method. After placing builder's plastic sheet over the levelled platform, strips of GSW mesh (hexagonal opening size of 50 mm across the flats, wire diameter 1 mm) of width slightly larger (at least by one mesh size on each side) than the thickness of the wall were laid. This mesh was the bottom mesh or foundation mesh of the wall specimen. The alignment of the bottom mesh should be such that the twisted side pointing outward from the face of the wall on each side (Figure 5.9). Over the mesh, a wall was built following the same procedures as in the case of unreinforced wall. A similar strip of GSW mesh was placed at an interval of 350 mm along the height.

Figure 5.9 Alignment of bottom mesh

(a) Inserted nail in the middle of untwisted sides of overlapped mesh

(b) First twist

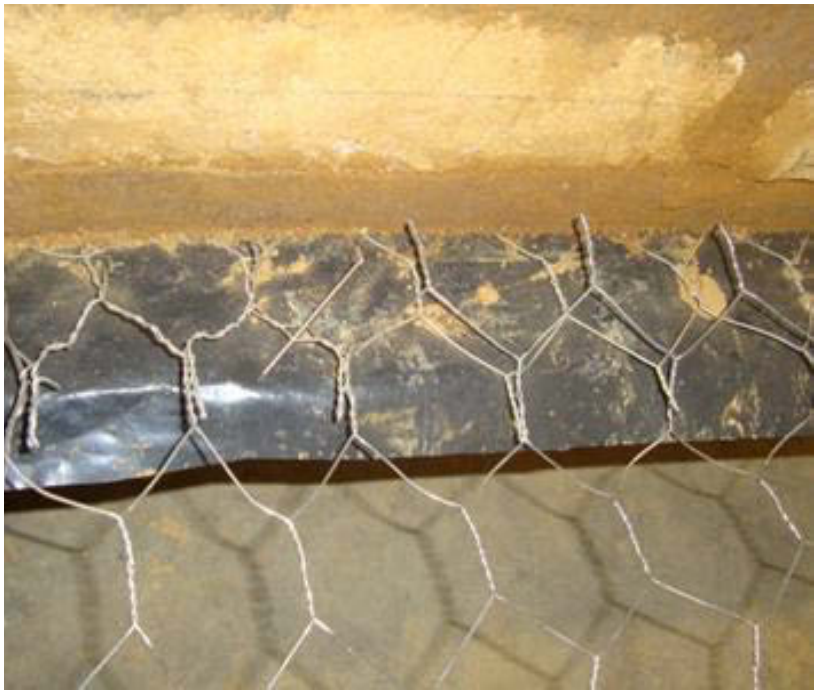

(c) Next twist

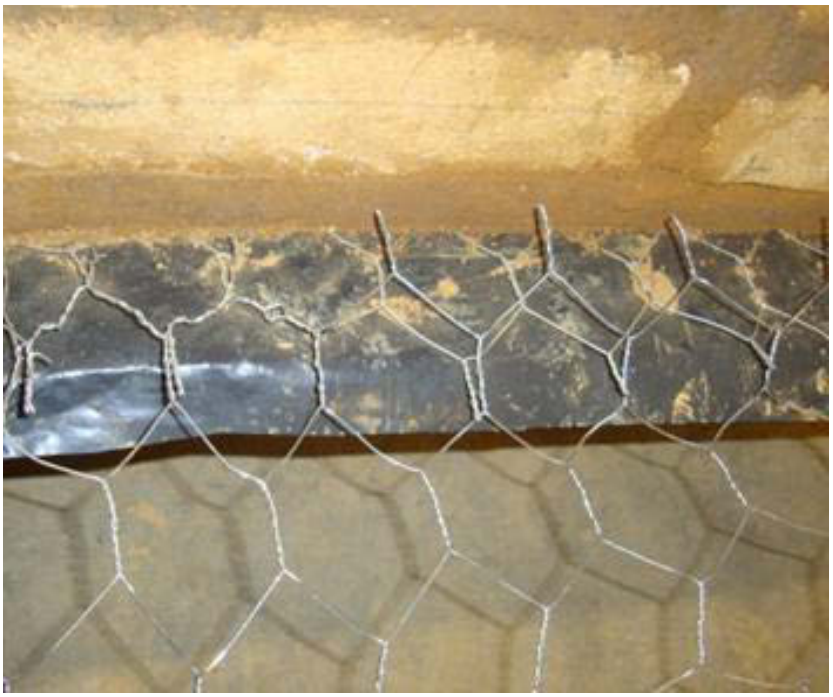

(d) Completed up to fourth side from left end

Figure 5.10 Steps for connecting meshes at the bottom

After completion of the wall, it was wrapped with GSW mesh reinforcement system. For that purpose, a strip of mesh of width equal to the side of the wall and length slightly greater than the height of the wall plus thickness of the wall was cut for each side of the wall. In this research, a simple technique was developed for connecting the wire meshes to each other effectively using a small slender object such as a nail.

Initially, meshes to be joined were overlapped up to the length of two cells in such a way that the untwisted side of the cell of both meshes fit exactly on top of one other. Then, a nail was inserted between the untwisted sides in the middle and the nail was turned to get the first twist. The nail was turned again to get the second twist. Following similar procedures, all meshes were connected to the meshes at the bottom (Figure 5.10).

After connecting meshes from all sides of the wall to the foundation mesh, meshes from opposite sides were brought closer to the wall and overlapped at the top. Excess length of the mesh beyond the other side of the wall was cut and meshes were joined at the top following similar procedures as in the case of bottom mesh (Figure 5.11). Four sides of a row of cells were joined to form a symmetrical joint. Then, sides of the adjacent meshes were joined to each other by twisting the vertical sides along the height of the wall (Figure 5.12). Finally, the wire meshes at opposite sides of the wall were tied to the wall using the twin wires of the strip inserted into the wall during the construction of the wall. The completed wall specimens are shown in Figure 5.13.

Figure 5.11 Connection of two meshes along the top of a wall

Figure 5.12 Connection of meshes along the side of a wall

Figure 5.13 Reinforced wall specimen using prefabricated mesh

5.1.3 Wall specimens for bending test in lateral span

The dimensions of wall specimens for bending in lateral span were chosen based on similar arguments for bending in vertical span. The thickness of the wall was taken as 350 mm and the length was 1400 mm. The height was adopted as 400 mm, which could accommodate at least 4 layers of stones as specified in the code (BS EN 1052-2:1999).

Testing of flexural strength of wall in lateral span was challenging. Due to two layers of stones joined by weak mortar along the thickness, allowing the specimen to slide on a smooth horizontal surface such as polytetrafluoroethylene sheet as in the case of brick masonry was not a good option. In addition, if the wall was allowed to slide

between two polytetrafluoroethylene sheets with some grease between them, the tensile strength of the sheet would have significant effect on the results because of low flexural strength of masonry. In order to solve this problem, a special method was developed.

In this method, a platform composed of two similar segments supported on spherical rollers was constructed so that it would offer very little resistance while moving in any direction. Each segment was similar to the bases used for bending test in vertical span as mentioned in previous section. However, in this case, each segment was supported on six spherical rollers each of 50 kg load bearing capacity.

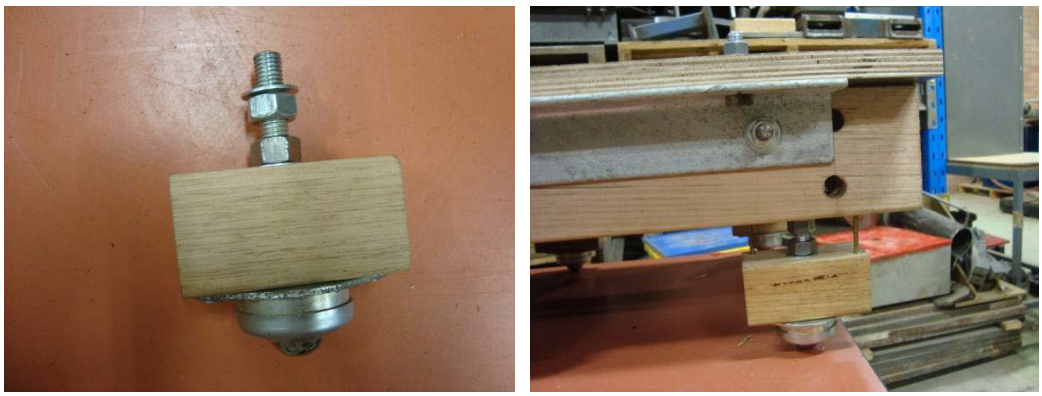

(a) Spherical roller support assembly (b) Connection details

Figure 5.14 A spherical roller support with a nut-bolt system

A purpose made spherical roller support with nuts (M10), washers and a bolt was fabricated and connected to the base segment through a 12 mm hole (Figure 5.14). The load on base segment was transferred to the bolt via upper nut and washer. The height of the base segment could be adjusted by turning the upper nut for levelling purposes. Initially, two segments were properly levelled and joined together using

M10 bolts and two equal angle sections of size 50 mm (5 mm thickness) placed one on each longitudinal side (Figure 5.15). The purpose of angles was to hold two segments together. A gap of 30 mm was maintained between two segments at the centre of the span to allow free rotation of the segments during testing once the angles were removed.

Figure 5.15 A base for supporting wall specimen for bending test in lateral span

In order to economize testing setup, two types of base were constructed: one supported on rollers and the other supported on bolts (Figure 5.16). The base with roller supports was used as a common support to all specimens during testing.

Figure 5.16 Fixed base on the top of roller supported base

The base segments supported on bolts were similar to roller supported bases except the support system. In bolt supported system, the hole on the frame of base segment was enlarged up to the depth just enough to hold the nut tightly. A M10 bolt was inserted through the nut. The height of the base segment could be adjusted by turning the bolt for levelling purposes.

Each set of base was pre-loaded with an expected load of wall for 24 hours for conditioning (Figure 5.17). Then, it was tested for levelling and adjusted if required and re-loaded similarly until there was no change in level.

A strip of 30 mm x 17 mm plywood was inserted in the gap and a sheet of builder plastic was laid over the platform supported on bolts. For the first layer, a head joint was created within the gap between two base segments. This was to ensure a section of the wall free from any influence provided by the support.

Figure 5.17 Bases under constant loading for conditioning

Figure 5.18 Wall specimens for bending test in lateral span.

The remaining portion of the wall was constructed following similar procedures as for bending in vertical span. Due to time constraints, three un-reinforced wall specimens and two reinforced wall specimens were built for bending test in lateral span (Figure 5.18). Prefabricated mesh as in the case of bending in vertical span was used for reinforced specimens. The specimens were dried in the laboratory environment for over four weeks.

5.2 Specimens for dynamic test

Stone walls with mud mortar are relatively weaker as compared to the walls with stiff mortar, such as, cement-sand mortar. Also, the traditional stone houses are normally built with flexible floors and roofs spanning only one way and heavily deficient for in-plane shear strength. In such cases, the out-of-plane bending strength of the walls is critical to earthquake performance (Spence & Coburn 1992). Therefore, it was decided to investigate the behaviour of stone wall for out-of-plane shaking.

While investigating out of plane response of a wall, a single cantilever wall will not be sufficient because interactions of the walls at the corner play a crucial role. The lateral support provided by the cross walls mobilises the bending strength of the main wall in the lateral span. Therefore, one storey single room specimen seems to be a minimum requirement for studying the response of walls for out-of-plane shaking. However, such specimen would be heavy for moving from the place of preparation to the shake table. In such scenario, there were two options: either building the specimen directly over the shake table or preparing a part of a room

containing a main wall and two wing walls at the end. The first option was not practicable due to busy schedule of shake table testing facility for other projects. Therefore, the second option was chosen.

An U-shaped platform fabricated by Dowling (2006) during his PhD research in the same lab was used for building a shake table specimen. Obviously, the dimensions of the specimen were based on the size of the platform. The length of main wall was chosen as 1.8 m, whereas the length of wing wall was 0.8 m. The thickness of the wall was chosen as 175 mm. An opening of size 0.45 m x 0.45 m was provided at the middle of the main wall (Figure 5.19). This was a half scale model of a part of a single storey room.

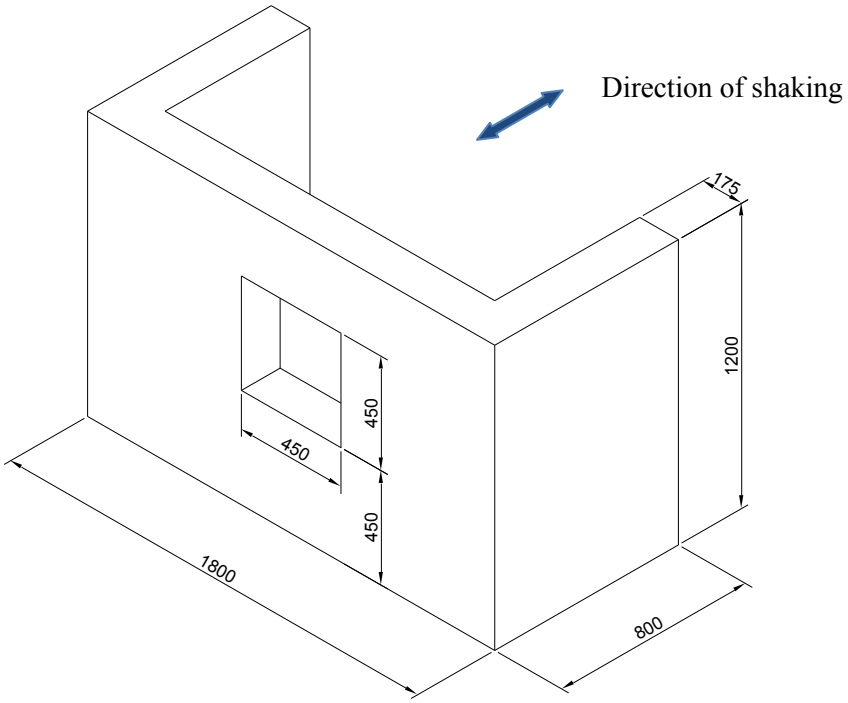

Figure 5.19 Schematic diagram of a shake table model

Observing the behaviour of the main wall for out of plane shaking mode was the prime objective of this test. The major functions of the wing walls were just to provide a lateral support to the main wall. In the worst case scenario, there might be an opening for a door at the end of wing wall of the specimen. Therefore, the end of wing wall was left free.

Using shear keys to fix the base of the wall to the platform is not suitable for stone walls with mud mortar because such wall is too fragile. During shaking, the shear keys easily tear the wall apart, which reduces the effectiveness of the fixity of the wall to the base. As a consequence, unrealistic shaking load will be transferred to the specimen.

In order to solve this challenge, a system for holding the specimen at the base was developed. In this scheme, a holding compartment of width slightly larger (2x20 = 40 mm) than the thickness of the wall was fabricated (Figure 5.20). The purpose of the gap of 20 mm on each side of the wall was to insert a wooden strip of width 20 mm. The compartment was fixed to the platform, by drilling through holes and using threaded rod of 10 mm and nuts at both ends. Holes were also drilled on the side frame of the compartment to insert M10 bolts. Towards the inside face of the compartment, the holes were enlarged up to the depth just enough to hold M10 nuts (Figure 5.21). These nuts will hold the bolts inserted through the holes from the outer side of the frame so that while tightening bolts, it will push the wooden strip towards the wall. As a consequence, the grip between walls and the holding compartment will be increased.

Figure 5.20 U-shaped platform for preparing a specimen for shake table test

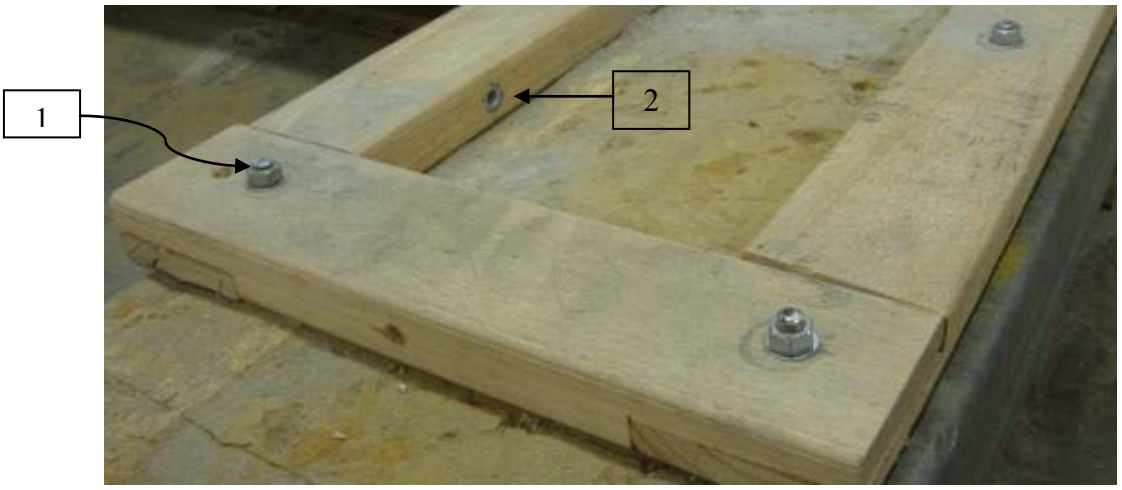

Notes: 1- A nut-bolt system for fixing the holding compartment to the platform
2- A nut for holding a side bolt for griping the wooden strip between wall and holding compartment.

Figure 5.21 Close up view of U-Shaped platform

Stone pieces were broken down to smaller size to suit the reduced scale (1:2) wall. As in case of wall specimen for static test, corner stones and other stones were prepared using a diamond saw. Similarly, mud mortar was prepared as in static test

specimen. Then, the wall specimen was built within the holding compartment leaving a gap of 20 mm along each side (Figure 5.22).

Figure 5.22 Un-reinforced specimen for shake table testing

Building a stone wall in reduced scale was a tough job due to small width of the wall, which needed more work in breaking every piece of stone as compared to a full scale wall. A considerable amount of time had been invested to build the specimen. After completion, it was left to dry in the laboratory environment over 4 weeks.

The gap between the wall and the holding compartment was cleaned and a wooden strip of thickness 20 mm and height 50 mm was inserted on each side of the wall. These strips were tightened using bolts inserted through holes in the side frames of the compartment (Figure 5.23).

Figure 5.23 Clamping system at the bottom of the specimen

Figure 5.24 Additional anchorage provided to the specimen

Additional anchorage to the wall was provided by driving screws through the wooden strips touching each piece of stone. Also, the screws were used to join wooden strips with the frame of the holding compartment (Figure 5.24).

Figure 5.25 Twin wires from inserted mesh for tying the outer mesh

Another identical wall specimen was also constructed and reinforced with steel wire mesh (wire diameter 0.56 mm, mesh size 13 mm across flats) following similar procedures mentioned in section 5.1.2. The bottom (foundation) meshes along the main wall and wing walls were overlapped at the corner. During the construction of the specimen, horizontal strips for providing a pair of binding wires were inserted into the wall at the following locations: middle height between bottom of the wall and sill level, sill level, middle height between sill and lintel, lintel level and middle height between lintel and top of the wall (Figure 5.25). These locations were chosen

for simplifying and economizing the construction technique. These strips were also overlapped at the corner of the specimen similar to bottom strips.

While tightening, the flexible mesh fits tightly around the outer corner of the building throughout the whole height. However, around the inner corner, the tendency of the mesh from two orthogonal walls will be to pull apart. The meshes will be held down by the inserted mesh in certain intervals along the height. As a consequence, the mesh may sag between each layer of inserted mesh. In order to avoid this, small strip of mesh (5 meshes width and length about wall thickness) were inserted in each layer of stones at the inner corner of the specimen on each side.

A vertical strip of wire mesh (width equal to the wall thickness and length equal to window height plus twice the wall thickness) was inserted in each side of window during the construction of the wall. This strip was folded away from the side of the widow (equal to wall thickness) and embedded in to the wall at the sill level and lintel level.

After completing the wall, the required pieces of reinforcement meshes were cut from a roll of wire mesh. Connecting procedures were similar as in case of reinforced specimen for static testing. The following sequence of connections was developed to get a tightly fitted mesh around the specimen.

1. Connection at the base
2. Connection at the top
3. Connection with adjacent meshes along sides

4. Connection along the inner corner and tying the mesh with twin wires from the inserted strips up to the width of smaller strips.
5. Connection along the outer corner
6. Connection along opening
7. Tightening the mesh
8. Tying the mesh with twin wires from the inserted strips

Figure 5.26 Meshes after connecting at the top

While connecting at the top, it is not necessary to make the meshes very tightly fitted to the wall at the beginning (Figure 5.26). It is just enough to pull the mesh gently and connect along the top throughout the whole length. However, it is advisable to maintain joints along a row of cells to provide symmetrical connections (Figure 5.27). Around the junction region on the top of the wall, this type of connection is

not possible. In this case, joints of overlapped meshes should be provided among the best possible matches between the sides of meshes. Tightness of the mesh with the wall increases gradually if the proper sequence is followed as mentioned above.

Figure 5.27 Connection along the top

For reinforcing the wall with a window opening, the whole wall was covered with the mesh initially and connected at the top and bottom as other walls. Then, the mesh was connected with the inserted strip at the sill and lintel level, following similar procedures to connect with the mesh at the bottom of the wall. Similarly, the strip inserted along the side of the window was connected to the mesh following the connecting procedures along the edge as mentioned in section 5.1.2 for prefabricated mesh. Then, the remaining portion of the mesh within the window was removed by cutting with a wire cutter (Figure 5.28).

(a) Overall view of a window

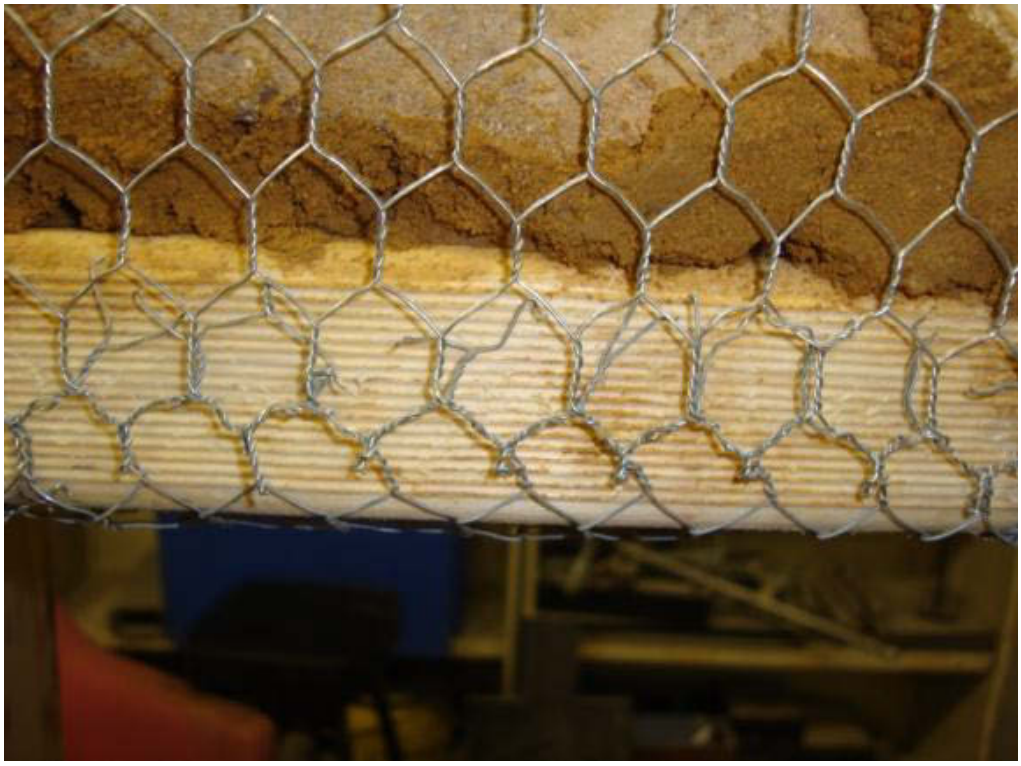

(b) Connection along lintel of a window

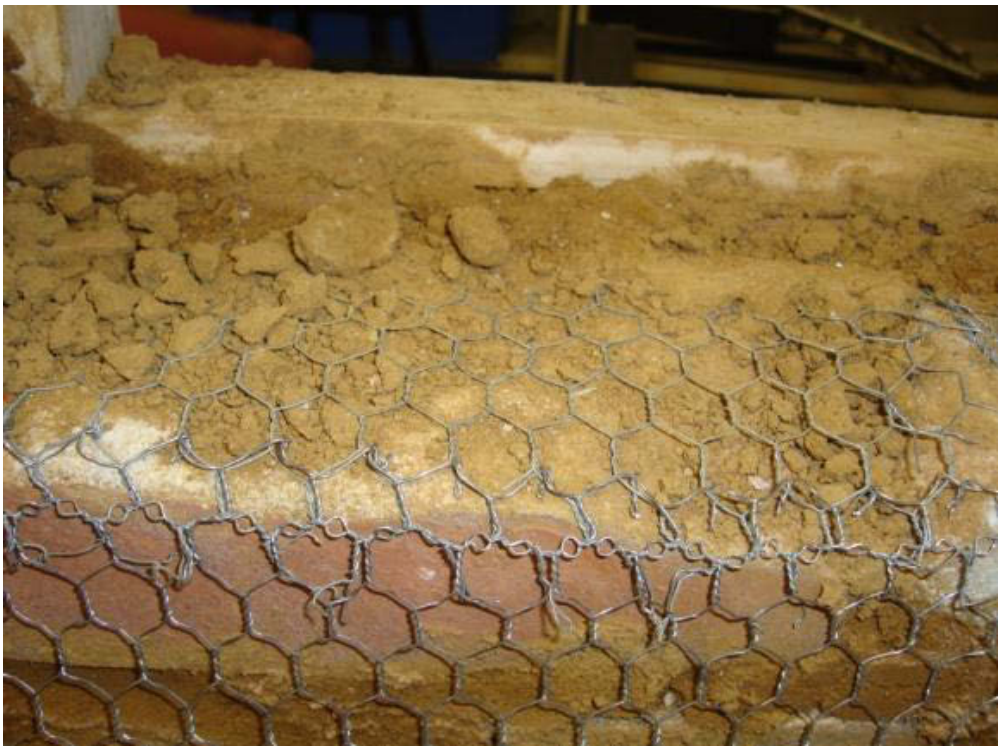

(c) Connection along sill of a window

(d) Connection along side of a window

Figure 5.28 Details of reinforcement around a window

The effectiveness of externally wrapped reinforcement system depends on tightness of the reinforcement attached to the wall (Section 6.1). The proposed sequence of steps mentioned above helps to fit the mesh tightly to the wall.

For step 7, one technique has been developed and applied for increasing the tightness of wrapping for hexagonal wire mesh during this research. In this method, a column of cells are collapsed by twisting two opposite vertical sides of a cell (Figure 5.29).

After this process, the original column of cells will be converted to a single line of twisted wire within a newly formed cell. This process reduces the number of cells along the horizontal length of a wall. As a result, the meshes are readjusted in both horizontal and vertical directions with increased tightness. The number of columns of cells to be collapsed depends on the dimensions of walls as well as initial tightness of fitting during connecting meshes at the top of the walls.

In this experiment, collapsing a single middle column of each segment (max width 900 mm, which was the width of the roll of mesh) of mesh was found adequate.

The final step for installing the reinforcement was to tie the outer mesh to the wall using twin wires of the inserted mesh at various levels during the construction of the wall. The pair of twin wires was twisted at least 3 times over the wire of the vertical mesh. This was adopted based on the recommendation of conventional twist for preparing netting (AS 2423-2002). Finally, excess wires beyond the twist were cut and the twisted ends were bent inward to the wall for avoiding injury from sharp end of the twisted wire.

(a) Initial condition (a cell selected- encircled)

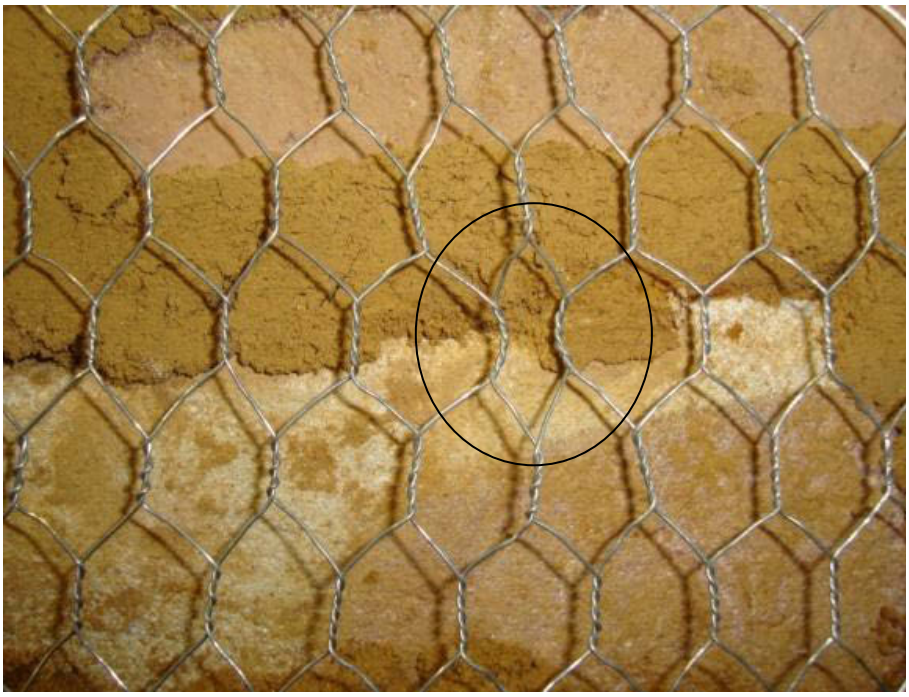

(b) Two parallel sides brought together (encircled)

(c) One cell collapsed (encircled)

(d) A column of cells collapsed

Figure 5.29 Cell collapsing technique for increasing tightness

As in the case of unreinforced specimen, the gap between the walls and the holding compartment was cleared and wooden strips (20 mm thickness and 50 mm height) were inserted and tightened using bolts through holes in side frames (Figure 5.30). Additional anchorage was provided using screws. The specimen was left to dry over four weeks in the laboratory environment.

Figure 5.30 Reinforced shake table specimen

5.3 Testing on walls

5.3.1 Static tests

5.3.1.1 Compressive strength of walls

Wall specimens were placed centrally in the testing machine, ensuring that both top and bottom of the specimen were in full contact with the testing machine (Figure

5.31). The load was maintained steadily around 0.15 N/mm^2/min and therefore failure occurred after 15 minutes to 30 minutes from the start of loading (BS EN1052-1:1999).

Figure 5.31 Wall specimen during compression testing

The compressive strength of masonry specimen was calculated using the Equation (2.1). The results of the compressive strength test are tabulated in Table 5.1.

Table 5.1 Compressive strength of wall specimens

Wall	Length	Breadth	Load	Stress	E
	mm	mm	kN	MPa	MPa
1	500	350	319.24	1.82	309
2	500	350	299.37	1.71	297
3	500	350	324.02	1.85	334
Average				1.80	313

Deformation was measured using LVDTs. The stress strain curves were observed as given in Figure 5.32. The modulus of elasticity, E, was calculated as a secant modulus at a stress equal to one third of the maximum stress as specified in the code (BS EN1052-1:1999). According to the code, the modulus of elasticity can be rounded to nearest 100 MPa. Following this rule, the average modulus of elasticity of the specimens can be taken as 300 N/mm^2. This rule seems to be intended for masonry specimen with cement or lime mortar, which normally has modulus of elasticity more than 1000 MPa. Therefore, for mud mortar specimens, rounding to 100 may not be a suitable option. Considering the modulus of elasticity in the range of 30% to 60% of ultimate stress, average modulus of elasticity seems to be 240 MPa.

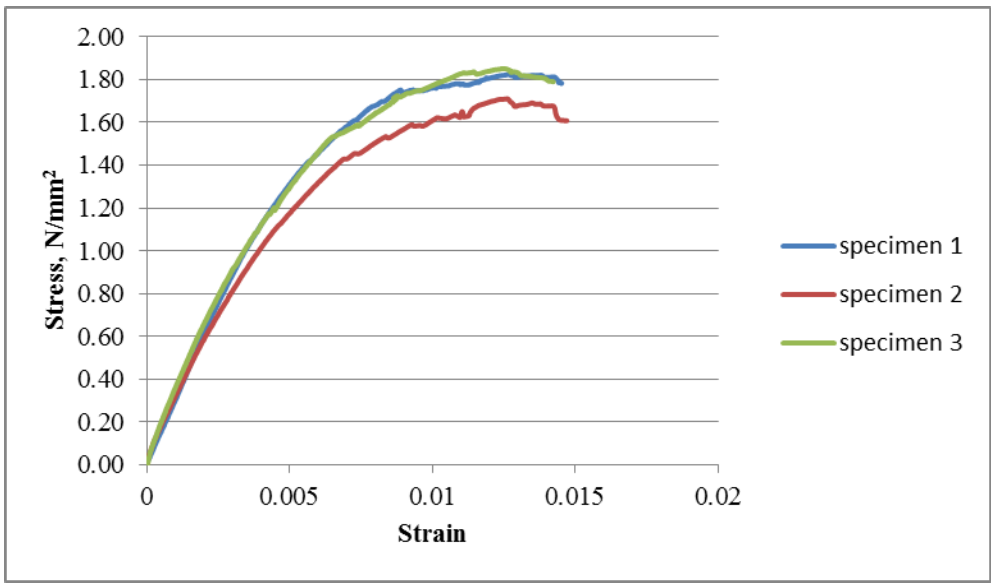

Figure 5.32 Stress strain curves of masonry specimens in compression

After crossing the peak value of the load, LVDTs were removed for the safety of the instruments. For the third specimen, the loading was continued until the specimen was on the verge of failure (Figure 5.33).

Figure 5.33 Wall specimen on the verge of collapse

The wall specimen could sustain compressive load up to a large deformation. As the cracks widened, the stiffness of the wall reduced considerably. However, the stability of the wall was maintained even after a wide opening of the cracks. The behaviour of wall throughout the whole loading period was as shown in Figure 5.34.

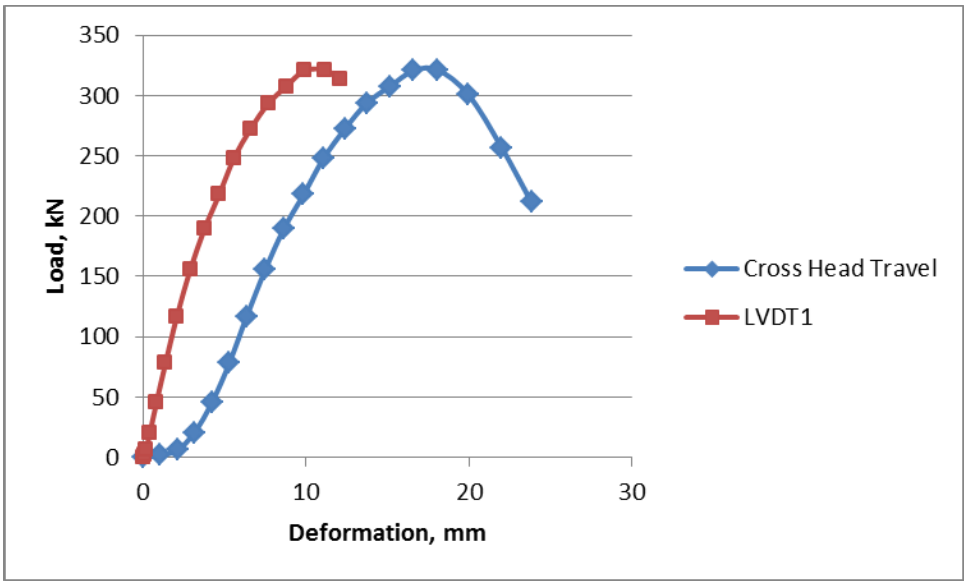

Figure 5.34 Behaviour of masonry specimen in compression

As a control measure of drying, moisture content of the mud mortar was measured after bending test. Average moisture content of the mortar after the compression testing was 3.85% (Table 5.2).

Table 5.2 Moisture content of mortar after compression testing of wall

Wall	Container g	Container + Mortar g	Container + Mortar (Dry) g	Moisture %
1	355.12	1495.55	1452.38	3.93
2	396.13	1217.57	1182.9	4.41
3	363.24	1377.07	1345.6	3.20
Average				3.85

5.3.1.2 Bending test of walls in vertical span

The wall specimens were tested using four point bending test in the vertical span (Figure 5.35). Two load skates were placed below the bottom of the specimen's platform to provide a rolling base. At each support and loading arm, a 50 mm diameter steel rod of length 600 mm was provided.

Figure 5.35 Wall specimen under bending test in vertical span

The load was applied using hydraulic jack assembly and measured with two load cells each of 5 kN capacity. The weight of loading arms was supported on a purpose made frame. One small load skate at each side of the loading arm was used to provide a rolling base over the guide of the frame. The distance of lower support from the bottom edge of the specimen was kept at 50 mm. The spacing between the inner load bearings was set at 500 mm (Figure 5.36).

The loading arm was located at a distance of 375 mm from the nearest support. A strip of Ethylene-vinyl acetate rubber sheet of thickness 12 mm and width 50 mm was inserted between the wall and the bearing at the support as well as at the loading arm to ensure proper contact with the wall.

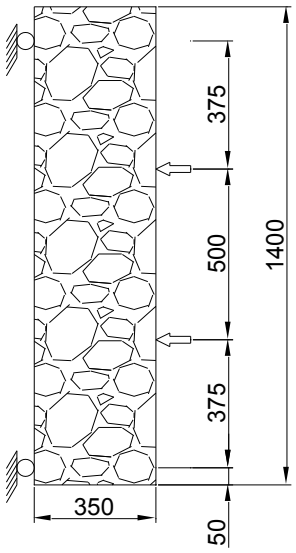

Figure 5.36 Schematic diagram of flexural test in vertical span

A piece of equal angle of size 40 mm and thickness of 3 mm was attached to the side of the wall near both ends of each support using epoxy for measuring the deflection of the rubber at the support. The loading was applied at a rate of 0.03 $N/mm^2/min$ (BS EN 1052-2:1999). Deflections were measured at the supports and mid span of the wall using LVDTs. Since the LVDTs were placed symmetrically at the supports and the mid span deflection was measured at the centre of the wall, the average of all four support deflections was equal to the contribution of the rubber deflection at the mid span. The net deflection at the mid span of the wall was obtained by subtracting the component of the rubber deflection. The load at the initiation of the crack was taken for calculating the bending stress using the Equation (2.3).

The weight of the wall was measured and weight density of the wall was calculated. The compressive stress at the level of crack was subtracted from the bending stress

of the wall to obtain the net bending strength of the unreinforced wall and the reinforced wall as shown in Table 5.3 and Table 5.4 respectively.

In Table 5.4, the first row represents the result of a reinforced wall prepared by direct weaving method as mentioned in section 3.3, whereas the second and third rows show the results of reinforced walls prepared by using prefabricated mesh.

The stability of wall specimens was maintained up to a large rotation after crack initiation. This phenomenon was observed even in unreinforced wall specimen (Figure 5.37) and much more pronounced in reinforced specimen (Figure 5.38).

Table 5.3 Flexure strength of unreinforced wall specimens (vertical span)

Wall	H	F_c	F_u	f_{tb}	W	γ	h_c	f_c	f_b
	mm	N	N	kPa	kg	kN/m^3	mm	kPa	kPa
1	1435	3504	5592	64	519	20.3	925	13	54.0
2	1365	2992	6050	55	491	20.2	900	09	45.6
3	1415	3028	4434	56	505	20.0	920	10	45.7
4	1440	3142	3632	58	520	20.2	900	11	46.8
5	1430	3565	5095	65	511	20.4	625	16	49.0
Average									48.2

Note: H = height of specimen, F_c = Load at crack initiation, F_u = ultimate load, f_{tb} = theoretical bending stress, W = weight, γ = weight density, h_c = height of crack from bottom, f_c = compressive stress, f_b = bending strength.

Table 5.4 Flexure strength of reinforced wall specimens (vertical span)

Wall	H	F_c	F_u	f_b	W	γ	h_c	f_c	f_b
	mm	N	N	kPa	kg	kN/m^3	mm	kPa	kPa
1	1448	3895	6898	72	515.0	19.94	800	13	58.6
2	1440	4353	8029	80	506.8	20.05	720	14	65.5
3	1430	3355	9395	62	506.8	20.05	840	12	49.8

Note: notations similar to Table 5.3

Figure 5.37 Crack in unreinforced wall specimen (Bending in vertical span)

Figure 5.38 Crack in reinforced wall specimen (Bending in vertical span)

The large deflection capability without significant loss of the load carrying capacity of the wall was also evident from the load deflection curves at the mid span of the wall as shown in Figure 5.39. The reinfored specimen sustained considerably higher load with increased deflection.

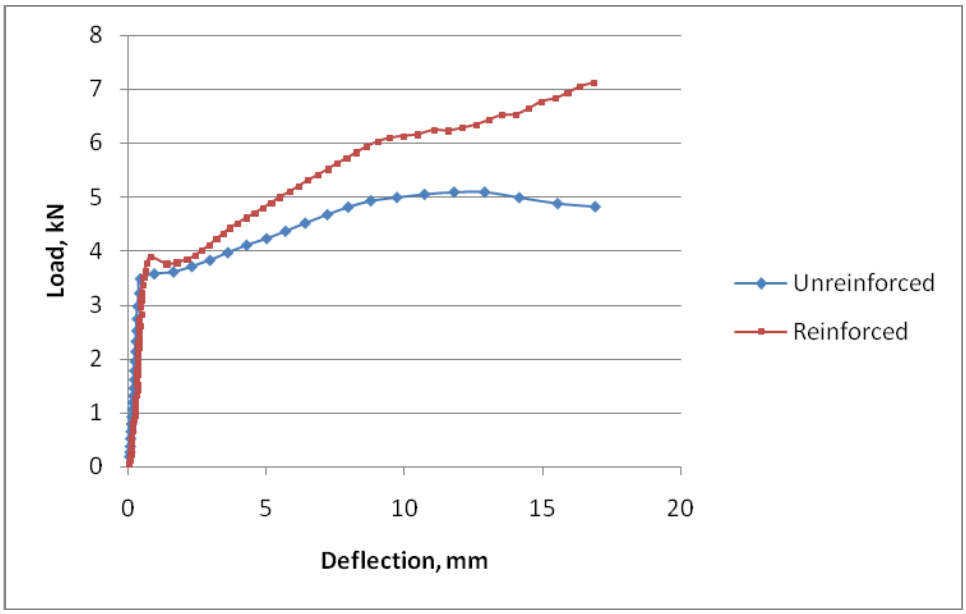

Figure 5.39 A typical load deflection curve (Bending in vertical span)

The moisture content of the mortar samples from the wall specimens at the time of testing was as shown in Table 5.5 and Table 5.6.

Table 5.5 Moisture content of unreinforced wall (flexural test vertical span)

Wall	Container g	Container + Mortar g	Container + Mortar (Dry) g	Moisture %
1	358.7	619.4	614.7	1.84
2	358.6	595.5	592.5	1.28
3	405.9	518.1	515.6	2.28
4	355.1	517.8	513.3	2.84
5	355.3	856.00	847.00	1.83
Average				2.01

Table 5.6 Moisture content of reinforced wall (flexural test vertical span)

Wall	Container g	Container + Mortar g	Container + Mortar (Dry) g	Moisture %
1	363.0	762.5	756.1	1.63
2	355.3	856.0	847.0	1.83
Average				1.73

5.3.1.3 Bending test of wall specimens in lateral span

Following exactly similar procedures as given in the last section, a loading setup for four point bending test of a wall in lateral span was prepared. Few modifications were required as the span had been changed from vertical to lateral. The weight of the loading arm was transferred by two stainless steel grooved rollers of 32 mm diameter to two guide rails (Figure 5.40).

(a) Grooved roller assembly (b) Guide rails

Figure 5.40 Arrangement for holding vertical loading arm

A properly leveled platform was prepared and a specially prepared base with roller supports (as mentioned in section 5.1.3) was placed on the platform. A wall

specimen was gently placed on the top of the base. The whole assembly was brought close to the position of testing by rolling the base over the platform towards the supports. The holding angles, attached to the base of the wall specimen, were removed gently. Plastic sheet at the bottom of the wall was cut along the gap. Finally, the angles of the base supported on the rollers, were also removed. Then, the specimen was loaded similarly as in the case of vertical span (Figure 5.41).

Figure 5.41 Bending test of a wall specimen in lateral span

The load at the initiation of the crack was taken for calculating the bending stress using Equation (2.3).

The results are shown in Table 5.7 and Table 5.8 for unreinforced wall specimens and reinforced wall specimens respectively.

Table 5.7 Flexural strength of unreinforced masonry specimen in lateral span

Wall	*l*	t	h	F_c	F_u	σ_b
	mm	mm	mm	kN	kN	kPa
1	1400	350	385	4.18	4.18	99.7
2	1400	350	395	3.39	3.39	78.7
3	1400	350	390	3.29	3.29	77.4
Average						85.3

Figure 5.42 Cracks in unreinforced wall (Bending in lateral span)

The unreinforced wall specimen could not bear any further load after cracking. There were no cracks in the stone unit. The crack path followed the mortar joint (Figure 5.42).

The reinforced wall sustained considerably high load up to a large deflection. As in unreinforced wall, crack path followed the mortar joint. Few joints of the cells were detached (Figure 5.43).

Table 5.8 Flexural strength of reinforced masonry specimen in lateral span

Wall	*l*	t	h	F_c	F_u	σ_b
	mm	mm	mm	kN	kN	kPa
1	1400	350	450	6.54	8.40	133.5
2	1400	350	460	5.99	7.58	119.6
Average						126.6

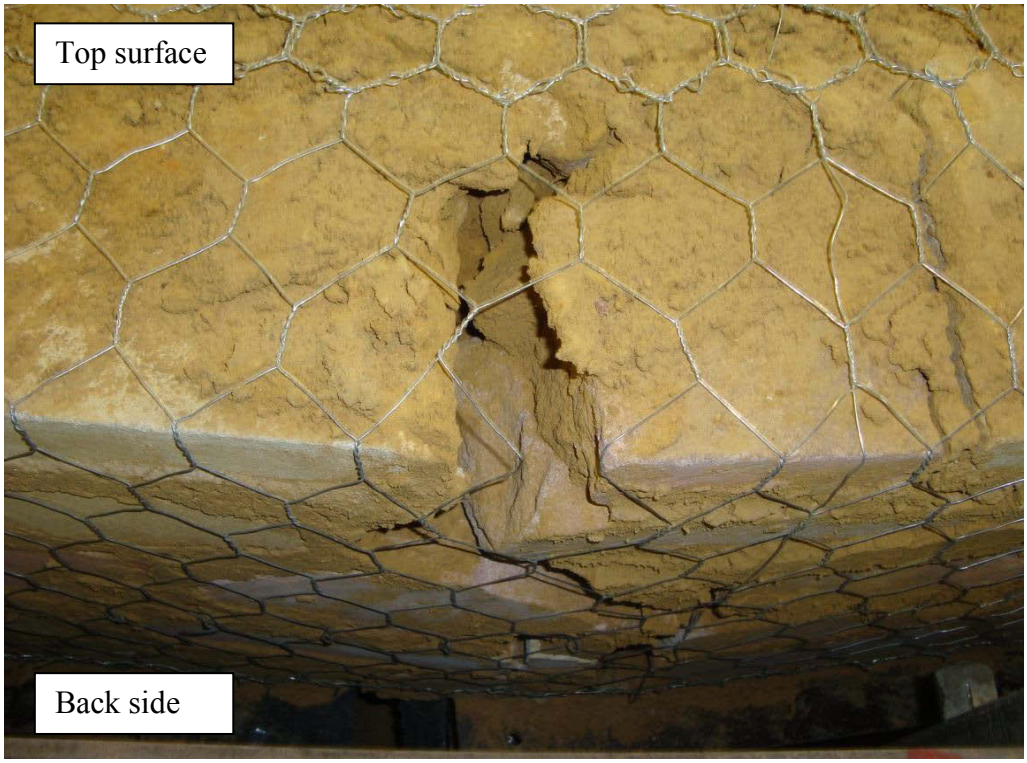

Figure 5.43 Crack on reinforced wall specimen (Bending in lateral span)

On the basis of the result on reinforced wall 1, loading on reinforced wall 2 was continued for longer duration than reinforced wall 1. Few humps were detected in

the load deformation curve (Figure 5.44). These correspond to the breakage of few joints in the mesh.

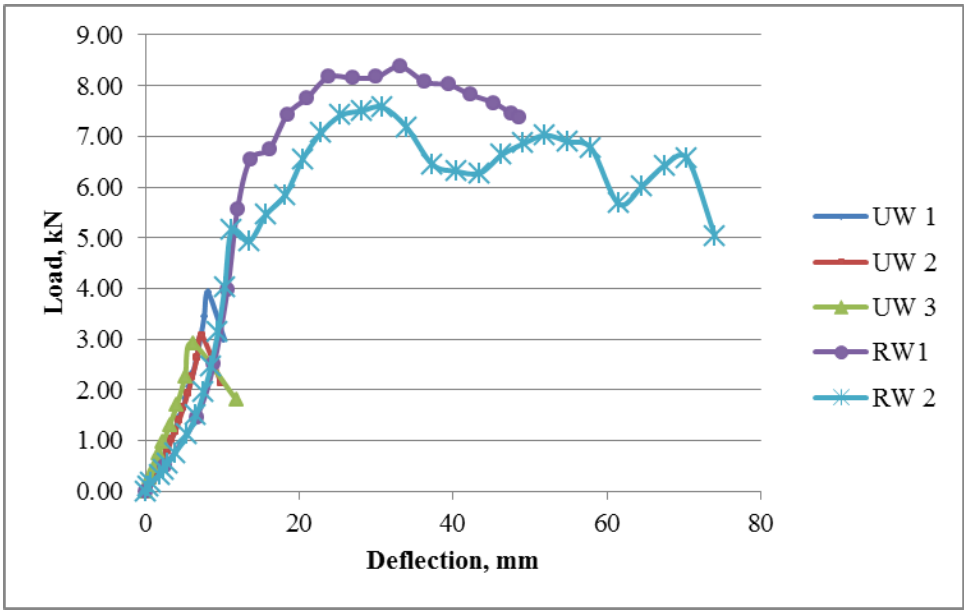

Note: UW = Unreinforced wall, RW = Reinforced wall

Figure 5.44 Load deflection curves (bending in lateral span)

Table 5.9 Moisture content of unreinforced wall specimens (flexural test lateral span)

Wall	Container g	Container + Mortar g	Container + Mortar (Dry) g	Moisture %
1	355.0	747.9	741.6	1.63
2	396.3	1036.3	1027.3	1.43
3	355.0	922.4	908.8	2.46
Average				1.84

Table 5.10 Moisture content of reinforced wall specimens (flexural test lateral span)

Wall	Container g	Container + Mortar g	Container + Mortar (Dry) g	Moisture %
1	396.0	1065.4	1043.4	3.40
2	354.8	1130.8	1100.6	4.05
Average				3.72

After the test, the moisture contents of the specimens were also measured (Table 5.9 and Table 5.10).

5.3.2 Dynamic tests

5.3.2.1 Earthquake Loading

As any earthquake event will never repeat again exactly in the same way, it is not necessary for testing of structures by applying a particular ground motion (Tomaževič & Velechovsky 1992). In this research, ground motion recording of 1940 El Centro Earthquake was selected as a representative of seismic loading (Figure 5.45). The magnitude of this earthquake was 6.9, which was the strongest recorded quake in Imperial Valley, California, USA (Southern California Earthquake Data Centre).

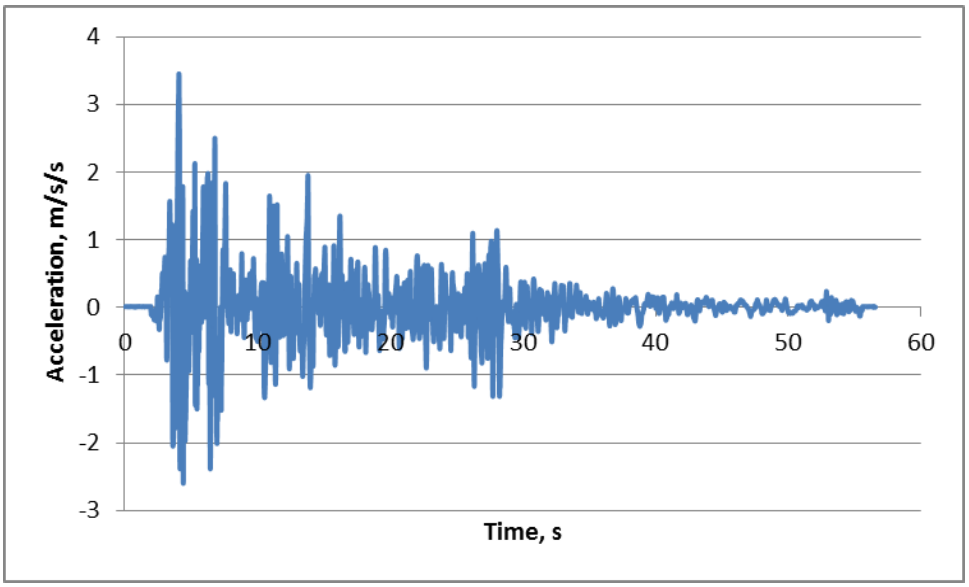

Figure 5.45 Ground motion recording during 1940 El Centro Earthquake

5.3.2.2 Capacity of the testing facility

The dynamic testing was carried out on the uniaxial shake table of 10 tones capacity. The size of the platform was 3m x 3m. It could handle accelerations up to ±2.5g with no pay load, velocity of ± 0.550 m/s and displacement of ± 0.1 m in the frequency range 0.1 to 50 Hz.

5.3.2.3 Shake table tests on unreinforced wall specimens

The specimen was transferred to the shake table and the base of the specimen was fixed firmly to the platform of the shake table using bolts. Nine accelerometers and five displacement transducers were installed at the various strategic locations of the specimens (Figure 5.46).

Figure 5.46 Locations of measured points

One accelerometer and one displacement transducer were also installed at the base of the specimen in order to record the input excitation. All the measuring instruments were connected to the data acquisition system.

The natural frequencies of the wall specimens were measured by sine sweep method. The amplitude of the input excitation was chosen as 0.0125g and frequency was varied from 1 to 50 Hz. The output of the sine sweep test was as shown in Figure 5.47. From this figure, the first natural frequency appears to be 21 Hz.

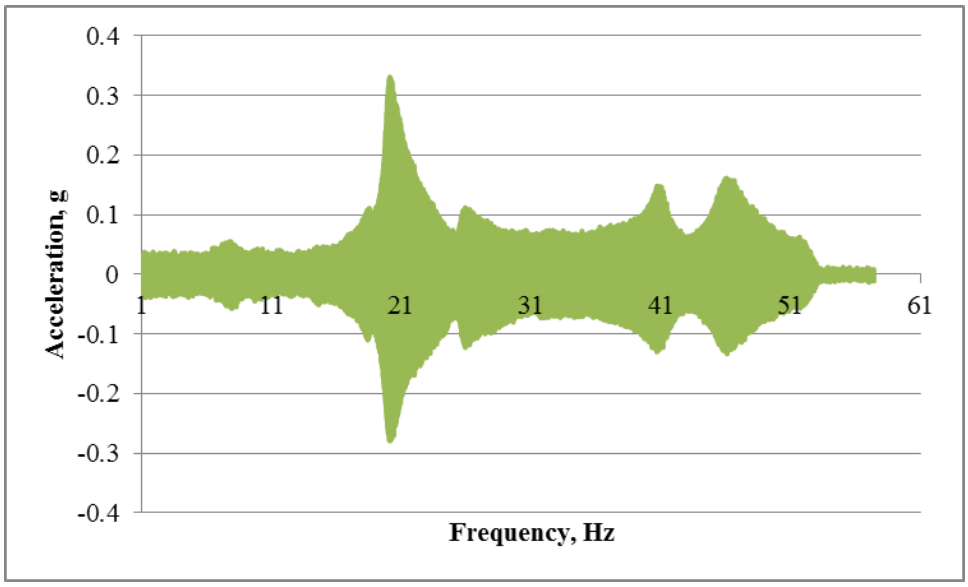

Figure 5.47 Initial sine sweep test

For scaling the input loadings, time scaling of 1/3 was used instead of 1/2 for the half scale model. This scale was chosen by comparing the frequency contents of the input signals (Figure 5.48) with the natural frequency of the model in order to increase the severity of vibration for this model. In this figure, the majority of excitation frequencies are below 5 Hz. Therefore, for the current model, reducing the time scale by 1/3 seems to have more severe damaging effect in the model.

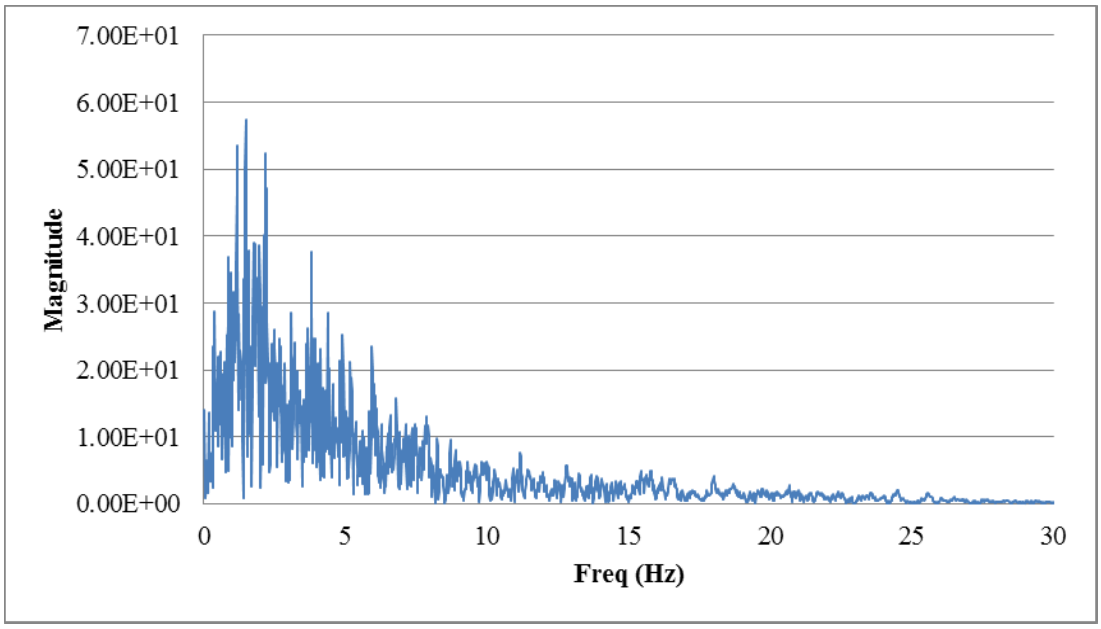

Figure 5.48 Frequency contents of input excitations

The first test was conducted at a shaking intensity of 25% of the original EL Centro record. In the subsequent runs, the intensity was increased at a rate of 25% in each step. At the intensity of 100%, there were no observable cracks in the specimen. At this stage, the displacement time history of the top of the main wall at mid-span was observed as shown in Figure 5.49.

Slight cracks were observed at the bottom of the wing wall when the intensity of shaking reached 175%. The peak load at this level was 0.62g, which in the full scale corresponds to 0.31g. This confirms that, during sine sweep testing, the specimen was subjected well below cracking level.

The propagation of cracks travelled towards the main wall at the intensity of 200%. Small inclined cracks also appeared in the main wall. A subsequent sine sweep test

was conducted to check the change in natural frequency of the damaged specimen. It was observed that the natural frequency dropped from 21 Hz to 16 Hz.

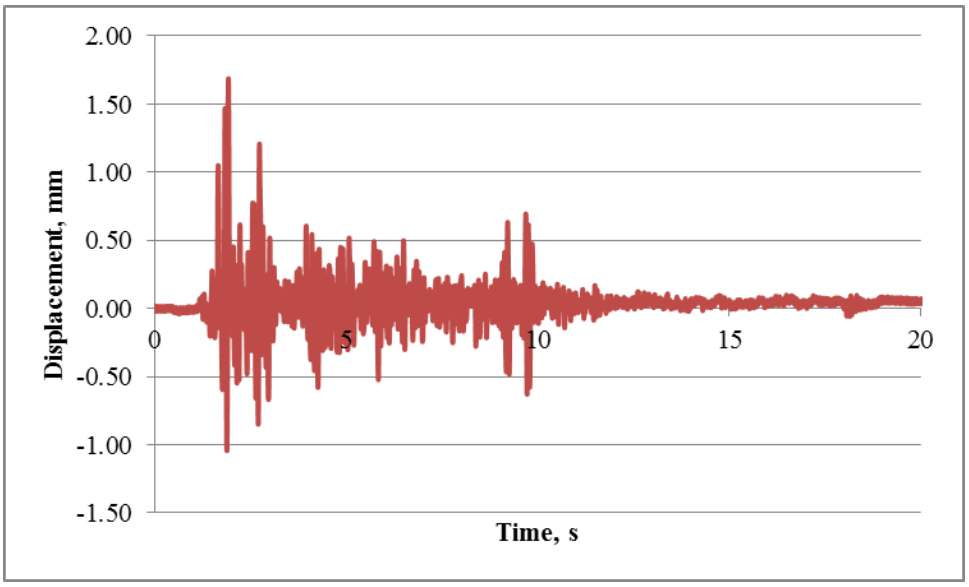

Figure 5.49 Mid span displacement of the wall at the top (100% intensity)

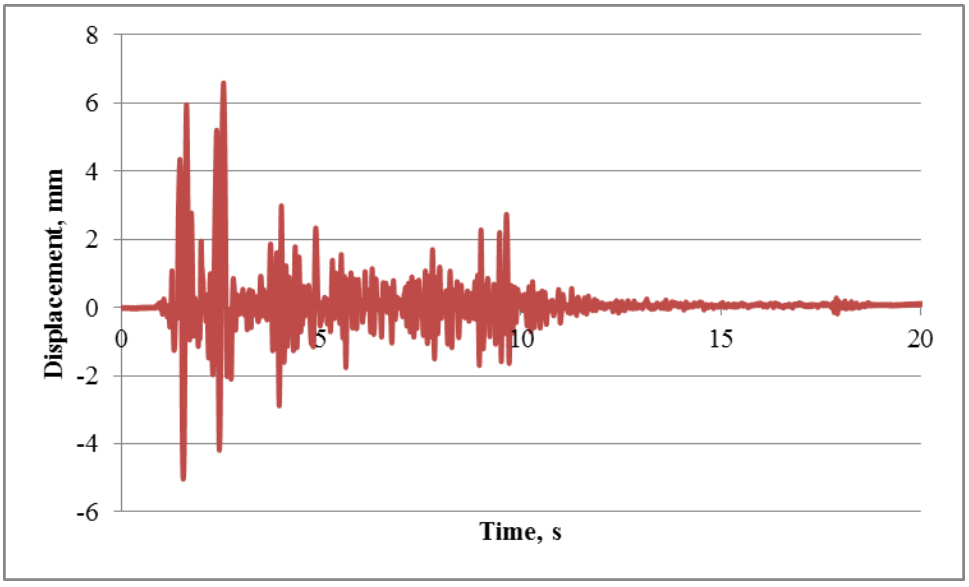

Figure 5.50 Mid span displacement of the wall at the top (200% intensity)

The mid span response of the top of the wall was observed as shown in Figure 5.50. Comparing this response with the previous case, the effect of the change in the natural frequency of the wall is evident. The profiles of the main wall at various loading intensities were observed as shown in Figure 5.51 and Figure 5.52.

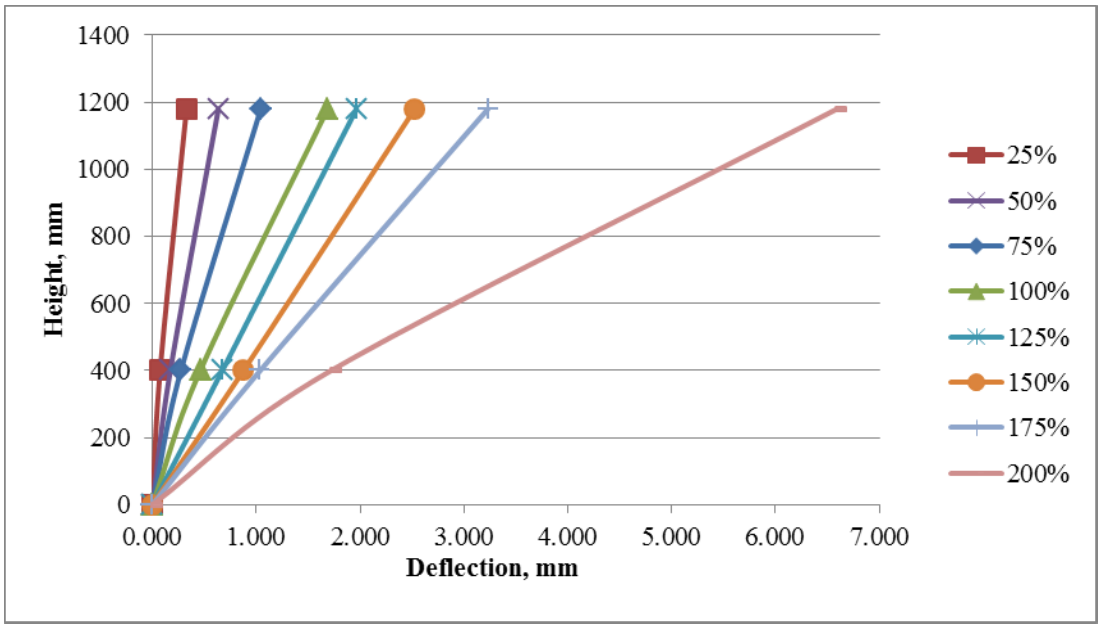

Figure 5.51 Profile of main wall at mid span at various loading intensities

In these figures, displacement has increased considerably from loading intensity of 175 % to 200%. This implies that cracks initiated at 175% intensity. As a consequence, the cracked section displaced significantly at 200% intensity level. Moreover, comparing the profile of the main wall at mid span and corner in Figure 5.51 and Figure 5.52 at the loading intensity of 200%, the displacements are almost similar. This indicates that there was corner separation at this loading level.

According to the reduced frequency, the time scaling was further reduced to 1/4 to produce a realistic situation. Testing was repeated from 100% to 200% intensity with

modified scaling. At this second round of testing, there was no visible change in the damage state of the specimen. However, a third sine sweep test was conducted at this stage. The natural frequency was further reduced to 13.6 Hz.

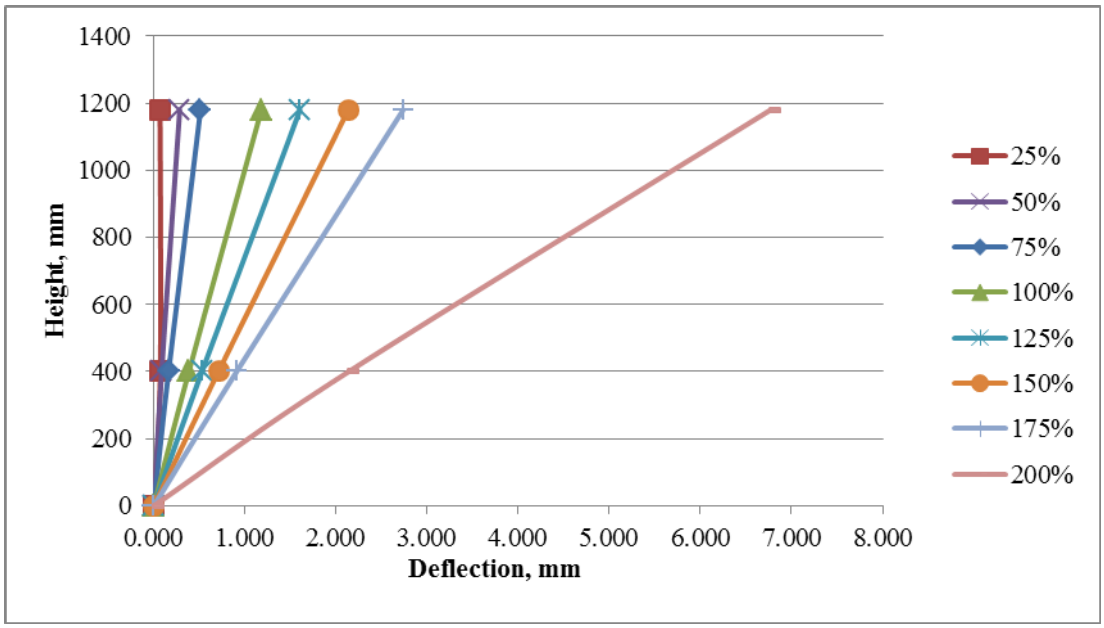

Figure 5.52 Profile of the main wall at the corner at various loading intensities

The next testing was carried out at 225% intensity. At this stage, crack width increased further. Vertical cracks were appeared near the corner following the path of the mortar joints. A fourth sine sweep test showed that the frequency of the specimen had further decreased to 12.5 Hz.

Instruments were removed and the specimen was subjected to 250% intensity record. Cracks widened and the damage to the specimen was severe. The specimen was on the verge of collapse. The crack patterns were as shown in Figure 5.53. The number near the crack shows the corresponding intensity level.

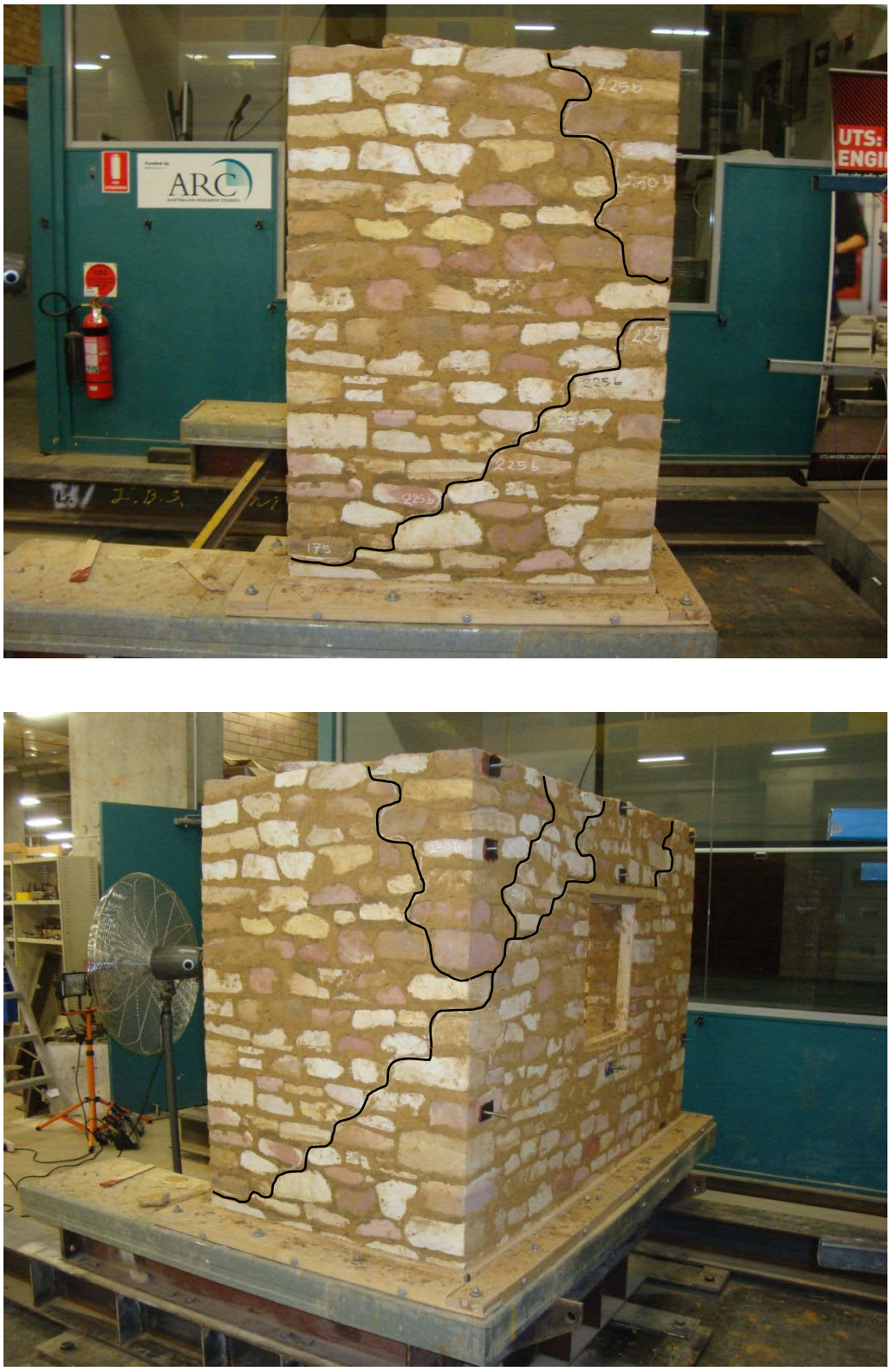

Figure 5.53 Cracks on the specimen.

The moisture content of the wall specimen was also measured as shown in Table 5.11.

Table 5.11 Moisture content of unreinforced shake table specimen

Sample	Container g	Container + Mortar g	Container + Mortar (Dry) g	Moisture %
1	354.0	738.7	733.4	1.40
2	395.1	695.4	691.6	1.28
3	362.3	567.6	564.7	1.45
Average				1.38

5.3.2.4 Shake table test on reinforced wall specimen

Reinforced wall specimen was tested under exactly similar conditions as in the case of unreinforced specimen (Figure 5.54).

Figure 5.54 Reinforced wall specimen during testing

The fundamental period of the vibration of the reinforced specimen was 26.1 Hz (Figure 5.55). Comparing with the unreinforced specimen, there was some improvement in the overall stiffness of the wall. This might be due to confinement provided by the tightly fitted mesh.

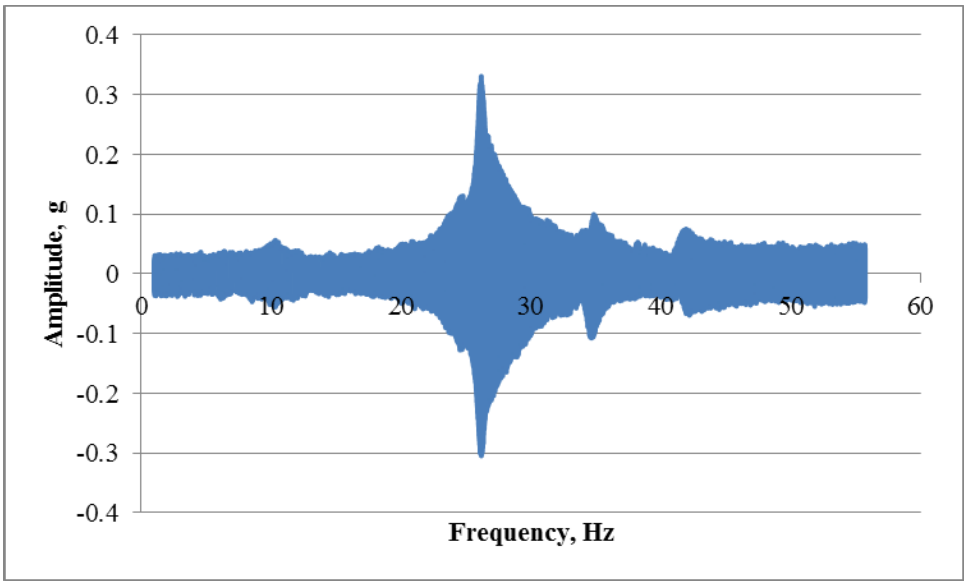

Figure 5.55 Initial sine sweep test of reinforced specimen

Though the natural frequency of the reinforced specimen was different than unreinforced specimen, the same time scaling with similar testing sequence was followed.

The displacement time history of the top of the wall at mid span with 100% intensity of loading was as shown in Figure 5.56. Comparing the profile of the main wall at mid span with unreinforced wall specimen (Figure 5.57), 40% improvement in the displacement was achieved with reinforced specimen at this loading stage.

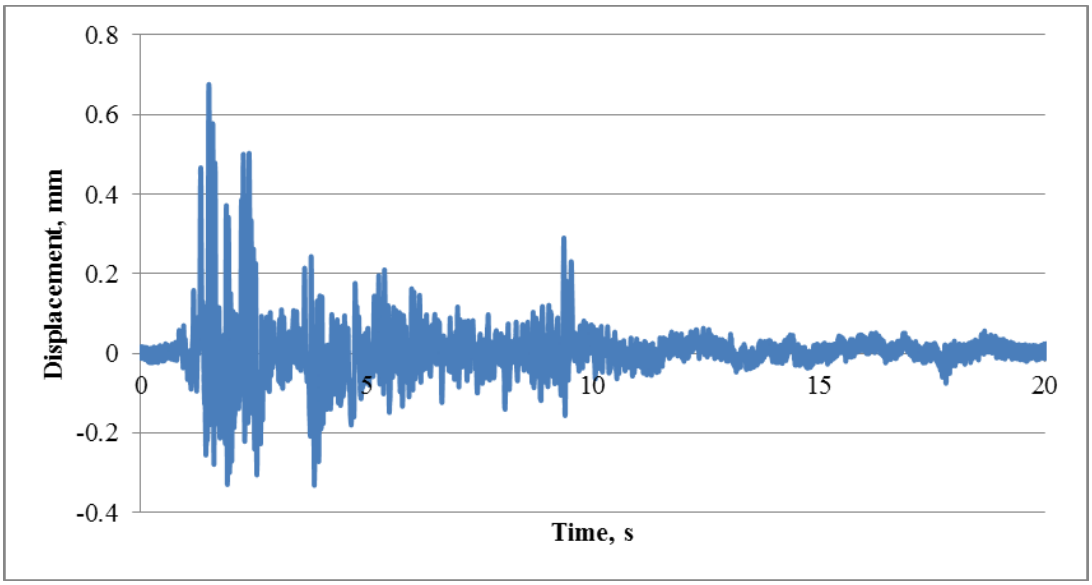

Figure 5.56 Mid-span top displacement of reinforced wall (100% intensity)

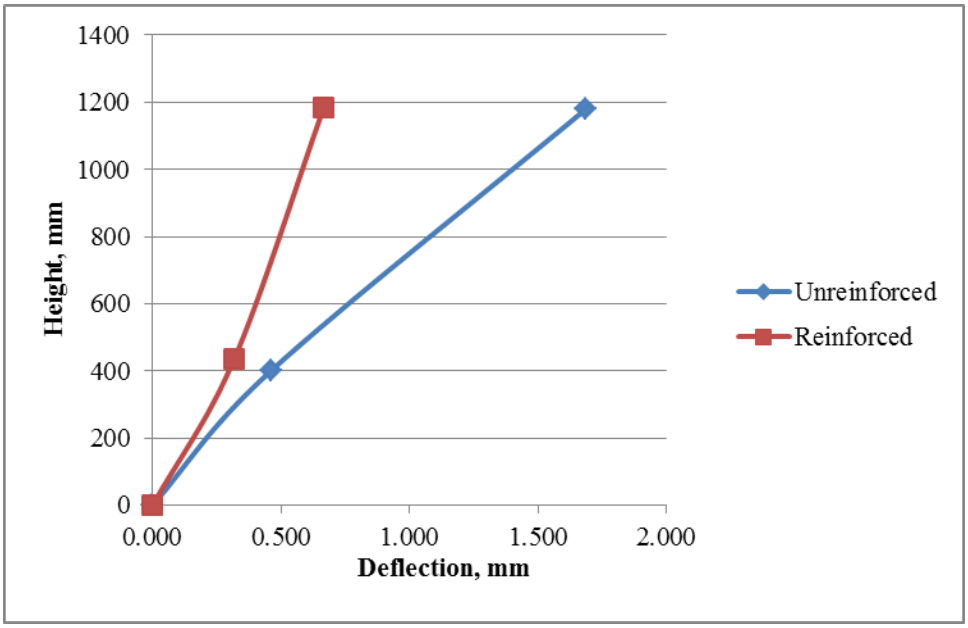

Figure 5.57 Comparison of profile of main wall at mid span at 100% intensity

There were no visible cracks up to 200% loading intensity. However, a sine sweep test was conducted after this stage. The natural frequency was observed as 20.5 Hz. The reduction in natural frequency implied that there were some changes in the

system. This may be either in the form of some minor cracks or relaxation of tension in the reinforcement mesh.

After 250% intensity, the natural frequency further decreased to 18.9 Hz. However, there were no visible cracks on the specimen. This loading intensity was the highest load applied to the unreinforced specimen. In the unreinforced specimen, the first crack was observed at 175% intensity level with 1/3 time scaling. Therefore, in the subsequent loading, frequency scaling was reverted back to 1/3 and continued with 25% increase in the intensity in each step.

The first minor cracks at the bottom of the wing walls were observed at 275% of the original record. This corresponds to 0.48g in full scale model. Comparing to the load at first cracking in the unreinforced model, this load level was 157% higher. At 300% loading intensity, the crack propagated further towards the corner. The frequency of the specimen after this stage was reduced to 17.3 Hz.

Minor cracks at the sill level of the main wall were detected at 350% intensity. Crack width at the bottom of the wing wall increased further. As a result, mesh elongated slightly. The natural frequency of the specimen reduced to 13 Hz.

A complete horizontal crack was developed along the sill level of the main wall at 375% loading intensity. Two joints along the connection of the reinforcement mesh at the bottom of wing wall were separated (Figure 5.58). This loading corresponds to 0.66g in full scale model. The fundamental frequency of the specimen was further down to 10 Hz.

Figure 5.58 Joint unwoven at 375% loading intensity

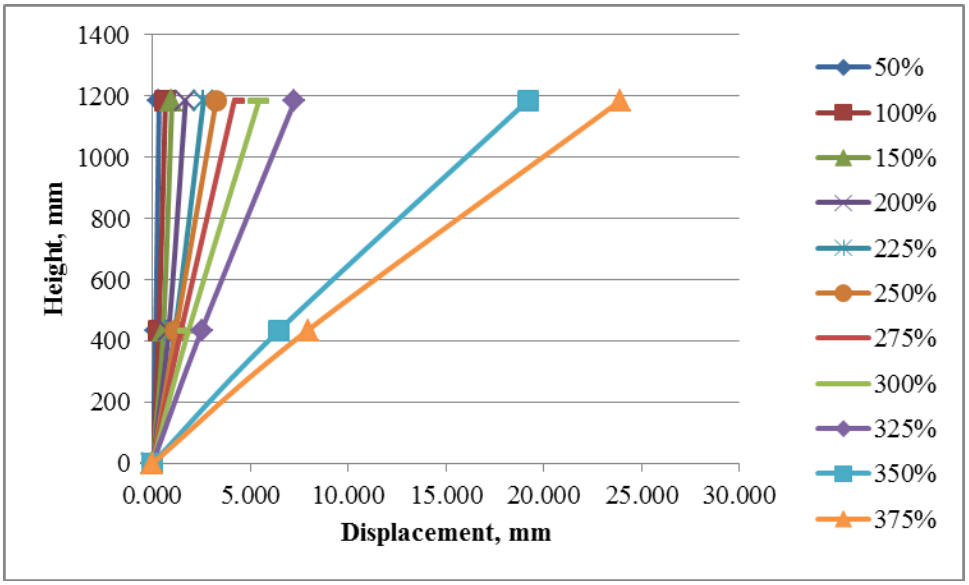

Figure 5.59 Profile of main wall at mid span (Reinforced specimen)

The variation of profile of the main wall at mid span with increasing loading intensity was as shown in Figure 5.59. A large shift in the profile at 350% intensity

was evident due to elongated meshes. The profile of the main wall at the corner was observed as shown in Figure 5.60.

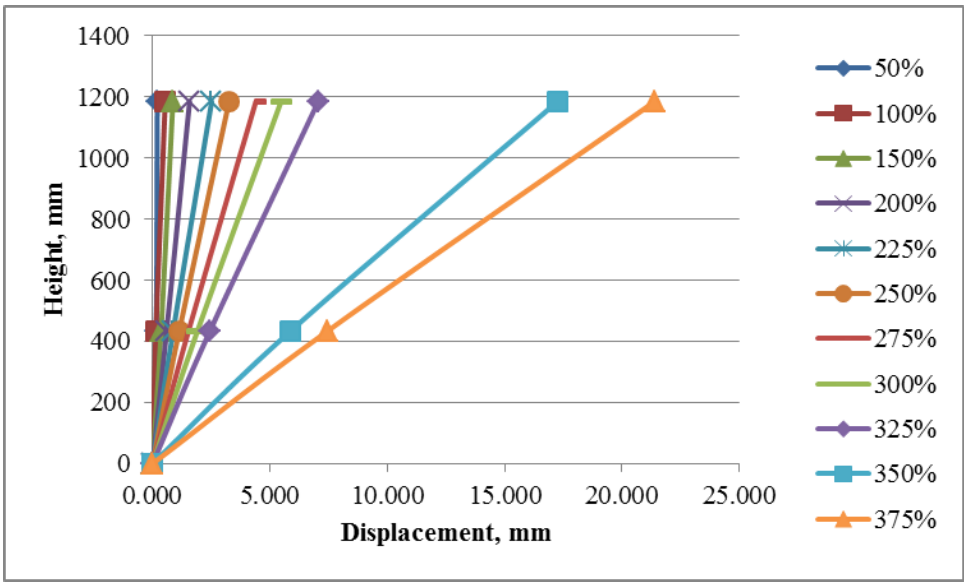

Figure 5.60 Profile of main wall at corner (Reinforced wall)

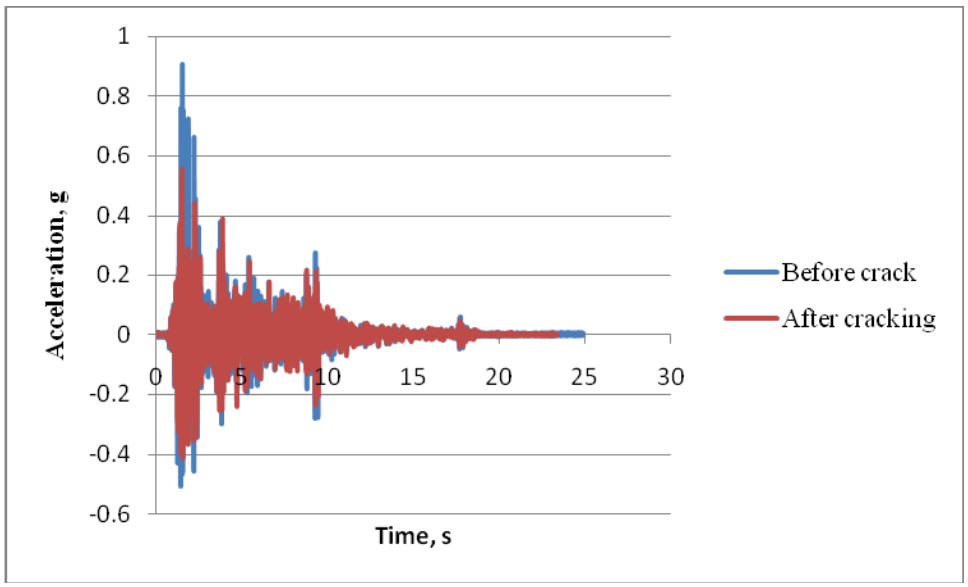

Figure 5.61 Response of the wall specimen before and after cracking

The wall specimen was again subjected to 100% intensity in order to compare with the response before cracking. It was found that the response was reduced considerably specially around peak region (Figure 5.61).

Instruments were removed and specimen was subjected to 400% loading intensity. The existing cracks enlarged. Few cracks appeared in the main wall starting from the middle of the wall at the top and inclined towards the corner around the middle height (Figure 5.62). The overall stability of the wall was still maintained.

Figure 5.62 Cracks in the main wall after 400% loading intensity

The moisture contents of the mortar specimens collected from the specimen after the test was observed as shown in Table 5.12.

Table 5.12 Moisture content of reinforced shake table specimen

Sample	Container	Container + Mortar	Container + Mortar (Dry)	Moisture
	g	g	g	%
1	362.7	1285.8	1269.6	1.79
2	356.8	1286.0	1269.4	1.82
3	354.0	1323.1	1304.7	1.94
Average				1.85

5.4 **Summary**

In order to maintain a smooth surface of wall specimens, every piece of stone was cut along one side using a diamond saw, whereas the corner stone was cut along two adjacent orthogonal sides. The remaining sides of the stone piece were maintained in their natural state so that it could behave as rubble wall.

Three unreinforced rubble wall specimens of size 500 mm x 350 mm x 1050 mm were prepared for testing in compression. A method was developed to create a smooth top surface of the wall. The average compressive strength of the wall specimens was 1.8 MPa. The average modulus of elasticity of wall at one third stress level was observed as 0.3 GPa.

The flexural strength of wall was determined by four point bending test in vertical span as well as lateral span. A purpose made platform and testing set up were developed for preparing and testing of wall specimens. Five unreinforced wall specimens of size 500 mm x 350 mm x 1400 mm were prepared and tested in vertical span. The average flexural strength (at crack initiation) in vertical span was observed as 48 kPa. However, the wall remained stable up to a large deflection after the initiation of cracking.

Three reinforced wall specimens (500 mm x 350 mm x 1400 mm) were also prepared and tested in similar condition in vertical span. In one wall specimen, reinforcement (GSW) was fabricated by direct weaving method. Pre-fabricated mesh was used for reinforcing the other two specimens. The initial cracking load was almost similar to unreinforced specimen. However, the ultimate load was almost double than that of unreinforced specimen.

Three unreinforced wall specimens of size 1400 mm x 350 mm x 400 mm were prepared and tested in lateral span. The average flexural strength of the specimens in lateral span was observed as 85 kPa. The strength of wall was lost immediately after initial cracking. This shows that the unreinforced wall specimens fail in brittle manner while bending in lateral span.

Using pre-fabricated mesh method, two reinforced wall specimens (1400 mm x 350 mm x 400 mm) were also prepared and tested in lateral span. The initial cracking strength of reinforced specimen was increased by almost 50% as compared to unreinforced specimen. Unlike unreinforced wall specimen, the reinforced wall specimen did not fail after the initial cracking. The specimen continued taking higher loads with increased deflection. The ultimate strength of the reinforced wall specimen was increased by almost 2.4 times that of unreinforced specimen. The reinforced wall showed a highly ductile behaviour.

Two identical U-shaped wall specimens were prepared for shake table testing. A window was provided in the main wall. One of the specimens was reinforced with GWS using pre-fabricated mesh method. The shake table specimen was a representative of a half scale model of a part of a single storey room. Ground motion

recording of 1940 El Centro Earthquake was selected as a representative of seismic loading.

The first test run was conducted at a shaking intensity of 25% of the original EL Centro record and it was increased at a rate of 25% in each step in the subsequent runs. The mid span deflection of the main wall of reinforced specimen was only half of the unreinforced specimen. The first crack in reinforced specimen appeared only after applying 1.5 times the loading level that caused initial cracking in unreinforced specimen. The unreinforced wall was at the verge of collapse at ground shaking of 2.5 times the El-Centro intensity, but the reinforced wall survived ground shaking in excess of 4.0 times El-Centro intensity.

6. Analytical and Numerical Studies

In this chapter, theory of externally wrapped reinforcement has been proposed and extended to a GSW reinforced wall. This is followed by the load deformation curves and ultimate strength of hexagonal GSW mesh in vertical as well as horizontal direction. Then, some useful parameters of the mesh are presented. In addition, discussion on the contribution of the horizontally inserted mesh and the performance of external mesh in resisting the lateral load are given. Finally, these findings have been applied for checking the adequacy of the GSW reinforcement for a single storey and double storey buildings in seismic loading.

6.1 Theory of externally wrapped reinforcement

In order to explain the behaviour of an externally reinforced system, a theory has been proposed and some relations have been derived. These derivations are based on idealistic situations, which may be further refined by including other parameters in future works.

Suppose an ideal beam (strong in compression but weak in tension) of a rectangular section of depth D and width B, simply supported across span L, reinforced (wrapped around but not attached) with a flexible and highly extensible external wire along the middle width, is being subjected to an uniformly distributed load of w/unit length as shown in Figure 6.1 (supports not shown for clarity). Also, suppose the surface of the beam and the reinforcement is smooth so that there is no friction between them. Moreover, assume the wire is passed through a rounded slot at all corners of the beam.

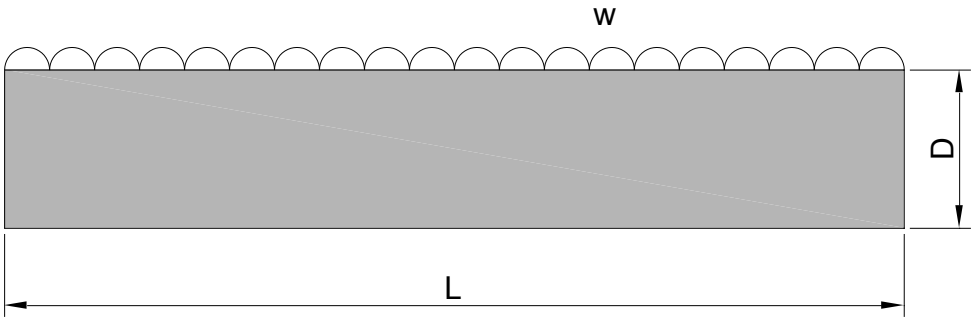

Figure 6.1 A simply supported ideal beam

As the load is increased, the bending stress will also be correspondingly increased. When the bending stress exceeds the flexural strength of the beam, a crack will be initiated on the bottom of the beam at mid span. The external reinforcement, which is not bonded with the beam, cannot come to action unless there is some rotation. Hence, the crack will propagate further into the whole depth and the beam tends to collapse. However, the external reinforcement will prevent the beam from complete collapse (Figure 6.2).

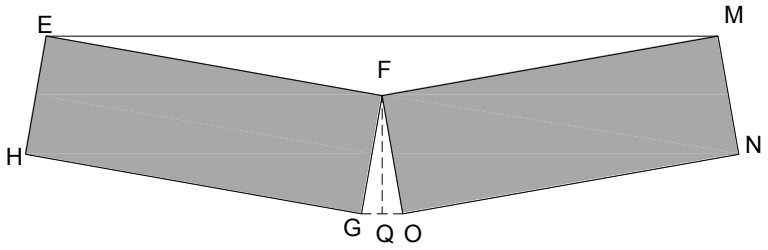

Figure 6.2 An externally wrapped beam after cracking

As the width of crack grows, there will be some rotation of the beam. Consequently, the external reinforcement at the bottom of the beam will be stretched and some

stress will be induced in the reinforcement. This tension is balanced by the compressive stress developed around point F. As a result, a couple will be formed, which will oppose further rotation of the beam. If the material is highly strong in compression, sufficient amount of tension can be induced in the reinforcement. The beam will be adjusted to a new equilibrium position such that the induced couple will be equal to the unbalanced moment due to the load. The amount of rotation of the beam depends on the deformation of the external reinforcement undergone to induce required amount of tension.

The reinforcement will be readjusted around the periphery of the beam. Therefore, the whole length of the cable will be in action.

Let the beam rotates by an angle θ.

Then,

EM = 2 (FM) cos θ = L cos θ

GO = 2 (GF) sin θ = 2 D sin θ

Total change in length of the wire,

ΔL= EM + MN + NO + GO + HG + HE - 2(L + D)

$$= L\ \cos\theta + D + \frac{L}{2} + 2D\sin\theta + \frac{L}{2} + D - 2(L + D)$$

$$\therefore \Delta L = L(cos\theta - 1) + 2D\sin\theta \qquad (6.1)$$

Differentiating both sides with respect to θ,

$$\frac{d(\Delta L)}{d\theta} = -L\ sin\theta + 2\ D\cos\theta$$

The change in length will be maximum when $\frac{d(\Delta L)}{d\theta} = 0$

or, $-L\sin\theta + 2\ D\ cos\ \theta = 0$

or, $\tan\theta = \frac{2D}{L}$

or, $\theta = tan^{-1}\frac{2D}{L}$ (6.2)

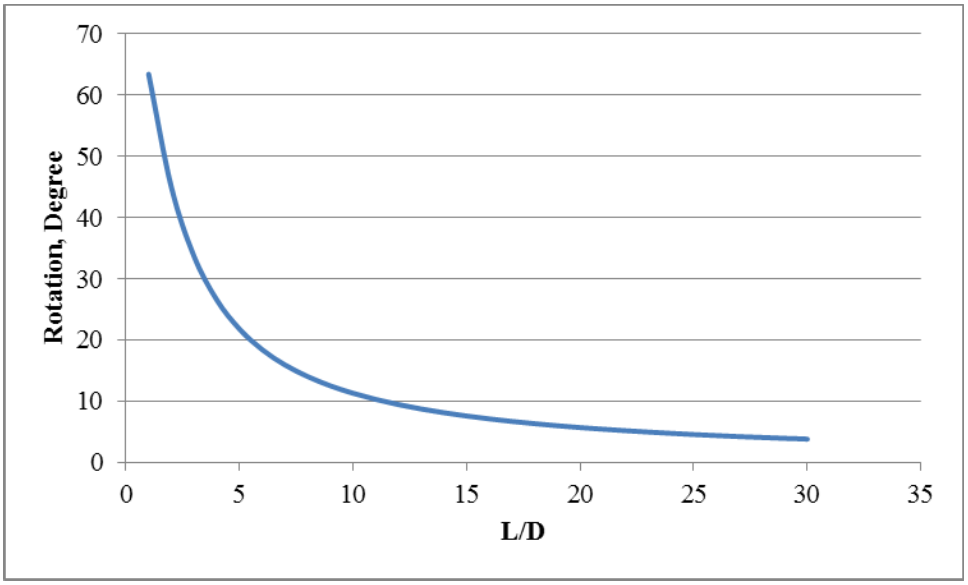

Figure 6.3 Variation of stable angle of rotation

Equation (6.2) gives the maximum angle of rotation up to which the beam will be stable. After exceeding this value, the beam will collapse. For instance, if the length

of wall is twice the depth, the beam will be unstable after a rotation of 45^0. This maximum angle of stability is plotted with respect to non-dimensional quantity L/D as shown in Figure 6.3. This figure shows that as the length of wall increases, it will become unstable even after a small amount of rotation.

As the length, L, cannot be zero, dividing by L on both sides in Equation (6.1) yields

$$\frac{\Delta L}{L} = \cos\theta - 1 + \frac{2D}{L}\sin\theta \tag{6.3}$$

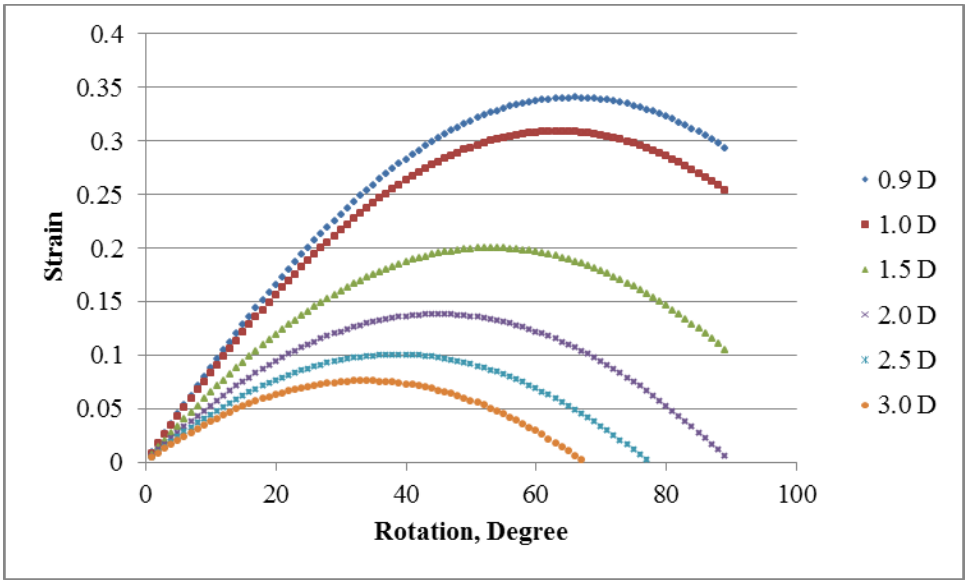

Figure 6.4 Variation of strain with rotation for different span

Equation (6.3) gives the strain induced in the reinforcement with the corresponding rotation. If a graph is plotted between the variation of the strain in the reinforcement with respect to rotation for different spans, it will be as shown in Figure 6.4. In this graph, span is chosen as a certain multiple of depth of the beam.

Suppose a rigid tie link is introduced at the middle of the beam. When the beam cracks, it will deflect as shown in Figure 6.5. Unlike the previous case, the tie wire will hold back the upper wire from lifting up (to be horizontal) and the reinforcement will be readjusted to the equilibrium position. This will improve the maximum angle of stability as well as stiffness of the system. The reinforcement will achieve higher strain at a lower rotation as compared to the previous case.

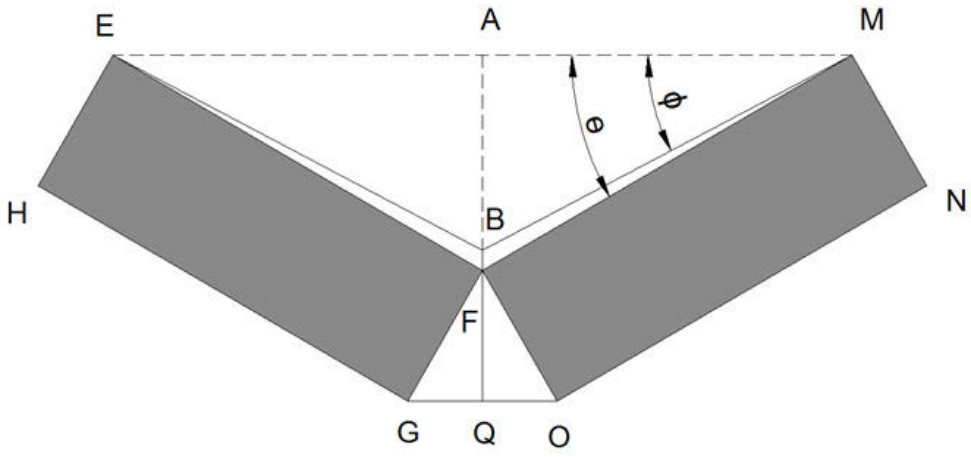

Figure 6.5 A beam with a tie link at middle span

From Figure 6.5, the change in length of the wire,

$\Delta L = EB + BM + MN + NO + OG + GH + HE - 2(L+D)$

Here,

$EB = BM;$

$(NO+GH) = L ;$

$MN = HE = D;$

OG = 2 D sin θ.

∴ ΔL = 2BM + 2D + L + 2 D sin θ - 2(L+D)

= 2 BM + 2 D sin θ – L

Also, $BM = \frac{AM}{COS\,\Phi} = \frac{AM}{\cos\left(tan^{-1}\left(\frac{AB}{AM}\right)\right)}$

Also, AB = AF – BF

$$= \frac{L}{2}\,sin\theta - (BQ - FQ)$$

$$= \frac{L}{2}\,sin\theta - (D - D\,cos\theta)$$

$$= \frac{L}{2}\,sin\theta - D(1 - \,cos\theta)$$

Also, $AM = FM\,cos\theta = \frac{L}{2}\,cos\theta$

$\therefore BM = \frac{AM}{COS\,\Phi} = \frac{AM}{\cos\left(tan^{-1}\left(\frac{AB}{AM}\right)\right)}$

Substituting these values, yields

$$\therefore \Delta L = 2\,\frac{AM}{\cos\left(tan^{-1}\left(\frac{AB}{AM}\right)\right)} + 2D\,sin\theta - L$$

$$or, \Delta L = 2\frac{\frac{L}{2}\cos\theta}{\cos\left(\tan^{-1}\left(\frac{\frac{L}{2}\sin\theta - D(1-\cos\theta)}{\frac{L}{2}\cos\theta}\right)\right)} + 2D\sin\theta - L$$

$$or, \Delta L = \frac{L\cos\theta}{\cos\left(\tan^{-1}\left(\frac{\frac{L}{2}\sin\theta - D(1-\cos\theta)}{\frac{L}{2}\cos\theta}\right)\right)} + 2D\sin\theta - L$$

$$or, \frac{\Delta L}{L} = \frac{\cos\theta}{\cos\left(\tan^{-1}\left(\frac{\frac{L}{2}\sin\theta - D(1-\cos\theta)}{\frac{L}{2}\cos\theta}\right)\right)} + 2\frac{D}{L}\sin\theta - 1 \quad (6.4)$$

Equation (6.4) was plotted with respect to rotation for different values of L (multiple of depth, D), as shown in Figure 6.6.

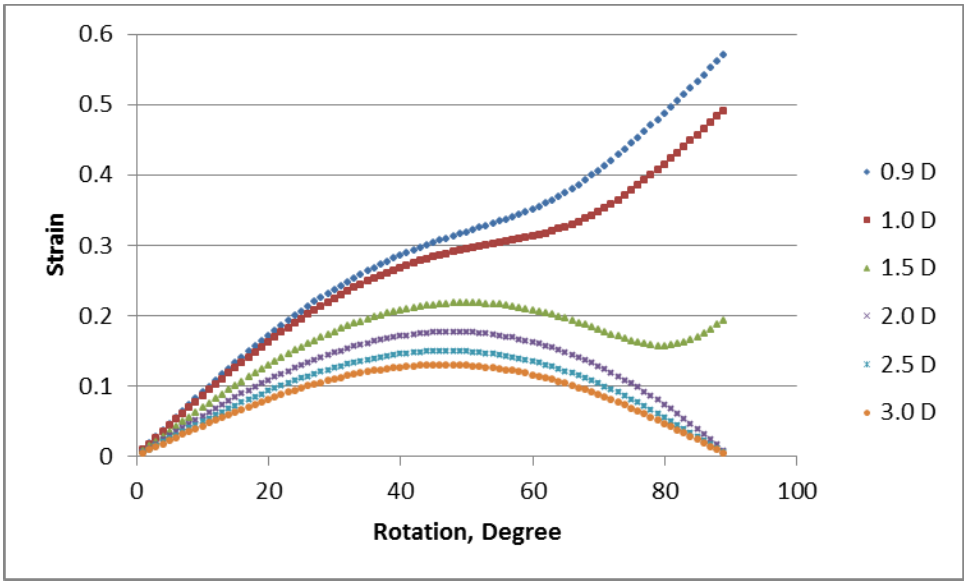

Figure 6.6 Variation of strain with rotation for a beam with a tie link at mid span

This graph shows that as long as the span of the beam is less than D, the beam remains stable for all values of rotation. If the span lies between the range D and just below 2D, the beam will not collapse even after exceeding the first maximum strain.

Combining both cases (with and without central tie link) the strain variation curves are obtained as shown in Figure 6.7. In this curve, NL stands for no link and WL means with link. This graph shows that use of tie links improves the strain induced in the external reinforcement with respect to rotation of the beam. Such an improvement is higher for longer span as compared to shorter span.

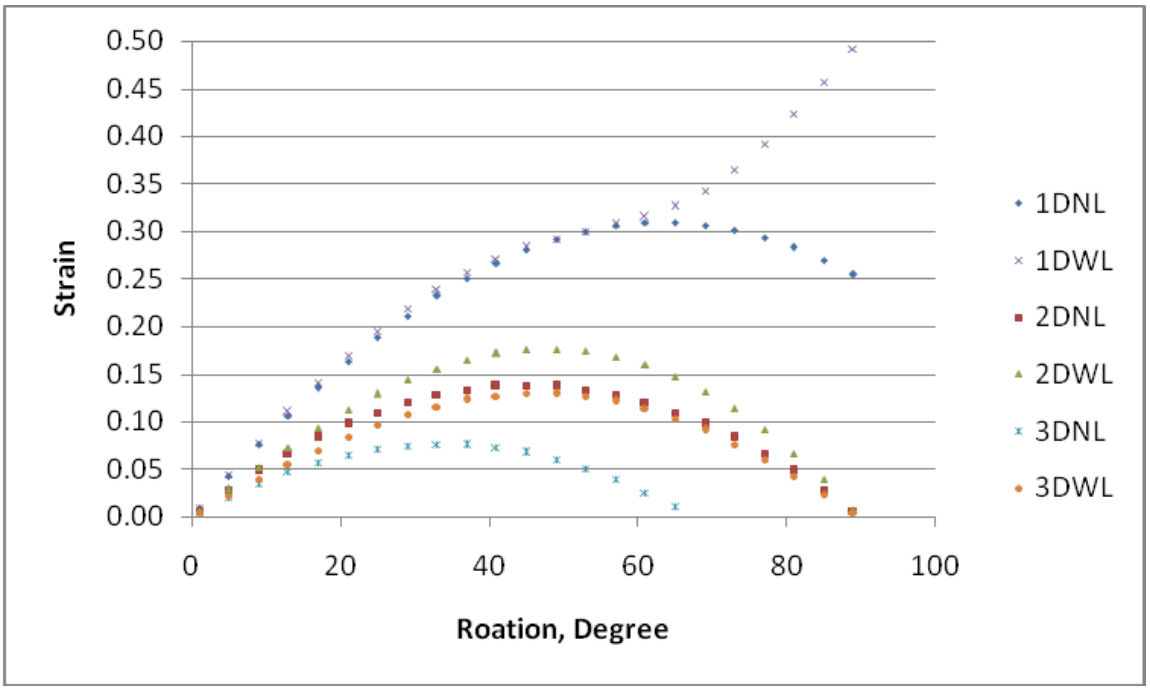

Figure 6.7 Overlapped strain variation curves

Suppose additional tie links are also introduced as shown in Figure 6.8. In this case, the scenario changes drastically. After a crack appears at the mid span, mostly the wire within the central two segments is mobilised, unless a new crack is formed at

either P or K due to tension in the wire. To simplify the case, suppose there is no crack at K and P.

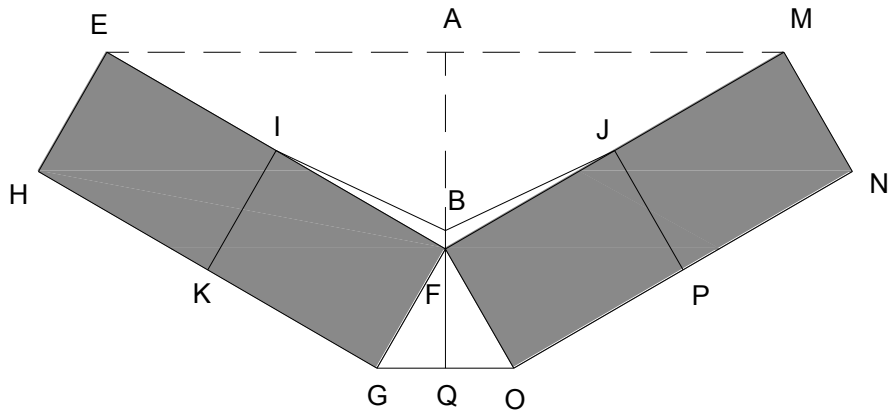

Figure 6.8 A beam with 3 tie links

Then,

change in length, $\Delta L = GO = 2\ D \sin\theta$

strain mobilised length, $s_m = 2\ S$

where, S = spacing of tie links

Strain in the wire is,

$$\varepsilon = \frac{2D \sin\theta}{s_m} \qquad (6.5)$$

Equation (6.5) is plotted against rotation for various spacing (multiples of depth) as shown in Figure 6.9. This shows that the effectiveness of strain mobilization

increases as the spacing is decreased. When spacing tends to zero, it will approach the externally bonded reinforcement case.

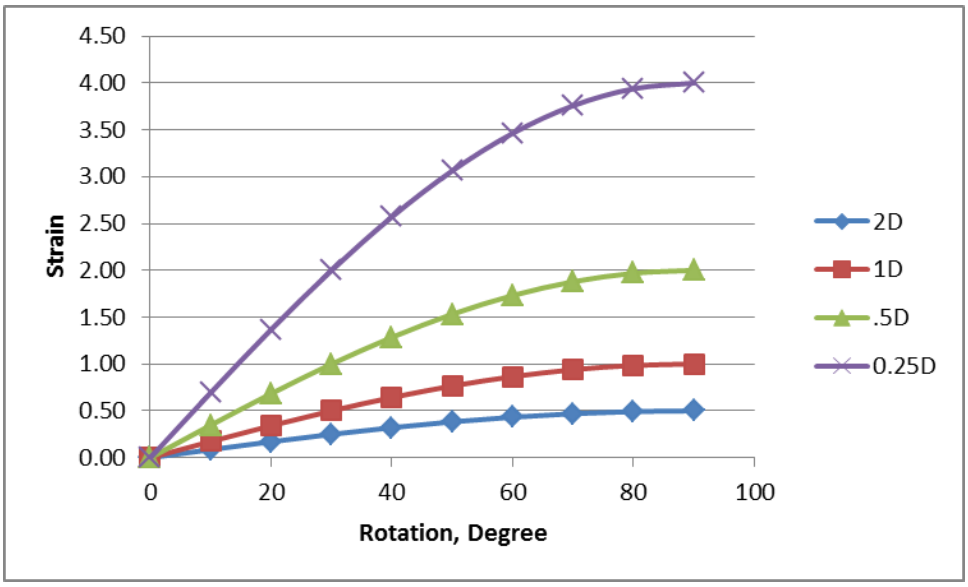

Figure 6.9 Strain variation for multi-link beam

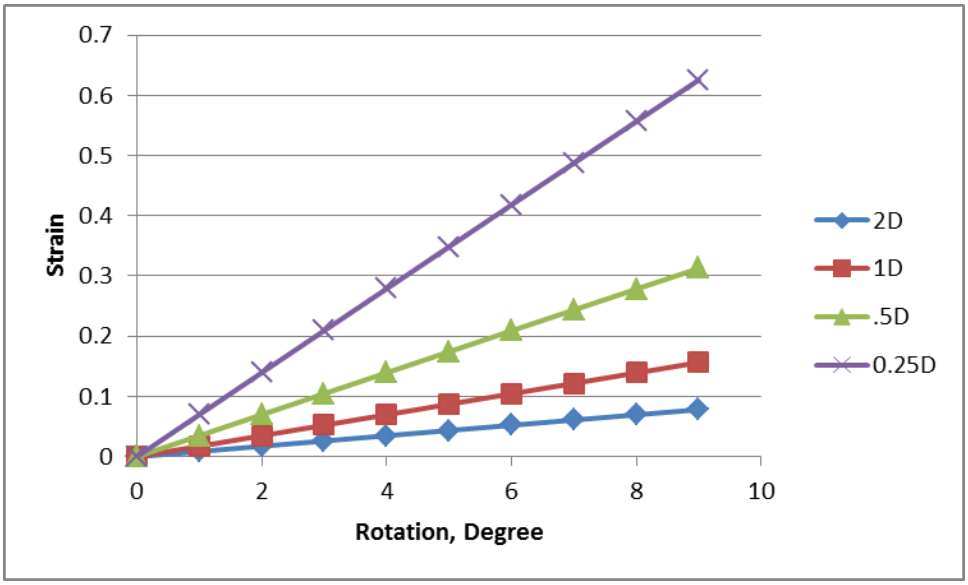

Figure 6.10 Strain variation for multi-link beam (Below 10^0)

From a practical point of view, behaviour of the reinforcement at higher degrees of rotation is not useful. To restrict within the limited rotation, only the lower part of the curve will be suitable, which is replotted in Figure 6.10.

As the bending strength of the thoroughly cracked beam is zero, the whole moment is balanced by the induced tension in the wire due to rotation of the beam.

Suppose M be the unbalanced moment on the half section of the beam. Considering only the right half section of the beam,

$$M = T D \cos\theta = f_t A D \cos\theta \quad (6.6)$$

where, T = Tension induced in the wire at the bottom of the beam

f_t = tensile stress in the reinforcement

A = area of cross-section of the reinforcement

Tensile stress in the reinforcement depends on the level of strain, Ɛ, which in turn depends on the angle of rotation as given by Equation (6.5). If the stress is within elastic range,

$$M = Ɛ E A D \cos\theta$$

where, E = modulus of elasticity

Using the value of Ɛ from Equation (6.5),

$$M = \frac{2 EAD^2}{S_m} \sin\theta \cos\theta \quad (6.7)$$

For small range of rotation, cos θ ≈ 1,

$$\theta = \sin^{-1}\left(\frac{s_m M}{2EAD^2}\right) \tag{6.8}$$

Equation (6.8) gives the approximate angle of rotation, θ (valid for small range), where the cracked beam will eventually be in equilibrium position.

In order to limit the deformation, the only way is to reduce the strain mobilised length of reinforcement. This can be achieved by decreasing the spacing of cross ties. Using a pair of wires as a cross tie at very small spacing is not practicable. However, a strip of horizontal mesh can be used instead of a pair of wires. In such a case, the spacing of the tie wire will reduce to the size of each cell of the mesh. This will considerably improve the deflection of the wall.

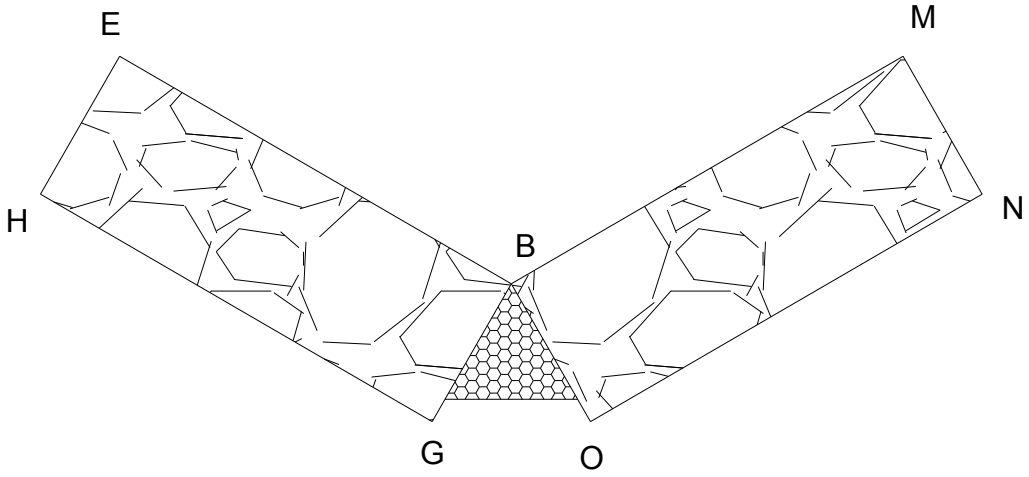

Figure 6.11 A wall with a horizontally inserted mesh (Plan view)

If a horizontal wire mesh is inserted in to a wall, the flexural behaviour of the wall will be improved. Without external wire mesh, the stone around points B and G/O

(Figure 6.11) may fall during reversible bending during an earthquake event. Also, the layer of horizontal wire mesh may slide into the wall. Therefore, reinforcing the wall with the horizontally inserted mesh alone is not so effective for resisting earthquake loading.

If the external mesh is tied with the inserted mesh, it will create a very effective system. This will not only stop stones falling from the region around points B and O/G but also prevent the inserted mesh from sliding into the wall (Figure 6.12). As a result, higher tensile stress will be mobilised in the inserted mesh as well as in the outer mesh along the connected region. Consequently, the flexural strength of the wall will increase significantly. Also, the deformation of the wall will be reduced accordingly.

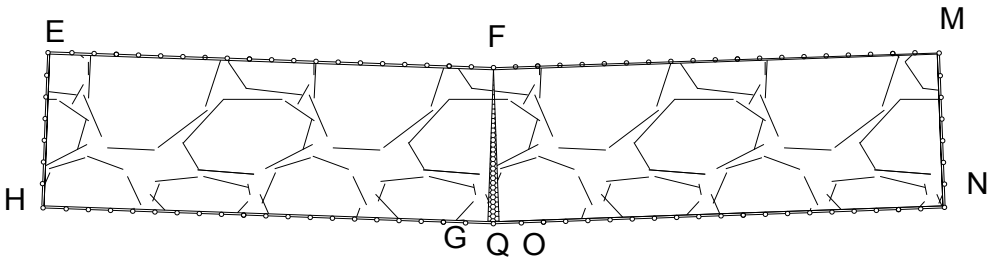

Figure 6.12 A wall reinforced with inserted mesh and external mesh (Plan view)

6.2 **Deformation characteristics of a hexagonal wire mesh**

A rubble is extremely less likely to be in a perfect hexagonal shape. Therefore, hexagonal wire mesh is useful for restraining the relatively smaller pieces of stone against falling from the wall during an earthquake event. However, the hexagonal wire mesh is more flexible than the wire used to weave the mesh. The flexibility of the mesh depends on support conditions along the side of the mesh. Therefore, the

equations developed in section 6.1 are not directly applicable in the case of hexagonal wire mesh.

In order to explain the behaviour of hexagonal mesh under vertical and horizontal loading, numerical models were created and analysed using finite element method. A unique numbering pattern (Figure 6.13) was developed for creating a hexagonal shape of the mesh. This numbering sequence can be repeated in regular intervals in order to create a series of mesh, which is very useful for generating the nodes or key points by writing command lines.

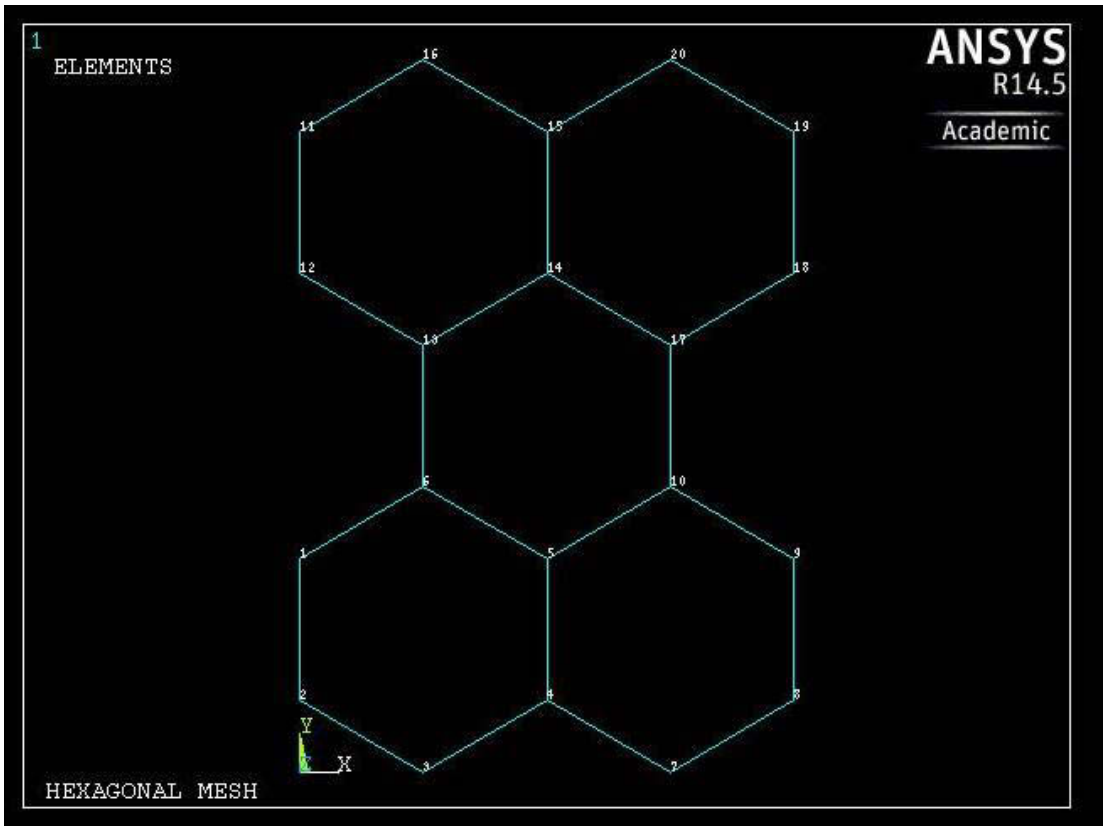

Figure 6.13 Numbering pattern of corner points

Each side of the mesh was modelled as a circular beam (BEAM188 in ANSYS). The vertical member of each cell of the hexagonal GSW mesh contains two wires,

whereas the inclined member is a single wire. Therefore, the vertical member was modelled as a member having twice the area of the inclined member. On the other hand, the inclined member is subjected to higher internal forces than the vertical member when the mesh is subjected to vertical or horizontal loading. Therefore, inclined members are more critical than the vertical members of the mesh.

6.2.1 Deformation along the vertical direction

For analysing the behaviour in the vertical direction, a model with a single hexagonal mesh of size (50 mm between parallel sides) was created and fixed at the bottom node. Initially, the diameter of the wire was taken as 1 mm and a bilinear stress strain curve was used. The ultimate strength of the wire was considered as 400 MPa.

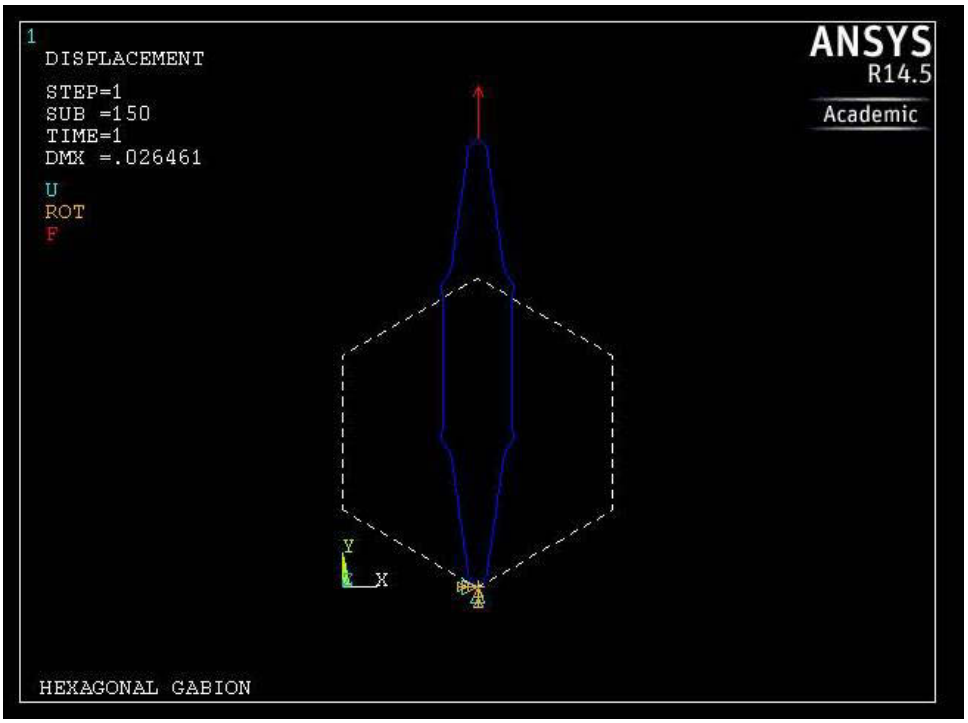

Figure 6.14 A single mesh with unrestrained sides under vertical loading

The model was subjected to a vertical point load at the top node. In the first stage, both left and right sides of the mesh were allowed to deform freely along the horizontal direction. The undeformed and deformed shape of the model was as shown in Figure 6.14. The mesh was highly stretched along the vertical direction even by a small amount of load (46 N).

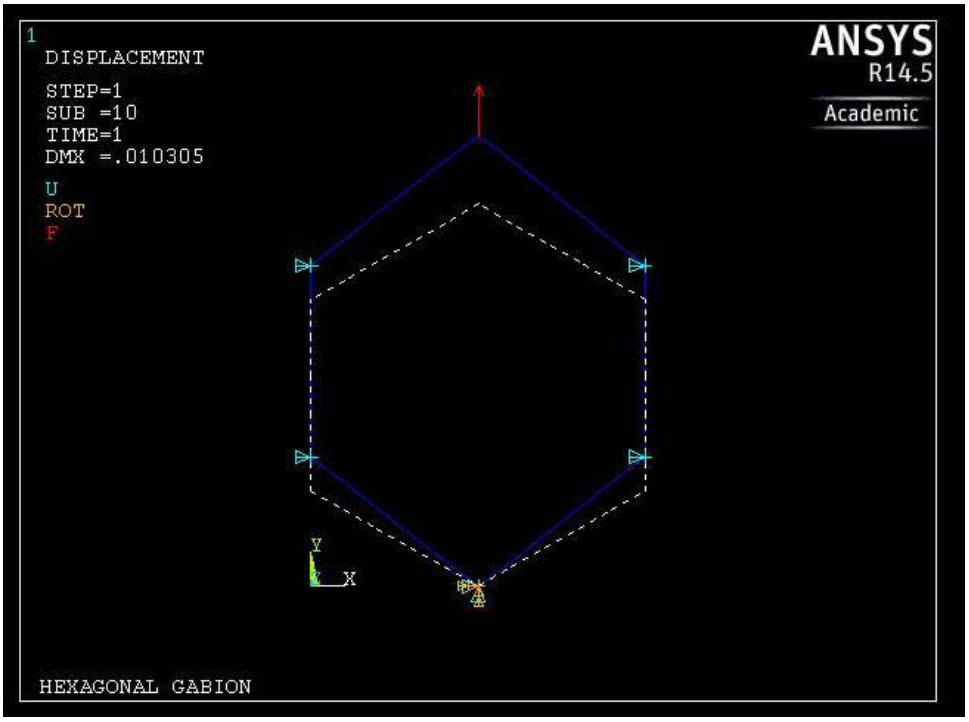

Figure 6.15 Vertical deformation of a single mesh with restrained sides

In fact, a mesh wrapped around the wall is not free to deform. The sides of the mesh on one face of the wall is restrained by the other meshes on orthogonal faces of the wall. Therefore, in the second stage, the sides of the model were restrained against horizontal deformation in order to create a similar situation as the mesh wrapped around the wall. In this case, the vertical deformation of the mesh was reduced considerably (Figure 6.15). This shows that externally wrapped mesh acts with

limited flexibility. The vertical load deformation curve of a constrained mesh with a single cell is shown in Figure 6.16.

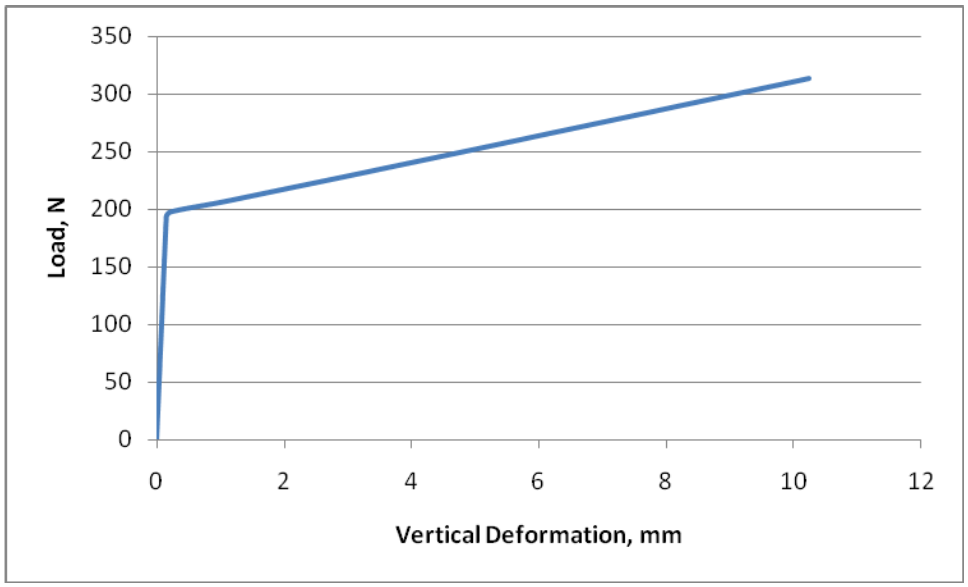

Figure 6.16 Vertical load deformation curve of a mesh with a single cell

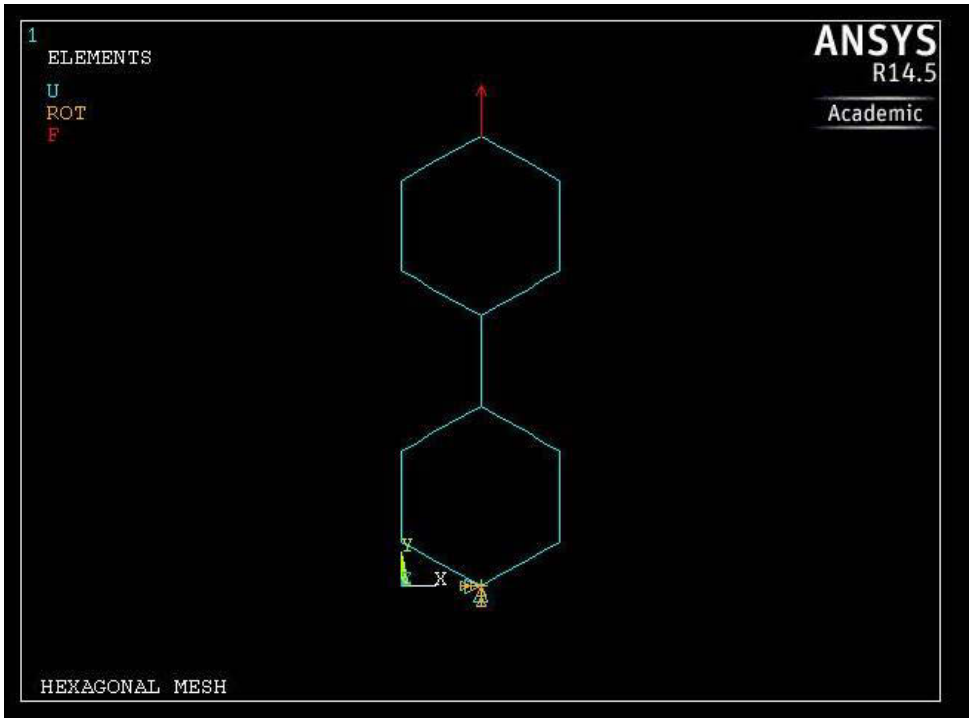

Figure 6.17 A single column model with two cells along the vertical direction

The influence of the height on the overall deformation of the mesh was further investigated by adding a number of cells along the vertical direction. For example, a mesh model having height of two cells is shown Figure 6.17.

Similarly, a series of other models were created by adding more and more cells on top of the other cells and the corresponding deformations were calculated. For simplicity, the number of cells along the height was increased in the order of 1,2,4,8 and 16.

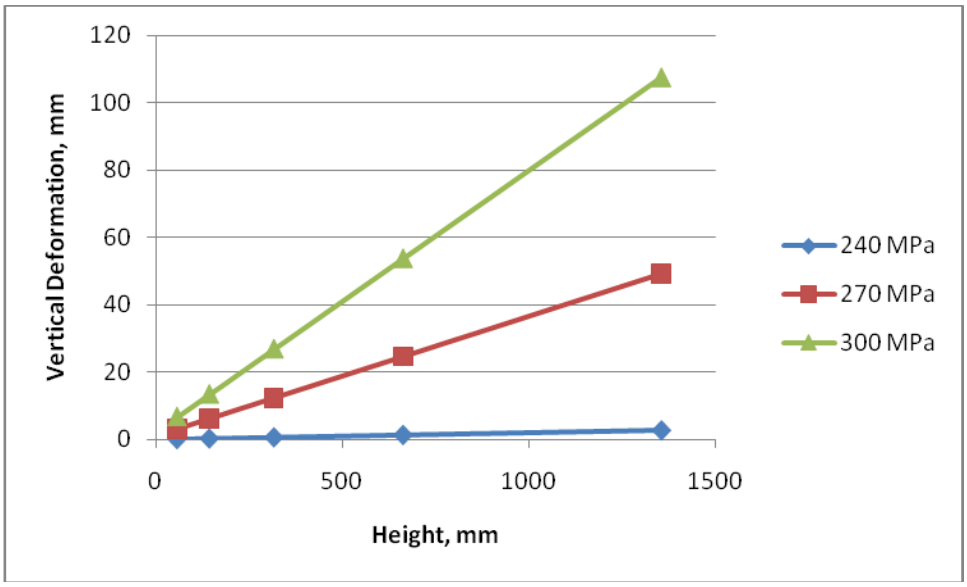

Figure 6.18 Vertical deformation of a mesh at various stress level

The deformation of the mesh depends on the stress level at each member. As the inclined member of the cell is the most critical one, the axial stress at the inclined member was taken as a reference for comparing the deformation as shown in Figure 6.18. Below the yield stress, the deformation of the mesh is significantly small. As the stress level exceeds the yield stress, the deformation increases considerably. However, the variation of deformation with height of the mesh at a particular stress

level is almost linear. This shows that hexagonal mesh behaves in a very stable manner.

Though the deformation of a constrained mesh is considerably lower than a unconstrained mesh, it is still higher than the deformation of a solid wire. As a result, wrapped (constrained) mesh imparts more flexibility to the wall as compared to a solid wire. The deformation of a mesh was compared with the deformation of an equivalent solid wire of the same height as the mesh.

As a vertical strip of a mesh with a single column of hexagonal cells is composed of two wires, the equivalent solid wire was taken as a wire having an area of cross-section twice the cross sectional area of a single wire. The same amount of loading was applied to the equivalent solid wire model as well as mesh model. The concept of an equivalent solid wire was envisaged to have an idea about how much deformation would be there using the same wires as straight form instead of a mesh.

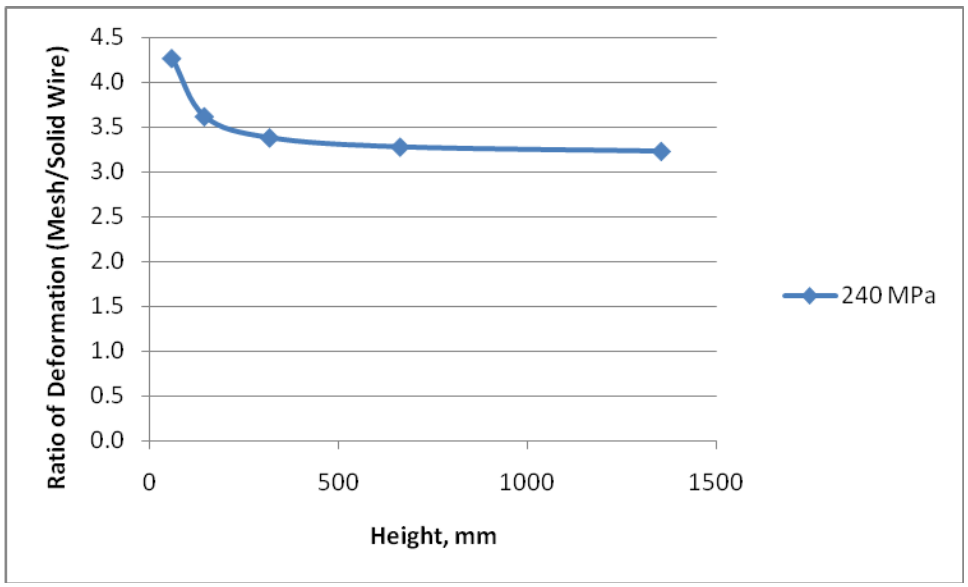

Figure 6.19 Variation of elastic deformation ratio (mesh/wire) along the height

Within elastic limit, the ratio of vertical deformation of a mesh with the deformation of the equivalent solid wire is as shown in Figure 6.19. This shows that as the height of a mesh increases, the deformation ratio (mesh/solid wire) decreases. However, this decrement converges to a certain value on further increase in the height of the mesh. Thus, the deformation of a mesh (higher than 8 cells height) is about 3.2 times higher than a solid wire within the elastic limit. Beyond elastic limit, such comparison is not useful because some parts of the mesh (inclined sides) will exceed elastic limit and other parts (vertical sides) will remain within elastic limit.

A mesh with a single column of cells is barely enough for covering a wall. Therefore, a mesh containing a number of rows and columns of cells will be required for reinforcing the wall. When additional columns of cells are accommodated between left and right sides of the mesh, the deformation behaviour may be different than the single column of cells. In order to study the effect of adjacent cells on the overall deformation of the mesh, the length was varied while keeping the height of the mesh constant. The length of the mesh was also increased in the order of 1,2,4,8 and 16 cells for a constant height of mesh (4 cells). One such models is shown in Figure 6.20.

The vertical deformation of each model was calculated and plotted at three different stress levels (on inclined member) as shown in Figure 6.21. As the length of a mesh increases, there is very slight increment in the vertical deformation. . This shows that the influence of change in the length of a mesh (height remaining constant) in the overall vertical deformation is negligible for a particular stress level.

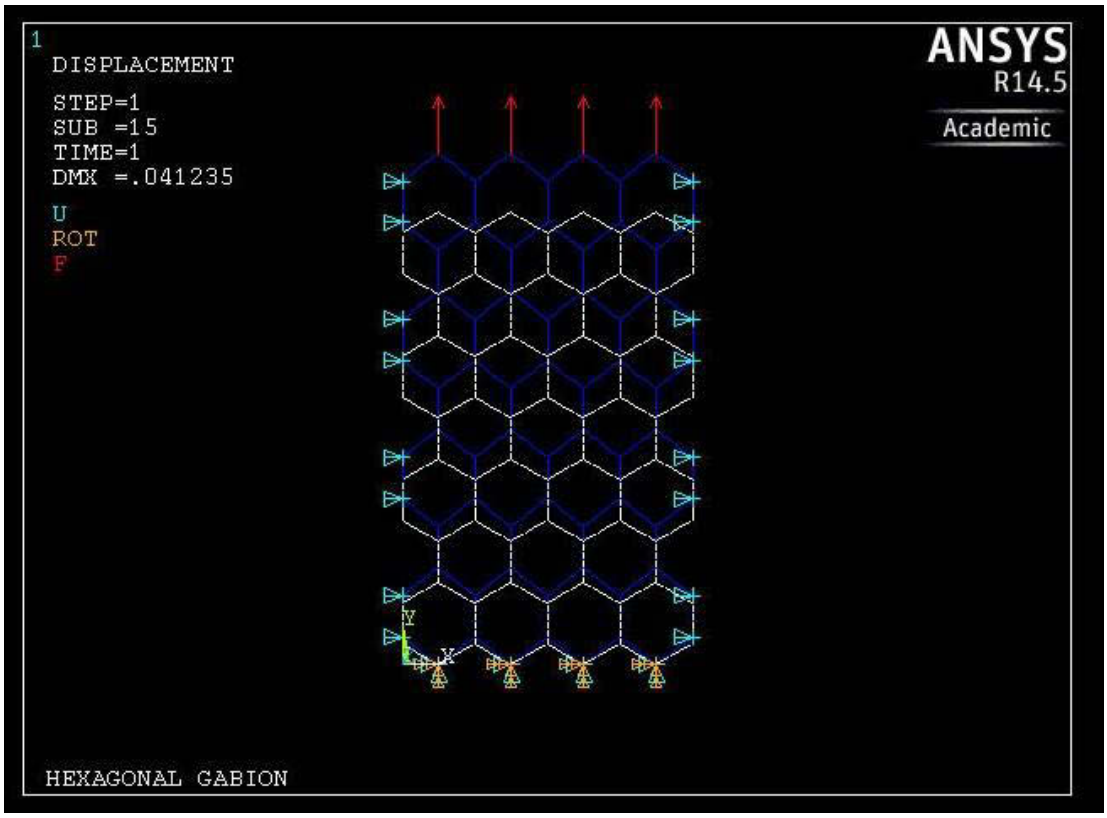

Figure 6.20 A multi-column mesh model with restrained sides

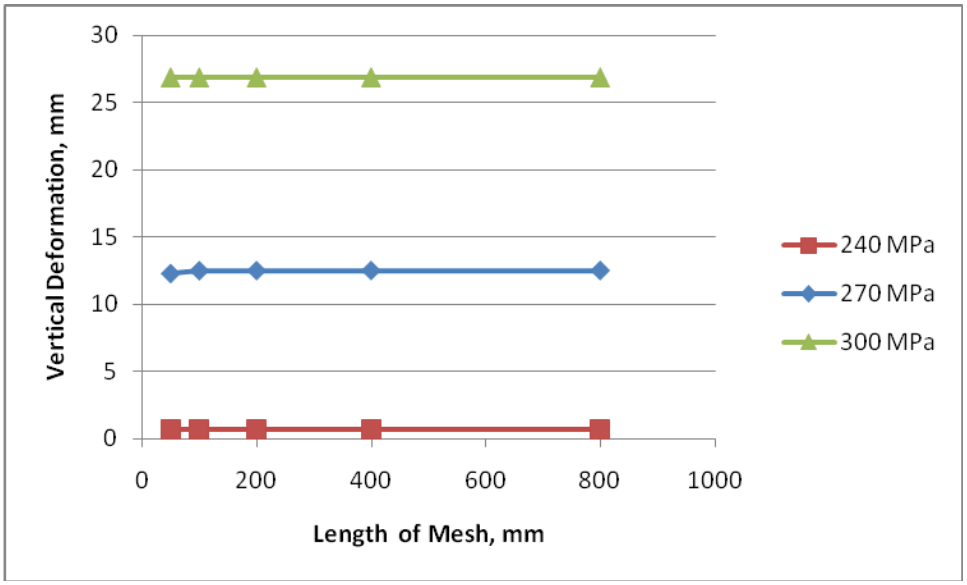

Figure 6.21 Deformation of a mesh of constant height with varying length

6.2.2 Deformation along the horizontal direction

In order to observe the behaviour in horizontal direction, the left side of the mesh was fixed, and the top and bottom corners of the cell were restrained against vertical deformation (Figure 6.22) for simulating a properly wrapped mesh around the wall.

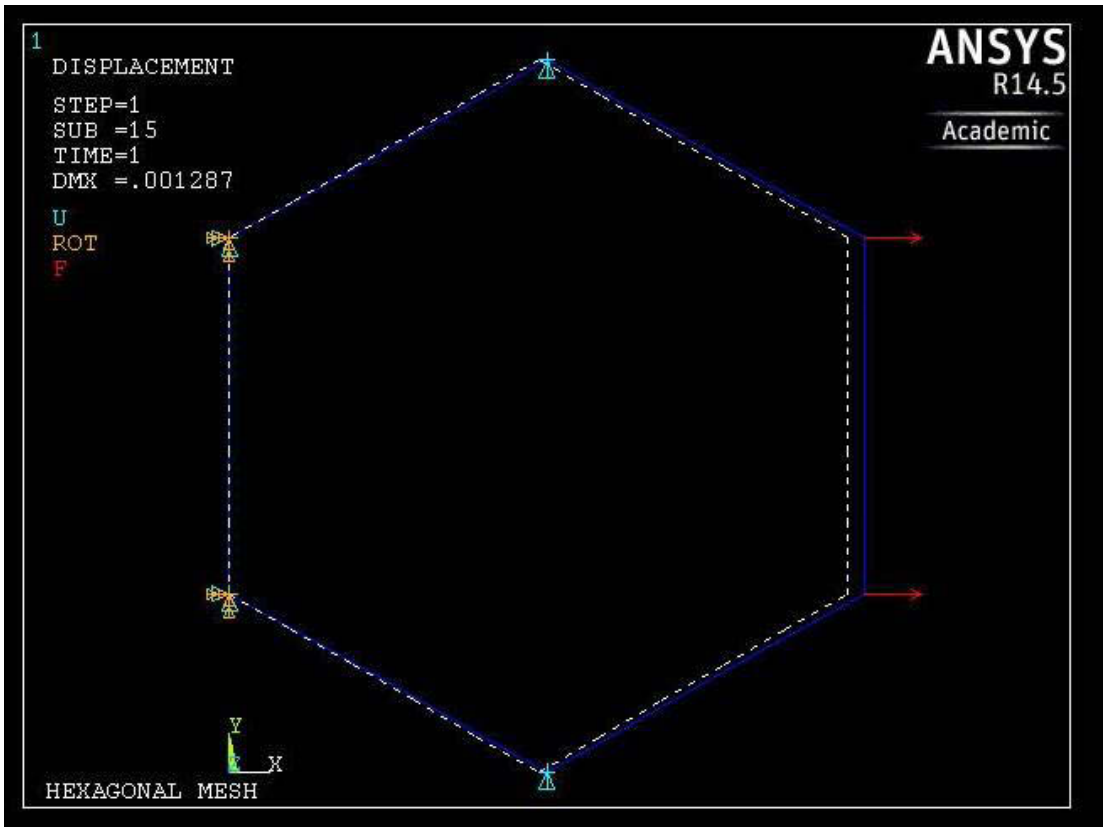

Figure 6.22 Horizontal deformation of hexagonal mesh with restrained sides

A horizontal point load was applied at each corner of the cell at the right side. The equivalence of load between horizontal and vertical direction was maintained by the concept of uniformly distributed load per unit length. The amount of horizontal UDL applied for horizontal deformation analysis was exactly the same as the load applied in the vertical deformation analysis.

Following similar steps as in the case of vertical direction, the length of the mesh was varied by adding additional cells to the right side (Figure 6.23) and corresponding deformation was calculated.

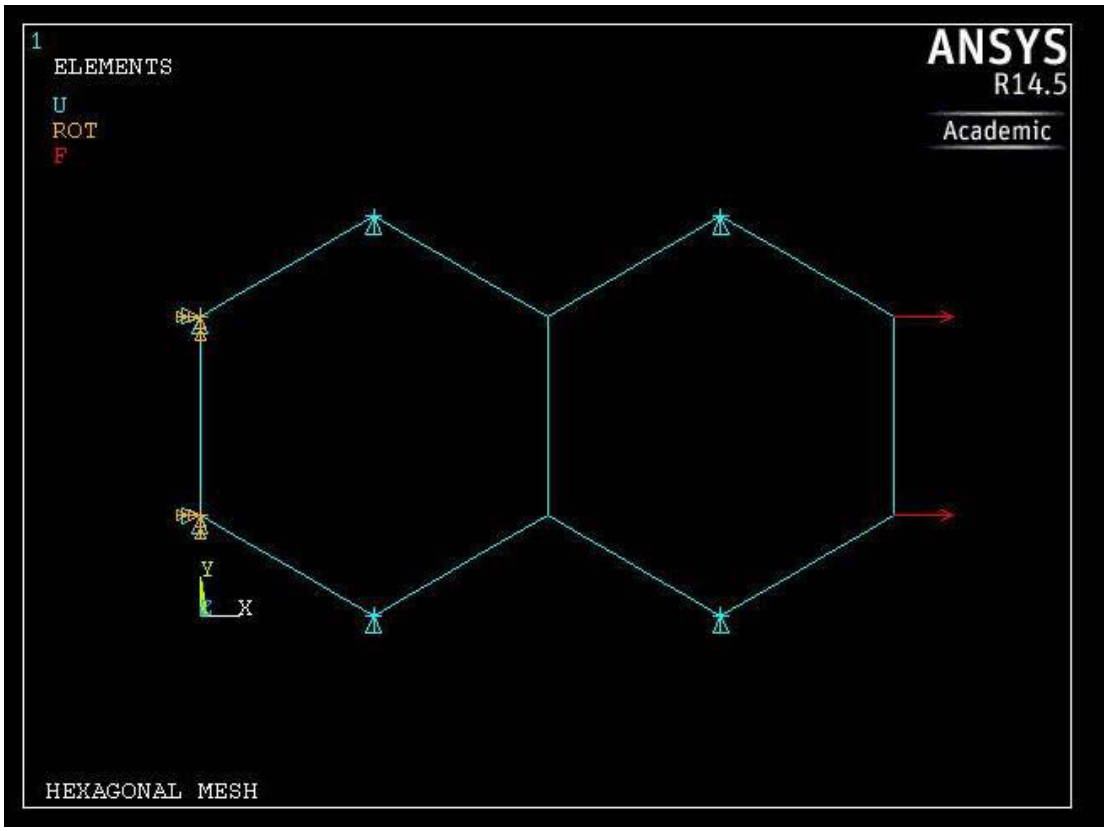

Figure 6.23 A single row mesh model with two cells

The variation of deformation at two stress levels (in inclined members) are shown in Figure 6.24. This figure shows that the change in deformation in the horizontal direction with the corresponding change in the length of the mesh follows almost a linear pattern.

The deformation of a mesh in horizontal direction was also compared with the deformation of an equivalent solid wire. In this case also, the equivalent solid wire

was taken as a wire having an area of cross-section twice the cross sectional area of a single wire and a length equal to the length of the mesh.

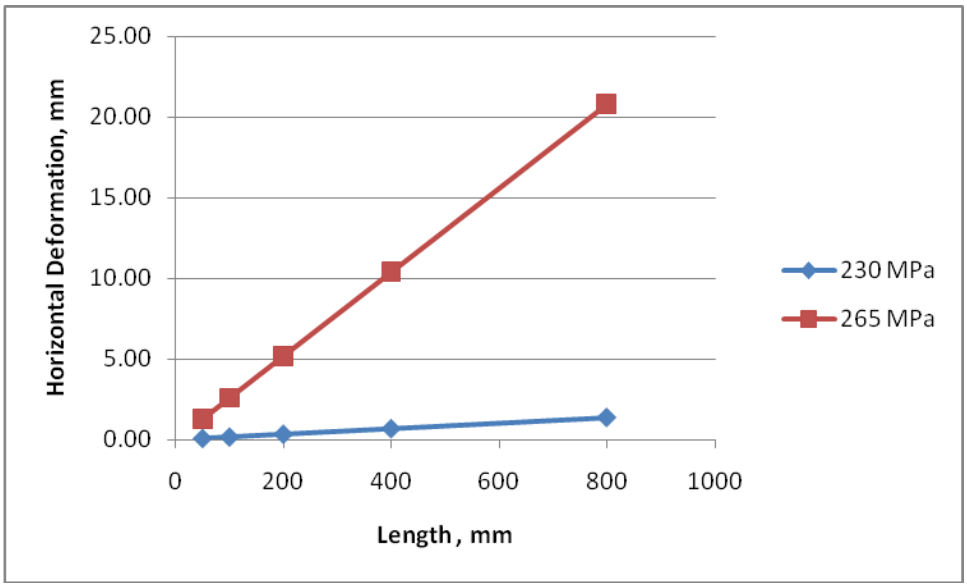

Figure 6.24 Horizontal deformation of a mesh at various stress levels

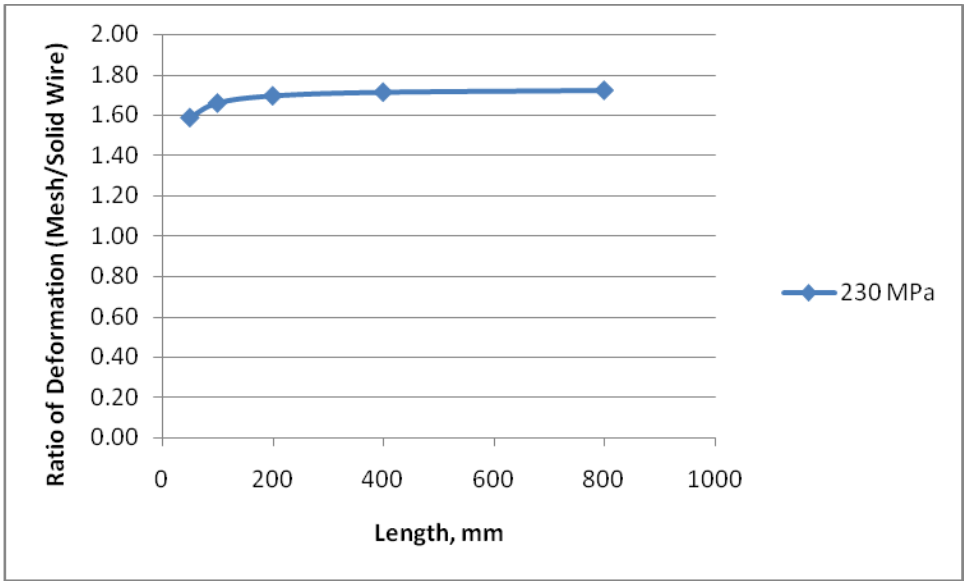

Figure 6.25 Variation of elastic deformation ratio (mesh/wire) along the height

Applying the same amount of loading to both the mesh model and the solid wire model, a deformation ratio curve for the stress level below the yield stress was obtained (Figure 6.25). This shows that as the length of a mesh increases, the deformation ratio (mesh/solid wire) also increases slightly. However, this value converges to a certain value with further increase in the length. Thus, the deformation of a mesh (longer than 8 cells) is about 1.7 times higher than a solid wire within the elastic limit. Comparing this value with deformation ratio in vertical direction, it shows that a row of hexagonal mesh is stiffer (in horizontal direction) than a column of hexagonal mesh (in the vertical direction). This is also obvious comparing the horizontal deformation of a single row of mesh and the vertical deformation of a single column mesh when subjected to an equal load per unit length (Figure 6.26).

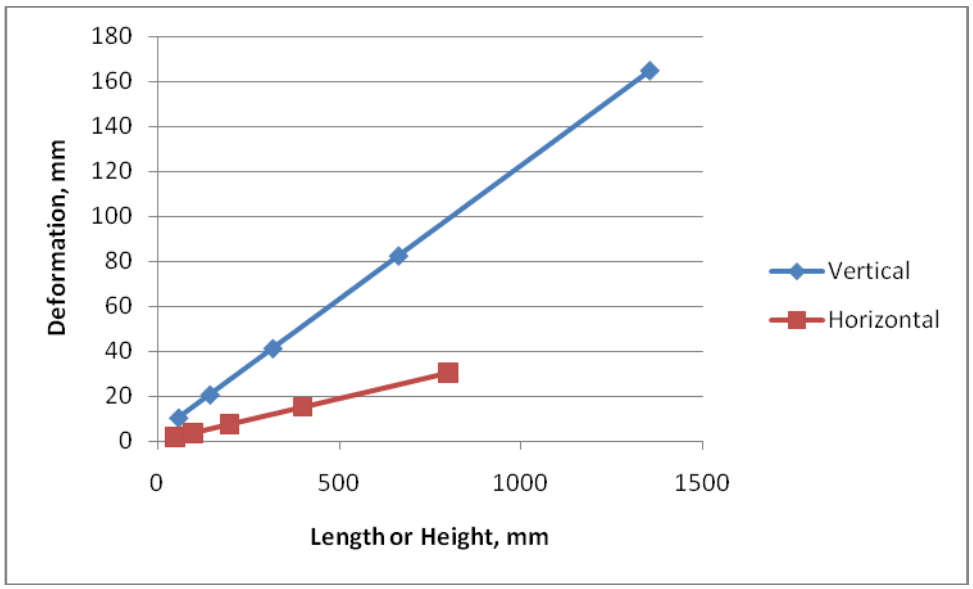

Figure 6.26 Deformation of a mesh under horizontal and vertical loading

The variation of horizontal deformation of a mesh with a constant length (4 cells) and varying height (1,2,4,8,16 cells) is shown in Figure 6.27 at two stress levels in the inclined member. This shows that as the height of the mesh increases, there is no significant change in the horizontal deformation of a mesh at a particular stress level.

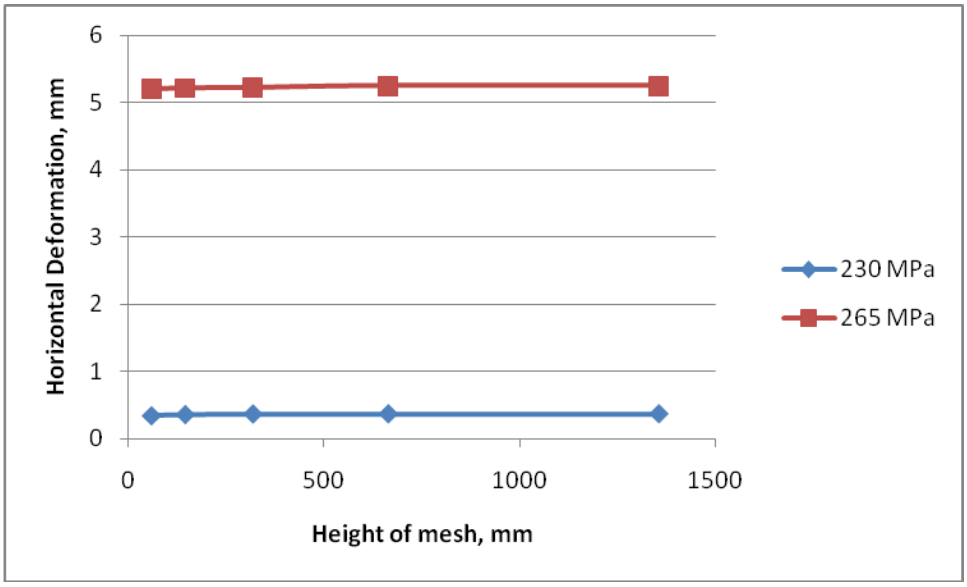

Figure 6.27 Deformation of a mesh of a constant length with varying height

6.2.3 Effect of cell size on the overall deformation of a mesh

Another set of mesh models were created with modified dimensions. The size of each hexagonal cell was increased to 100 mm (between parallel sides). The diameter of the wire was also increased to 2 mm in order to create a realistic mesh. The stress in both cases were maintained at the same level. The deformation of mesh having cell size of 100 mm (Mesh 100) was compared with the deformation of mesh having cell size of 50 mm (Mesh 50) as shown in Figure 6.28.

The deformations of both types of meshes fit exactly along the same line. This indicates that the deformation of a mesh is independent of opening size of the cell for a particular stress level. As a consequence, the deformation is proportional to the height or length of the mesh depending upon the direction of loading for a given material. This finding is very helpful for predicting the deformation of a mesh having any opening size on the basis of a set of predefined load deformation curves at various stress levels of a particular opening size.

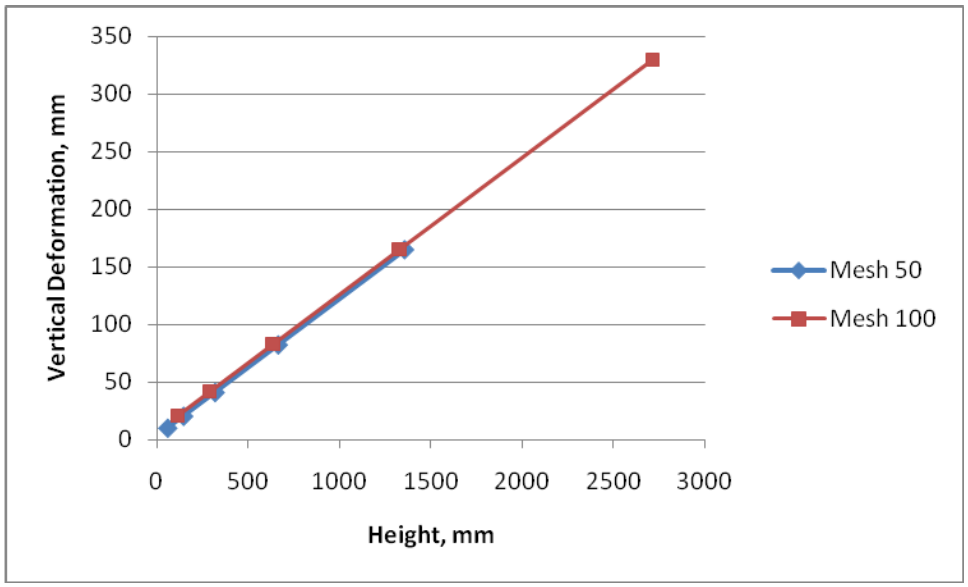

Figure 6.28 Comparison of deformation of mesh with different cell size

6.3 Ultimate strength of a mesh

The ultimate strength of a mesh is governed by the most critical member of the mesh. As explained in section 6.2, the most critical part of a hexagonal mesh is the inclined member.

6.3.1 Ultimate strength along the vertical direction

Suppose, a hexagonal mesh model is fixed at the bottom node and both sides corner nodes restrained against horizontal deformation (Figure 6.29). Consider, P to be a vertical point load acting at the top node, θ be the angle of inclined member with the horizontal.

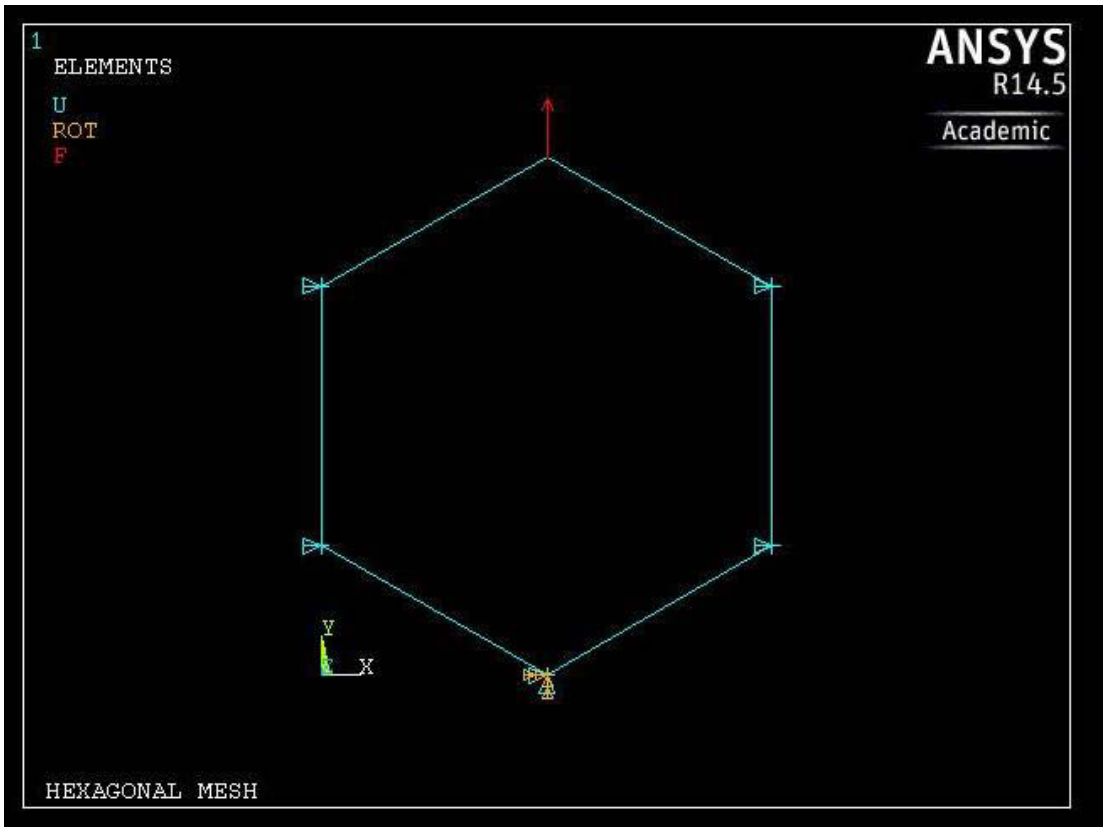

Figure 6.29 A hexagonal mesh with a single cell loaded in vertical direction

Then, the axial force, F_{av} on the inclined member is given by,

$$F_{av} = \frac{P}{2 \sin \theta} \tag{6.9}$$

And,

$$f_{av} = \frac{F_{av}}{A} = \frac{P}{2\,A \sin\theta} \qquad (6.10)$$

where,

f_{av} is the axial stress in the inclined member subjected to a vertical load,

A is the cross-sectional area of the member.

The ultimate strength of the wire was taken as 400 MPa. For a hexagonal mesh, initial value of θ is 30^0. If the wire was composed of inextensible material, the value of θ would not be changed for any value of load P. In that case, using Equation (6.10), the ultimate load carrying capacity of each cell would be 314 N for a wire of 1 mm diameter. However, in the case of real materials, as the load increases the value of θ increases due to extension of the member. As a result, more load can be carried by the inclined member. Therefore, the ultimate strength of the mesh depends on the stress strain curve of the material. Using the same parameters of the materials as used in the previous section, the ultimate capacity of the mesh (per cell) appears to be 450 N. On the other hand, the ultimate load capacity of the two straight wires of 1 mm diameter will be 628 N. Thus, the ultimate strength of a mesh is always less than the ultimate strength of solid wires used for weaving the mesh. However, by sacrificing of the strength, flexibility is introduced by the mesh.

Twenty cells (size 50 mm) can be accommodated per meter length of the mesh. Having 450 N load carrying capacity for each cell, the overall strength of the mesh (50 mm opening size, 1 mm diameter wire) will be 9.0 kN/m load distributed along the length of the mesh.

6.3.2 Ultimate strength along the horizontal direction

Suppose a horizontal point load, Q, is applied at each corner node of the right side of a hexagonal mesh having a single cell (Figure 6.30). The left side corner nodes are fixed, and the top as well as the bottom corner nodes are restrained against vertical deformation. Let θ be the angle of inclined member with the horizontal.

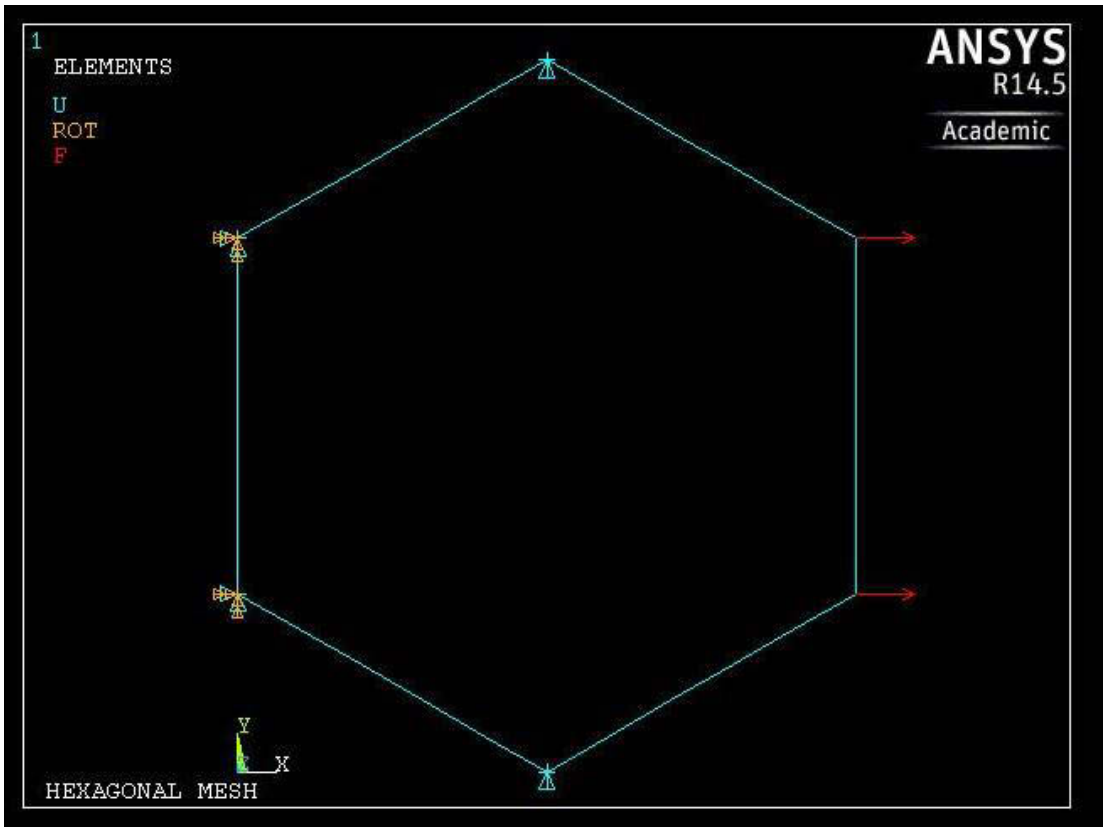

Figure 6.30 A hexagonal mesh with a single cell loaded in horizontal direction

Then, axial force, F_{ah} on the inclined member is given by,

$$F_{ah} = \frac{Q}{\cos\theta} \tag{6.11}$$

And, axial stress in the inclined member,

$$f_{ah} = \frac{F_{ah}}{A} = \frac{Q}{A\cos\theta} \qquad (6.12)$$

If the material was inextensible, the ultimate capacity of the mesh would be 2 x 272 = 544 N. However, for a real material, as the load increases, the length of member increases. As a result, the angle θ will decrease. Few iterations may be needed to determine the ultimate strength of the member. Using the same parameters as in the previous case, the ultimate load carrying capacity of the mesh with a single cell was obtained as 2 x 288 = 576 N. Comparing with the previous case, a single cell is stronger in horizontal direction than in the vertical direction. However, this is not valid for the strength of a mesh containing more than a single row and a single column of cells.

The length of each side and the height of a hexagonal cell with 50 mm opening size between parallel sides will be 28.9 mm and 57.7 mm, respectively. In the horizontal direction, a hexagonal mesh can be considered as a series of horizontal rows of cells interconnected with a rows of vertical sides. Almost 12 rows of cells can be accommodated per meter height of the mesh. The total height of 12 rows will be 1.01 m. Therefore, the ultimate capacity of 576 N per cell in the horizontal direction is equivalent to 6.84 kN/m along the height of the mesh.

Comparing this value with the ultimate strength of the mesh in the vertical direction, it seems that the hexagonal mesh is about 30% stronger in the vertical direction than in the horizontal direction.

6.4 Some useful parameters of a hexagonal mesh

Some parameters of a hexagonal mesh, which may be used for evaluating the deformation of the mesh subjected to various loading conditions have been evaluated and presented in this section. As the deformation of the mesh for a given height (or length) remains almost constant when the other dimension (length or height) exceeds by 8 cells, a mesh model having 12 cells height and 20 cells length was used in order to calculate these parameters.

6.4.1 Deformation per unit height or length of a mesh

Figure 6.31 shows the vertical deformation per meter height of a mesh (cell size of 50 mm between two parallel sides and wire diameter of 1 mm) for a uniformly distributed load (UDL) per unit width of a mesh applied vertically. The vertical UDL was varied gradually and the corresponding deformation was obtained. In order to get the deformation per unit height, the vertical deformation was divided by the total height of the mesh model (12 cells high, 20 cells long).

This chart may be useful to calculate the vertical deformation of the hexagonal mesh for a specific value of a uniformly distributed load. For example, if a mesh (cell size of 50 mm, wire diameter of 1 mm) of height 2.4 m is subjected to a vertical UDL of 4.5 kN/m width of the mesh, the deformation per metre height corresponding to 4.5 kN is 31.5 mm (using Figure 6.31). Then, the total vertical deformation of the mesh will be 31.5 x 2.4 = 75.6 mm.

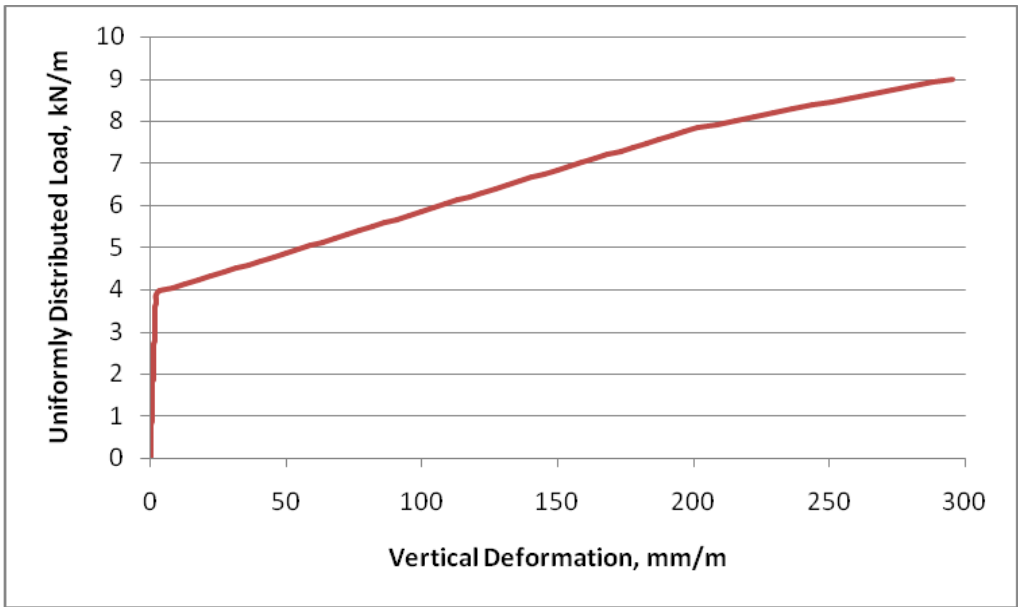

(a) Deformation up to 300 mm

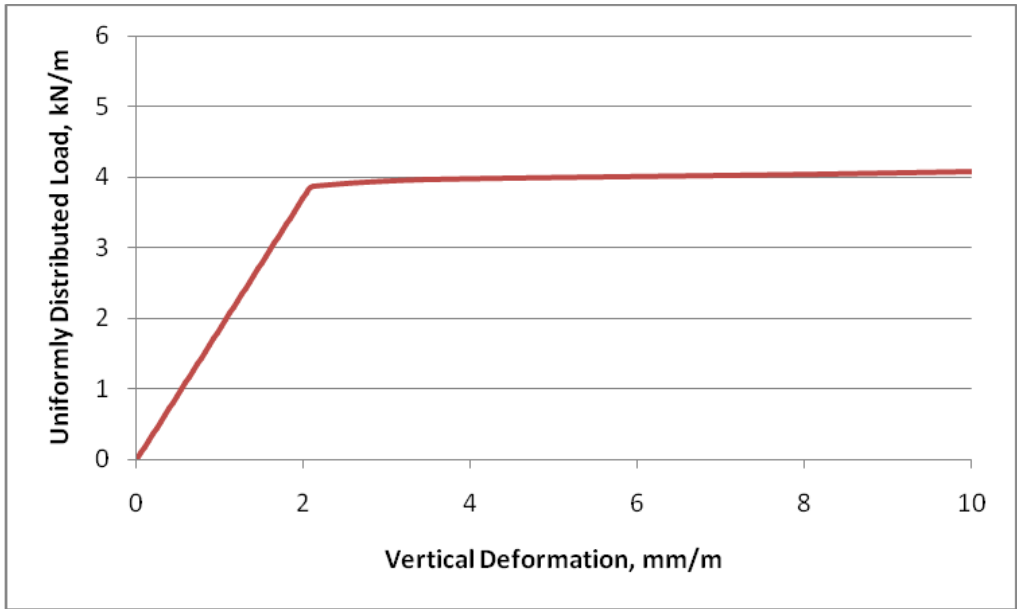

(b) Deformation below 10 mm

Figure 6.31 Vertical load-deformation curve (Mesh 50 mm, ϕ 1 mm)

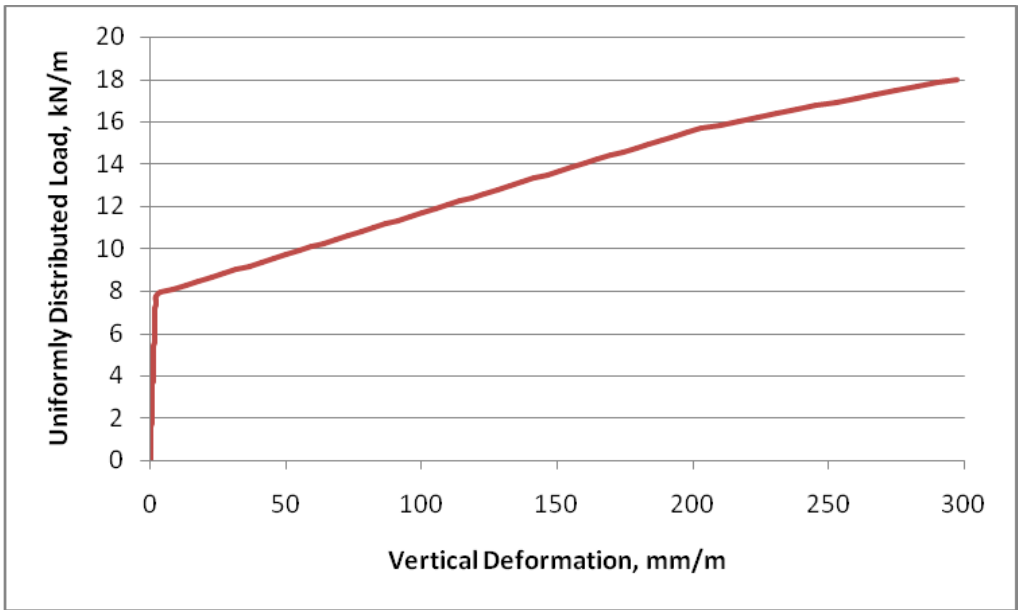

(a) Deformation up to 300 mm

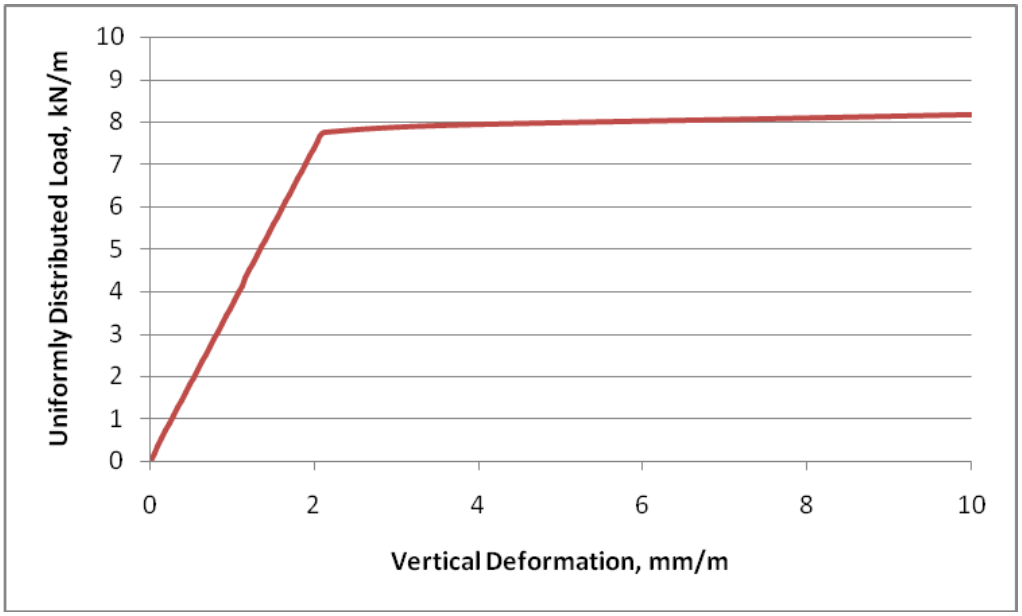

(b) Deformation below 10 mm

Figure 6.32 Vertical load-deformation curve (Mesh 100 mm, ϕ 2 mm)

If the cell size of the mesh is increased to 100 mm (between parallel sides) and the diameter of the wire to 2 mm, the vertical deformation per unit height of the mesh will be as shown in Figure 6.32. In this case, the load carrying capacity of the mesh

has doubled as compared to previous size of the mesh for a specific value of the deformation.

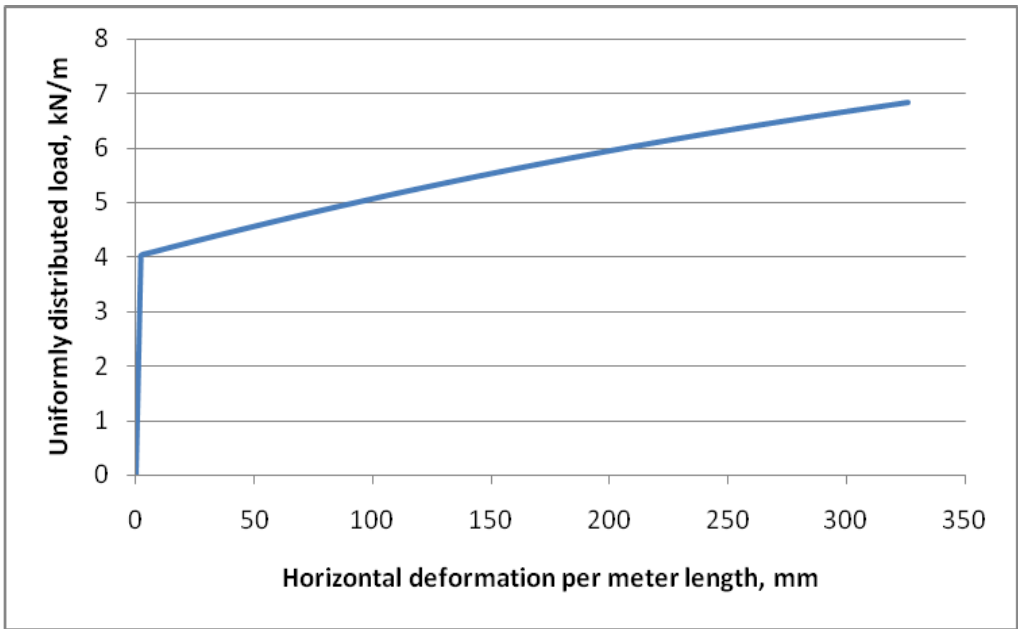

(a) Deformation up to 330 mm

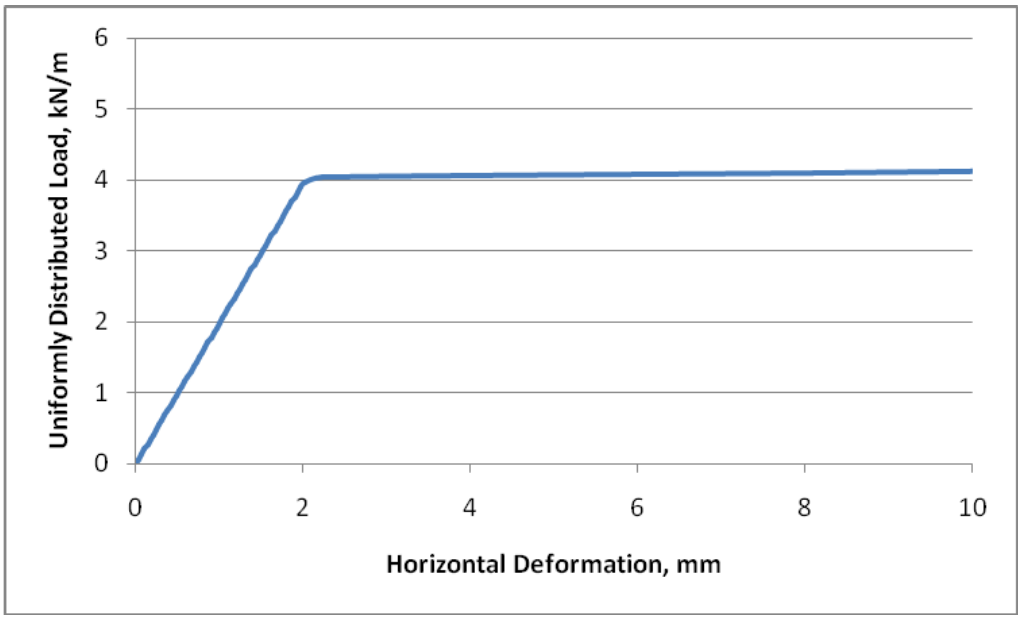

(b) Deformation below 10 mm

Figure 6.33 Horizontal load-deformation curve (Mesh 50 mm, ϕ 1 mm)

The horizontal deformation per meter length of a mesh (cell size of 50 mm, wire diameter of 1 mm) for a horizontal UDL per meter height of the mesh is given in Figure 6.33.

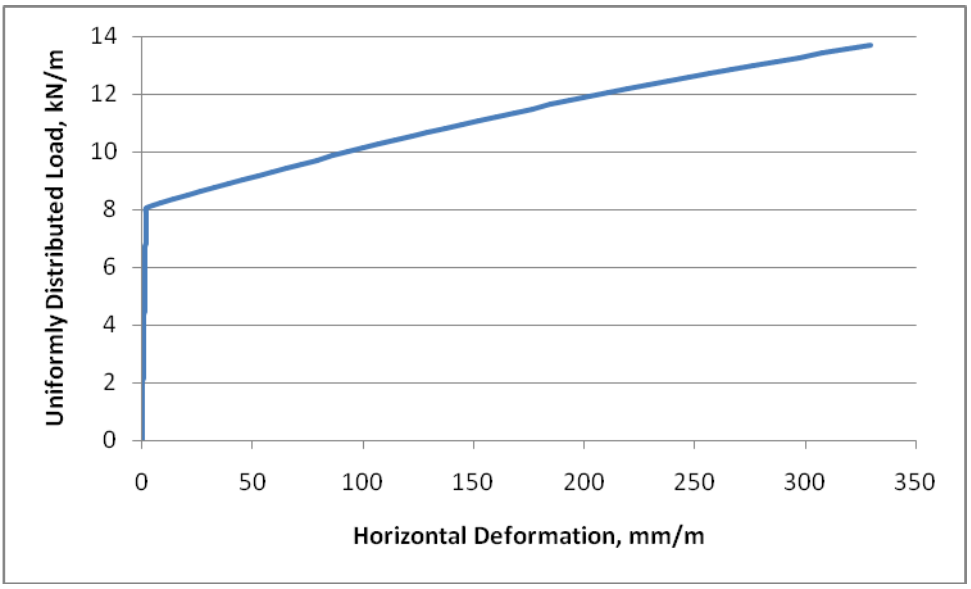

(a) Deformation up to 330 mm

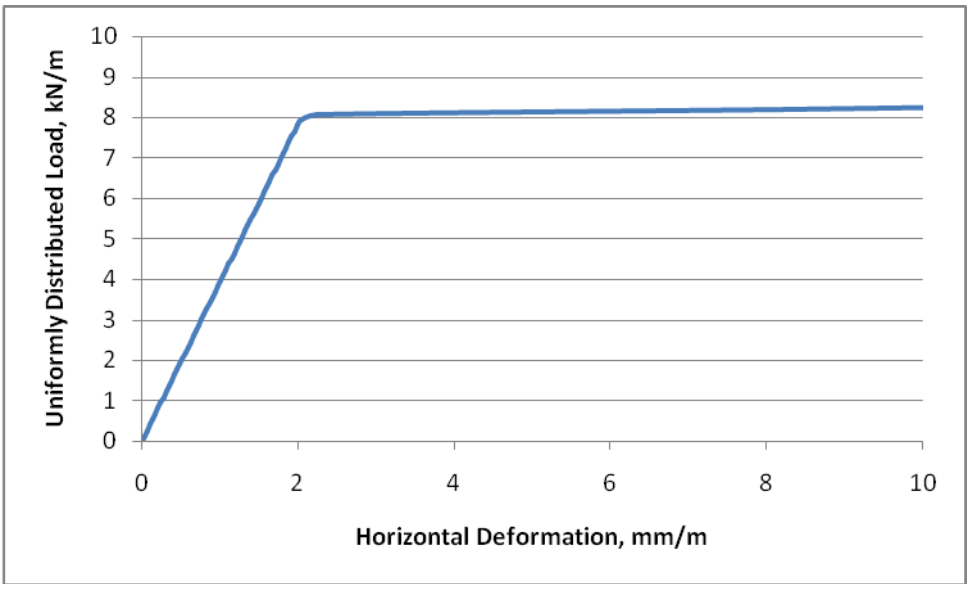

(b) Deformation below 10 mm

Figure 6.34 Horizontal load-deformation curve (Mesh 100 mm, ϕ 2 mm)

Following similar procedures, horizontal deformation of a mesh of given length can be calculated using this chart. Figure 6.34 shows the same parameter for a mesh of cell size 100 mm with wire diameter of 2 mm.

6.4.2 Equivalent stress strain curve of a mesh

All relations derived in section 6.1 for externally wrapped reinforcement are based on a single straight wire. As the deformation of a mesh is higher than a wire, the stress strain curve of the wire is not valid in the case of the mesh when using these equations.

In section 6.4.1, deformation of a mesh per meter height or length for a varying level of UDL in the vertical and horizontal direction have been evaluated. If the value of UDL is divided by the area of total number of wires effectively taking part in the direction of loading (per unit width), it will give an equivalent stress. Similarly, the value of the deformation of the mesh in mm per meter can be easily converted to equivalent strain by changing the deformation in meters. With these new values of stress and strain, the mesh is converted to a hypothetical wire having similar load deformation properties to the mesh as shown in Figure 6.35 and Figure 6.36.

Equivalent stress is always less than actual stress in the inclined member of the mesh. However, total force generated in the mesh can be calculated by multiplying the equivalent stress with an equivalent area. Similarly equivalent strain is always greater than the strain of a solid wire for a given stress level. The equivalent modulus of elasticity of the mesh in the vertical direction is 6.0×10^4 MPa, whereas in the horizontal direction it is 1.06×10^5 MPa.

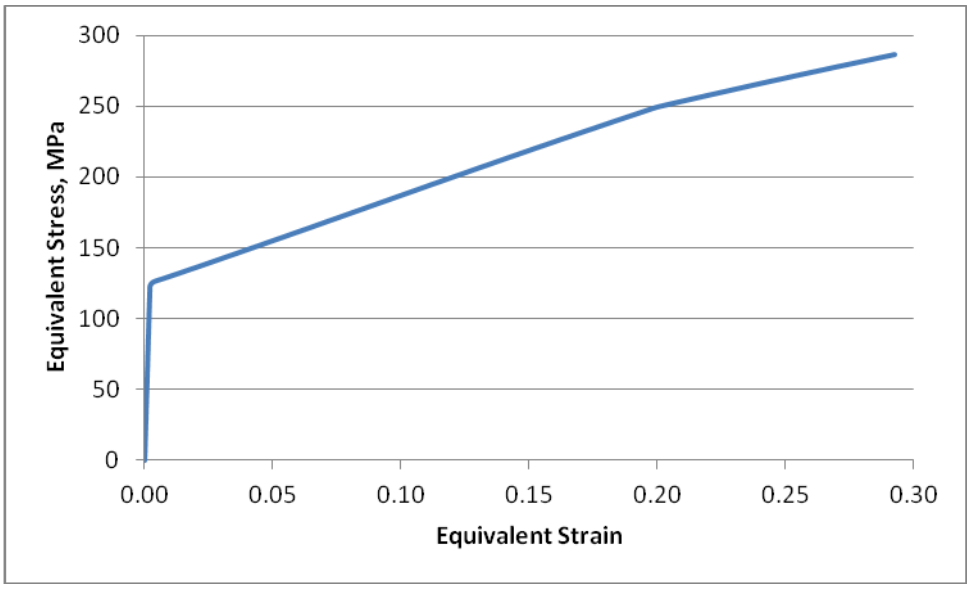

(a) Equivalent strain up to 0.29

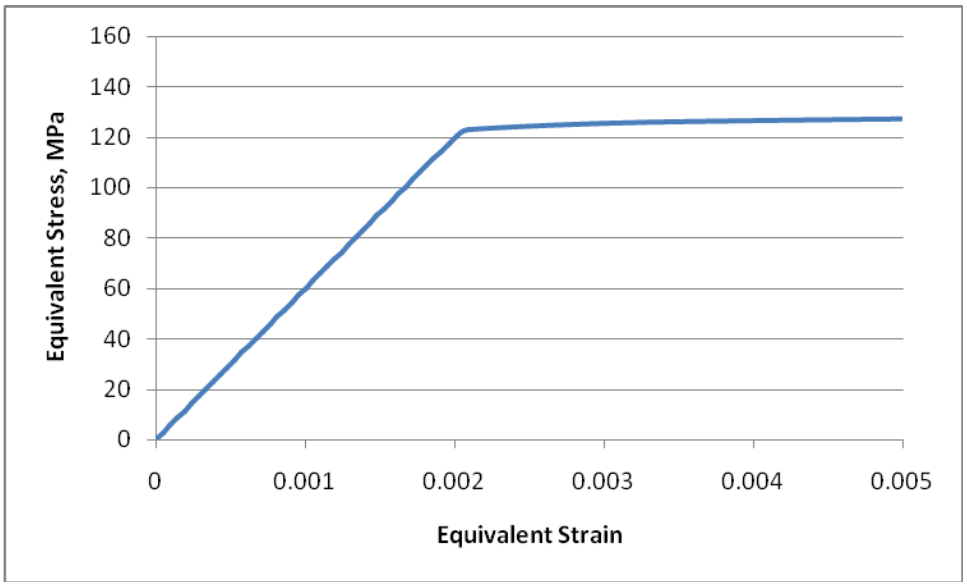

(b) Equivalent strain below 0.005

Figure 6.35 Equivalent stress strain curve of a mesh in vertical direction

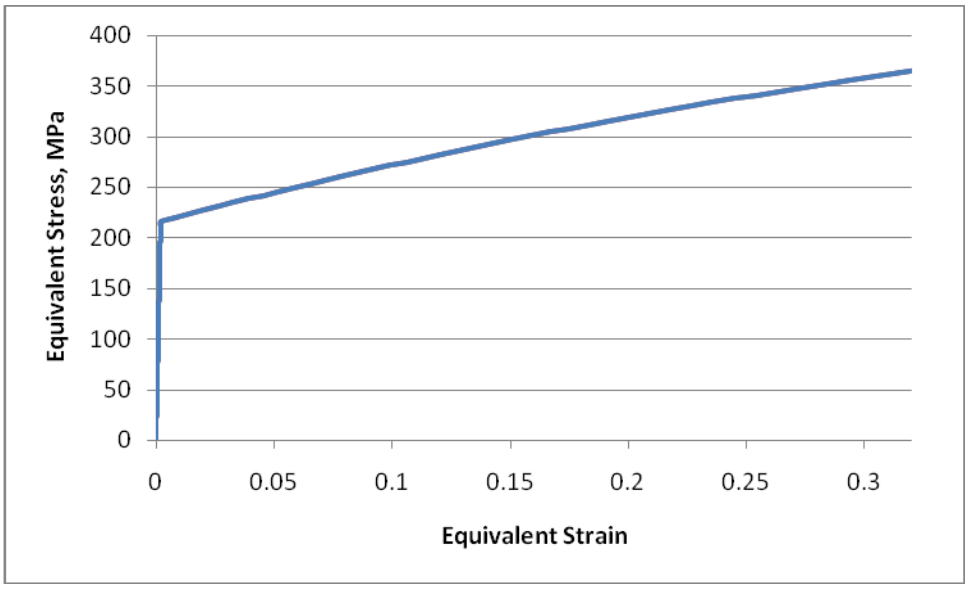

(a) Equivalent strain up to 0.33

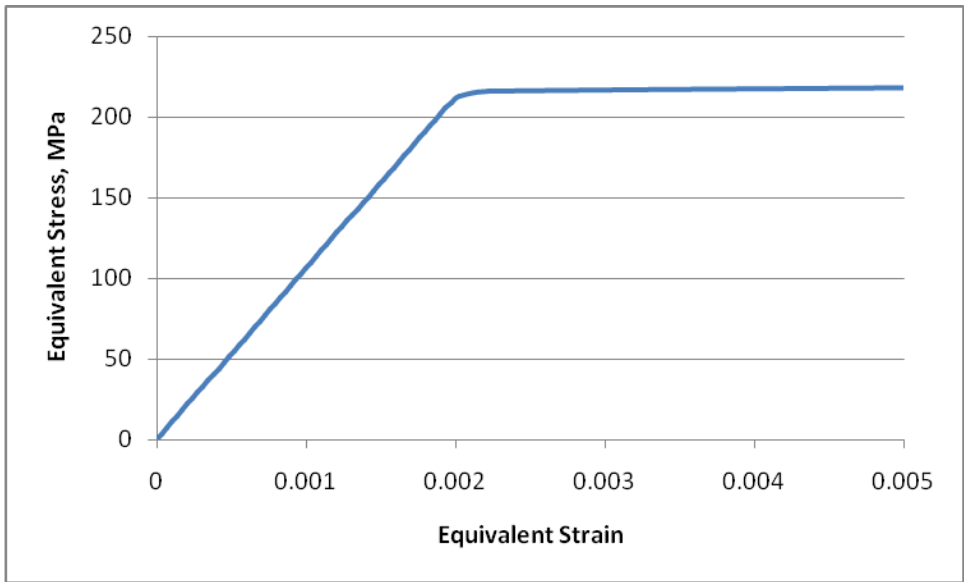

(b) Equivalent strain below 0.005

Figure 6.36 Equivalent stress strain curve of a mesh in horizontal direction

6.5 Contribution of external mesh

6.5.1 Bending behaviour along the lateral span

The horizontally inserted mesh are provided at a certain interval along the height of the wall due to practical and economic considerations. As a result, only a small strip of the outer mesh is connected along the inserted mesh and the remaining part between two inserted meshes is free throughout the whole length. Therefore, the bending performance of outer mesh along the horizontal direction is composed of two components. The first component consists of the role played by a portion of the mesh along the level of horizontally inserted mesh. This part is highly strained because of the restraint provided by the interconnected internal mesh. Usually, this portion is restricted within a single row of cells. The most probable strain mobilising length within this region is supposed to be twice the size of the cell (spacing of equivalent tie links) as given in section 6.1. The deformation of the mesh depends upon the angle of rotation, θ, of the cracked wall. The corresponding equivalent stress can be evaluated using Figure 6.36.

The second component consists of the contribution from remaining portion of the outer mesh. In this case, the strain will be mobilised within the whole length of the mesh. Therefore, the value of the strain will be less than in restrained region. The equivalent stress can be evaluated using Figure 6.36. The equivalent cross-sectional area will be reduced by the area involved in the first component. The resisting moment is evaluated by calculating the contribution from both parts separately using Equation (6.6) and added to get the final value.

6.5.2 Contribution in resisting the corner separation

The rotation of the wall at the corner is resisted by the tension developed in the reinforcement. The deformation of the mesh at the corner crack is half the deformation at the mid span crack. Therefore, the strain developed in the mesh will also be half of the strain at the mid span crack for a particular value of rotation. However, the stress may not always be half depending upon whether the strain level in each location is elastic or plastic. The calculation procedures are similar as in the case of mid span moment.

6.5.3 Bending behaviour along the vertical direction

Interconnection with the horizontally inserted mesh divides the outer mesh into distinct parts along the vertical direction. This helps the external mesh to be strained almost uniformly throughout the whole width at a given height. Therefore, Equation (6.6) can be used in order to determine the resisting moment with equivalent stress in the mesh.

6.6 Contribution of horizontally inserted mesh

6.6.1 Along the lateral span

The horizontal layer of a mesh inserted in the wall increases the bending strength, and at the same time, helps to reduce the deflection. The stress induced in the mesh depends on the angle of rotation of the wall.

Consider a segment of a wall with an embedded horizontal layer of hexagonal mesh as shown in Figure 6.37. The arrows show the direction of stress developed in the

mesh. In order to calculate the resisting moment contributed by the horizontal wire mesh, each row of cells was considered one at a time. The distance of each row of cells was calculated from the point of rotation, A. The deformation of the mesh at the mid height of each row of cells was calculated based on the angle of rotation. For example, if y_1 is the distance of first row of cells at mid height B from point A and θ is the angle of rotation of the wall, then deformation at the mid height is given by,

$$\Delta L = 2\, y_1 \tan\theta \tag{6.13}$$

Similarly, deformation of other rows of cells at respective mid height can be evaluated.

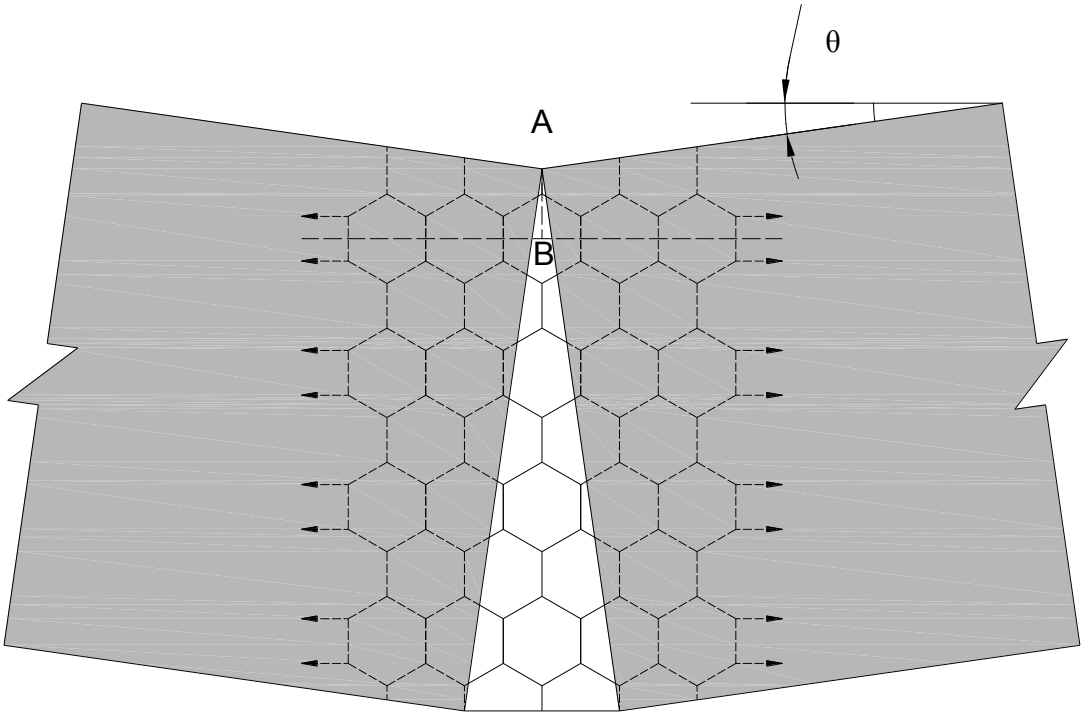

Figure 6.37 A portion of a wall near the cracked section (Plan View)

The mud mortar is not firm enough to provide anchorage to the inserted mesh at the immediate vicinity of the crack. Therefore, a considerable amount of length will be mobilised in order to provide the required anchorage. The inserted horizontal mesh is connected with the external wire mesh at an interval of the distance between parallel sides of the mesh. If a crack in the wall is developed along the vertical sides of the inserted mesh, the supporting length across the crack will be twice the cell size. Therefore, equivalent strain at the mid height of each row of cells can be obtained by dividing the ΔL by twice the distance between two parallel sides of the mesh. With these values of strains, Figure 6.36 provides corresponding values of equivalent stress. Multiplying these equivalent stresses by the cross-sectional area of a pair of wires, the force developed in each row of cells can be evaluated.

As long as the outer mesh can hold the wall around the cracked compressive zone, a strip of contact area with a tiny width will be enough to resist compressive stresses due to high strength of stone in compression. Therefore, the moment of the tensile force developed in the mesh can virtually be taken at the opposite face of the wall. The product of the distance of mid height of each row of cells from point A and the force induced in that row of cells will be the resisting moment of that row of cells about point A. Then, the total resisting moment of the inserted horizontal mesh about point A is given by,

$$M = \sum_1^n f_i A_i y_i \qquad (6.14)$$

where,

f_i = stress induced in i^{th} row of cell

A_i = area of an equivalent twin wires in i^{th} row

y_i = distance at the mid height of i^{th} row of cells from point A

n = number of rows of cells

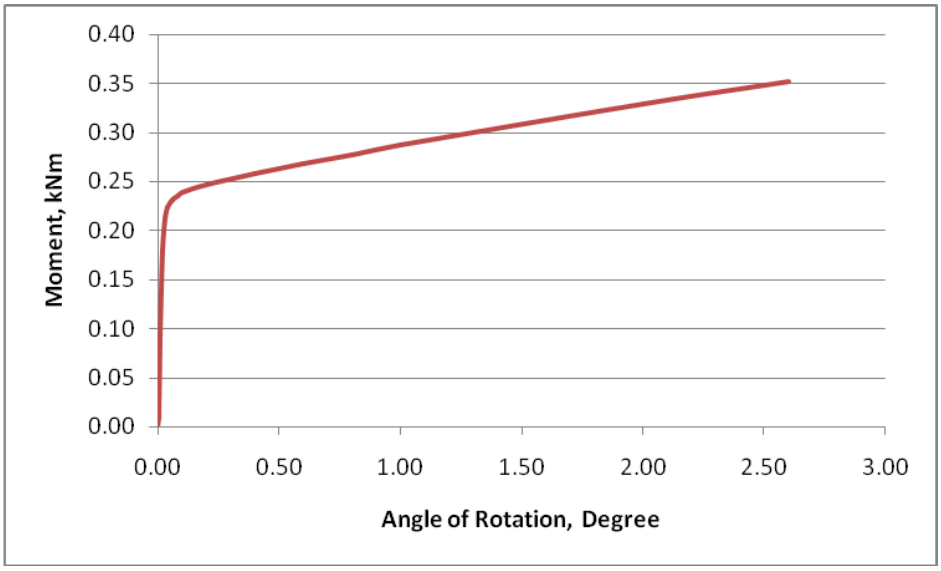

(a) Rotation up to 2.6^0

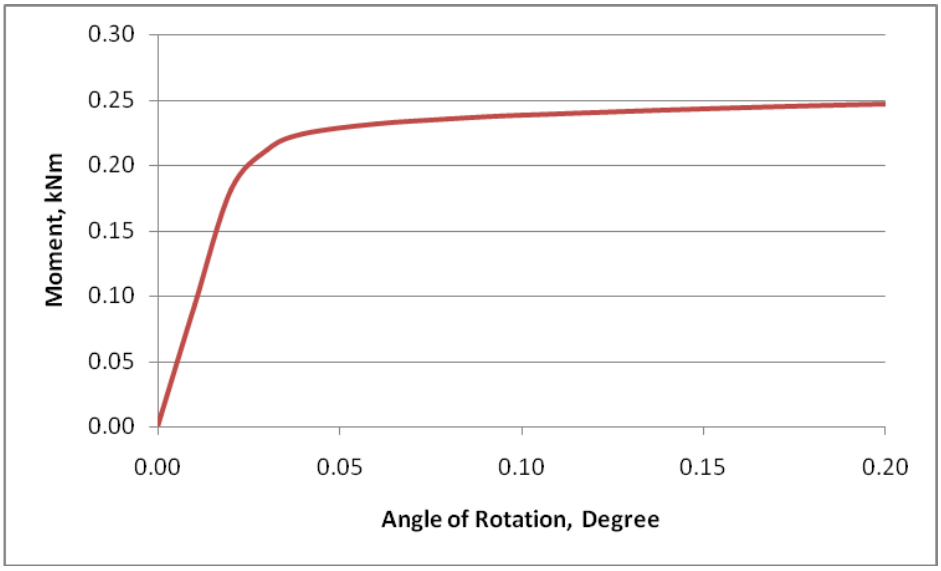

(b) Rotation below 0.2^0

Figure 6.38 Moment at mid span due to inserted mesh (Mesh 50 mm, ϕ 1 mm)

Equation (6.14) was plotted with varying degrees of rotation for a mesh of 50 mm opening size with 1 mm diameter wire as shown in Figure 6.38. From this figure, the resisting bending moment induced in the horizontal wire mesh can be obtained for a given value of rotation of the wall.

Similarly, Figure 6.39 shows a plot of Equation (6.14) for a mesh of 100 mm opening size with 2 mm diameter wire. With larger opening size of the mesh, the spacing of tie nodes with the external mesh increases. As a consequence, more rotation of the wall will be required to produce the same amount of strain as in the case of smaller opening.

Four rows of cells are accommodated within the wall thickness (350 mm) in the case of a mesh with 50 mm opening size, whereas only two rows of cells are enclosed for opening size of 100 mm. Therefore, there is relatively smooth transition from elastic to plastic deformation of resisting moment curve for 50 mm cell size.

Initially, the deformation of the inserted mesh will be smaller than the deformation given by curves in Figure 6.38 and Figure 6.39. This is because of the confinement provided by the mud mortar and the compressive stress of the weight of wall above the inserted horizontal wire mesh. Therefore, the actual deformation of the wall will be less in the elastic range. This means, the inserted mesh will help the wall to remain intact during minor earthquakes.

Once the wall cracks and undergoes a couple of reversible shakings, the additional support provided by the mortar and compressive stress will virtually vanish within the cracked zone. In that case, the deformation characteristics of the mesh will be

similar to a constrained mesh. On this basis, curves in Figure 6.38 and Figure 6.39 have been prepared.

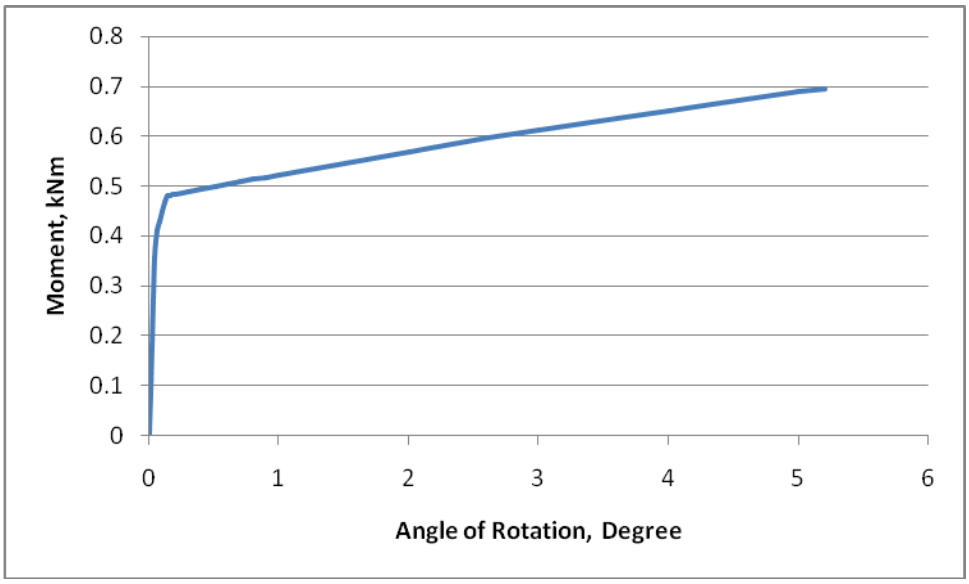

(a) Rotation up to 5.2^0

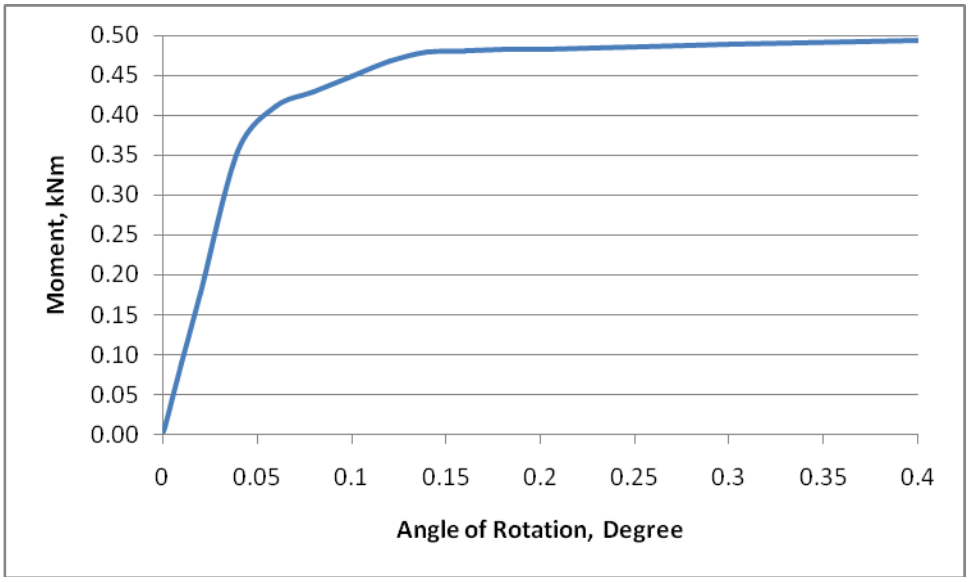

(b) Rotation below 0.4^0

Figure 6.39 Moment at mid span due to inserted mesh (Mesh100 mm, ϕ 2 mm)

6.6.2 Around the junction

After vertical cracks are formed at the corner due to seismic shaking, the out of plane wall tends to fall from the corner. However, this will be prevented by the combined action of inserted mesh and the outer mesh.

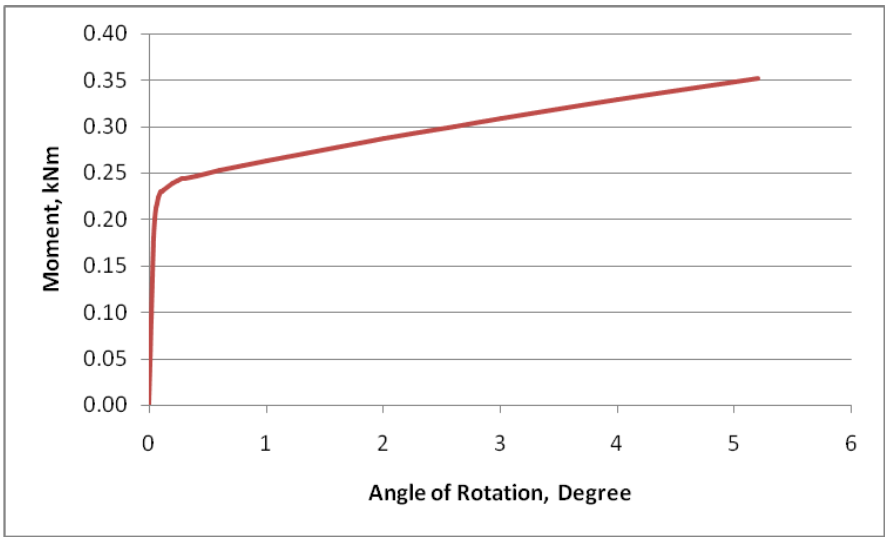

(a) Rotation up to 5.2^0

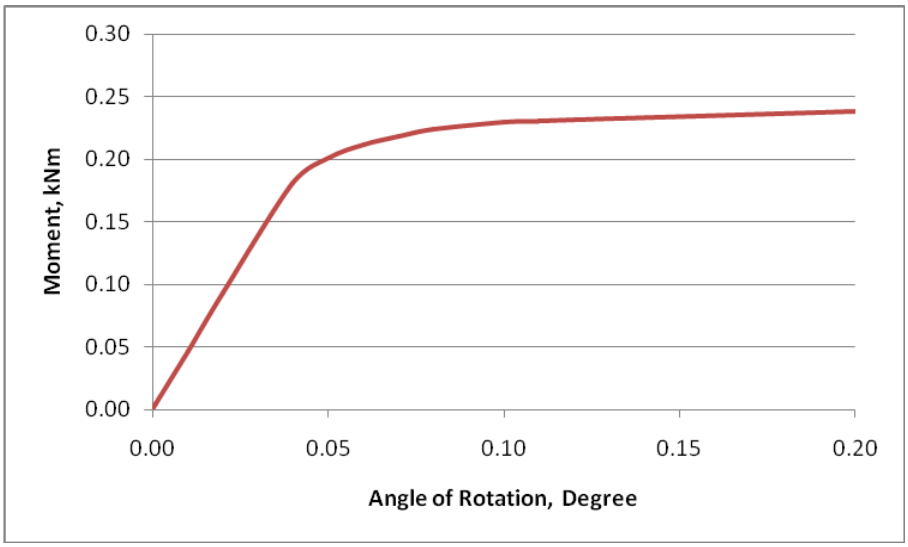

(b) Rotation belwo 0.2^0

Figure 6.40 Moment at corner due to inserted mesh (Mesh 50 mm, ϕ 1 mm)

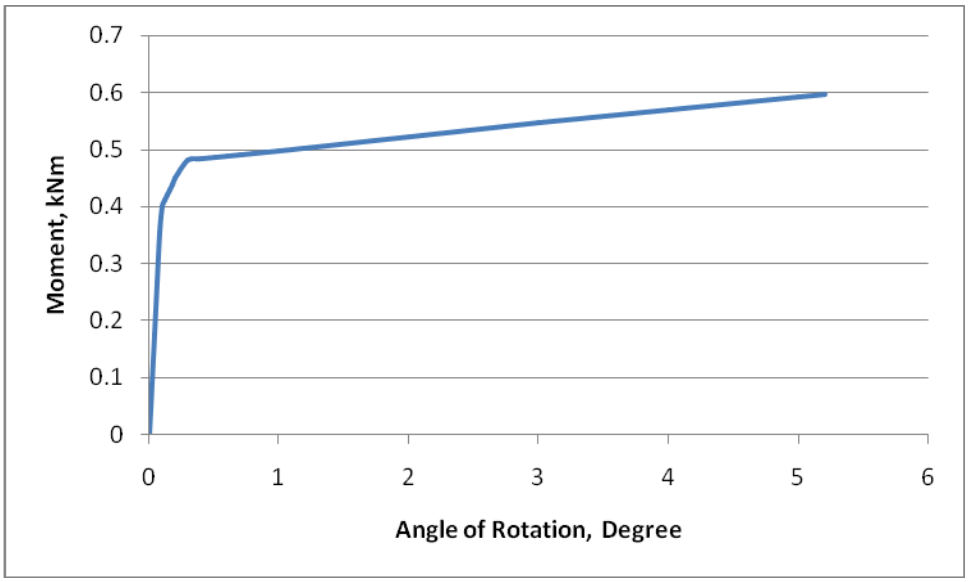

(a) Rotation up to 5.2^0

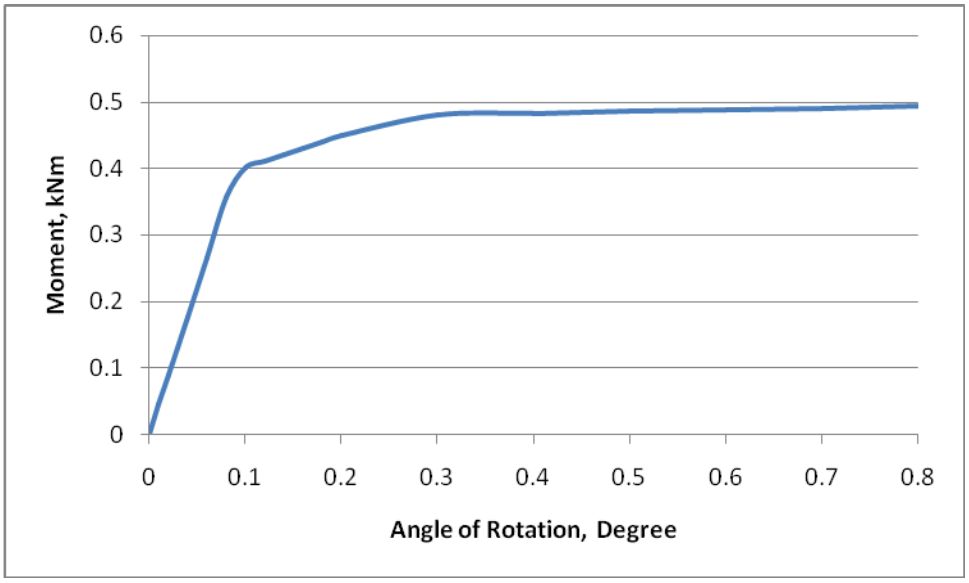

(b) Rotation below 0.8^0

Figure 6.41 Moment at corner due to inserted mesh (Mesh 100 mm, ϕ 2 mm)

As in the case of external mesh, the strain induced in the inserted mesh will be half the strain at mid span cracking. The resisting moment due to inserted mesh can be

obtained in a similar way as in the case of mid span as shown in Figure 6.40 and Figure 6.41.

6.6.3 Along the vertical span

Inserted mesh in the wall restrict the stress mobilising length of the outer mesh along the vertical span. This is very helpful in order to restrict the deformation of the external mesh along the height. As a result, the horizontal deflection of the wall while bending in the vertical span will be highly reduced.

6.7 Experimental verification

The relations derived above have been applied to predict the strength of a reinforced specimen and compared with the experimental result. Wall specimen for flexural test in the lateral span was wrapped with a hexagonal GSW mesh of 50 mm opening size with 1 mm diameter wire. A similar mesh was also inserted at the mid height of the specimen. The maximum angle of rotation not to exceed the ultimate strain in the outer mesh of this size is 2.6^0.

At this angle of rotation,

the moment of resistance contributed by the internal mesh = 0.352 kNm (Using Figure 6.38).

The deformation of the outer mesh = 2 x 350 x sin (2.6^0) = 31.8 mm

Strain in the outer mesh = 31.8 / (2 x 50) = 0.318

Stress induced = 364 MPa (Using Figure 6.36)

Area of wire within highly strained zone = 1.57 mm^2

Moment induced = 0.200 kNm

Strain in the remaining portion of the outer mesh = 0.023

Stress induced = 229 MPa

Height of the specimen = 460 mm.

Fraction of rows of cells accommodated within weight = 5.64

Total equivalent area of mesh = 8.86 mm^2

Net area of mesh = 8.86 - 1.57 = 7.29 mm^2

Moment contributed by remaining portion of the outer mesh = 0.584 kNm

Total resisting moment of the reinforcement = 0.352 + 0.200 + 0.584 = 1.14 kNm

External moment applied at the maximum load = 1.42 kNm

Percentage of moment predicted by analytical method = 80 %

This shows that the analytical solution can predict fairly close to the experimental result. The higher value of the test result implies that there is some reserved strength due to the constraints provided by the mud mortar. Thus, theoretical relations derived in this research will provide a conservative solution.

6.8 **Performance of reinforced wall in lateral loading**

6.8.1 Deflection in lateral span

Usually, the fixity at the corner of the orthogonal walls is not so high. Therefore, the out of plane wall most likely breaks at mid span when the bending stress exceeds the flexural strength of the wall. After mid span crack, the support moment will be higher due to cantilever action. Consequently, cracks occur around the corner region. One possible location for crack initiation is just opposite of point J near point C on line BC (Figure 6.42). However, the corner region may not be strong enough to withstand the rotation and let the negative moment build up sufficiently. Therefore, the most probable location of the crack is along JQ.

After cracking at two locations, the broken part of the wall tends to rotate further. However, this rotation will be resisted by the couple developed at the cracked locations due to combined action of the external mesh as well as the internal mesh.

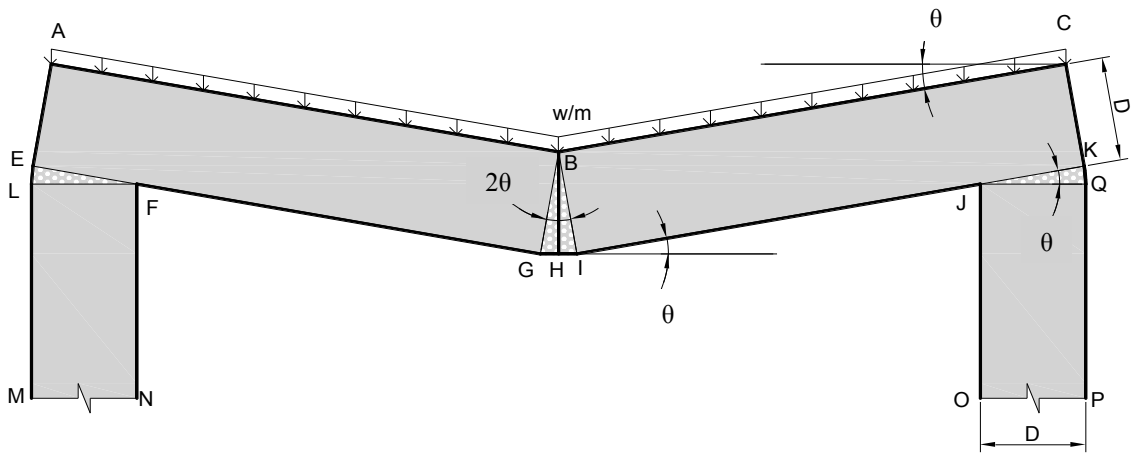

Figure 6.42 Most probable failure mechanism of wall in lateral load (Top View)

If M is the unbalanced moment on the right half section, the following relation will be valid.

$$M = M_B + M_J \tag{6.15}$$

where, M_B = Resisting moment induced at B

M_J = Resisting moment induced at J

Each of M_B and M_J is composed of contributions from inserted mesh as well as external mesh, which depend on the rotation of the wall. The cracked wall will rotate up to an angle θ, such that enough moment will be induced at point B and J in order to balance the external moment. For a particular rotation, the contribution of the internal mesh for M_B and M_J can be determined using Equation (6.14) or Figures 6.38 to 6.41, whichever is applicable.

For the external mesh, the following relation will be valid within the elastic limit

$$M = \frac{2\,EAD^2}{S_m}\sin\theta\cos\theta + \frac{EAD^2}{S_m}\sin\theta\cos\theta = \frac{3EA\,D^2}{S_m}\sin\theta\cos\theta \tag{6.16}$$

where, notations are similar to Equation (6.7).

For small range of rotation, cos θ ≈ 1,

$$\theta = \sin^{-1}\left(\frac{M s_m}{3EAD^2}\right) \tag{6.17}$$

When the strain exceeds the elastic range, the role played by the external mesh can be evaluated using Equation (6.6) along with Figure 6.35 and Figure 6.36 for mid

span and corner separately and added together. This means, the following relation will be applicable.

$$M = f_{t1}\, AD \cos\theta + f_{t2}\, AD \cos\theta \qquad (6.18)$$

where,

f_{t1} = stress induced at mid span crack,

f_{t2} = stress induce at corner crack,

and other notations are similar to Equation (6.6).

The final angle of rotation can be determined using few iterations until it converges to a particular value.

6.8.2 Deflection in vertical span

Once the bending stress at the bottom of the wall exceeds the bending strength, crack will appear at the base and the wall tends to rotate around the toe. The strain mobilizing length will be restricted mostly within a single spacing of inserted mesh. The deformation of the mesh will be '$D_u \sin\theta$', where D_u is the length of the uplifted portion.

The rotation of the wall will be resisted by the action of external mesh. The resisting moment of the external mesh can be evaluated using similar relation as Equation (6.6) with 'D' replaced by D_u. Within the elastic range, the angle of rotation is given by the following equation.

$$\theta = \sin^{-1}\left(\frac{Ms_m}{EAD_u^2}\right) \quad (6.19)$$

where, notations are similar to Equation (6.7) except D_u as noted above.

While using Equation (6.19), the unbalanced moment M is to be calculated using flexure formula corresponding to net bending stress at the bottom of the wall as given below.

$$M = \frac{fI}{D_t} \quad (6.20)$$

where,

f = net tensile bending stress

I = second moment of area of cross-section of wall

D_t = distance of outer face of wall at tension side with respect to the neutral axis

The wall will rotate until enough tension is induced in the external mesh in order to balance the external moment.

6.9 Step by step procedures for calculating the deflection

The main function of the external reinforcement is to limit the post cracking deformation and allow the cracked parts to be shaken within a confined zone so that most of the energy of seismic excitation will be absorbed without further damage to the building. With the help of confinement provided by external mesh, the inserted mesh is very effective to limit the deformation of the building.

In order to evaluate the adequacy of the GSW reinforcement system for resisting seismic loading, it seems logical to assess it based on the probable deformation of the building. The maximum allowable deflection can be extended to a value, which is adequate for collapse prevention. The following simplified steps might be useful for checking the deflection of the building.

1. Estimate the earthquake loading

2. Select the most critical region of the wall for out of plane bending, assess the maximum bending stress in a strip of wall of unit width and check against bending strength.

3. If the bending stress is less than the bending strength of the wall, there will be no crack in the wall. In such case the deflection can be calculated using elastic analysis. However, finding the elastic deflection is of no interest for the current study.

4. If the bending stress exceeds the bending strength of the wall, there will be cracking in the wall. In this case, the following steps will be useful for estimating the deflection.

5. Calculate the approximate angle of rotation, θ using Equation (6.17). Take stress mobilising length equal to the length of the wall.

6. With this rotation, calculate the contribution of inserted mesh at mid span and the corner using Figures 6.38 to 6.41, whichever is applicable.

7. For the value of θ calculated in step 5, calculate the strain in the external mesh at the mid span using Equation (6.5) and evaluate equivalent stress using Figure 6.35 or Figure 6.36. Calculate the area of the pair of wires and determine the moment using Equation (6.6). Strain in the corner crack will be half of the mid span strain. With this strain, calculate the moment as for mid span.

8. Calculate the net moment to be resisted by the remaining portion of the external mesh (excluding the row of cells along the interconnection with inserted mesh).

9. Calculate the revised value of rotation using Equation (6.17) for resisting the moment calculated in step 8. Take the net area of the external mesh by subtracting the area along the inserted mesh. Take the length of wall as strain mobilising length. Then, calculate the corresponding strain in the external mesh at mid span using Equation (6.5). If the value of strain is within the elastic range (Figure 6.36), the calculated value of θ is valid. Compare this angle of rotation with the calculated θ in step 5. If the values are almost similar, this is the angle at equilibrium. Otherwise, repeat steps 6 to 9 with the newly calculated angle until the value converges. On the other hand, if the value of strain calculated at this stage lies in the plastic range, the calculated value of θ using Equation (6.17) is invalid. In this case, use Equation (6.18) to calculate the resisting moment for the rotation in step 5. If the recently calculated moment is less than the moment to be resisted as calculated in step 8, increase the value of rotation and repeat steps 6 to 9 until the value of

moment converges. If the strain exceed the ultimate value, increase the size of reinforcement and repeat the process from steps 5 to 9 until the value of rotation or moment converges.

10. After calculating the angle of rotation at equilibrium, calculate the deflection of the wall using simple geometric relations. For example, the mid span deflection, Δ_m, is given by

$$\Delta_m = 0.5\ l\ \sin\theta \tag{6.21}$$

where,

l = the effective span

11. If the deflection exceeds the allowable limit, repeat the process from step 5 to 10 with increased size of reinforcement. However, in the case of marginally exceeding value, it might be enough due to other factors, not considered when performing the calculation as given in section 6.7.1.

12. For checking the deflection in the vertical span, calculate the overturning moment and check for uplift.

13. If there is no uplift, deflection can be calculated using elastic analysis, which is of no interest for current study.

14. If there is some uplift, calculate the angle of rotation using Equation (6.19), and check for strain. If the strain is within the elastic limit, the angle of rotation

just calculated is valid. If the strain is in plastic range, determine the angle of rotation by iteration using Equation (6.6).

15. The deflection at the top of each storey, Δ_t, is given by

$$\Delta_t = H \sin\theta \tag{6.22}$$

6.10 Few examples on checking the adequacy of reinforcement

On the basis of above mentioned discussion, the adequacy of the hexagonal mesh reinforcement for improving the seismic performance of a stone masonry building has been investigated in this section. Equivalent static analysis has been used to calculate the earthquake forces. As GSW reinforcement is mostly useful for seismically active regions, such as, South Asia, Indian Standard (IS 1893 (Part 1): 2002) has been followed when calculating the earthquake load.

6.10.1 Single storey building

Consider, a single storey stone masonry building of size 4.00 m x 3.50 m (Figure 6.43) is located on firm soil in a zone with severe seismic intensity. Suppose, the thickness and the height of the wall are 0.35 m and 2.40 m, respectively. One window of size 0.90 m x 0.9 m is centrally located in the rear wall at a height of 0.90 m. Also a door of size 0.90 m x 1.8 m is placed in the front wall. A light roof is provided at the top (not shown for clarity).

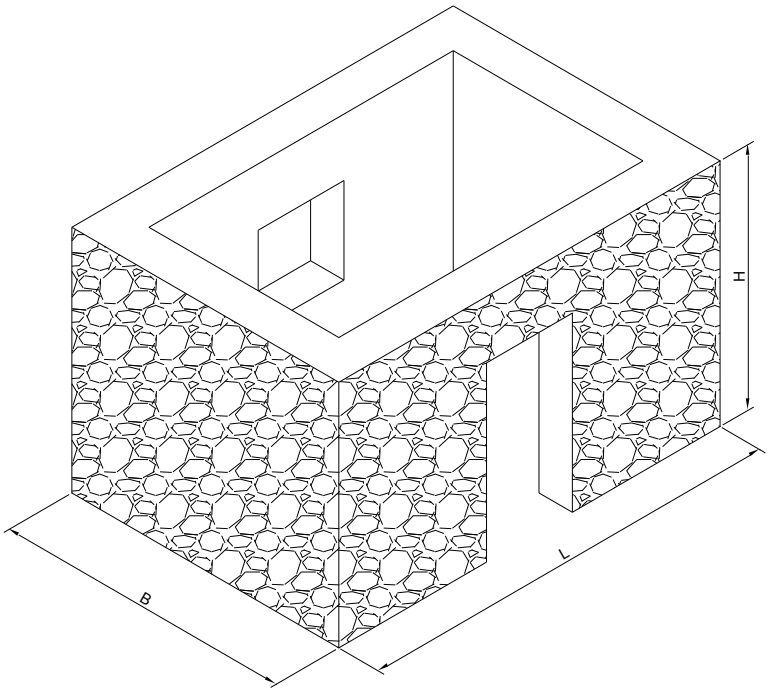

Figure 6.43 A single storey building

(a) Calculation of base shear

According to Indian Standard (IS 1893 (Part 1): 2002) the design horizontal seismic coefficient, A_h is determined by the following expression:

$$A_h = \frac{ZIS_a}{2Rg} \qquad (6.23)$$

where,

z = Zone factor

I = Importance factor

R = Response reduction factor

Sa/g = Average response acceleration coefficient

In this example,

Z = 0.36 (Zone V, very severe seismic intensity)

I = 1.0 (Residential building)

R = 3 (Load bearing masonry with horizontal bands and vertical reinforcement at corners and jambs). This category is chosen on the basis of the best available option.

Sa/g is chosen based on natural vibration period of the building.

The approximate fundamental natural vibration period, T_a, in seconds,

$$T_a = \frac{0.09\,h}{\sqrt{d}} \tag{6.24}$$

where,

h = Height of the building

d = Base dimension of the building at the plinth level, in m, along the considered direction of the lateral force.

Then, T_a = 0.12 s,

Sa/g = 2.5 (For $0.10 \leq T \leq 0.55$) for medium soil sites.

Substituting all parameters in Equation (6.23),

A_h = 0.15, indicating that the seismic load is 15% of the seismic weight,

The total design lateral force or design base shear, V_B, is given by,

$V_B = A_h W$

where,

W = Seismic weight of the building

Considering unit weight of roof = 0.85 kN/m^2,

Total roof load = 11.9 kN.

Considering unit weight of sand stone wall = 22 kN/m^3,

Total weight of wall = 232.6 kN (considering reduction for wall opening)

Seismic weight at roof level = 11.9 + 0.5 x 232.6 = 128.2 kN

Total seismic weight, W = 128.2 kN

Therefore, $V_B = A_h W$ = 0.15 x 128.2 = 19.2 kN

(b) Checking for uplift of the base

Total overturning moment at the base = 19.2 x 2.4 = 46.2 kNm, neglecting any eccentricity.

Assuming the reinforcement system helps to maintain the whole building as a box system,

Second moment of wall area = 8.25 m^4, neglecting the opening

Bending stress at the base = ± 9.78 kPa

Total dead load = 244.5 kN

Compressive stress due to dead load = - 51.4 kPa

Net stress = -41.6, -61.2 kPa. Therefore, there will be no uplift.

(c) Checking for deflection in horizontal direction

Suppose the roof is connected to the long wall. Considering a horizontal strip of wall of 1 m height at the roof level, lateral load = 0.15 x (0.85 x 3.5/2+0.35 x 22) = 1.38 kN/m

Neglecting the fixity at the support,

Bending moment at the mid span, $M = 1.38 \times 3.65^2/8 = 2.30$ kNm

Corresponding bending stress = 0.112 MPa > 0.085 MPa

Therefore, the wall will be cracked at the mid span.

Suppose the building is reinforced with a GSW mesh of 50 mm cell size between parallel sides and 1 mm wire diameter. For 50 mm cell size, the number of rows of cells within 1 m height of the mesh will be almost 12. Therefore, total area of equivalent wire, $A = 18.3$ mm^2.

The equivalent modulus of elasticity of the mesh in horizontal direction (Figure 6.36), $E = 1.06 \times 10^5$ MPa.

Initially, considering the strain mobilising length, 2s = 4000 mm (whole length of external mesh) and using Equation (6.17), the approximate angle of rotation,

$\theta = 0.738^0$

In fact, the actual angle of rotation will be smaller than this value due to the contribution of internal horizontal mesh as well as interconnection with the external mesh. Therefore, few iteration may be necessary in order to get the final result.

Corresponding to this rotation, resisting moment developed in the inserted horizontal wire mesh at mid span and at the corner are 0.274 kNm (Figure 6.38) and 0.256 kNm (Figure 6.40) respectively. At least two layers of horizontal wire mesh will be accommodated within 1 m height of external wire mesh. Therefore, total resisting moment of the internal mesh will be 0.548 kNm at the mid span and 0.512 kNm at the corner.

The deformation of outer mesh at the location of inserted mesh,

$\Delta L = 2\ D \sin\theta = 9.01$ mm

As assumed in section 6.1, the most probable length of strain mobilisation is twice the spacing of tie wire or opening size of inserted mesh. Therefore the strain mobilising length for the outer mesh along the interconnected region with the inserted mesh, $s_m = 100$ mm.

The influence of interconnection between external and internal mesh on the strain mobilising length will be restricted to a single row of cells. Therefore, the total equivalent area of wire of a single row of cell = 1.57 mm^2.

Strain induced within $s_m = 0.0901$

Corresponding equivalent stress = 267 MPa (Using Figure 6.36)

Resisting moment = 0.147 kNm

Total resisting moment = 2 x 0.147 = 0.293 kNm (corresponding to two locations of inserted mesh). This is a part of the contribution of outer mesh to the resisting moment.

Similarly, strain induced in external mesh at corner = 0.5 x 0.0901 = 0.045.

Stress induced = 242 MPa (Figure 6.36).

Moment induced = 0.133 kNm

Total resisting moment of outer mesh at corner crack = 2 x 0.133 = 0.266 kNm

Moment to be resisted by remaining portion of the outer mesh

= 2.30 - 0.548 - 0.512-0.293-0.532 = 0.675 kNm

Equivalent area of remaining portion of the outer mesh = 16.7 mm^2

Angle of rotation of the wall for resisting 0.675 kNm = 0.237^0 (Using Equation 6.17)

Strain in the outer mesh with this rotation = 0.00072. This lies in the elastic range (Figure 6.36). Therefore, the calculated value of θ is valid.

This angle of rotation is smaller than initially calculated value. This implies that the strain mobilised in the internal horizontal mesh and outer mesh as calculated above is higher than actual strain induced. Therefore, the next round of iteration is to be carried out.

Following a similar procedure, starting with the new value of rotation (0.237^0), second iteration was conducted. At the end of second iteration, angle of rotation was obtained as 0.285^0. Continuing the iteration in similar manner, the angle of rotation

was converged to 0.280^0 after the fifth iteration. At this stage, the deflection of the wall at the mid span = 9.0 mm.

6.10.2 Double storey building

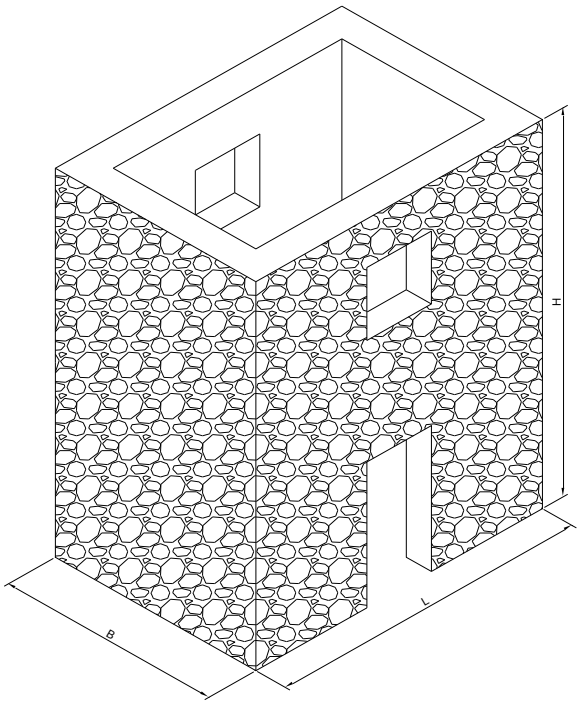

Figure 6.44 A double storey building

Consider, a double storey stone masonry building having a similar ground storey as in the previous case as shown in Figure 6.44. Suppose, the floor height of the top storey is also 2.40 m. One window of size 0.90 m x 0.90 m is centrally located in the back as well as the front wall of the building at a height of 0.90 m from the floor. A light roof is provided at the top (not shown for clarity).

(a) Calculation of base shear

Most of the parameters except those which are relevant to the building height will be similar as in the case of the single storey building in section 6.9.1. The fundamental vibration period will be different due to change in the height of the building.

Approximate time period, T_a = 0.23 s

Average response acceleration coefficient, Sa/g = 2.5

Then, design horizontal seismic coefficient, A_h = 0.15

Considering unit weight of roof = 0.85 kN/m^2,

Total dead load of roof = 11.9 kN.

Taking the unit weight of floor = 0.5 kN/m^2,

Total dead load of the floor = 4.62 kN

Taking the live load as 2 kN/m^2

Total live load = 18.5 kN

Considering the unit weight of sand stone wall = 22 kN/m^3,

Total weight of top storey wall = 238.9 kN (considering reduction for wall opening)

Total weight of ground storey wall = 232.6 kN

Seismic weight at roof level = 11.9 + 0.5 x 238.9 = 131.3 kN

Seismic weight at floor level = 4.62 + 0.5 x 238.9 + 0.5 x 232.6 + 0.25 x 18.5

= 245 kN.

Total seismic weight, W = 376.3 kN

Therefore, $V_B = A_h W = 0.15 \times 376.3 = 56.4$ kN

The vertical distribution of base shear to different floor levels is given by the following expression.

$$Q_i = \frac{W_i h_i^2}{\sum_{j=1}^{n} W_j h_j^2} \quad (6.25)$$

where,

Q_i = Design lateral force at floor i

W_i = Seismic weight of floor i

h_i = Height of floor i measured from the base

n = Number of storeys

Using this equation, the lateral load will be distributed as shown in Table 6.1.

Table 6.1 Vertical distribution of base shear

Floor	W_i kN	h_i m	$w_i h_i^2$	Q_i kN
Top floor	131.3	4.8	3025.8	38.5
Ground floor	245.0	2.4	1411.1	18.0
Total			4436.8	

(b) Checking for uplift at the base

Total overturning moment at the base = 38.5 x 4.8 + 18 x 2.4 = 228 kNm, (neglecting any eccentricity).

Assuming the reinforcement system helps to maintain the whole building as a box system,

Second moment of wall area = 8.25 m^4, (neglecting opening)

Bending stress at the base = ± 0.011 MPa

Total vertical load = 506 kN

Compressive stress due to vertical load = -0.106 MPa

Net stress = - 0.117, -0.095 MPa. Therefore, there will be no uplift.

(c) Checking for deflection in horizontal direction

The wall in top storey will be more critical for out of bending than in ground storey.

Lateral coefficient for top storey = 38.5/131.3 = 0.29

Suppose the roof is connected along the long wall. Considering a horizontal strip of wall of 1 m height at the roof level,

lateral load = 0.29 x (0.85 x 3.5/2 + 0.35 x 22) = 2.69 kN/m

Neglecting the fixity at the support,

Bending moment at the mid span, M = 1.38 x 3.65^2/8 = 4.48 kNm

Corresponding bending stress = 0.220 MPa > 0.085 MPa

Therefore, the wall will be cracked at the mid span.

Suppose the building is reinforced with a GSW mesh of 50 mm cell size with 1 mm wire diameter.

For 50 mm cell size, the fraction of cells per meter height of the mesh will be almost 12. Therefore, total area of equivalent wire, A = 18.3 mm^2.

The equivalent modulus of elasticity of the mesh in horizontal direction (Figure 6.36), E = 1.06 x 10^5 MPa.

Initially, considering the strain mobilising length, s_m = 4000 mm (whole length of external mesh) and using Equation (6.17), the approximate angle of rotation,

$\theta = 1.44^0$

Corresponding to this rotation, the resisting moment developed in the inserted horizontal wire mesh at mid span and at corner are 0.306 kNm (Figure 6.38) and 0.273 kNm (Figure 6.40), respectively. At least two layers of horizontal wire mesh will be accommodated within 1 m height of external wire mesh. Therefore, the total resisting moment of the internal mesh will be 0.612 kNm at the mid span and 0.546 kNm at the corner.

The deformation of outer mesh at the location of inserted mesh,

$\Delta L = 2\ D \sin\theta = 17.6$ mm

Strain mobilising length, s_m for the outer mesh along the inserted mesh = 100 mm.

Strain induced within s_m = 0.176

Corresponding equivalent stress = 309 MPa (From Figure 6.36)

The total equivalent area of wire of a single row of cells = 1.57 mm^2.

Resisting moment = 0.170 kNm

Total resisting moment = 2 x 0.170 = 0.340 kNm (corresponding to two locations of inserted mesh). This is a part of the contribution of outer mesh to the resisting moment.

Similarly, strain induced in external mesh at corner crack = 0.5 x 0.176 = 0.088

Stress induced = 266 MPa (Figure 6.38).

The total equivalent area of wire of a single row of cells = 1.57 mm^2.

Moment induced = 0.146 kNm

Total resisting moment of outer mesh at corner cracking = 2 x 0.146 = 0.292 kNm

Moment to be resisted by remaining portion of the outer mesh

= 4.48 - 0.612 - 0.546 - 0.340 - 0.292 = 2.69 kNm

Equivalent area of remaining portion of the outer mesh = 16.7 mm^2

For resisting 2.69 kNm, the angle of rotation of the wall = 0.237^0 (Using Equation 6.17).

Strain in the outer mesh with this rotation = 0.0028. This lies in the plastic range (Figure 6.36). Therefore, the calculated value of θ is invalid. In such case, the angle of rotation can be determined by checking the moment induced in the outer mesh for

a particular angle of rotation and comparing this value with the moment to be resisted by the outer mesh. This iteration process is to be continued until these two values converge.

For the angle of rotation $\theta = 1.44^0$,

Strain in outer mesh caused by mid span crack = 0.0044

Stress induced = 218 MPa (Figure 6.36)

Moment induced = 1.27 kNm

Strain in outer mesh caused by crack at the junction = 0.0022

Stress induced = 216 MPa (Figure 6.36)

Moment induced = 1.26 kNm

Total moment = 2.53 kNm, which is less than the moment to be resisted 2.69 kNm. This means, the wall needs to have more rotation in order to balance the moment.

Next iteration:

The ultimate strain in the outer mesh (50 mm cell size) along the interconnected region with the inserted mesh (50 mm cell size) will reach at an angle of rotation of about 2.6^0 (Equation (6.5) and Figure 6.36). Calculating all the parameters with this angle will verify whether the reinforcement is enough for the loading considered.

Corresponding to this rotation, the resisting moment developed in the inserted horizontal wire mesh at mid span and at corner are 0.352 kNm (Figure 6.38) and 0.300 kNm (Figure 6.40), respectively. At least two layers of horizontal wire mesh

will be accommodated within 1 m height of external wire mesh. Therefore, the total resisting moment of the internal mesh will be 0.704 kNm at the mid span and 0.600 kNm at the corner.

At this angle, the total deformation = 25.7 mm

Strain mobilising length, s_m for the outer mesh along the inserted mesh = 100 mm.

Strain induced within s_m = 0.257

Corresponding equivalent stress = 342 MPa (From Figure 6.36)

The total equivalent area of wire of a single row of cells = 1.57 mm^2.

Resisting moment = 0.200 kNm

Total resisting moment = 2 x 0.200 = 0.400 kNm (corresponding to two locations of inserted mesh). This is a part of the contribution of outer mesh to the resisting moment.

Similarly, strain induced in the external mesh at corner crack = 0.5 x 0.257 = 0.128

Stress induced = 301 MPa (Figure 6.36).

The total equivalent area of wire of a single row of cells = 1.57 mm^2.

Moment induced = 0.165 kNm.

Total resisting moment of outer mesh at corner cracking = 2 x 0.165 = 0.330 kNm

Moment to be resisted by remaining portion of the outer mesh

= 4.48 - 0.704 - 0.600 - 0.400 - 0.330 = 2.45 kNm

Equivalent area of remaining portion of the outer mesh = 16.7 mm^2

For resisting 2.45 kNm, the angle of rotation of the wall = 0.896^0 (Using Equation 6.17)

Strain in the outer mesh with this rotation = 0.0026. This lies in plastic range (Figure 6.36). Therefore, the calculated value of θ is again invalid. In such case, the angle of rotation can be determined by checking the moment induced in the outer mesh for a particular angle of rotation and comparing this value with the moment to be resisted by the outer mesh. This iteration process is to be continued until these two values converge.

For the angle of rotation θ = 2.6^0,

Strain in the outer mesh caused by mid span crack = 0.0079

Stress induced = 220 MPa (Figure 6.36)

Moment induced = 1.29 kNm

Strain in outer mesh caused by the crack at the junction = 0.0039

Stress induced = 217 MPa (Figure 6.36)

Moment induced = 1.27 kNm

Total resisting moment = 2.56 kNm, which is more than the moment to be resisted, 2.45 kNm. This means, the required rotation of wall is less than 2.6^0 in order to balance the moment. Also, it suggests that the current reinforcement is enough for

sustaining the load under consideration. However, the exact rotation is to be determined using further iterations.

Using a similar procedure as above, a few more iterations were conducted by varying the angle of rotation. Finally, it was converged at the rotation of 2.1^0.

At this angle, the deflection of wall = 67 mm. Though this deflection is high for general consideration, the building may not collapse if the roof is stable and enough bearing is provided.

If the deflection is to be limited, a wire mesh of 100 mm cell size with 2 mm diameter wire is to be adopted.

In that case, the fractions of cells per meter height of the mess will be 6.1.

Therefore, the equivalent area of wire mesh per meter height = 38.4 mm^2.

Strain mobilising length = 200 mm.

Area of a pair of wires = 6.28 mm^2.

Following similar procedures as given above, and using Figure 6.39 and Figure 6.41 to calculate the contribution of inserted mesh at mid span and corner, respectively, the mid span deflection was obtained as 4.5 mm (calculations not shown for brevity).

Similarly, as a next alternative, using internal mesh of 100 mm size with 2 mm diameter wire and outer mesh of 50mm size with 1 mm diameter yields a deflection of 23 mm.

6.10.3 Maximum length of a wall

Maximum dimension of a wall can be determined either by ensuring that no parts of the reinforcement has exceeded the ultimate stress or the maximum deflection of the wall have not exceeded the allowable value. The most critical part of the reinforcement is the outer mesh along the interconnected region with the internal mesh. This is because of two reasons. Firstly, this region has been restrained due to connected nodes with inserted mesh. Therefore, this portion will be highly strained as compared to remaining portion of the mesh. Secondly, this region is the farthest part as compared to inserted mesh from the compressive zone forming the couple.

In the case of mesh with 50 mm cell size and 1 mm diameter wire, the ultimate equivalent strain in the outer mesh along the horizontally inserted mesh will occur at angle of rotation of about 2.6^0. At this value of rotation, the resisting moment of an inserted mesh will be 0.352 kNm at mid span and 0.300 kNm at the corner. Assuming two inserted meshes per meter of height of the wall, the remaining unbalanced moment is to be resisted by the outer mesh. For a particular length and breadth, the corresponding unbalanced moment can be compared with the resisting moment of outer mesh.

Flowing a similar procedure as given in section 6.9.1, it was found that the mesh with 50 mm cell size and 1 mm wire diameter could be used to reinforce a single storey room having a maximum size of 5.30 m x 5.30 m. In this case, the deflection will be 112 mm. Limiting the size of the room to 5.0 m x 5.0 m, the deflection of reinforced wall will reduce to 50 mm.

Rotation of the wall with reinforcement mesh having 100 mm cell size and 2 mm diameter wire can undergo up to 5.2^0 before the occurrence of the ultimate strain in the outer mesh. In this rotation, the deflection of the wall may be unacceptable for a large span. Therefore, allowable deflection governs the maximum span of the wall in this case. Flowing a similar procedure as given in section 6.9.2, the maximum dimension of a room in a two storey building was calculated. If the maximum deflection of top storey is allowed up to 130 mm, the maximum size of a room is 5.50 m x 5.50 m.

6.11 **Summary**

Externally wrapped reinforcement comes into action only when there is some rotation of the beam. Therefore, such reinforcement is useful especially for post cracking performance. After cracking, the beam will rotate until sufficient tension is induced in the external reinforcement so that enough resisting moment is generated for balancing the external moment. The required amount of rotation will be considerably reduced if the external reinforcement on the opposite face of the beam are tied to the wall in small intervals.

A mesh with hexagonal opening is highly flexible if sides of the mesh are free to deform. In a wall wrapped with a mesh, the sides of the mesh on each face of the wall are restrained along the height. In such case, the deformation of the mesh is considerably reduced. However, the deformation is still higher than a solid wire. Within the elastic limit, a single column of hexagonal cells of GSW mesh (with constrained sides) deforms about 3.2 times more than a solid wire in the vertical

direction (loading parallel to twisted sides). The change in vertical deformation of the hexagonal mesh of a constant height with increase in the width of the mesh is almost negligible. This is also equally applicable for the horizontal deformation (loading perpendicular to twisted sides). This means the influence of change in the height of the mesh of a constant length in the horizontal deformation is insignificant. An elastic deformation of a single row of hexagonal cells of GSW mesh in horizontal direction is about 1.7 times higher than the deformation of an equivalent solid wire. Interestingly, the deformation of a hexagonal mesh is independent of cell size, provided the same stress level is maintained.

The inclined member is the most critical part of the hexagonal mesh, which governs the load carrying capacity of a mesh. The ultimate strength of the mesh is always less than the ultimate strength of solid wires used for weaving the mesh. A single hexagonal cell is stronger in horizontal direction than in the vertical direction. However, the GSW hexagonal mesh is about 30% stronger in the vertical direction than in the horizontal direction.

Vertical deformation per unit height of a mesh due to uniformly distributed vertical loading throughout the whole width of the mesh was derived for two mesh sizes: mesh with 50 mm opening size having 1 mm diameter wire and mesh with 100 mm opening size with 2 mm diameter. Similarly, horizontal deformation per unit width of the mesh due to uniformly distributed horizontal loading throughout the height of the mesh was also calculated for both sizes. These values may be useful for quickly assessing the total deformation of a mesh once the uniformly distributed load is known. Moreover, equivalent stress strain curve for a hexagonal mesh derived from

above relation will be useful for evaluating the stress level in the mesh for a given value of strain.

The performance of outer mesh in resisting the bending in lateral span composed of two components. The first part consists of the contribution by the portion of the mesh along the level of horizontally inserted mesh. This region is highly strained due to restraint provided by the inserted mesh. The second part consists of the role played by the remaining portion of the mesh. In the vertical span, the external mesh is almost uniformly strained due to distinctly divided segments throughout the whole length by the inserted mesh. Therefore, the contribution of the external mesh in resisting the unbalanced moment in the vertical direction can be directly determined for a given value of rotation of the wall. In all of the above cases, the theory developed in section 6.1 is applicable using parameters derived in section 6.4.

Horizontal layer of the inserted mesh provides additional support to the resisting moment of the external mesh and helps to reduce the deflection of the wall. The contribution of the inserted mesh along the lateral span was evaluated considering each row of cells at a time and summing them together to get the total results. In the vertical span, the inserted mesh tends to confine the strain within distinct segment, which is very helpful in inducing the resisting moment within a small angle of rotation. This is highly desirable for reducing the deflection of the wall.

The relations derived for the GSW mesh reinforcement has been experimentally verified by comparing the predicted value of resisting moment using the analytical method with the test results. It has been observed that the analytical solutions produce results about 80% of the experimental results, and hence conservative.

The overall performance of the reinforced wall is composed of contributions from internal mesh as well as external mesh. The most probable sequence of cracking seems to be initiated at mid span of the wall followed by cracking at the corner. At every crack, there will be resistance against further rotation from both internal as well as external mesh. As the contribution of both meshes depends on the rotation of the wall, the final value of the rotation can be obtained through an iterative procedure.

Checking the adequacy of the given size of mesh for seismic loading by assessing the probable deflection of the building was considered reasonable for the type of building under consideration. A set of procedures were developed and applied for assessing a typical single storey and double storey buildings. This assessment method has shown that a GSW mesh with 50 mm cell size and 1 mm diameter is adequate to reinforce a single storey building with a light roof up to 5 m x 5 m room size. Using 100 mm cell size with 2 mm wire diameter, a two storey building can be reinforced up to dimensions of 5.5 m x 5.5 m. In both cases, no consideration is given to the deterioration of the GSW with time.

7. Discussions

In this chapter, overall features of this research are discussed. The results are critically analysed based on the observations made during testing and analysis. The probable reasons behind each and every outcome of the investigation are discussed. Results obtained in this research are compared with relevant data available in the literature.

This research was challenging in many ways. The first hurdle began with the collection of materials. Though this research involved natural materials, these were not easily available in the market. In Sydney, most of the stone quarries have already been closed down. The stone was collected from a quarry, who consider themselves as Sydney's last quarry (Sandstone Sales 2010). Similarly, suppliers for mud mortar soil were not located near the city because there is no real demand for this item. Therefore, it was hard to locate them even on the internet.

The second challenge was involving bulky and fragile items. The rubble masonry by nature could not be built in a single layer. As a consequence, wall specimens were large and heavy. Therefore, preparation of the specimens was physically demanding. A considerable amount of time and effort were invested for preparing the specimens. It was not practical to prepare many specimens to achieve more statistically reliable results. On the other hand, these specimens were too fragile and brittle. Therefore, handling heavy items with care was another great challenge. Because of huge size of some specimens, space requirement in the laboratory for construction and storage of specimens was another constraint.

The third challenge was absence of available standard methods of testing for such specimens. Therefore, certain modifications were necessary to be developed. As a result, fabricating some sorts of testing set up was required in every testing.

The fourth problem was the lack of available data. Testing was necessary to find out all basic properties of the specimens. Because of this requirement, scope of the research was enormously wide spread.

The fifth challenge was in numerical simulation. In the absence of reliable data, it would have been of little value whatever efforts were made in numerical analysis. Moreover, due to many influencing factors, in addition to the variation of the shape and size of the rubble, numerical modeling was extremely complex. Numerous unsuccessful attempts were made in order to produce numerical explanation of the test results. These have not been included in this thesis for brevity.

Obviously besides these major challenges, there were many associated hurdles. Overcoming these obstacles, some fruitful results have been achieved. The outcomes of these investigations are summarized below.

7.1 **Mud mortar properties**

At the beginning of the experimental program, plastic limit and liquid limit of the soil for mud mortar were investigated. The main reasons behind the need for these tests were related to the probable sources of different types of soil for mortar. As the soil extracted from the building sites can be used for mud mortar, there may be many variations of mortar soil. Therefore, testing of soil for identifying the type and composition was envisaged to set out a reference for the mud mortar. These results

will be useful for comparing any future work in the laboratory as well as on the building site involving mud mortar.

In this research, mud mortar soil with 18% of plastic limit and 25% of liquid limit were used.

Thus, the plasticity index, PI = LL-PL = 7 %.

Comparing these values in plasticity chart (Budhu 2011) as shown in Figure 7.1, this shows that the type of soil used in this research was inorganic silty clay with low plasticity.

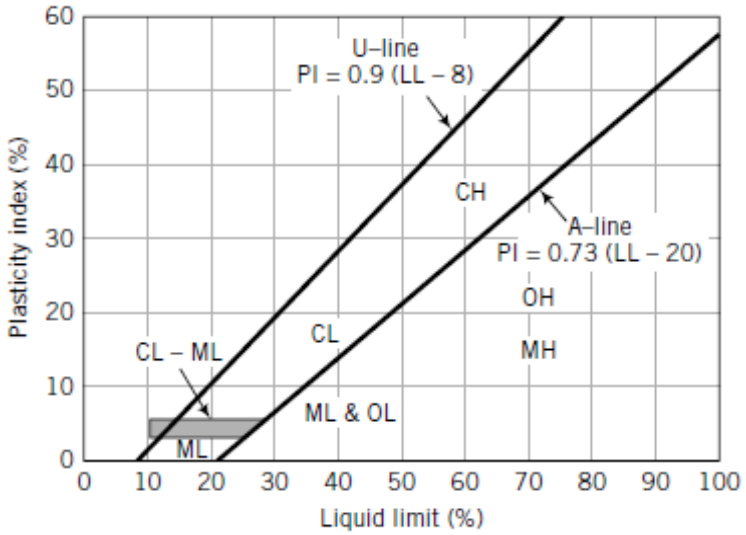

Figure 7.1 Plasticity chart (Budhu 2011)

Also, from the chart, the equation of U-line,

PI = 0.9 (LL-8) %

= 0.9 (25-8) %

= 15.3% > 6.5 %

This confirms the validity of the test results.

As compared to soil used by other researchers, the mortar soil used in this research has shown low Atterberg limits (Table 7.1). Due to low plasticity index of mortar, it can quickly get stiff when losing small amounts of moisture. Therefore, shrinkage will be relatively small, which is the desired property of mortar. Moreover, the moisture content of the mud mortar was maintained around 23% during the construction of specimens. This moisture content was selected based on the visual observation of the mortar with few trials as suggested by Walker (HB 195 - 2002). As the selected moisture content was close to liquid limit, the mud mortar was soft enough so that it could be spread easily filling the gap between the stone pieces.

Table 7.1 Comparison of physical parameters of soil

Parameter	Zhong et al. (2008)		Wu et al.(2011)	This research
	Site 1	Site 2	Site 1	Site 1
Liquid Limit, %	42.0	34.6	36.3	24.5
Plasticity Limit, %	24.9	22.7	19.2	18.0
Plasticity Index, %	17.0	11.9	17.1	6.5

The water binder ratio for preparing the mud mortar depends on the composition of the soil. In this research, sedimentation test was included for finding the proportion of sand, silt and clay of the soil. Since the sedimentation test can be conducted in the field, it will be helpful for comparing the soil of any building site with these results. The percentage of sand, silt and clay of the mortar soil were within the recommended values as shown in Table 7.2. Comparing with the recommended ranges, the portion of sand in the mortar was at the upper limit, whereas the contents of silt and clay were in the medium range. The higher percentage of sand helps in

reducing shrinkage. Also, the lower range of plasticity index of this mortar soil could be attributed to the higher value of sand content. While comparing with the soil used by Dowling (2005), sand and silt are of almost similar proportions. However, Dowling used considerably low clay content.

Table 7.2 Comparison of composition of mud mortar soil

Composition	Recommended (HB 195) %	Dowling (2005) %	This Research %
Clay	10-40	2-6	14
Silt	10-30	20-35	20
Sand	30-75	65-75	66

The research on the effects of particle size distribution in the strength of mortar is not available in the literature. However, sieve analysis was included for observing the trend of particle sizes of the sand and also confirming the fraction of fine particles obtained in sedimentation test. The shape of particle size distribution curve (Figure 4.13) indicates that the sand particles are almost well graded. However, the slight twist of the curve in the range of six to eight microns indicates that a larger fraction of particles are within this range. Moreover, the percentage passing through 75μm sieve is 32%, which is comparable with combined percentage of silt and clay obtained from the sedimentation test.

The flexural strength of nine mortar prisms are presented in Figure 7.2. All test data have shown consistent results. The proposed method for preparing top surface of mortar prisms has proven advantageous. The average value of the bending strength was 470 kPa. This value seems reasonable with the specified rage of bending strength (0-500 kPa) of mud bricks (Walker & Standards Australia HB 195 - 2002).

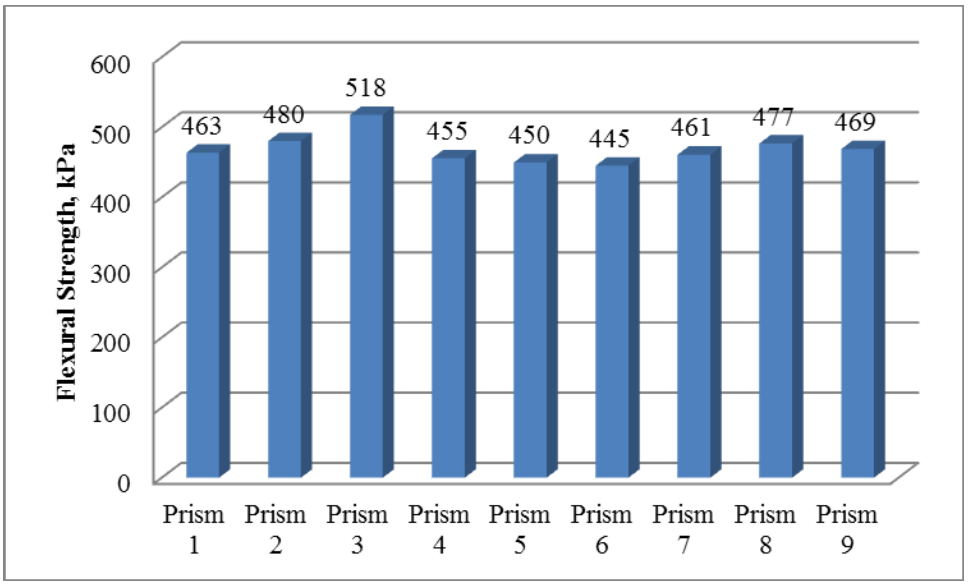

Figure 7.2 Bending test results of mortar prisms

The average compressive strength of 16 mortar specimens was 1.56 MPa with a coefficient of variation of 5.1%. The shape of the broken piece of the prism was hourglass type (Figure 4.16 b). The variations of test results of each mortar prism were as shown in Figure 7.3.

Comparing with the specification of compressive strength for mud bricks (1-5 MPa) in the Australian Standard handbook (HB 195 - 2002), the mud mortar used in this experiment seems to be of lower strength. However, it is comparable to the values obtained by other researcher (Table 7.3).

Table 7.3 Comparison of mud mortar properties

	Compressive strength MPa	Modulus of elasticity MPa	Tensile Strength MPa
Silveira et al. 2012	1.32	225	0.17
Dowling 2006	1.50	151	-
This research	1.56	207	0.47

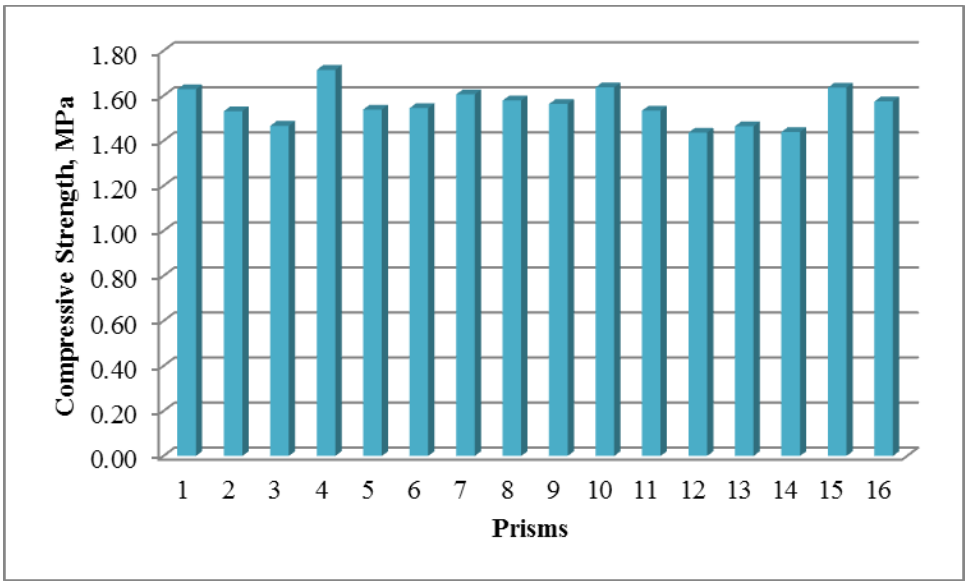

Figure 7.3 Compressive strength test results of mortar prisms

Table 7.3 shows that the modulus of elasticity of mud mortar prism is fairly close to the values acquired by Silveira et al. (2012). However, it is higher than the case of Dowling (2006). The modulus of elasticity calculated by bending test seems significantly higher than that obtained from compression test. This suggests that mud mortar behaves differently in compression and tension.

7.2 Stone specimens properties

The average compressive strength of 11 stone cubes was found to be 38 MPa. The minimum recommended value for sand stone is 30 MPa (IS 1597.1 : 1992). This implies that the sandstone used in this experiment is relatively soft. The strength of each of the specimens is presented in Figure 7.4. The result for specimen 7 seems relatively low compared to other specimens. Therefore, this value was discarded while calculating the average compressive strength of stone.

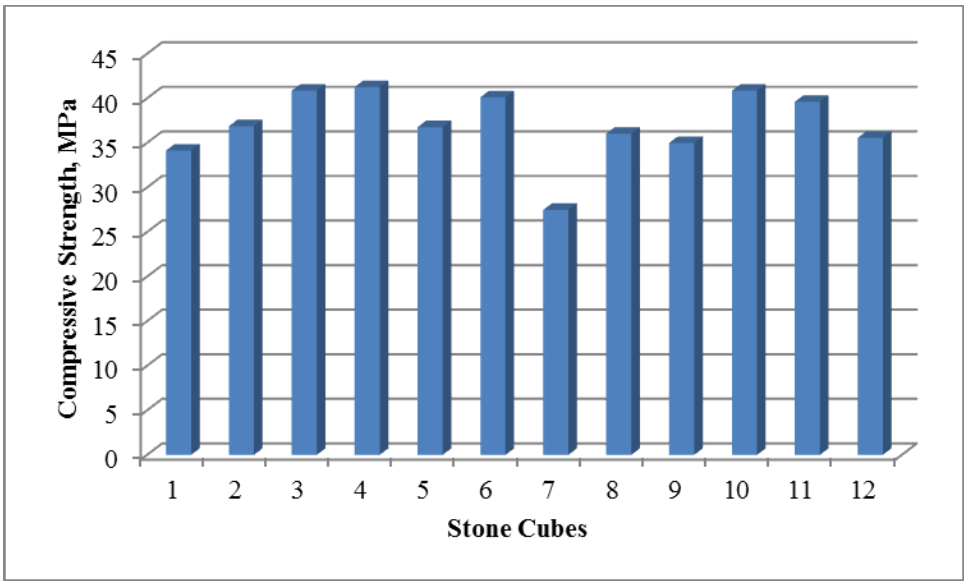

Figure 7.4 Compressive strengths of stone cubes

The flexural strengths of 10 stone prisms were as shown in Figure 7.5. Majority of the results were on the lower side. Therefore, two higher results were discarded to get the average strength of 8 prisms as 3.3 MPa.

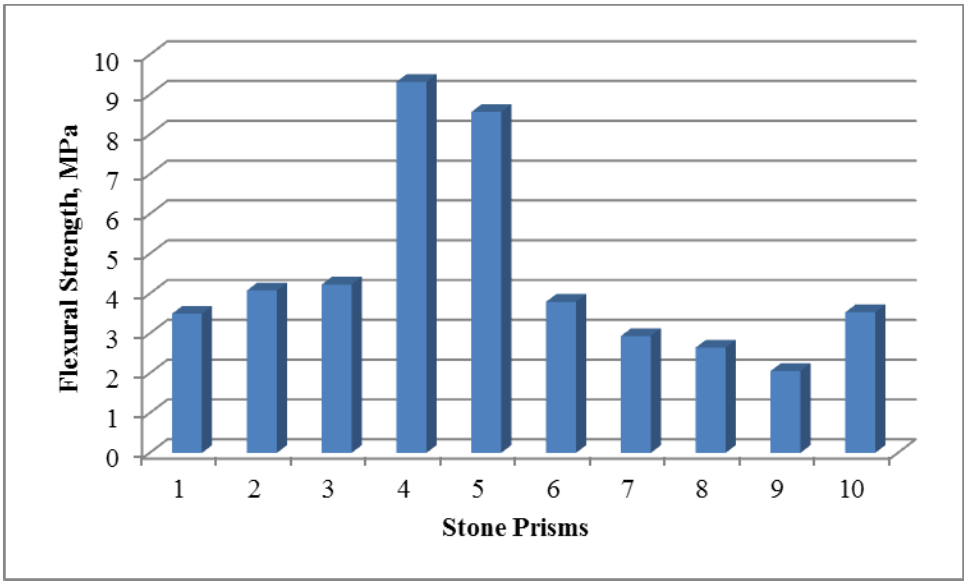

Figure 7.5 Flexural strength of stone prisms

7.3 Wall specimens - compression tests

The compressive strengths of three wall specimens were reasonably consistent as shown in Figure 7.6. While comparing the compressive strengths of stone, mortar and wall specimens, the strength of wall lies between the strength of mortar and stone (Figure 7.7). This is in line with the results of other researchers (Table 7.4).

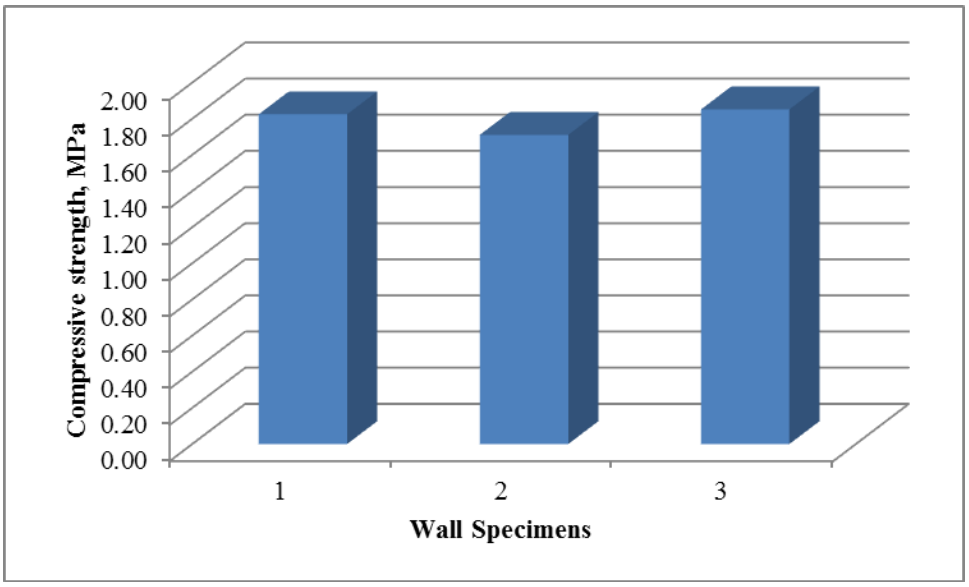

Figure 7.6 Compressive strength of wall specimen

From Table 7.4, it seems that just 5% of the compressive strength of stone has been mobilised in the compressive strength of the wall. This is similar with finding of Gracia et al. (2012) for rubble masonry with low strength mortar. All other values presented in this table are for stack bonded prisms (like ashlar masonry). This clearly suggests that the mechanisms of rubble masonry are different from other masonry.

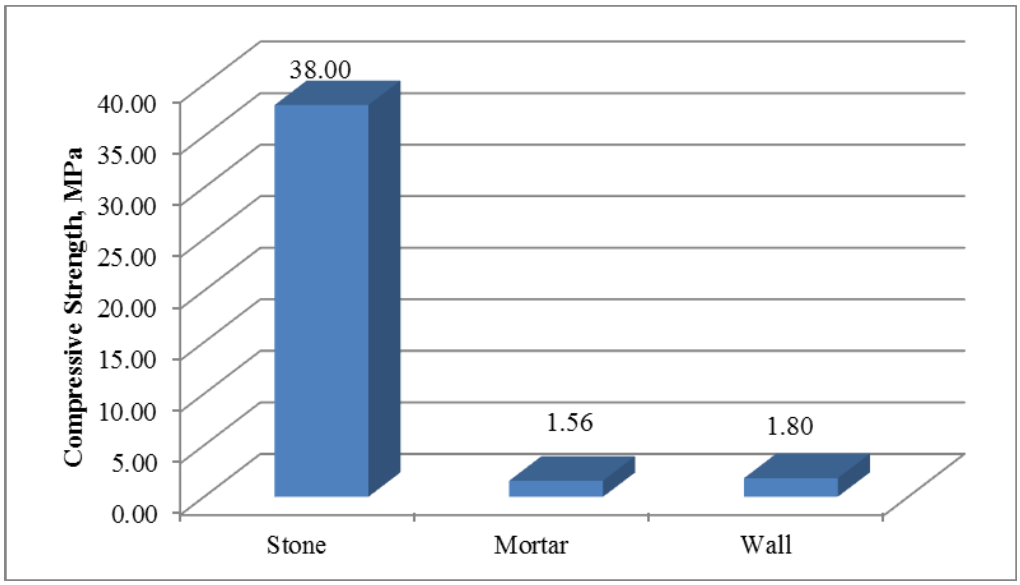

Figure 7.7 Comparison of compressive strength of stone, mortar and wall

Table 7.4 Compressive strength of stone wall with strengths of its components

	Stone	Mortar	Prisms/Wall	Ratio of wall strength to	
	MPa	MPa	MPa	Stone	Mortar
Rao, Reddy & Jagadish (1997)	86.1	9.4	38.60	0.45	4.11
Rao, Reddy & Jagadish (1997)	86.1	2.8	30.40	0.35	10.86
Oliveira (2000)	91.6	DJ	62.30	0.68	NA
Vasconcelos & Lourenco (2009)	73.0	DSJ	69.20	0.95	NA
Vasconcelos & Lourenco (2009)	73.0	DRJ	51.90	0.71	NA
Vasconcelos & Lourenco (2009)	73.0	LM	37.00	0.51	NA
Vasconcelos & Lourenco (2009)	73.0	MM	64.20	0.88	NA
Zeng (2010)	55.2	15.9	40.70	0.74	2.56
García et al (2012)	40.0	0.26	1.84	0.05	7.08
This Research	37.9	1.56	1.80	0.05	1.15

Notes: DJ = Dry Joint, DSJ = Dry Smooth Joint, DRJ = Dry Rough Joint, LM = Lime Mortar (strength not measured), MM = Mud Mortar (strength not measured), NA = Not Applicable

Masonry with regular unit in compression fails in tri-axial compression state of mortar and biaxial tension state of unit (Hendry et al. 1997). However, in rubble masonry with low strength mortar, such condition may not always be truly valid.

A new failure pattern has been proposed to address this case in this research. In the absence of sharp corners, the effective mortar joints are usually larger than the gap between two units (Figure 7.8). As a consequence, a relatively soft pocket provided by the mud mortar will be enough to create differential settlement/displacement to the rubble bridging this joint. Due to brittle nature of the stone, this deformation will be enough to break the stone in bending.

Figure 7.8 Close up view of mortar joint in rubble masonry

In order to verify this proposition, a simple analytical explanation has been offered. Suppose, there is a uniform stress distribution inside the wall specimen subjected to compression testing. Considering the effective span over the vertical mortar joint,

flexural stress on the stone above the joint was calculated. By varying the effective span from 20 to 60 mm based on the shape of the stones and assuming the end condition as lying between fixed and free support, the flexural stress for the stone with three different depths was obtained as shown in Figure 7.9 for the compressive stress of 1.8 MPa. Comparing with the flexural strength of the stone unit (3.3 MPa), the stone unit with 50 mm thickness may fail if the effective spacing of the joint is around 40 to 50 mm. This spacing is reasonable to be valid for the rubble masonry. This further indicates that for flat stone rubble masonry with mud mortar, the thickness of vertical joint is more critical than horizontal joint for the compressive strength.

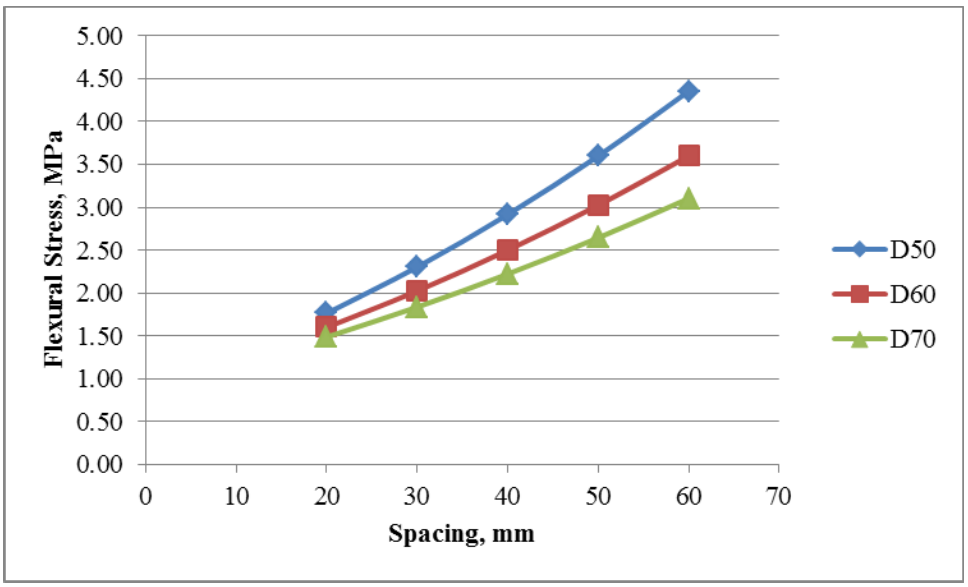

Note: D50 = Depth with 50 mm and so on

Figure 7.9 Variation of flexural stress in the stone along the mortar joint

Reinforced wall specimen was not prepared for compression testing because of two reasons. Firstly, it was supposed that the improvement in the compressive strength

by externally wrapped reinforcement system would not be significant. This was based on the logical comparison of the current case with the compression testing results of gabion (Wheen 2009). Secondly, it was not necessary to increase the compressive strength of unreinforced rubble masonry to deal with the type of structures under study.

7.4 Wall specimens - vertical flexural tests

The flexural strength of 5 unreinforced wall specimens in the vertical span was 48 kPa. The bending strength was calculated based on the loading at the initiation of the crack. This load depends on where the crack is formed. Most often, cracks appear at the stone mortar joint near the top support because this is the least counter balanced part due to the self-weight of the wall above this level. If the joints in that portion are stronger for any reasons, the crack appears at the lower part. In that case, the crack load will be higher but the net bending strength will be similar to the previous case because of the same reason.

The flexural strength of the wall in vertical span is the measure of the bond strength between mortar and stone interface. Though the bending strength of the mortar is not directly related to the flexural strength of the wall in the vertical span, this can be used as an indirect measure of the bond strength of the wall. Comparing these two values, it can be seen that the bond strength of the wall is about 10% of the bending strength of the mortar beam (Figure 7.10).

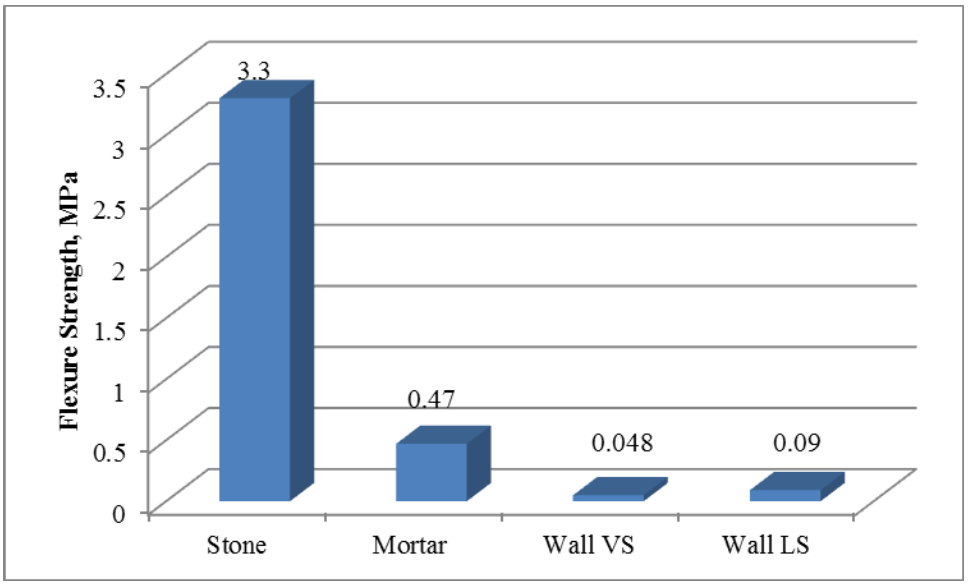

Notes: VS = vertical span, LS = Lateral Span

Figure 7.10 Comparison of flexural strengths of wall and its components

The ultimate load was not taken into consideration while calculating the bond strength of the wall (Table 5.3). During the test, it was observed that load sustained by the specimen was increasing even after a wide crack had developed in the wall (Figure 5.37). In fact, this is because of the rigid body movement of the wall after cracking. Interestingly, the wall remains stable up to a large displacement, also with increased load (Figure 5.39). Such capacity is imparted to the wall mainly because of two reasons. The first reason is the large thickness of the wall which is helpful for maintaining the stability up to a large rotation. The second reason is the upright position of the wall. Unlike a beam, self-weight is advantageous for the wall in resisting lateral load even after exceeding its flexural strength.

After the initiation of cracking, the slope of the load deflection curve changes drastically. However, the wall continues taking further load up to a large deflection.

This shows that the system of walls will be flexible after cracking. This might attract less seismic input depending upon its vibration period after cracking. If by any means integrity of the wall is maintained, such wall will behave satisfactorily during earthquake loading.

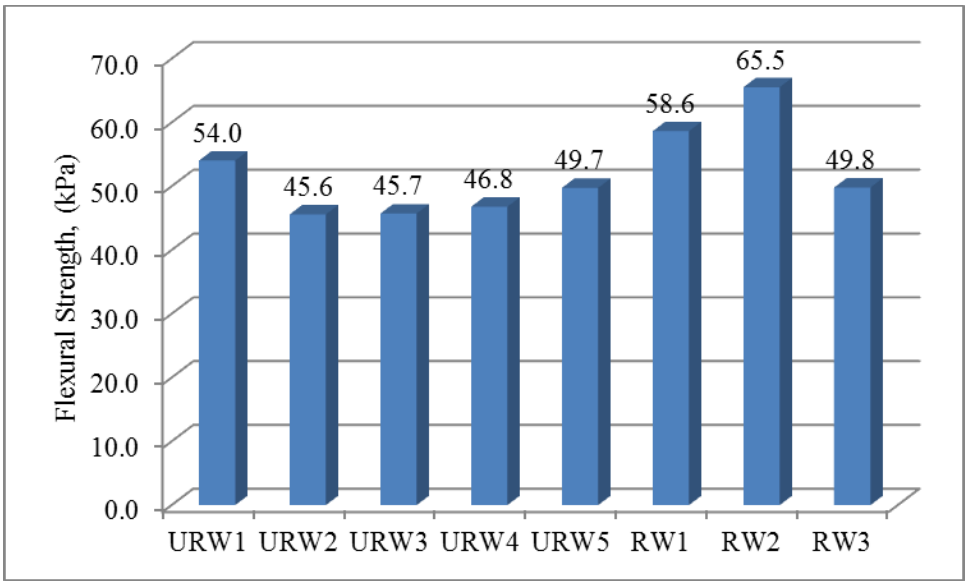

Notes: URW = Unreinforced Wall, RW = Reinforced Wall

Figure 7.11 Flexural strength of walls (Vertical Span)

The flexural strengths of three reinforced wall specimens for bending in vertical span (VS) are comparatively shown with five unreinforced wall specimens in Figure 7.11. This shows that the contribution of the GSW reinforcement to the bending strength of the wall is insignificant. This is because the externally applied reinforcement comes into action only when there is a considerable wall deflection. Because of fragile nature of stone masonry in mud mortar, wall gets easily cracked after a small deformation. Therefore, the significance of GSW mesh appears only after initiation of cracks in the wall. Slight improvement in the bending strength of the reinforced

wall is attributed to the initial confinement imparted by the mesh tightness attached to the wall.

The effect of GSW mesh reinforcement in the strength of wall can be observed while comparing with ultimate load (Fig. 7.12) sustained by the specimens. In this chart, yield load is the load taken just before initiation of the crack in the wall, whereas the ultimate load is the maximum load taken by the wall. In this case, the author prefers to use the term ultimate load instead of ultimate strength in order to emphasise that this is a different case from the most commonly used term "ultimate strength". After cracking, the flexural strength of the wall reduces to almost zero but the wall can continuously carry further lateral loads.

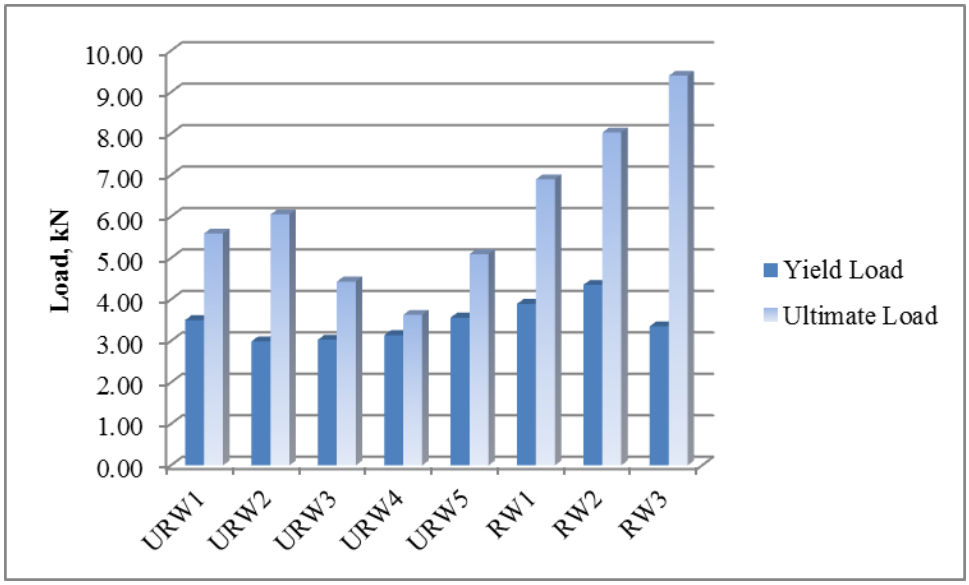

Figure 7.12 Comparison of load at initial crack and ultimate load (Vertical Span)

The chart shows that there is a significant improvement on the ultimate load carrying capacity of the wall with GSW mesh reinforcement. As the width of crack starts increasing, the reinforcement prevents it from widening further with the support

from relatively high compressive strength of stone wall. During this process, the wall can have large deflection with sustained load as shown in load deflection curve (Figure 5.39). A similar type of curve with large displacement and very flat initial slope was observed by Spence & Coburn (1992) for timber reinforced stone wall with mud mortar

The load deformation curve clearly indicates that, the initial stiffness of the wall is not improved by the GSW reinforcement for bending in the vertical span. However, post cracking behaviour of the reinforced wall is considerably improved. This system of reinforcement has performed in accordance with the requirements of the reinforcement technique envisaged by the authors during testing on unreinforced walls (Pun, Samali & Valipour 2012a). Based on their observations, authors concluded that for making stone houses earthquake resistant, it will be enough to develop a reinforcement system which will maintain the integrity of the wall after initiation of the crack during the reversible shaking of the earthquake.

Moreover, the load deflection curve has shown that post cracking stiffness of the reinforced wall is slightly improved but still well below the stiffness before cracking. As a consequence, the wall seems to be flexible enough to attract less seismic input depending upon its vibration period. In addition, the load carrying capacity of the wall increases with the increment in deflection of the wall. Both of these characteristics of the reinforced wall are helpful in improving the seismic performance.

7.5 Wall specimens - horizontal flexural tests

The horizontal flexural strengths of three unreinforced wall specimens and two reinforced wall specimens were as shown Figure 7.13. The bending strength of unreinforced wall specimens in lateral span was almost double than in vertical span (Figure 7.10). However, the load carrying capacity drops significantly after the initiation of the crack (Figure 5.44) in lateral span. Therefore, it is a brittle failure.

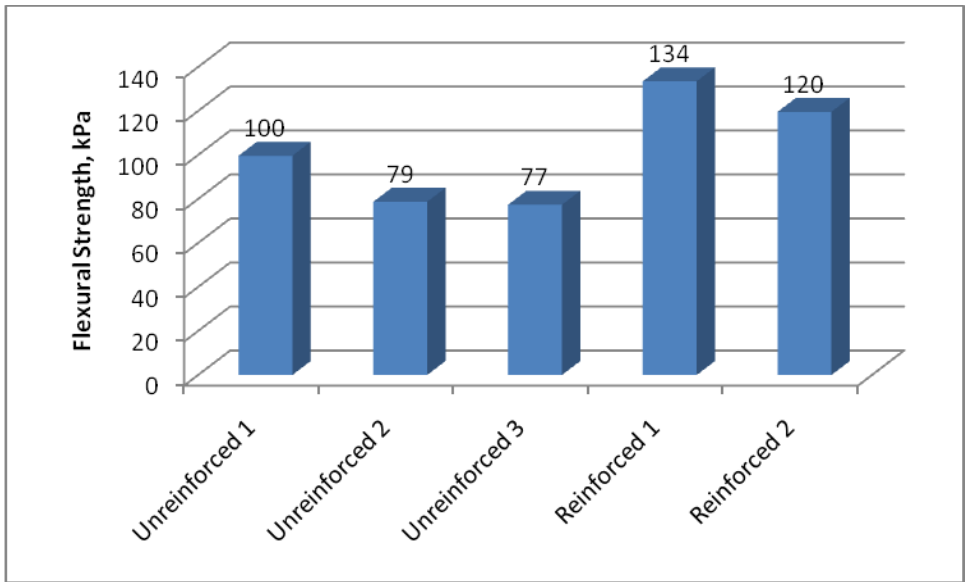

Figure 7.13 Flexural strength of reinforced and unreinforced walls (Lateral Span)

Unlike in the vertical span, there is a considerable improvement in the load carrying capacity of the reinforced wall while bending in lateral span. This was due to the closely spaced tie wire. With reduced spacing, mobilization of the strain in the external mesh was significant with small rotation as indicated in the proposed Equation (6.5). Figure 5.44 also shows that the stiffness of the reinforced wall in lateral span does not reduce after cracking. Few humps in the curves correspond to the failure of some parts of the mesh. The wall can carry load even after the failure

of few meshes. This suggests that this reinforcement system turns the brittle wall in to considerably ductile structure.

7.6 Wall specimens - shake table tests

In general, small scale masonry model testing shows the overall behaviour of the structural system, and not the behaviour of structural elements (Tomaževič & Velechovsky 1992). The shake table testing has shown that freshly built stone wall with mud mortar can withstand a considerable amount of seismic shaking. Initial cracking appeared only after input excitation was 1.75 times El-Centro. This might not be true for old structures. As time passes, the ingress of moisture may loosen the mud mortar. In that case, the strength of the building may not be in the same condition as in the freshly built condition.

Though the roof load and compensating load for the reduced scale was not considered, the overall response of the shake table specimen was good. The lintel beam prevented the formation of vertical crack in the mid-span of the main wall. The wall specimen was on the verge of collapse at ground shaking level 2.5 times El-Centro.

The reinforced shake table specimen performed considerably better than the unreinforced specimen. Initial crack appeared only after shaking intensity 2.75 times El Centro. As the shaking intensity increased, horizontal cracks were developed along the wall as expected. This has proven the fact that the wall in the lateral span will be stronger than in the vertical span using the proposed reinforcement scheme. The confining action of external mesh assisted by internal tie wire keeps the wall

intact between the cracked sections. Cracking at the corner were noticeably reduced. The reinforced wall specimen survived even after ground shaking 4 times El-Centro.

7.7 Moisture content

The moisture content was monitored through all tests. In most cases, it was below 2%. In the case of compression test of unreinforced wall and flexural test of reinforced wall in lateral span, the moisture contents were relatively higher than other tests. Therefore, the results obtained in these two cases may be slightly lower than those with reduced moisture contents.

7.8 Analytical modelling and numerical studies

An analytical study has revealed that the effectiveness of externally wrapped reinforcement increases considerably when the spacing of tie links connecting the reinforcements on opposite sides is reduced. In the lateral span, spacing of tie links can be reduced using the pair of wires from the inserted mesh to connect with the external mesh. However, it will be concentrated along the inserted mesh only. In the vertical span, the spacing of the tie links is governed by the spacing of the horizontally inserted mesh.

All relations derived for the externally wrapped reinforcement is not directly applicable for the GSW mesh reinforcement. This is because the deformation of a hexagonal mesh is different than a solid wire. Therefore, the deformation characteristics of a hexagonal mesh was investigated in the vertical as well as horizontal direction. The concept of vertical and horizontal deformation was introduced based on the way an installed mesh around the wall would deform. In

fact, vertical deformation represents stretching along the diagonally opposite corner, whereas the horizontal deformation is the elongation perpendicular to the parallel sides of the mesh (Figure 6.29 and Figure 6.30) . However, in the case of GSW mesh fabricated either by direct weaving method or double twisted method, two vertical sides (only two out of 6 parallel sides of a hexagonal mesh) consists of double wire. Therefore, the vertical and horizontal deformation of the hexagonal mesh used in this thesis represent unique quantities.

The hexagonal mesh deforms more in the vertical direction than in the horizontal direction. It is evident from the comparison of deformation ratio of mesh and equivalent solid wire. The elastic deformation of a single column of hexagonal cells in the vertical direction is about 3.2 times higher than equivalent solid wire, whereas this ratio in horizontal deformation of a single row of hexagonal cells is around 1.7. Therefore, a single column of cells of a GSW mesh is stiffer in the horizontal direction than in the vertical direction.

The major contribution to the overall deformation of a mesh is played by the inclined members. In the case of vertical deformation, the top and bottom pairs of inclined members contribute in series (Figure 6.15), whereas in the case of horizontal deformation, both pairs act in parallel. This is the main reason for having more deformation in the vertical direction.

The deformation of a hexagonal mesh is proportional to the length of the mesh. However, it is independent of opening size of the cell as long as the same stress level is maintained. This shows that the hexagonal mesh behaves in the most stable configuration acting as an equivalent solid wire with more flexibility.

In a hexagonal mesh, the internal force in the inclined member is always more than in the vertical member for vertical or horizontal loading. In addition, in a GSW hexagonal mesh, the vertical member consists of two wires and inclined member is a single wire. Therefore, the inclined member is the most critical part of the hexagonal GSW mesh. As a consequence, the ultimate strength of the mesh is always less than the ultimate strength of solid wires used for weaving the mesh. The ultimate strength of a single hexagonal cell in the vertical direction is about 72% of the equivalent solid wire, whereas in the horizontal direction it is about 92%. However, overall load carrying capacity of the hexagonal mesh is about 30% more in the vertical direction than in the horizontal direction. In fact, the distance between the parallel sides of a hexagonal cell is smaller than the distance between opposite corners. Therefore, the number of columns of cells accommodated per unit length of the mesh is more than the number of rows of cells per unit height. Columns of cells contribute to the strength in the vertical direction, whereas rows of cells are responsible for the strength in the horizontal direction.

Deformation of a hexagonal mesh per unit length is useful in two ways. Firstly, it can be used to calculate the total deformation of the mesh for a given value of UDL. Secondly, it quickly gives an idea about how much the mesh would deform for restraining the given UDL. As the deformation depends on the cell size and diameter of wire, a curve is valid only for that type of mesh. On the other hand, the equivalent stress strain curve is applicable for all sizes of mesh and diameters of wire. However, either equivalent stress or equivalent strain of the mesh should be a known parameter for using this curve.

Though the inserted mesh is helpful in reducing the spacing of the tie link in the lateral span, it does so only along the interconnected region of the external mesh. The remaining portion of the outer mesh between two inserted meshes is free to deform throughout the whole length. As the rotation of the wall in lateral span increases, the portion of the external mesh along the inserted mesh will be highly stressed near the crack in the wall as compared to remaining portions of the mesh. For resisting the unbalanced moment in the vertical span, the whole length of the external mesh will be stressed almost uniformly near the cracked region.

The strain level in the inserted mesh varies in each row of cells. The maximum strain level will be always less than the maximum strain in the external mesh. The equivalent stress in each row of cells can be obtained using the equivalent stress strain curve of the mesh in horizontal direction. The total resisting moment will be the summation of contributions from each row of cells.

The theoretical relations derived for the external and inserted GSW mesh were experimentally verified by comparing with the test results. The analytically predicted value was about 80% of the test results. The higher values of the experimental results were due to the constraints provided by the mud mortar. However, after a couple of shaking cycles, the additional contribution of the mud mortar may disappear and the real strength might come closer to the predicted value by the analytical method. If the strength of mortar does not degrade so much, it will provide additional safety.

The performance of the reinforced wall is the combined outcomes of the inserted as well as external mesh. In the lateral span, the crack will most probably initiate along the mid span, which alters the boundary conditions of the wall, making the corner

region more vulnerable. As a consequence, crack will appear along the corner of the wall. As the wall starts to rotate, strain in the internal as well as external mesh will be initiated and the resisting moment will be induced. The cracked wall will rotate until sufficient resisting moment is induced in order to balance the external moment.

Using fragile materials like stone and mud with flexible reinforcement, it is not reasonable to expect the building to remain intact during the earthquake event. If the collapse of the building can be prevented, the probability of survival of the occupants will be increased. Limiting the maximum deformation of the building, the chances of collapse can be reduced.

A set of procedures were developed in order to calculate the deflection of the GSW reinforced wall and applied to single storey and double storey buildings. This assessment method has produced quite reasonable results. When the angle of rotation of the wall increases, there might be a considerable drop in the transfer of input excitation. This factor has not been taken into consideration in this method. Therefore, the actual deflection might be significantly less than the calculated value. Further research is necessary in this regard.

8. Conclusions and Recommendations for Future Research

8.1 Summary and conclusions

Stone masonry with mud mortar is highly vulnerable to earthquake loading. There are still large stocks of stone masonry houses in many earthquake prone regions around the world as this type of building typologies are the most viable options in the mountainous areas. Unfortunately, this is the least considered field in research activities.

Developing an effective and applicable seismic improvement technique for stone masonry houses built with mud mortar is still highly demanding in earthquake prone hilly regions. Improving out of plane bending performance of such type of masonry is one of the major steps towards solving this challenge.

This research has set up a path toward reducing earthquake vulnerability of traditional stone masonry houses. The outcome of this research has demonstrated the effectiveness of the proposed GSW reinforcement for improving the seismic performance of residential houses made from natural stone with mud mortar. This technique seems equally applicable for using rubble from damaged houses in earthquake disasters to build seismic resistant houses, which will be useful during reconstruction phase for clearing up sites and building safer houses side by side.

The seismic performance of GSW reinforcement was concluded through a series of static and dynamic testing and supported by analytical and numerical modeling. During this journey, a collection of basic properties of walls and its components has also been established. Randomly selected sand stone pieces and mud mortar soil

were chosen as representative materials of traditional stone masonry houses, which were used for preparing wall specimens.

The liquid limit test and plastic limit test have shown that the type of soil used for preparing mud mortar was inorganic silty clay with low plasticity. The mortar soil was composed of 14% clay, 20% silt and 66% sand. Following systematic procedures, compressive strength, bending strength and modulus of elasticity of the mud mortar were determined. New procedures proposed for preparing the top surface of dried mud mortar specimens have proven highly effective. This method will be useful for obtaining the consistent results of dried mud mortar specimens due to reduced uncertainties caused by undulated surface. The modulus of elasticity of mud mortar prism calculated by bending test was considerably higher than obtained from compression test. This implies that the mud mortar behaves differently in compression and tension.

Compressive strengths of rubble walls with mud mortar were determined using full scale specimens prepared in the laboratory. The dimensions of the specimen were finalised based on the nature of the wall and indirect correlation with the existing standard methods for other types of wall specimens. Stress strain curves, as well as modulus of elasticity, were also determined. The compressive strength of wall specimen was obtained in the range between the strength of mortar and stone specimen, which is in line with findings of other researchers. However, only 5% of the compressive strength of stone specimen was mobilised in the strength of wall in compression. Moreover, it has been observed that the rubble wall specimen with

mud mortar subjected to compressive load fails more likely in bending rather than splitting. As a consequence, the thickness of vertical joints are more critical than thickness of horizontal bed joint of rubble walls for the compressive strength. The pattern of load deformation curve as well as modulus of elasticity of the wall specimen was almost similar with mud mortar. This implies that the deformation characteristics of rubble wall specimen largely depend on the properties of mud mortar.

The flexure strength of rubble wall built with mud mortar was determined in the vertical span as well as lateral span. The terms of bending strengths in the vertical and lateral span seem more suitable for addressing the flexural behaviour of rubble masonry. A set of purpose made testing accessories was developed to determine the flexural strength of wall specimens. Such walls are stronger by almost twice in lateral span than in vertical span. However, the wall remains stable up to a large rotation while bending in the vertical span. The behaviour of unreinforced wall in lateral span has shown a brittle failure.

The outcomes of experimental investigation on unreinforced specimens in bending have highlighted the main cause of poor performance of such type of masonry in earthquakes and also its positive aspects which can be mobilised for improving seismic performance. As widely accepted, the inherent weakness of stone-mortar interface seems the main cause of damage of such walls in the seismic shakings. The bond strength of this type of wall can hardly reach about one tenth of the bending strength of mud mortar. This implies that the weak wall gets easily cracked during early phases of the seismic load, which is normally small. This makes the wall ready

to undergo peak loads with reduced seismic response due to increased flexibility so long as its integrity is maintained.

In order to maintain the integrity of the wall, a relatively cheap, durable and simple reinforcement system using galvanized steel wire mesh has been proposed and tested for effectiveness in this research. Two types of reinforcement schemes were developed for reinforcing the wall specimens. In the first method, reinforcement mesh was woven around the wall specimen using galvanized steel wire. In the second method, pre-fabricated mesh was wrapped around the wall. Connection procedures between pre-fabricated meshes was developed, which was the major breakthrough for the second type of reinforcement scheme, otherwise it was not possible for using pre-fabricated mesh effectively for reinforcing the wall. In addition, a simple method for tightening the mesh after wrapping around the wall was also developed. This tightening technique makes the GSW reinforcement system more superior in seismic performance than other types of externally applied mesh by allowing limited deformation of the building during ground shaking.

Wall specimens wrapped with the GSW mesh were tested for bending in static loading and also in dynamic loading using a shake table. Though there was no significant improvement in the initial stiffness as well as load at crack initiation in the wall while bending in the vertical span, the GSW reinforcement system improved post cracking performance considerably. The reinforcement system increased the bending resistance of the wall by more than 150% and remained stable up to a large deflection.

In the lateral span, this reinforcement scheme improved the bending strength by almost double before crack initiation. Post cracking stiffness was also maintained at considerably higher levels up to a large deflection. After a mesh was broken, the load carrying capacity was dropped slightly. However, it was increased again before the failure of another mesh. This has shown that GSW reinforcement makes the wall highly ductile even in bending in lateral span.

This performance has been observed in dynamic loading as well. The first cracking load of reinforced specimen was improved by 150%. The mid span deflection of reinforced wall was about half of unreinforced wall. The unreinforced wall was at the point of collapse at ground shaking 2.5 times the El-Centro quake. On the other hand, the reinforced wall specimen survived ground shaking in excess of 4.0 times El-Centro intensity.

Though the roof load and additional compensational loads were not taken into account in the model, from comparative analysis it has been proven that such reinforcement system performs highly satisfactorily during earthquake loading.

The mesh provided confinement to the wall, which helped to avoid the most common seismic deficiencies of the stone masonry. As a consequence, the integrity of the whole building was maintained during the earthquake loading.

Analytical modelling has shown that the effectiveness of GSW reinforcement system increases with reducing the spacing of the tie wire for connecting the mesh to the wall and increasing the tightness of the mesh to the wall. Using horizontal strip of

internal mesh instead of twin tie wires, closer spacing of the equivalent tie wires can be achieved.

A hexagonal mesh behaves in a very stable configuration. The hexagonal mesh is stiffer in horizontal direction than in vertical direction. An individual cell of a hexagonal mesh is stronger in the horizontal direction. However, overall load carrying capacity of a hexagonal mesh is about 30% higher in the vertical direction.

Analytical relations derived for the reinforced wall has predicted about 80% of the strength of the wall. This has not only validated the theoretical relations but also indicated that these relations are conservative.

Horizontally inserted hexagonal mesh in the wall interconnected with the external mesh can contribute considerably to enhance the seismic performance of the wall. Assuming the inserted mesh have been provided at an interval not exceeding 500 mm along the height, the following results have been observed. Without considering the effect of corrosion, a hexagonal GSW mesh having 50 mm opening size with 1 mm diameter seems adequate to reinforce a light roof single storey building up to 5 m span. Similarly, a mesh having 100 mm opening size with 2 mm wire diameter, most likely be adequate to reinforce a two storey building with light floor and roof up to 5.5 m span.

GSW reinforcement system was found to be relatively easy to fabricate. It constitutes only a single additional material, which is helpful in reducing the complexity during implementation. Below the plinth level, covering the mesh with cement plaster will be helpful for prolonging the life of the mesh.

Because of randomness and variations in the properties of stone, mud mortar and workmanship, these findings will not be sufficient to be generalised to all types of random masonry construction. However, the improvement achieved using galvanized wire mesh will be applicable to all types of walling.

8.2 Recommendation for future research

This research has opened the way to many exciting areas for further studies. For example, roof or floor systems were not incorporated in this study. Usually, double storey stone masonry houses are more common than single storey dwellings. A thorough investigation including roof or floor would provide realistic behaviour of low strength stone masonry buildings during major earthquakes, which could be directly applicable in the fields.

Shear strength testing of the stone masonry with mud mortar was removed from the experimental investigation due to time constraints in this research. Though it is challenging because of fragile nature of wall specimens, shear strength might be determined by adopting methods specified in ASTM International Standard (ASTM E519/E519M-2010).

A study on the durability of the GSW in the rural environment will be a useful topic for implementing such reinforcement system. It would be better to investigate the durability of the GSW in two separate environments: one below the plinth level and the other above the plinth level.

Rubble masonry is relatively faster to construct and hence a cheaper option than other types of stone masonry. However, such types of masonry are still more time

consuming than brick or block masonry. Shaping of each piece of rubble is required for proper adjustment in order to avoid a continuous vertical joint. In such scenario, investigating the properties of mud concrete could be a better alternative. Similar to conventional concrete, mud concrete is a mixture of soil, sand and gravel/rubble. By varying the size of rubble and ratio of mud/rubble, strength of mud concrete in compression, tension and flexure can be studied to find the optimum size of rubble or grading of rubble and mud/rubble ratio. With externally applied mesh reinforcement, such construction could be an economical alternative for seismic resistant construction. If verified, it would be the best low cost housing solution, even during reconstruction phase after an earthquake disaster.

This research has provided a pool of experimental data. A separate detailed analytical and numerical study to expand on the preliminary analytical studies carried out in this thesis will be a useful research topic.

References

Arya, A.S. 2001, *Improving Earthquake Resistance of Buildings - Guidelines*, Building Materials & Technology Promotion Council, New Delhi.

ASTM Standard ASTM A 641/A 641M: 2009, *Standard Specification for Zinc-Coated (Galvanized) Carbon Steel Wire*, ASTM International.

ASTM Standard ASTM A 975 : 2003, *Standard Specification for Double - Twisted Hexagonal Mesh Gabions and Revet Mattresses*, ASTM International.

ASTM Standard ASTM C 1072 - 2006, *Standard Test Method for Measurement of Masonry Flexural Bond Strenght*, ASTM International, USA.

ASTM Standard ASTM E519/E519M-2010, *Standard Test Method for Diagonal Tension (Shear) in Masonry Assemblages*, ASTM International.

Australian Standard AS1289.3.2.1-2009, *Methods of testing soils for engineering purposes* - Standards Australia Limited, Sydney, Australia.

Australian Standard AS 1289.2.1.1-2005, *Methods of testing soils for engineering purposes*, Standards Australia Limited, Sydney, Australia.

Australian Standard AS 1289.3.1.1-2009, *Methods of testing soils for engineering purposes*, Standards Australia Limited, Sydney, Australia.

Australian Standard AS 1391 - 2007, *Metallic materials - Tensile testing at ambient temperature*, Standards Australia Limited.

Australian Standard AS 2423-2002, *Coated steel wire fencing products for terrestrial, aquatic and general use*, Standards Australia International Ltd.

Australian Standard AS 3638-1993, *Test Sieving procedures*, Australian Standards Limited, Sydney, Australia.

Australian Standard AS 3700 - 2011, *Masonry structures*, Standards Australia Limited, Sydney, Australia.

Australian/New Zealand Standard AS/NZS 4534: 2006, *Zinc and Zinc/aluminium-alloy coatings on steel wire*, Standards Australia/Standards New Zealand.

Bairrão, R. & Falcão Silva, M.J. 2009, 'Shaking table tests of two different reinforcement techniques using polymeric grids on an asymmetric limestone full-scaled structure', *Engineering Structures*, vol. 31, no. 6, pp. 1321-30.

Bayraktar, A., CoSkun, N. & Yalçin, A. 2007, 'Damages of masonry buildings during the July 2, 2004 Dogubayazit (Agri) earthquake in Turkey', *Engineering Failure Analysis*, vol. 14, no. 1, pp. 147-57.

Bayraktar, A., Nart, C. & Ali, Y. 2007, 'Performance of Masonry Stone Buildings during the March 25 and 28, 2004 Askale (Erzurum) Earthquakes in Turkey', *Journal of Performance of Constructed Facilities*, vol. 21, no. 6, pp. 432-40.

Benedetti, D., Carydis, P. & Pezzoli, P. 1998, 'Shaking table tests on 24 simple masonry buildings', *Earthquake Engineering & Structural Dynamics*, vol. 27, no. 1, pp. 67-90.

Binda, L., Pina-Henriques, J., Anzani, A., Fontana, A. & Lourenço, P.B. 2006, 'A contribution for the understanding of load-transfer mechanisms in multi-leaf masonry walls: Testing and modelling', *Engineering Structures*, vol. 28, no. 8, pp. 1132-48.

Blondet, M., Vargas, J. & Rubiños, Á. 2009, 'Construction of safe and healthy adobe houses after the Pisco 2007 earthquake in Peru', *11th International Conference on Non-conventional Materials and Technologies (NOCMAT 2009)*, Bath, UK.

Bothara, J. & Brzev, S. 2011, 'A Tutorial: Improving the Seismic Performance of Stone Masonry Buildings', Earthquake Engineering Research Institute, viewed 14 December 2014 < ttp://www.world-housing.net/wp- content/uploads/2011/06/ Stone_Masonry_English.pdf >.

Bothara, J.K. & Hiçyılmaz, K.M.O. 2008, 'General observations of buildings behaviour during the 8th October 2005 Pakistan earthquake', *Bulletin of the New Zealand Society for Earthquake Engineering Inc*, vol. 41, no. 4, pp. 209-33.

British Standard BS 5628-3 : 2001, *Code of practice for use of masonry*, British Standard Institution, London.

British Standard BS EN1052-1:1999, *Methods of test for masonry-determination of compressive strength*, British Standard Institution, London.

British Standard BS EN1052-3: 2002, *Methods of test for masonry - determination of initial shear strength*, British Standard Institution, London.

British Standard BS EN 1052-4: 2000, *Determination of shear strength including damp proof course*, British Standard Institution, London.

British Standard BS EN 1052-5: 2005, *Determination of bond strength by the bond wrench method*, British Standard Institution, London.

British Standard BS EN 1926:2006, *Natural stone test methods - determination of uniaxial compressive strength*, British Standard Institution, London.

British Standard BS EN 12372:2006, *Natural stone test methods - Determination of flexural strength under concentrated load*, British Standards Institution, London.

British Standard Institution BS EN 1015-11:1999, *Methods of test for mortar for masonry* British Standard Institution, London, UK.

British Standards BS 5390 : 1976, *Code of practice for stone masonry*, British Standards Institution, London.

British Standards BS EN 1015-11:1999, *Methods of test for mortar for masonry* - British Standards Institution, London.

British Standards BS EN 1052-2:1999, *Methods of test for masonry - determination of flexural strength*, British Standards Institution, London.

Brooks, P., Adams, S. & Fowler, W. 2001, *Civilizations exploration and conquest : charts the amazing progress of humankind, from the Stone Age to the Space Age*, Hermes House, London.

Budhu, M. 2011, *Soil mechanics and foundations*, 3rd edn, Wiley, Hoboken, NJ.

Charleson, A. 2011, *Seismic strengthening of earthen houses using straps cut from used car tires: a construction guide*, 51, Earthquake Engineering Research Institute, viewed 13 November 2014, <http://www.world-housing.net/wp- content/uploads/2011/ 06/Seismic_strengthening_of_earthen_houses_using_tire_straps_English2.pdf>.

Chiras, D.D. 2000, *The natural house : a complete guide to healthy, energy-efficient, natural homes*, Chelsea Green Pub., White River Junction, Vt.

Coburn, A. & Spence, R.J.S. 2002, *Earthquake protection*, 2nd edn, Wiley, Chichester.

Corradi, M., Borri, A. & Vignoli, A. 2002, 'Strengthening techniques tested on masonry structures struck by the Umbria-Marche earthquake of 1997-1998', *Construction and Building Materials*, vol. 16, no. 4, pp. 229-39.

Decanini, L., De Sortis, A., Goretti, A., Langenbach, R., Mollaioli, F. & Rasulo, A. 2004, 'Performance of masonry buildings during the 2002 Molise, Italy, earthquake', *Earthquake Spectra*, vol. 20, p. S191.

Dowling, D. 2006, 'Seismic strengthening of adobe-mudbrick houses', PhD thesis, University of Technology, Sydney, Australia.

Dowling, D., Samali, B. & Li, J. 2005, 'An improved means of reinforcing adobe walls – external vertical reinforcement', *SismoAdobe 2005*, Lima, Peru.

Gago, A., Proença, J., Cardoso, J., Cóias, V. & Paula, R. 2009, 'Seismic strengthening of stone masonry walls with glass fiber reinforced polymer stips and mechanical anchorages ', *Experimental Techniques*.

García, D., San-José, J., Garmendia, L. & San-Mateos, R. 2012, 'Experimental study of traditional stone masonry under compressive load and comparison of results with design codes', *Materials and Structures*, vol. 45, no. 7, pp. 995-1006.

Global Synthetics, *Link Gabions and Mattresses Design Booklet*, viewed 5 May 2014, <http://www.globalsynthetics.com.au/files/data_sheets/booklet_gabions.pdf>.

Harris, H.G. 1999, *Structural modeling and experimental techniques*, CRC press.

Hendry, A.W. & Khalaf, F.M. 2001, *Masonry wall construction*, E&FN Spon, New York.

Hendry, A.W., Sinha, B.P., Davies, S.R. & ebrary Inc. 1997, *Design of masonry structures*, 1st edn, E & FN Spon, viewed 7 August 2014, <http://site.ebrary.com/lib/ utslibrary/ Doc?id=10061004>.

Indian Standard IS 1597.1 : 1992, *Construction of stone masonry code of practice, Part 1: Rubble Stone Masonry*, Bureau of Indian Standards.

Indian Standard IS 1597.2 : 1992, *Construction of stone masonry code of practice, Part 2: Ashlar Masonry*, Bureau of Indian Standards.

Indian Standard IS 13935: 1993, *Repair and seismic strengthening of buildings - guidelines*, Bureau of Indian Standards, New Delhi, India.

Indian Standards IS 1893 (Part 1): 2002, *Criteria for Earthquake Resistant Design of Structurers*, Bureau of Indian Standards, New Delhi.

International Association for Earthquake Engineering (IAEE) 1986, *Guidelines for Earthquake Resistant Non-Engineered Construction*.

Karantoni, F.V. & Bouckovalas, G. 1997, 'Description and analysis of building damage due to Pyrgos, Greece earthquake', *Soil Dynamics and Earthquake Engineering*, vol. 16, no. 2, pp. 141-50.

Karantoni, F.V. & Fardis, M.N. 1992, 'Effectiveness of Seismic Strengthening Techniques for Masonry Buildings', *Journal of Structural Engineering*, vol. 118, no. 7, pp. 1884-902.

Koseki, J., Meguro, K., Mayorca, P. & Johansson, J. 2002, *The June 23, 2001 Atico Earthquake, Peru*.

Li, L. 1984, 'Base Isolation Measure for Aseismic Buildings in China', *Eighth World Conference in Earthquake Engineering*, vol. VI, San Francisco, California, pp. 791-8.

Lourenço, P. & Rots, J. 1997, 'Multisurface Interface Model for Analysis of Masonry Structures', *Journal of Engineering Mechanics*, vol. 123, no. 7, pp. 660-8.

MACCAFERRI, *Gabions*, viewed 23 November 2013, <http://www.maccaferri.com.au/ wawcs0137319/idDetails=166/Products-Gabions>.

Magenes, G., Penna, A. & Galasco, A. 2010, 'A full-scale shaking table test on a two-storey stone masonry building', *14th European Conference on Earthquake Engineering*.

Maxlow, J. & Maxlow, A. 1984, *Rock solid : building a stone house in Australia*, Night Owl, Shepparton, Vic.

Mayorca, P. & Meguro, K. 2004, 'Proposal of an efficient technique for retrofitting unreinforced masonry dwellings', *Thirteenth World Conference on Earthquake Engineering,* , Vancouver, British Columbia, Canada

McAfee, P. 2001, *Stone buildings : conservation, repair, building*, O'Brien Press, Dublin.

Meguro, K., Navaratnaraj, S., Sakurai, K. & Numada, M. 2012, 'Shaking Table Tests on 1/4 Scaled Shapeless Stone Masonry Houses with and without Retrofit by

Polypropylene Band Meshes', *15th World Conference on Earthquake Engineering*, Lisbon, Portugal.

Milani, G. 2010, '3D FE limit analysis model for multi-layer masonry structures reinforced with FRP strips', *International Journal of Mechanical Sciences*, vol. 52, no. 6, pp. 784-803.

Milosevic, J., Lopes, M., Gago, A.S. & Bento, R. 2013, 'Testing and modeling the diagonal tension strength of rubble stone masonry panels', *Engineering Structures*, vol. 52, pp. 581-91.

Morel, J.C., Mesbah, A., Oggero, M. & Walker, P. 2001, 'Building houses with local materials: means to drastically reduce the environmental impact of construction', *Building and Environment*, vol. 36, no. 10, pp. 1119-26.

Nepal National Building Code NBC 203: 1994, *Guidelines for earthquake resistant buildings construction: low strength masonry*, Kathmandu, Nepal.

Newlin, J.A. & Trayer, G.W. 1956, *Deflection of beams with special reference to shear deformations*, National Advisory Committee for Aeronautics, USA, 1309.

Nienhuys, S. 1999, *The development of the wire-mesh knotting equipment*, pamphlet, Gilgit, Pakistan.

Nienhuys, S. 2006, 'Galvanized Wire Reinforcement Technology', Aga Khan Planning and Building Service, Pakistan.

Oliveira, D.V. 2000, 'Mechanical characterization of stone and brick masonry', *report 00-Dec/E-4, Universidade do Minho, Departamento de Engenharia Civil, Guimarães, Portugal*.

Pun, R., Samali, B. & Shreshta, B. 2010, 'Major factors in reinforcing stone masonry for sustainable construction practice', *21st Australasian Conference on the Mechanics of Structurers and Materials*, Melbourne, Australia, pp. 547-52.

Pun, R., Samali, B. & Valipour, H. 2012a, 'Flexural strength of stone wall in mud mortar', *Australasian Structural Engineering Conference 2012*, Perth, Australia.

Pun, R., Samali, B. & Valipour, H. 2012b, 'Seismic performance improvement of stone masonry buildings in mud mortar', *22nd Australasian Conference on the Mechanics of Structures and Materials*, Sydney, New South Wales, Australia, pp. 479-84.

Ramalho, M.A., Taliercio, A., Anzani, A., Binda, L. & Papa, E. 2008, 'A numerical model for the description of the nonlinear behaviour of multi-leaf masonry walls', *Advances in Engineering Software*, vol. 39, no. 4, pp. 249-57.

Sandstone Sales 2013, viewed March 2013, <http://www.sandstonesales.com.au/>.

Senthivel, R. & Lourenço, P.B. 2009, 'Finite element modelling of deformation characteristics of historical stone masonry shear walls', *Engineering Structures*, vol. 31, no. 9, pp. 1930-43.

Severn, R.T., Stoten, D.P. & Tagawa, Y. 2012, 'The contribution of shaking tables to earthquake engineering', *15th World Conference on Earthquake Engineering*, Lisbon, Portugal.

Silveira, D., Varum, H., Costa, A., Martins, T., Pereira, H. & Almeida, J. 2012, 'Mechanical properties of adobe bricks in ancient constructions', *Construction and Building Materials*, vol. 28, no. 1, pp. 36-44.

Smoljanović, H., Živaljić, N. & Nikolić, Ž. 2013, 'A combined finite-discrete element analysis of dry stone masonry structures', *Engineering Structures*, vol. 52, pp. 89-100.

Southern California Earthquake Data Centre, *Imperial Valley Earthquake*, viewed 16 February 2014, <http://www.data.scec.org/significant/imperial1940.html>.

Spence, R. & Coburn, A. 1992, 'Strengthening buildings of stone masonry to resist earthquakes', *Meccanica*, vol. 27, no. 3, pp. 213-21.

Spence, R. & D'Ayala, D. 1999, 'Damage assessment and analysis of the 1997 Umbria-Marche earthquakes', *Structural engineering international*, vol. 9, no. 3, pp. 229-33.

Stuff 2011, *Christchurch quake - the first image,* viewed 23 February 2011, <http:// www. stuff.co.nz/national/4688271/Christchurch-quake-the-first-images>.

Sutton, M.A., Wolters, W.J., Peters, W.H., Ranson, W.F. & McNeill, S.R. 1983, 'Determination of displacements using an improved digital correlation method', *Image and Vision Computing*, vol. 1, no. 3, pp. 133-9.

Thakkar, S.K. & Agarwal, P. 2000, 'Seismic evaluation of earthquake resistant and retrofitting measures of stone masonry houses', *12th World Conference on Earthquake Engineering*, Auckland, New Zealand.

Tomazevic, M. 1999, *Earthquake-resistant design of masonry buildings*, Imperial College, River Edge, NJ.

Tomaževič, M. & Velechovsky, T. 1992, 'Some aspects of testing small-scale masonry building models on simple earthquake simulators', *Earthquake Engineering & Structural Dynamics*, vol. 21, no. 11, pp. 945-63.

Turer, A., Korkmaz, S.Z. & Korkmaz, H.H. 2007, 'Performance improvement studies of masonry houses using elastic post-tensioning straps', *Earthquake Engineering & Structural Dynamics*, vol. 36, no. 5, pp. 683-705.

Turer, A. & Özden, B. 2008, 'Seismic base isolation using low-cost Scrap Tire Pads (STP)', *Materials and Structures*, vol. 41, no. 5, pp. 891-908.

USGS, '(United States Geological Survey), Significant Earthquake and News Headlines Archive', <http://earthquake.usgs.gov/earthquakes/eqinthenews/>.

Valluzzi, M., Binda, L. & Modena, C. 2002, 'Experimental and analytical studies for the choice of repair techniques applied to historic buildings', *Materials and Structures*, vol. 35, no. 5, pp. 285-92.

Valluzzi, M., da Porto, F. & Modena, C. 2004, 'Behavior and modeling of strengthened three-leaf stone masonry walls', *Materials and Structures*, vol. 37, no. 3, pp. 184-92.

Vasconcelos, G. & Lourenço, P.B. 2009, 'Experimental characterization of stone masonry in shear and compression', *Construction and Building Materials*, vol. 23, no. 11, pp. 3337-45.

Venu Madhava Rao, K., Venkatarama Reddy, B.V. & Jagadish, K.S. 1997, 'Strength characteristics of stone masonry', *Materials and Structures*, vol. 30, no. 4, pp. 233-7.

Vintzileou, E. 2008, 'Effect of Timber Ties on the Behavior of Historic Masonry', *Journal of Structural Engineering*, vol. 134, no. 6, pp. 961-72.

Vintzileou, E. & Miltiadou-Fezans, A. 2008, 'Mechanical properties of three-leaf stone masonry grouted with ternary or hydraulic lime-based grouts', *Engineering Structures*, vol. 30, no. 8, pp. 2265-76.

Walker, P. & Standards Australia HB 195 - 2002, *The Australian Earth Building Handbook*, Standards Australia International Ltd.

Wheen, R.J. 2009, 'Post-earthquake Reconstruction using Chainwire as Reinforcement', *Concrete 09, 24th Biennial Conference of Concrete Institute of Australia*, Concrete Institute of Australia, Sydney, Australia.

Worakanchana, K., Mayorca, P., Guragain, R., Navaratnaraj, S. & Meguro, K. 2008, '3-D Applied Element Method for PP-Band Retrofitted Masonry', *Seisan Kenkyu*, vol. 60, no. 2, pp. 128-31.

World Housing Encyclopedia, 'Housing Reports/Stone Masonry House', Viewed 17 April 2013, <http://www.world-housing.net/category/masonry/stone-masonry>.

Wu, F., Li, G., Jia, J.Q. & Li, H.N. 2011, 'Mechanical Properties of Adobe Masonry in Shear Test', *Applied Mechanics and Materials*, vol. 71, pp. 3691-4.

Yamaguchi, N., Narafu, T., Turer, A., Iiba, M. & Imai, H. 2008, 'Shaking table test of simple and affordable seismic isolation', *The 14th World Conference on Earthquake Engineering* Beijing, China.

Zeng, F. 2010, 'Numerical modeling and experimental investigation of masonry structures', PhD Thesis thesis, The City University of New York.

Zhong, T., Zhishou, C., Zhineng, G. & Chunjie, J. 2008, 'Experimental Behaviour of Adobe and Rammed Earth Wall of Rural Houses used in Yunnan Province', *The 14th World Conference on Earthquake Engineering* Beijing, China.